Piezoelectric Actuator Design via Multiobjective Optimization Methods

zur Erlangung des akademischen Grades eines
DOKTORS DER INGENIEURWISSENSCHAFTEN (Dr.-Ing.)
der Fakultät für Maschinenbau
der Universität Paderborn

genehmigte
DISSERTATION

von
M. Eng. Bo Fu
aus Sichuan, VR China

Tag des Kolloquiums: 09.06.2005
Referent: Prof. Dr.-Ing. Jörg Wallaschek
Korreferent: Prof. Dr. Michael Dellnitz

Foreword

Piezoelectric actuators find widespread applications in almost all fields of engineering. Ultrasonic welding, traveling wave motors or ultrasonic scalers are examples of systems operated in resonance. Diesel injection valves, optical scanners and atomic force microscope are examples of systems operating in a quasistatic mode.

The performance of piezoelectric actuators in a given application is mainly determined from the tuning of the actuator characteristics to the load characteristics. Except for some very limited special cases, no simple general design guidelines can be given today. Mathematical methods for the optimization of piezoelectric actuators are therefore a very important tool for the system designer.

In most engineering design tasks, multiple optimization criteria must be met. Despite tremendous progress in the mathematical sciences, knowledge on methods and algorithms for multicriteria optimization problems is limited in the engineering community.

Bo Fu was a scholar at the Paderborn Institute for Scientific Computation (PaSCo) and his thesis work was funded within the DFG-Graduiertenkolleg “Scientific Computation: Application-oriented Modeling and Development of Algorithms”. His thesis concentrates on the study of multicriteria optimization problems arising in the design of piezoelectric actuators and on mathematical methods which were developed for this class of optimization problems. Classical and novel methods are studied in detail and applied to various typical design problems of piezoelectric transducers. The results are of interest for all engineers working on the design of piezoelectric actuators, which are interested in mathematical background of multicriteria optimization, as well as for all mathematicians working in multicriteria optimization, which are interested in engineering applications.

Paderborn, September 2005

(Prof. Dr.-Ing. Jörg Wallaschek)

Acknowledgments

First of all, I would like to express my sincere gratitude and appreciation to my thesis advisor, Prof. Dr.-Ing. Jörg Wallaschek, for his continuous encouragement, support and patience throughout my Ph.D. study. His observations and comments helped me to establish the overall direction of my research and to move forward with investigation in depth, and his technical and editorial advice was essential to the completion of this dissertation. I thank him for giving me the opportunity to work with him.

I would also like to thank my co-advisor, Prof. Dr. Michael Dellnitz, for providing many valuable comments and suggestions during the work. I am furthermore grateful to the other members of my examining committee, Prof. Dr.-Ing. Roland Span and Prof. Dr.-Ing. Ansgar Trächtler, for their valuable comments.

I would additionally like to thank all members of the Mechatronics and Dynamics research group at the Heinz Nixdorf Institute for their help and support over the last few years. Particular thanks go to Dr.-Ing. Tobias Hemsel for the valuable comments that were very helpful in improving the presentation and contents of this dissertation. Thanks also to Dipl.-Ing. Reinhard Böer, Dr.-Ing. Thomas Sattel, Dipl.-Ing. Michael Brökelmann, Dipl.-Ing. Maik Mracek, Dipl.-Ing. Rafal Krol und Dipl.-Ing. Christian Potthast for their discussions and support. Special thanks to Mrs. Marina Kassühlke and Mrs. Kerstin Hille for their help and support throughout my Ph.D. study.

All the members of the Graduiertenkolleg of the Paderborn Institute for Scientific Computation (PaSCo) are also due many thanks for the pleasant environment, assistance and friendship. Particular thanks to M.Sc. Fang Wang for several disscussions and Dipl.-Ing. Nicolai Neumann for proof-reading some of the chapters.

I gratefully acknowledge the China Scholarship Council, the Graduiertenkolleg of the PaSCo and the Heinz Nixdorf Institute for providing scholarships to pursue doctoral studies in Germany.

Finally, last, but not least, I would like to thank my family, my wife Ling and son Yiheng, for their love, encouragement, patience and understanding during the past few years.

Thank you all.

To my mother, my father, my wife and my son

Contents

List of Symbols

α	electromechanical transformation factor
A_p	cross area of piezoelectric elements
A_b	cross area of metal blocks
$\boldsymbol{\beta}^{\mathbf{S}}, \boldsymbol{\beta}^{\mathbf{T}}$	dielectric impermeability matrix
c	modal stiffness
c_L	load stiffness
$\mathbf{c}^{\mathbf{D}}, \mathbf{c}^{\mathbf{E}}$	elastic modulus (Young's modulus) matrix
c_p, c_m	wave speed
C	electric capacitance
d	modal damping
d_L	load damping
$\mathbf{d}$	piezoelectric charge constant matrix
D_p	diameter of piezoelectric elements
D_t	outer diameters of back blocks, front blocks, input side of horns and piezo-rings
D_{t2}	outer diameter of the output end of horns
$\mathbf{D}$	dielectric displacement vector
$\boldsymbol{\varepsilon}^{\mathbf{S}}, \boldsymbol{\varepsilon}^{\mathbf{T}}$	absolute dielectric constant matrix
$\mathbf{e}$	piezoelectric constant matrix
f	frequency
E	elastic modulus (Young's modulus)
$\mathbf{E}$	electric field strength vector
E_c	coercive field strength
F	force

$\mathbf{g}$	piezoelectric voltage constant matrix
h_p	thickness of piezoelectric rings/discs
$\mathbf{H}$	piezoelectric constant matrix
j	$\sqrt{-1}$
k, k_{eff}	coupling factor
k_p	wave number
$\mathbf{K}_{\varphi\varphi}$	dielectric matrix
$\mathbf{K}_{uu}$	stiffness matrix
$\mathbf{K}_{u\varphi}$,$\mathbf{K}_{\varphi u}$	piezoelectric matrix
L_b	length of back and front blocks
L_{f1}, L_{f2}	length of the first part of horns, length of the second part of horns
L_p	length of piezoelectric elements
L_m	mechanical inductance
λ_p	power efficiency
m	modal mass
M	piezoelectric quality number
$\mathbf{M}_p$	mass matrix
N	number of piezoelectric rings, population size
η	efficiency
η_e	electrical loss factor
η_m	mechanical loss factor
η_p	piezoelectric loss factor
φ_e, φ_m	phase difference
φ	electric potential field
p_e	electrical power

P	polarization
P_a, P_{ma}	apparent electrical and mechanical power
P_e, P_m	effective electrical power and mechanical power
P_r	remanent polarization
Pr	prestress
ρ	density
Q	electric charge
Q_m	mechanical quality factor
R	electric resistance
$\mathbf{s}^{\mathbf{D}}, \mathbf{s}^{\mathbf{E}}$	elastic compliance matrix
$\mathbf{S}$	strain vector
t	time
$\tan\delta$	loss factor
Typ_b	material of back and front blocks
Typ_f	material of horns
Typ_p	material of piezo-rings
$\mathbf{T}$	stress vector
u, u_3	displacment
U	voltage
v	velocity
ω	angular frequency
w_1, w_2	pseudo-weight of objective 1, pseudo-weight of objective 2
Ω	exciting angular frequency
ζ	diameter transformation ratio

In this dissertation, complex quantities are characterized by underline. Amplitudes are characterized by a hat “^”.

Parts of this work have already been published in terms of conference contributions:

Fu, Bo; Hemsel, Tobias; Wallaschek, Jörg: Model-based Diagnosis for Sandwiched Ultrasonic Transducers. Proceedings of the 18th International Congress on Acoustics, ICA 2004, Kyoto, Japan Bd. 3, 2004, S. 2243-2246

Fu, Bo; Hemsel, Tobias; Wallaschek, Jörg: Multiobjective Optimization of Piezoelectric Transducers using Evolutionary Algorithms. Proceedings of 2nd International Workshop on Piezoelectric Materials and Applications in Actuators, Paderborn, 2005, (in print)

Fu, Bo; Hemsel, Tobias; Wallaschek, Jörg: Piezoelectric Transducer Design via Multiobjective Optimization. World Congress Ultrasonics 2005, Beijing, P. R. China, (to be published in 2006)

1 Introduction

1.1 Motivation

Over the last decades the demand for piezoelectric actuators has been increased significantly. Different types of piezoelectric actuators such as high strain multilayers, ultrasonic transducers, converters and ultrasonic motors etc. have been developed. They have been widely used in engineering fields like e.g. micro-positioning, active vibration control, ultrasonic welding and machining. Piezoelectric actuators, like almost all mechanical systems, are always expected to be “optimal”. However, the design of piezoelectric actuators is a difficult task, because the overall characteristics of piezoelectric actuators are affected by various factors such as dimensions of active and passive parts, inherent properties of piezoelectric materials, electrical and mechanical boundary conditions, etc. Obviously, empirical and intuitive design methods cannot well accomplish the design task. Systematic optimization techniques are the most appropriate tool to be used in the design task of piezoelectric actuators.

The design of a piezoelectric actuator can be described as a process of finding optimal design variables like e.g. the dimension and material types of piezoelectric elements and mechanical parts, which minimize or maximize a certain number of objectives like e.g. output amplitude, input power, output power, subject to a certain set of specified requirements, like e.g. resonance frequency, limits on input voltage and pre-stress, geometric constraints, etc. This is a constrained multiobjective optimization problem (MOP) involving continuous and discrete design variables. Commonly, in this problem some of the multiple objectives are conflicting to each other and it is impossible to find a solution at which each objective function gets its optimal value simultaneously. In this case, one tries to find a set of optimal compromises namely Pareto-optimal solutions from which the designer can select one.

MOPs are often solved by traditional methods based on scalarization techniques. The common ground of these methods is to convert a multiobjective (vector) optimization problem into a single (scalar) optimization problem. After transformation the widely developed theory and methods for single objective optimization can be used. However, traditional methods show some difficulties. For example, they require some problem knowledge before optimization is performed. Some techniques may be sensitive to the shape of the Pareto-optimal front. Moreover, they require several optimization runs to obtain an approximation of the Pareto-optimal set. Evolutionary algorithms (EAs), on the other hand, are able to find multiple Pareto-optimal solutions in a single simulation run due to their population-approach. They are well suited for multiobjective optimization and the problems with discrete variables. Indeed, from the point of view of engineering only one best solution needs to be implemented. If one knows the exact trade-off among objectives before the problem is solved, there is no need to find multiple solutions. The exact trade-off between objective functions, however, is usually not clear before optimization is performed. Therefore, it is better to find the Pareto-optimal set and then select one solution by some criteria.

Over the past decades many multiobjective optimization methods in particular multiobjective evolutionary algorithms (MOEAs) have been developed. It is meaningful to apply them in the design of piezoelectric actuators in order to improve performances of products and reduce the cost of the product development. Although some studies concerning optimization of piezoelectric actuators have been published and some optimization methods have been used, these studies mainly concentrate on single objective optimization and continuous variables. Multiobjective optimizations of piezoelectric actuators including continuous and discrete design variables, especially the formulation of problems and the application of various MOEAs have not been reported. Obviously, there is a need for a contribution to this topic.

1.2 Objective

The objective of this thesis work is to present an integrated procedure for piezoelectric actuator design via multiobjective optimization methods. The work concentrates on the formulation of MOPs, the application of different multiobjective optimization methods, the evaluation of optimized results and the determination of the preferred design. There exist a large variety of multiobjective optimization methods and it is not possible to apply every existing method. The thesis mainly concentrates on the application of MOEAs. Regarding classical scalarization methods the algorithms of single objective optimization will not be stressed but the ways to converting the MOP to a single objective problem will be pointed out. As far as optimization problems of piezoelectric actuators are concerned, one practical MOP, namely the two-objective optimal design of Langevin-type transducers involving continuous and discrete design variables, is considered. The transfer matrix method based on continuum models of piezoelectric and mechanical rods and the lumped parameter method based on the electromechanical analogies are mainly applied in formulation of optimization problems.

1.3 Scope

The present thesis work is organized as follows:

In chapter 2, fundamentals of piezoelectric actuators are presented. First, the piezoelectric effect and typical piezoelectric actuators are introduced. Then, four models of piezoelectric actuators namely nonparametric models, continuum models, finite element models and lumped parameter models based on the electromechanical analogies are described. After that, typical design goals for typical piezoelectric actuators are presented. Finally, the state of the art of optimization of piezoelectric actuators is reviewed.

Chapter 3 presents multiobjective optimization methods. The basic concepts of multiobjective optimization are first introduced. Classical multiobjective optimization methods (scalarization methods) are then described briefly. Finally, five MOEAs are studied.

Chapter 4 presents the multiobjective optimization of Langevin-type transducers. First, the Langevin transducer is introduced. Then performance criteria for the transducer are described. After that, optimal prestress of the Langevin transducer for multiple objectives is discussed. The modeling of the transducer using the transfer matrix method based on continuum models is then described. Finally, MOPs for the design of Langevin-type transducers are formulated. These problems are then solved by two-level optimization using MOEAs described in chapter 3. The first level optimization is performed in this chapter.

In chapter 5, the second level optimization is preformed and the preferred design is determined. First, the non-dominated solutions are searched in the results of the first level optimization obtained in chapter 4 for the transducers with 2, 4 and 6 piezo-rings. Second, the results of the second level optimization are analyzed and the preferred design is determined using various methods. Finally, the load characteristics of the Pareto-optimal transducers are discussed.

The last chapter gives a summary to this thesis work and outlook for future work.

2 Piezoelectric Actuators

For the optimization of piezoelectric actuators two different kinds of techniques are needed. One is the modeling of the actuators; the other is an appropriate optimization method. In this chapter the most important fundamentals concerning piezoelectric actuators are described. First, the piezoelectric effect and piezoelectric actuators are introduced. The models of piezoelectric actuators are then described. After that, the typical design goals for different types of piezoelectric actuators are present and the state of the art of optimization of piezoelectric actuators is reviewed.

2.1 Piezoelectric Effect

The piezoelectric effect was first discovered by Pierre and Jacques Curie in 1880. They found that when mechanical stress T was applied to a particular crystal material, electrical charges Q were generated and a voltage U between the surfaces of the material was generated. About one year later the inverse piezoelectric effect, which is the fundamental for applying piezoelectric elements as actuators, was also examined by the Curies [Ike96].

The piezoelectric effect can appear only in crystals which have polar axes, i.e. in the crystals which possess no center of symmetry. Many naturally occurring crystals, e.g. quartz, tourmaline and Rochelle salt have this character. Piezoelectric ceramics (PZT-based ceramics), which are probably the most important piezoelectric materials, may be considered as a mass of randomly oriented piezoelectric crystallites. These materials have a perovskite crystal structure. In the high temperature no-polar phase there is no spontaneous polarization because the crystallites are cubic symmetric. Below the transition temperature known as the Curie point, i.e. in a non-centrosymmetric ferroelectric phase, spontaneous polarization occurs and the crystallites exhibit the tetragonal or rhombohedral structures. In the unpolarized state, the polarizations of grains (crystallites making up a polycrystalline ceramic) or domains are randomly oriented so that no overall polarization or piezoelectric effect appears. The piezoelectricity of the polycrystalline ceramics may, however, be aligned in any chosen direction by a poling treatment which involves applying a strong electric field (>3 kV/mm) to align the polarization direction of each grain or domain as much as possible, heating the material to beyond its Curie point and cooling the material below this point to “lock” the domain structure. The polycrystalline ceramic therefore becomes anisotropic and has a permanent polarization as if it were a single-domain crystal [Cul96] and [Uch97]. Details concerning the configuration and fabrication of piezoelectric ceramics are described in [JC71], [Phi 88] and [Set02].

The piezoelectric effect couples the electrical and mechanical behavior. It can be approximately described by the following linear piezoelectric constitutive fundamental equations [Ike96], [Phi91] and [Hem01]:

$$\begin{aligned}\mathbf{S} &= \mathbf{s}^{\mathbf{E}}\mathbf{T} + \mathbf{d}_{\mathbf{t}}\mathbf{E} \\ \mathbf{D} &= \mathbf{d}\mathbf{T} + \boldsymbol{\varepsilon}^{\mathbf{T}}\mathbf{E}\end{aligned} \tag{2.1}$$

In the above equations the full tensor notation has been abbreviated into simpler matrix notation. **D, E, S** and **T** are the vectors of the dielectric displacement, the electric field strength, the strain and the stress respectively. $\boldsymbol{\varepsilon}^{\mathbf{T}}$ **,** $\mathbf{s}^{\mathbf{E}}$ and **d** are the matrices of the absolute dielectric constant, the elastic compliance and the piezoelectric charge constant. The superscripts **T** and **E** refer to the quantities to be kept constant (**T=E=0**) when measuring material constants [IE87], [DI483] and [DI324]. Similar relations are found for various choices of independent variable sets. The constitutive equations can be arranged in several ways and the four types of the piezoelectric constitutive equation set are shown in Table 2.1. By calculations one set of constants can be expressed by another, see e.g. [DI483] and [DI324].

As poled piezoelectric ceramics are anisotropic, the material constants depend on the directions of the stimulation and reaction. These are described by a (right hand) Cartesian coordinate system. Usually the direction of polarization is taken to be that of the 3-axis (z axis), see Fig. 2.1. The material constants are complied in the following elastoelectric matrix, see Table 2.2. The material constants are generally written with two subscripts. The first subscript indicates the direction of the excitation, and the second gives the direction of of the system response. It is worth noticing that not all elements of the elastoelectric matrix are occupied.

These material constants are identified by the measurement on geometrically simple specimens under a small electric excitation [DI324] and [Rus95]. They are only applied for the description of the small signal behavior and subject to a high fluctuation range [DI324] and [Hem01].

Table 2.1 Types of fundamental piezoelectric constitutive equations

Independent variable	Piezoelectric constitutive equation	
T, E	$\mathbf{S} = \mathbf{s}^{\mathbf{E}}\mathbf{T} + \mathbf{dE}$ $\mathbf{D} = \mathbf{dT} + \boldsymbol{\varepsilon}^{\mathbf{T}}\mathbf{E}$	
S, D	$\mathbf{T} = \mathbf{c}^{\mathbf{D}}\mathbf{S} - \mathbf{hD}$ $\mathbf{E} = -\mathbf{hS} + \boldsymbol{\beta}^{\mathbf{S}}\mathbf{D}$	(2.2)
S, E	$\mathbf{T} = \mathbf{c}^{\mathbf{E}}\mathbf{S} - \mathbf{eE}$ $\mathbf{D} = \mathbf{eS} + \boldsymbol{\varepsilon}^{\mathbf{S}}\mathbf{E}$	(2.3)
T, D	$\mathbf{S} = \mathbf{s}^{\mathbf{D}}\mathbf{T} + \mathbf{gD}$ $\mathbf{E} = -\mathbf{gT} + \boldsymbol{\beta}^{\mathbf{T}}\mathbf{D}$	(2.4)

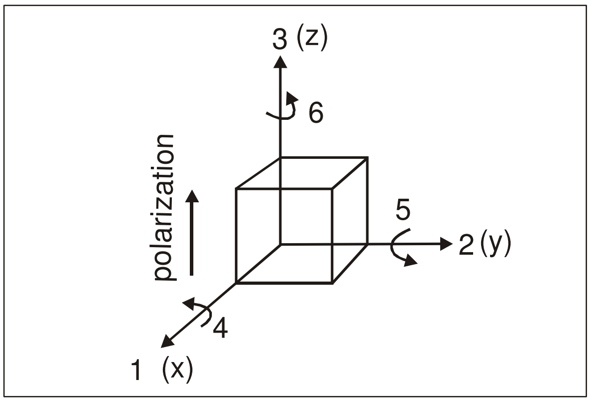

Fig. 2.1 Coordinate System

For large mechanical strains and large electrical field strengths the material behaves nonlinear. Fig. 2.2(a) shows the relationship between the applied electric field strength E and the induced polarization P. There appears a hysteresis caused by the transition of the spontaneous polarization between the positive and negative directions. Fig. 2.2(b) shows the relationship between the applied electric field and the strain, i.e. the so-called butterfly hysteresis curve. When the applied field is small, the induced strain is nearly proportional to the field. The piezoelectric constant can be obtained from the slope. As the field becomes larger (i.e. greater than about 100V/mm), the strain curve deviates from this linear trend and significant hysteresis is exhibited. If the drive electric field passes the coercive field, the hysteresis changes into a butterfly shape. Such strain hysteresis during an electric field cycle is caused by the change of the ferroelectric domain status. The detailed physical interpretations on hysteresis are shown in e.g. [Sch96] and [Uch97]. Commonly, the losses can be approximately described by complex material constants [Wal00] and [Hem01].

Piezoelectric ceramics are also temperature-dependent and exhibit total depolarization above the Curie point, which, depending on the composition, ranges from 150°C to 400°C. As the Curie point is approached the values of the piezoelectric constants decrease.

Table 2.2 Elastoelectric matrix for the stress T and the electric field E as independent variables

	T_1	T_2	T_3	T_4	T_5	T_6	E_1	E_2	E_3
S_1	s_{11}	s_{12}	s_{13}						d_{31}
S_2	s_{12}	s_{11}	s_{13}						d_{31}
S_3	s_{13}	s_{13}	s_{33}						d_{33}
S_4				s_{44}				d_{15}	
S_5					s_{44}		d_{15}		
S_6						$2(s_{11}-s_{12})$			
D_1					d_{15}		ε_{11}		
D_2				d_{15}				ε_{11}	
D_3	d_{31}	d_{31}	d_{33}						ε_{33}

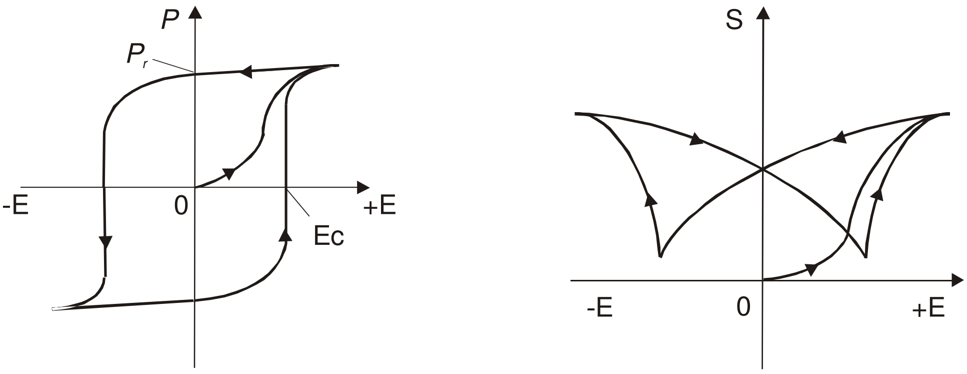

a) b)

Fig. 2.2 a) Polarization P as a function of field strength b) Mechanical deformation (strain) as a function of field strength

2.2 Piezoelectric Actuators

Piezoelectric actuators convert voltage and charge into force and motion. According to the electrical drive method, they can be divided into two categories: the resonant driven piezoelectric actuators and the non-resonant driven piezoelectric actuators. The resonant driven piezoelectric actuators include e.g. ultrasonic transducers (converters), ultrasonic motors and piezoelectric transformators. The non-resonant driven piezoelectric actuators include various one-stroke actuators. Their operating frequency range is from quasistatic up to about half of the first resonant frequency of the mechanical system.

In practice a variation of the electric field strength will deform a piezoelectric body in different directions with different intensities. According to the type of the utilized piezoelectric effect (the directions of the applied electric field and the extension), piezoelectric actuators can be divided into three main groups, see Fig. 2.3.

In longitudinal actuators, also called d_{33}-actuators, the applied electric field, the utilized extension and the polarization have the same direction. They are usually used for small movements and high forces and generally have because of high stiffness. Transversal actuator actuators, also called d_{31}-actuators, have the electric field applied in the direction of the polarization and the main deformation is in the direction perpendicular to the polarization. They are also used for small movements and high forces and also have high stiffness. In flexural actuators, also known as d_{15}-actuators or bimorphs, the electric field is applied in the direction perpendicular to the polarization and the flexural deformation is utilized. They are mainly used for large movements and have low stiffness.

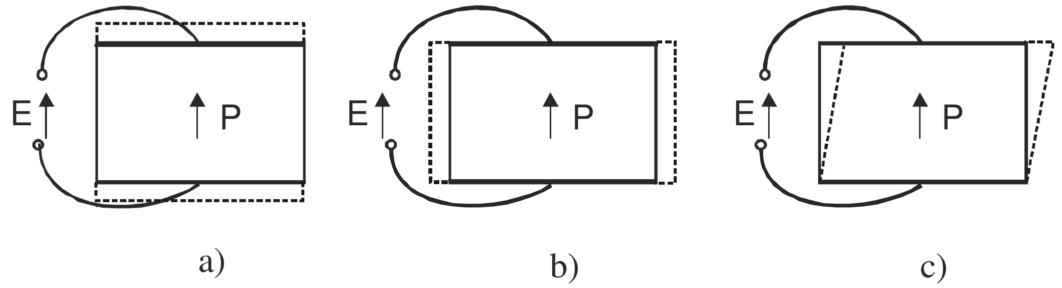

Fig. 2.3 Piezoelectric actuators a) d_{33} ; b) d_{31}; c) d_{15}

Typical strain levels that can be obtained by piezoelectric actuators are in the region of 0.1%, occurring at field strength in the region of 1000V/mm. This maximum field strength is limited to approximately 0.75 of the value of the coercive field. In order to increase the total displacement capability of a piezoelectric ceramic actuator, multilayer stacks as well as amplifying mechanisms are often used [Cul96] and [Hen01].

In addition to hysteresis, other effects such as zero point drift, creep and aging are also encountered in piezoelectric actuators [Sch96] and [Uch97].

A piezoelectric actuator commonly consists of several components including piezoelectric ceramics and metal housing, which are assembled to form an integral entity. Piezoelectric actuators have been widely used in various fields such as micro-positioning of tools, active vibration control, ultrasonic welding and machining, common rail diesel injection systems.

2.3 Models of Piezoelectric Actuators

In any optimization problem two phases can be distinguished: formulation and solution. Broad experience in solving problems has shown that the time needed to formulate a problem makes up 70-85% of the total time required for a complete treatment, from the formulation to results [SM95]. An adequate mathematical model is the fundamental of the formulation of optimization problems. This section presents four models which can be used to describe the dynamic behavior of piezoelectric actuators. In order to interpret the models more clearly, a typical longitudinal piezoelectric actuator as shown in Fig. 2.4 a) is used as an example for modeling.

2.3.1 Nonparametric Models

The nonparametric model deals with the piezoelectric actuator as a type of "black box" and directly estimates the impulse or the frequency response of the system. This model does not impose any assumptions about the actuator, other than that of linearity. In this context, a piezoelectric actuator can be regarded as an electromechanical four-pole network element, which has electric input quantities (the voltage U and the current I) and mechanical output quantities (the force F and the velocity v) , see Fig. 2.4 (b).

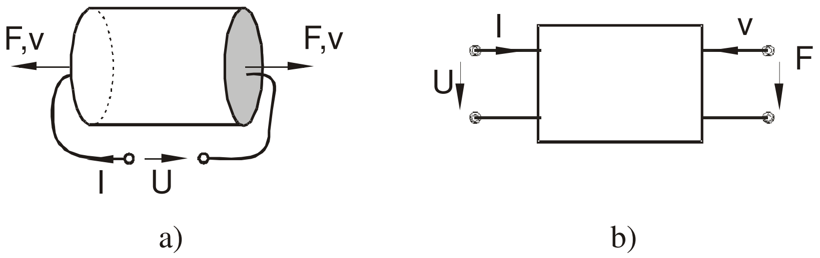

Fig. 2.4 a) Piezoelectric actuator b) Piezoelectric actuator as a four-pole network element

For harmonic vibrations of the piezoelectric actuator, the relation between inputs and outputs can be written as

$$\begin{bmatrix} \underline{\hat{I}} \\ \underline{\hat{v}} \end{bmatrix} = \begin{bmatrix} \underline{y}_{11} & \underline{y}_{12} \\ \underline{y}_{21} & \underline{y}_{22} \end{bmatrix} \cdot \begin{bmatrix} \underline{\hat{U}} \\ \underline{\hat{F}} \end{bmatrix}, \tag{2.5}$$

where $\underline{\hat{U}}$, $\underline{\hat{I}}$, $\underline{\hat{F}}$ and $\underline{\hat{v}}$ are complex amplitudes. $\underline{Y}$ is the transfer matrix, which also is called the conductance matrix. The elements of the transfer matrix are defined as follows:

$$\underline{y}_{11} = \frac{\underline{\hat{I}}}{\underline{\hat{U}}} \quad \text{: the short-circuit input admittance} \tag{2.6}$$

$$\underline{y}_{21} = \frac{\underline{\hat{v}}}{\underline{\hat{U}}} \quad \text{: the short-circuit core admittance (forward)} \tag{2.7}$$

$$\underline{y}_{12} = \frac{\underline{\hat{I}}}{\underline{\hat{F}}} \quad \text{: the short-circuit core admittance (backward)} \tag{2.8}$$

$$\underline{y}_{22} = \frac{\underline{\hat{v}}}{\underline{\hat{F}}} \quad \text{: the short-circuit output admittance} \tag{2.9}$$

Fig. 2.5 shows the typical variation of the amplitude magnitude and phase shift of the short-circuit input admittance $\underline{y}_{11}$ as a function of frequency (Bode plot) for a piezoelectric actuator. Fig. 2.6 gives the corresponding locus of $\underline{y}_{11}$ in the complex plane (Nyquist plot). According to Fig. 2.6, a piezoelectric quality number is geometrically defined as follows [LeI75].

$$M = \frac{Y_r}{Y_c} \tag{2.10}$$

where $Y_r = Y_{max} - Y_{min}$ is the diameter of the locus of $\underline{y}_{11}$ as shown in Fig. 2.6. Y_{max} and Y_{min} are the values of $\underline{y}_{11}$ at the frequencies f_m and f_n, respectively.

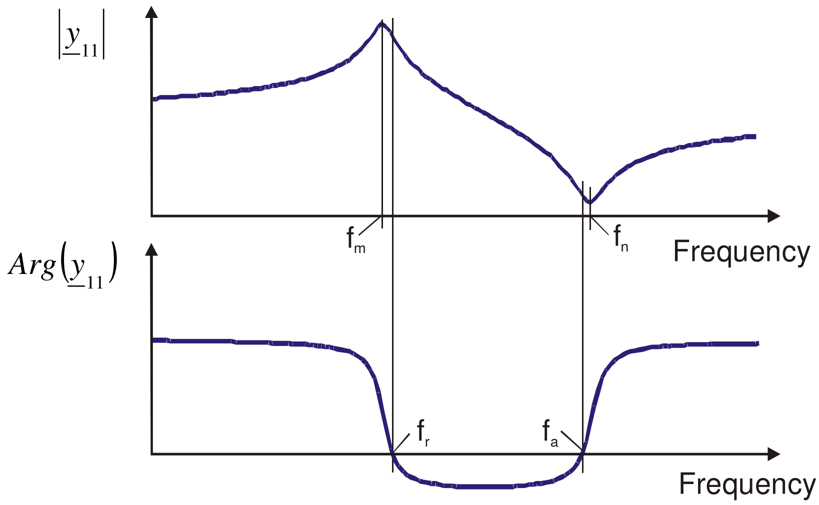

Fig. 2.5 Variation of admittance magnitude and phase angle with frequency

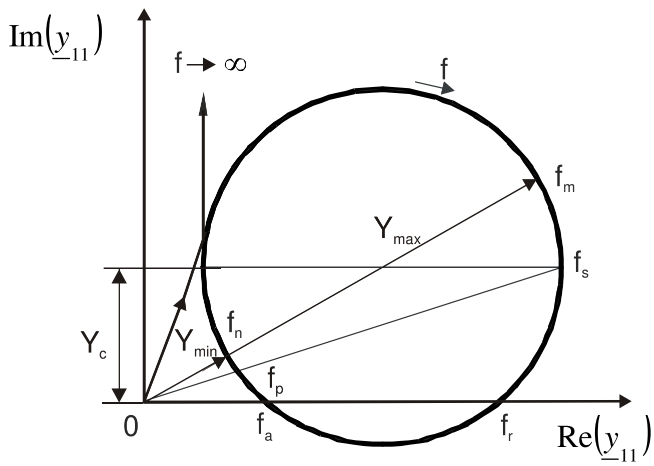

Fig. 2.6 Frequency response in the complex plane

There are three pairs of characteristic frequencies, which are characteristic for these plots, namely f_s and f_p , f_m and f_n as well as f_r and f_a . The series resonant frequency f_s is the frequency at which the admittance in the equivalent model becomes infinite if the electrical loss R and the mechanical loss d are neglected (see section 2.3.4). The parallel resonant frequency f_p is the frequency at which the admittance in the equivalent model becomes zero if R and d are neglected (also see section 2.3.4). The frequency f_m is the frequency at which the admittance becomes maximum and the frequency f_n is the frequency at which the admittance becomes minimum. The resonant frequency f_r and antiresonant frequency f_a are the frequencies at which the phase angle of $\underline{y}_{11}$ is equal to zero. These frequencies are approximately equal for the piezoelectric ceramics with a piezoelectric quality number M>>2, i.e. $f_s \approx f_r \approx f_m$ and $f_p \approx f_a \approx f_n$.

The coupling factor k is a measure of the effective energy conversion in the piezoelectric actuator. For quasistatic operation, the coupling factor k is defined as follows [Ike96]:

$$k^2 = \frac{\text{transformed, stored mechanical energy}}{\text{supplied electrical energy}} \tag{2.11a}$$

or

$$k^2 = \frac{\text{transformed, stored electrical energy}}{\text{supplied mechanical energy}} \tag{2.11b}$$

This definition gives a conceptual picture of the coupling factor, but it is not effective in determining the value of k^2 of an actual actuator. It is possible to express the coupling factor based on the frequencies defined above. This results in [Phi91]

$$k^2 = \frac{f_p^2 - f_s^2}{f_p^2} \tag{2.12}$$

As an approximation, when $k << 1$ one may write

$$k^2 = 2\frac{f_p - f_s}{f_p} = 2\frac{\Delta f}{f_p} \tag{2.13}$$

It is worth to point out that though a high k^2 is usually desirable for efficient transformation, the coupling factor must not be mistaken for efficiency, since the losses are not considered in the coupling factor. The unconverted energy is not necessarily lost (converted into heat) and can mostly be recovered.

The mechanical quality factor Q_m is used as a measure for the resonance rise of the piezoelectric actuator. It can be derived from the 3dB bandwidth of the admittance at f_s if $k^2Q_m>10$ [Rus95] resulting in

$$Q_m = \frac{f_s}{\Delta f_s(3dB)} = \frac{f_s}{f_2 - f_1} \tag{2.14}$$

The frequencies f_1 and f_2 are frequencies that correspond to the admittances that are 3dB lower than the maximal admittance, respectively.

The advantage of nonparametric models is that they are able to analyze the dynamic behaviors of all types of piezoelectric actuators, without knowing the concrete structure of the system. As no parameters are used in the models, obviously, they are not suitable to the optimization problem. Nonparametric models, however, play an important role in the experimental characterization of dynamic behaviors of piezoelectric actuators.

2.3.2 Continuum Models

In continuum models the piezoelectric actuator is considered as a mechanical continuum with additional degrees of freedom for the electrical behavior. Its behavior is described by the partial differential equations of motion, which involve derivatives with respect to spatial coordinates as well as with respect to time. Moreover, the electromechanical coupling of the piezoelectric material is approximately described by the constitutive equations [BCJ64] and [WH00].

It is difficult to find an analytical solution of the partial differential equations of motion of continuous systems having complex geometry and boundary conditions. Therefore, continuum models are mostly used for piezoelectric actuators with simplified geometry (rod, beam, plate etc.) and boundary conditions.

In the following the continuum model of the piezoelectric actuator shown in Fig. 2.4(a) will be described. Fig. 2.7 gives its dimensions.

Assumptions: It is assumed that the actuator has the shape of a slender rod and only the longitudinal vibration is taken into account. The problem is then reduced to the one-dimensional case by following assumptions:

- $D_p < \lambda/4$ (slender rod, λ is wavelength)
- $T_1 = T_2 = T_4 = T_5 = T_6 = 0$ (uniaxial stress condition)
- $E_1 = E_2 = 0$ (non leakage electrical field)
- $D_1 = D_2 = 0$ (surrounding medium air)

Governing equations The fundamental piezoelectric constitutive relation (*T, E*)-type (see Table 2.1) for loss-free piezoelectric material is

$$S_3 = s_{33}^E\, T_3 + d_{33}\, E_3 \tag{2.15}$$

$$D_3 = d_{33}\, T_3 + \varepsilon_{33}^T\, E_3 \tag{2.16}$$

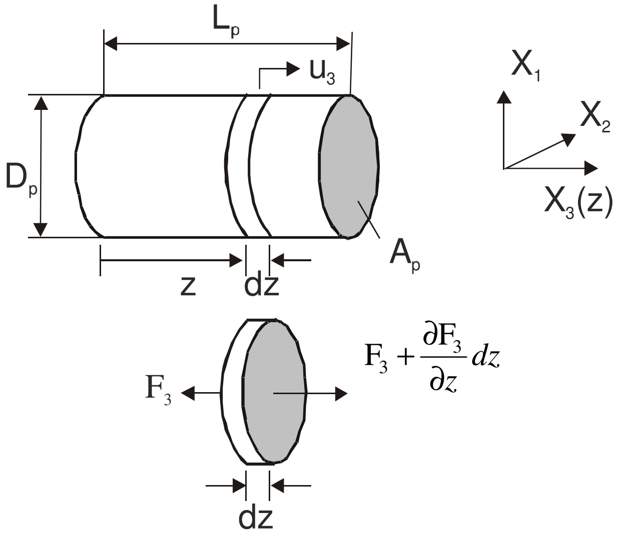

Fig. 2.7 Dimensions of the piezoelectric actuator

This is rearranged to give the relation of (*S, E*)-type as follows

$$T_3 = c_{33}^E S_3 - e_{33} E_3 \tag{2.17}$$

$$D_3 = e_{33} S_3 + \varepsilon_{33}^S E_3 \tag{2.18}$$

where $c_{33}^E = 1/s_{33}^E$, $e_{33} = d_{33}/s_{33}^E$, $\varepsilon_{33}^S = \varepsilon_{33}^T - d_{33}^2/s_{33}^E$

Eliminating E_3 gives

$$T_3 = c_{33}^D S_3 - \frac{e_{33}}{\varepsilon_{33}^S} D_3 \tag{2.19}$$

where $c_{33}^D = c_{33}^E + e_{33}^2/\varepsilon_{33}^S$

When the energy losses in the piezoelectric materials should be taken into account, the following complex moduli can be introduced into the model

$$\underline{s}_{33}^E = s_{33}^E(1 - j\eta_m) \tag{2.20}$$

$$\underline{\varepsilon}_{33}^T = \varepsilon_{33}^T(1 - j\eta_e) \tag{2.21}$$

$$\underline{d}_{33} = d_{33}(1 - j\eta_p) \tag{2.22}$$

Equations (2.20), (2.21) and (2.22) describe mechanical loss, dielectric loss and piezoelectric loss, respectively. The loss factors η_m, η_e and η_p describe the phase shifts between the stress and the strain, between the electric field strength and dielectric displacement as well as between the strain and the electric field strength, respectively. The application of complex moduli in the modeling will be discussed further in chapter 4.

Considering an element of length *dz*, the application of Newton's second law to the free body of the element shown in Fig. 2.7 yields

$$\frac{\partial T_3}{\partial z} = \rho \frac{\partial^2 u_3}{\partial t^2} \tag{2.23}$$

and the conservation of charge leads to

$$\frac{\partial D_3}{\partial z} = 0 \tag{2.24}$$

Substituting equations (2.17) and (2.18) into equations (2.23) and (2.24) as well as using

$$S_3 = \frac{\partial u_3}{\partial z} \tag{2.25}$$

and

$$E_3 = -\frac{\partial \varphi}{\partial z} \tag{2.26}$$

yield the following governing equations

$$\frac{\partial^2 u_3}{\partial t^2} = c_p{}^2 \frac{\partial^2 u_3}{\partial z^2} \tag{2.27}$$

$$\frac{\partial^2 \varphi}{\partial z^2} = \frac{e_{33}}{\varepsilon_{33}^S} \frac{\partial^2 u_3}{\partial z^2} \tag{2.28}$$

Equation (2.27) is the one-dimensional wave equation, in which the wave speed is given by $c_p = \sqrt{c_{33}^D / \rho}$.

Solutions of governing equations

The solution of the wave equation (2.27) is generally obtained by means of the separation-of-variables method, where $u_3\ (z,\ t)$ is expressed as the product of a function of time and a function of the space coordinate. The solution $\varphi\ (z,\ t)$ of the governing equation (2.28) can also be obtained by means of the same method. If the input voltage is a harmonic vibration with frequency Ω , the displacement u and the electric potential φ are also considered as harmonic vibrations with the same frequency. Therefore, the function of time in the separation-of-variables method can be directly expressed as $e^{j\Omega t}$. Using complex variables to express the displacement and potential fields yield

$$\underline{u}_3(z,t) = \underline{\hat{u}}_3(z) e^{j\Omega t} \tag{2.29}$$

$$\underline{\varphi}(z,t) = \underline{\hat{\varphi}}(z) e^{j\Omega t} \tag{2.30}$$

Substituting equations (2.29) and (2.30) into equations (2.27) and (2.28) yields the following governing equations

$$\frac{d^2 \underline{\hat{u}}_3}{dz^2} + k_p{}^2 \underline{\hat{u}}_3 = 0 \tag{2.31}$$

$$\frac{d^2 \underline{\hat{\varphi}}}{dz^2} = \frac{e_{33}}{\varepsilon_{33}^S} \frac{d^2 \underline{\hat{u}}_3}{d z^2} \tag{2.32}$$

where $k_p = \Omega / c_p$ is called wave number.

Since two arbitrary constants are required in the solution of a second-order ODE, the general solution of the equation (2.31) has the following complex form

$$\underline{\hat{u}}_3(z) = \underline{C}_1 e^{jk_p z} + \underline{C}_2 e^{-jk_p z} \tag{2.33}$$

Introducing equation (2.33) into equation (2.32) the solution $\underline{\hat{\varphi}}$ can be expressed as follows

$$\underline{\hat{\varphi}}(z) = \frac{e_{33}}{\varepsilon_{33}^{S}}\left(\underline{C}_1 e^{jk_p z} + \underline{C}_2 e^{-jk_p z}\right) + \underline{C}_3 z + \underline{C}_4 \tag{2.34}$$

The undetermined constants $\underline{C}_1$, $\underline{C}_2$, $\underline{C}_3$ and $\underline{C}_4$ can be computed from electrical and mechanical boundary conditions. For example, when the piezoelectric actuator shown in the Fig. 2.4(a) and Fig. 2.7 is fixed at one side ($z=0$) and a harmonic force $\underline{F}_3(t) = \underline{\hat{F}}_3 e^{j\Omega t}$ is applied at the other side ($z = L_p$), the boundary conditions are:

$$\begin{aligned} &\underline{\hat{u}}_3(z=0) = 0, \quad \underline{\hat{T}}_3(z=L_p) = \frac{\underline{\hat{F}}_3}{A_p} \\ &\underline{\hat{\varphi}}(z=0) = 0, \quad \underline{\hat{\varphi}}(z=L_p) = -\underline{\hat{U}} \end{aligned} \tag{2.35}$$

After introducing these boundary conditions into equations (2.33), (2.17), (2.34) and (2.34) four linear equations in terms of $\underline{C}_1$, $\underline{C}_2$, $\underline{C}_3$ and $\underline{C}_4$ can be obtained. The unknown constants are then determined based on solving the four linear equations ($\underline{\hat{F}}_3$ and $\underline{\hat{U}}$ are assumed as given quantities). Therefore, the complex amplitudes of the vibration displacement and electric potential are obtained according to the equations (2.33) and (2.34), respectively.

Similarly, the dielectric displacement $D_3(z,t)$ can also be described by means of the separation-of-variables method as follows

$$\underline{D}_3(z,t) = \underline{\hat{D}}_3(z) e^{j\Omega t} \tag{2.36}$$

Considering the equations (2.25) and (2.26) and introducing the equations (2.36), (2.29) and (2.30) into the equation (2.18) it follows

$$\underline{\hat{D}}_3(z) = e_{33}\frac{d\underline{\hat{u}}_3(z)}{dz} - \varepsilon_{33}^{S}\frac{d\underline{\hat{\varphi}}(z)}{dz} \tag{2.37}$$

Substituting the equations (2.33) and (2.34) into the equation (2.37) and with simple computations, the complex amplitude of the dielectric displacement is given by

$$\underline{\hat{D}}_3(z) = -\varepsilon_{33}^{S}\underline{C}_3 \tag{2.38}$$

The electric current can be derived through integrating the dielectric displacement over the area A_p of the electrode and then calculating the derivative with respect to time. Considering $\frac{\partial D_3}{\partial x_1} = \frac{\partial D_3}{\partial x_2} = 0$ the electric current is given by

$$\underline{\hat{I}} = j\Omega \underline{\hat{D}}_3 A_p \tag{2.39}$$

The vibration velocity at the free side (z = L_p) of the actuator can also be obtained through differentiating the displacement with respect to time. Its complex amplitude is given by

$$\underline{\hat{v}} = j\Omega\underline{\hat{u}}_3 \tag{2.40}$$

Consequently, the electromechanical transfer behaviors of the actuator as shown in Fig. 2.4 (a) are well-established. In the same way, a four-pole network element which has two input quantities and two output quantities as shown in the Fig. 2.4 (b) can be used. Its transfer functions can be described by the same form as expression (2.5). According to the equations (2.39) and (2.40), the expressions of the elements of the conductance matrix are

$$\underline{y}_{11}(\Omega) = \frac{j\Omega A_p k_p L_p \varepsilon_{33}^S ({e_{33}}^2 + c_{33}^E \varepsilon_{33}^S)\cos(k_p L_p)}{k_p {L_p}^2 (e_{33}^2 + c_{33}^E \varepsilon_{33}^S)\cos(k_p L_p) - {e_{33}}^2 \sin(k_p L_p)} \tag{2.41}$$

$$\underline{y}_{12}(\Omega) = \underline{y}_{21}(\Omega) = \frac{j\Omega e_{33} \varepsilon_{33}^S \sin(k_p L_p)}{k_p {L_p}^2 (e_{33}^2 + c_{33}^E \varepsilon_{33}^S)\cos(k_p L_p) - {e_{33}}^2 \sin(k_p L_p)} \tag{2.42}$$

$$\underline{y}_{22}(\Omega) = \frac{j\Omega L_p \varepsilon_{33}^S \sin(k_p L_p)}{A_p k_p {L_p}^2 (e_{33}^2 + c_{33}^E \varepsilon_{33}^S)\cos(k_p L_p) - A_p {e_{33}}^2 \sin(k_p L_p)} \tag{2.43}$$

Obviously, the analytical model makes the "black box" in the nonparametric model clear and into a "white box". In the present case a four-pole network element was obtained. For more general boundary conditions, piezoelectric actuators can also be considered as a six-pole network element. This will be discussed further in chapter 4.

Using the expression of the short-circuit input admittance $\underline{y}_{11}$ shown in equation (2.41) the series and parallel resonant frequencies of the piezoelectric actuator fixed at one side and free at the other side can be calculated. According to the definitions described in section 2.3.1, the series resonance frequency is the frequency at which the admittance $\underline{y}_{11}$ becomes infinite if the energy losses in the piezoelectric material are neglected. This can be achieved when the denominator of the expression of $\underline{y}_{11}$ is equal to zero. Therefore, the series resonant frequency can be determined by solving the characteristic equation

$$k_p {L_p}^2 (e_{33}^2 + c_{33}^E \varepsilon_{33}^S)\cos(k_p L_p) - {e_{33}}^2 \sin(k_p L_p) = 0 \tag{2.44}$$

Similarly, the parallel resonant frequency can be obtained by solving the equation

$$\cos\left(\frac{\Omega L_p}{c_p}\right) = 0 \tag{2.45}$$

As continuum models are based on material data and geometrical parameters, they can generally be used already in the design process for the formulation of optimization problems of piezoelectric actuators.

2.3.3 Finite Element Method

The finite element method (FEM) is an approximation of the continuum models that is particularly well suited to computation. Generally it is applied in the computation of the vibration behavior of piezoelectric actuators with complex geometry and boundary conditions. In the FEM, the continuous structure of the piezoelectric actuator is discretized into a number of finite elements. Besides the mechanical degrees of freedom u_i (translation and rotation displacements), an electrical degree of freedom φ_i (electrical potential) is added at each node. The FEM solution vector consists of the displacement values u_i and electric potential values φ_i at the nodes i. The displacement and voltage fields at arbitrary locations within the element are assumed as a linear combination of the nodal values of these fields, respectively. The coupled electromechanical field is described by means of the linear piezoelectric constitutive equations. The analysis then proceeds to writing a set of differential equations of motion and Maxwell's equations [Ler90] and [Abb98]. For the nodes of finite elements a coupled equation system can be obtained as follows [Ans01] and [HKL98]:

$$\begin{bmatrix} \mathbf{M}_p & 0 \\ 0 & 0 \end{bmatrix} \cdot \begin{bmatrix} \ddot{u} \\ \ddot{\varphi} \end{bmatrix} + \begin{bmatrix} \mathbf{K}_{uu} & \mathbf{K}_{u\varphi} \\ \mathbf{K}_{\varphi u} & \mathbf{K}_{\varphi\varphi} \end{bmatrix} \cdot \begin{bmatrix} u \\ \varphi \end{bmatrix} = \begin{bmatrix} F \\ Q \end{bmatrix} \tag{2.46}$$

where $\mathbf{M}_p$, $\mathbf{K}_{uu}$, $\mathbf{K}_{\varphi\varphi}$, $\mathbf{K}_{u\varphi}$ ($\mathbf{K}_{\varphi u}$) are the mass, stiffness, dielectric and piezoelectric matrices, respectively. F and Q are the nodal mechanical force and nodal electrical charge vectors, respectively. In the case of damped systems, a proportional damping, i.e., a damping matrix, which can be expressed as a linear combination of the mass and stiffness matrixes, is generally added [Gen95].

Considering time harmonic excitation the above system of equations can be transformed into an algebraic equation system:

$$\begin{bmatrix} \mathbf{K}_{\mathbf{uu}} - \Omega^2 \mathbf{M}_p & \mathbf{K}_{u\varphi} \\ \mathbf{K}_{\varphi u} & \mathbf{K}_{\varphi\varphi} \end{bmatrix} \cdot \begin{bmatrix} \underline{\hat{u}} \\ \underline{\hat{\varphi}} \end{bmatrix} = \begin{bmatrix} \underline{\hat{F}} \\ \underline{\hat{Q}} \end{bmatrix} \tag{2.47}$$

where $\underline{\hat{u}}$, $\underline{\hat{\varphi}}$, $\underline{\hat{F}}$ and $\underline{\hat{Q}}$ are complex amplitudes. The displacement field and electrical field can be first obtained by solving this algebraic equation system taking into account boundary conditions. The eigenfrequencies and eigenfuctions can be obtained by solving eigenvalue problems [WH00] and [SK99]. The time of numerical calculation will rise remarkably if damping is considered in the FEM model. For more details concerning FEM applied to piezoelectric actuators, refer to [Hem01], [HKL98], [Ans01] and [Abb98].

If optimization problems are formulated by means of the FEM, the number of the variables is usually very large. The cost of numerical computation in the FEM is notably higher than the cost in continuum models. Therefore, the FEM is not well suited for optimization problems occurring in the early design stages where the optimal results usually need to be obtained in short time and without high costs. The FEM, however, is usually used when the accurate geometrical details of the actuator need to be specified.

2.3.4 Lumped Parameter Models

The dynamic behavior of a linear system subjected to a harmonic excitation can usually be described accurately by superposing only a few of the normal modes. Each normal mode dominates the vibration behavior of the system in the range of the respective eignenfrequency. Therefore, if the system is driven in the range of one of its eigenfrequencies, its behavior can be described with reasonable accuracy by a model with only one degree of freedom.

Based on electro-mechanical analogies the vibration behavior of a piezoelectric actuator operating in the vicinity of one of it's eigenfrequencies can be described by an equivalent mechanical or electrical model as shown in Fig. 2.8 [Len75], [Wal00] and [Hem01]. In these models *m*, *c,* and *d* are modal mass, modal stiffness and modal damping, respectively. *C* and *R* are electric capacitance and electric resistance. α is the electromechanical transformation factor that describes the transmission ratio of electrical and mechanical quantities. *U* and *Q* are input voltage and charge, *u* and *F* are modal displacement and mechanical load.

According to these models, the dynamics of the system can be described by

$$m\ddot{\underline{u}} + d\dot{\underline{u}} + c\underline{u} = \alpha\underline{U} + \underline{F} \tag{2.48}$$

$$\frac{1}{C}\left(\underline{Q} - \alpha\underline{u}\right) + R\left(\dot{\underline{Q}} - \alpha\dot{\underline{u}}\right) = \underline{U} \tag{2.49}$$

The conductance matrix for oscillations with harmonic excitation $\underline{U}(t) = \hat{\underline{U}} \cdot e^{j\Omega t}$ can be obtained as

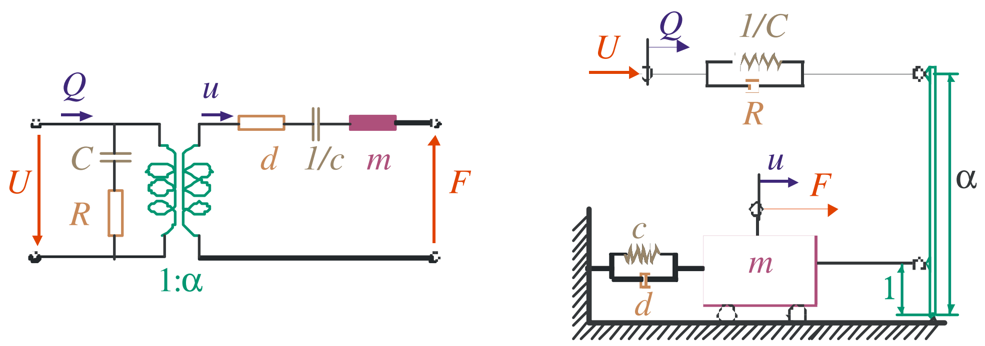

a) b)

Fig. 2.8 Equivalent models for a piezoelectric actuator

$$\begin{bmatrix} \underline{\hat{I}} \\ \underline{\hat{v}} \end{bmatrix} = j\Omega \begin{bmatrix} \dfrac{1}{jR\Omega + \dfrac{1}{C}} + \dfrac{\alpha^2}{-m\Omega^2 + jd\Omega + c} & \dfrac{\alpha}{-m\Omega^2 + jd\Omega + c} \\ \dfrac{\alpha}{-m\Omega^2 + jd\Omega + c} & \dfrac{1}{-m\Omega^2 + jd\Omega + c} \end{bmatrix} \begin{bmatrix} \underline{\hat{U}} \\ \underline{\hat{F}} \end{bmatrix} \tag{2.50}$$

where $\underline{\hat{I}} = j\Omega\underline{\hat{Q}}$ and $\underline{\hat{v}} = j\Omega\underline{\hat{u}}$.

In particular the following admittance functions can be obtained:

$$\underline{y}_{11} = \frac{\underline{\hat{I}}}{\underline{\hat{U}}} = \frac{j\Omega}{jR\Omega + \dfrac{1}{C}} + \frac{j\Omega\alpha^2}{-m\Omega^2 + jd\Omega + c} \tag{2.51}$$

$$\underline{y}_{21} = \frac{\underline{\hat{v}}}{\underline{\hat{U}}} = \frac{j\Omega\alpha}{-m\Omega^2 + jd\Omega + c} \tag{2.52}$$

The frequency responses of the above admittance functions can be described by the Bode plot similar to Fig. 2.5 as well as the Nyquist plot similar to Fig. 2.6. Fig. 2.9 shows the Nyquist plot of the $\underline{y}_{11}$ given by equation (2.51) in the case of R=0. As described in section 2.3.1 there exist three pairs of characteristic frequencies: ω_s and ω_p, ω_m and ω_n as well as ω_r and ω_a , which are approximately equal for a piezoelectric actuator with a piezoelectric quality number $M >> 2$.

These frequencies can be derived from the expressions shown in (2.51) as follows:

- The series resonant frequency $$\omega_s = \sqrt{\frac{c}{m}} \tag{2.53}$$

  The parallel resonant frequency $$\omega_p = \sqrt{\frac{c + \dfrac{\alpha^2}{C}}{m}} \tag{2.54}$$

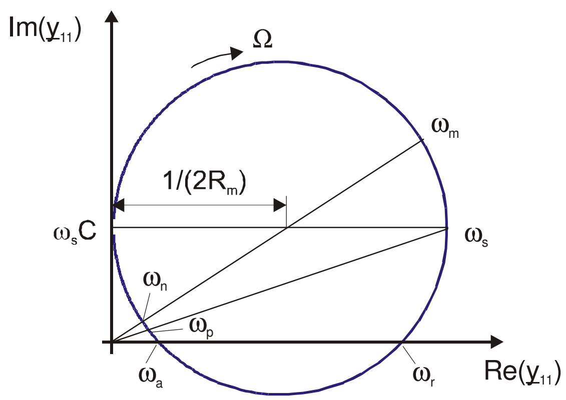

Fig. 2.9 The frequency response of the admittance $\underline{y}_{11}$ in the complex plane

- The maximum admittance frequency ω_m for $|\underline{y}_{11}|_{\max}$

  The minimum admittance frequency ω_n for $|\underline{y}_{11}|_{\min}$

- The resonance frequency ω_r for $\mathrm{Im}(\underline{y}_{11}) = 0$

  The antiresonance frequency ω_a for $\mathrm{Im}(\underline{y}_{11}) = 0$

Several performance criteria of piezoelectric actuators can be readily expressed by means of model parameters of the equivalent model. According to equation (2.52) the ratio between the amplitude of the modal displacement $\underline{\hat{u}}$ at the resonance frequency ω_s and its static counterpart can be calculated. This ratio represents the mechanical quality factor Q_m. It can be expressed as

$$Q_m = \frac{\sqrt{cm}}{d} = \frac{c}{\omega_s d} \tag{2.55}$$

The equivalent models can be reduced by transforming mechanical quantities into the electrical side of the models using the transformation factor α. Fig. 2.10 shows the reduced equivalent electrical model, where R_m, C_m and L_m are the mechanical resistance, capacitance and inductance respectively. They are as follows:

$$R_m = \frac{d}{\alpha^2},\; C_m = \frac{\alpha^2}{c},\; L_m = \frac{m}{\alpha^2} \tag{2.56}$$

Then the admittance corresponding to the mechanical characteristic of the actuator is

$$Y_m = 1\Big/\left(R_m + \frac{1}{j\Omega C_m} + j\Omega L_m\right) \tag{2.57}$$

In general, the value of R representing the electric loss (mainly dielectric loss) of the piezoelectric material is small and can be neglected [Uch04]. In the case of $R = 0$, the admittance corresponding to the electrical characteristic of the actuator is

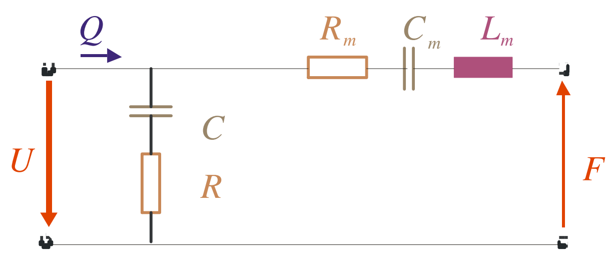

Fig. 2.10 The reduced equivalent electrical model

$$Y_e = j\Omega C \tag{2.58}$$

Therefore the admittance function $\underline{y}_{11}$ is given by:

$$\underline{y}_{11} = Y_e + Y_m \tag{2.59}$$

The ratio between the magnitudes of the Y_m and Y_e at the resonance frequency ($\Omega = \omega_s = \sqrt{c/m}$) defines a piezoelectric quality number

$$M = \frac{|Y_m|}{|Y_e|}_{at\ \Omega=\omega_s} = \frac{1/R_m}{\omega_s C} = \frac{\alpha^2}{\omega_s dC} = Q_m \frac{C_m}{C} \tag{2.60}$$

The piezoelectric quality number is an important performance parameter. It presents the extent of the phase rise or phase drop of the admittance functions and is appropriate to classifying piezoelectric actuators concerning electrical behaviors. Fig. 2.11 and Fig. 2.12 show the Bode plot and the Nyquist plot of the admittance function $\underline{y}_{11}$ for three groups of special values of M (here the electric loss R is neglected), respectively. It is noted that $M = 2$ is a critical value, at which the 0°-line is tangential to the phase-frequency plot of the $\underline{y}_{11}$ (see Fig. 2.11) and the real axis is tangent to the Nyquist plot (see Fig. 2.12). When $M > 2$ the 0°-line intersects the phase-frequency plot and the real axis intersects the Nyquist plot correspondingly. When $M<2$, the intersections do not exist any more. The values of M will affect the design of the power electric device for driving the piezoelectric actuator. This will be further discussed in Chapter 4.

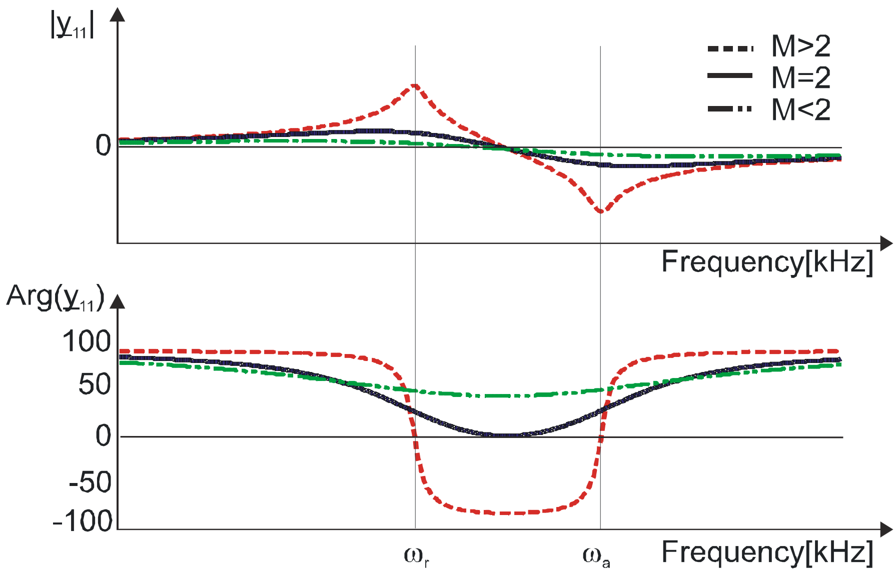

Fig. 2.11 $\underline{y}_{11}$ as a function of the frequency for three groups of the quality number M

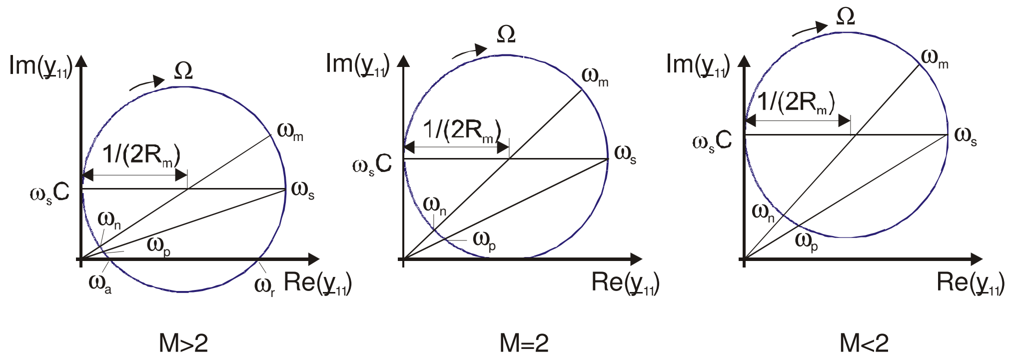

Fig. 2.12 $\underline{y}_{11}$ *as a function of the frequency in the complex plane for three groups of the quality number M*

The above lumped parameter models can well describe the vibration behavior of the piezoelectric actuator operating in the vicinity of one of it's resonant frequencies. Fig. 2.13 shows comparisons of measured and calculated admittance frequency responses for a piezoelectric actuator. As shown in the figure, the calculated results from the expressions (2.51) and (2.52) do agree with experimental results quite well. Generally, the values of model parameters can be estimated by experiments [Fu04]. They can also be obtained by the analytical calculation or FEM. Therefore, the equivalent model can be considered as a "gray box" model of the piezoelectric actuator. The advantage of equivalent models is that the dynamic behavior of the actuator can be described by simple algebraic equations and it is convenient to formulate the performance criteria of actuators.

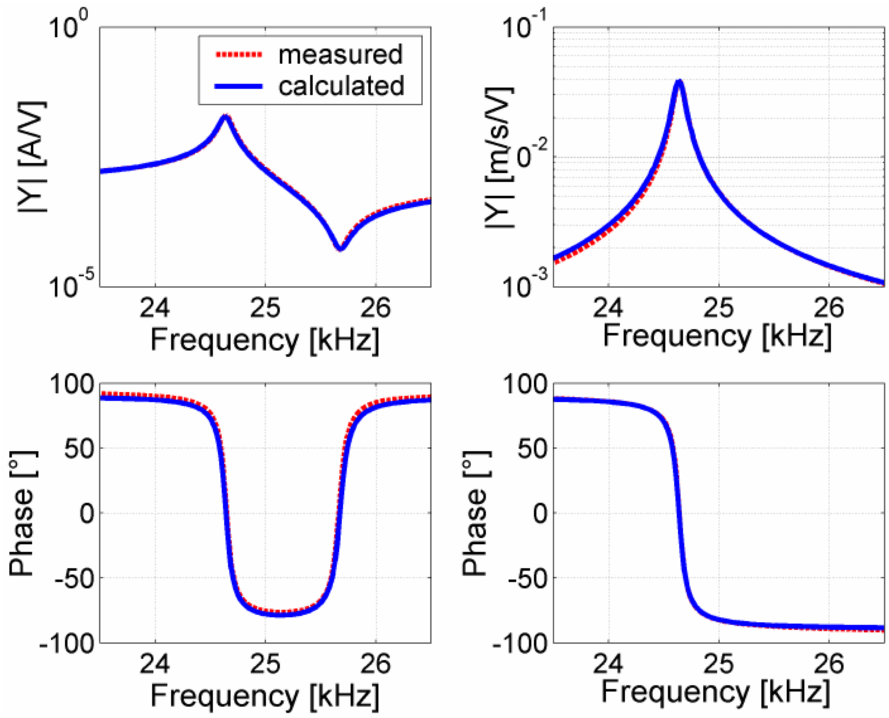

Fig. 2.13 Comparisons of the frequency responses $\underline{y}_{11}$ *and* $\underline{y}_{21}$ *measured and calculated from lumped parameter models*

2.4 Typical Design Goals

Piezoelectric actuators have been widely used in different fields. For different applications there exist different design goals. It is very difficult to describe all design goals for all application fields. In this section, only typical design goals of piezoelectric actuators for one stroke driving and resonant driving will be discussed.

2.4.1 One Stroke Driving

The piezoelectric actuators for one stroke driving generally operate well below the fundamental resonance frequency. They may be divided into two classes. One is usually used in precision instrumentation, which requires precise but minute motion (<10μm), where the positioning precision is a typical design goal and only small forces are required. The other one, which often has displacement amplifying mechanisms, is used in the fields, where large stroke (>200μm) is needed at large forces, like e.g. the control of helicopter rotors [DLL00]. Here the maximum stroke or maximum magnification factor is a typical design goal while the accuracy is of minor interest. For piezoelectric actuators used for one stroke driving, the typical design goals can be concluded as follows

- large stroke per unit of length
- positioning with high precision
- fast response time
- large mechanical energy density
- low power consumption
- compact size

2.4.2 Resonant Driving

The most widely used piezoelectric actuators for resonant driving are piezoelectric transducers and ultrasonic motors. Piezoelectric transducers are extensively used in acoustic wave generation devices such as power ultrasonic transducers used in industrial machining, welding, etc. [Lit03]. For these applications the typical design goals are

- specified mechanical resonance frequency
- sufficient frequency separation between the primary and all secondary (undesired) resonance frequencies
- high efficiency, low energy loss
- compact size
- low cost

In [Hem01] typical design goals for a piezoelectric linear motor were summarized. Different design requirements for the vibrator, contact and rotor were proposed.

Most of the piezoelectric transducers used in ultrasonic machining and bonding has a sandwich construction. They are known as Langevin transducers. In chapter 4, the practical design goals for the special piezoelectric transducers will be further discussed.

2.5 State of the Art of Optimization of Piezoelectric Actuators

The performance of piezoelectric actuators can usually be remarkably improved, if mathematical optimization methods are applied in their development. According to the different applications, there exist various optimization problems. As piezoelectric actuators couple the electric and mechanical quantities, their optimization characterizes multidisciplinary optimization problems. In recent decades, a number of optimization problems of piezoelectric actuators have been studied. Some optimization algorithms have been used successfully. In this section, the state of the art of optimization of piezoelectric actuators is briefly reviewed. The review will mainly concentrate on the formulation of optimization problems and the applied optimization methods.

A large number of studies have been carried out into optimization problems of piezoelectric actuators in intelligent structures. An intelligent structure is the structure that can actively sense and react to its environment via onboard sensors, actuators and computational/control capabilities [SC93]. Such a structure provides an efficient method to implement various tasks such as active control, shape control and health monitoring, see e.g. [CL87], [Cra94], [LOM00], [CTS02] and [Pre02]. Among the various available materials for actuators of intelligent structures, piezoelectric materials are excellent since they are light weight and can be easily incorporated into a structure by surface bonding or embedding. They produce only less significant inertial loads [CSe94]. It is important to determine optimal dimension, placement and controls of piezoelectric actuators in the intelligent structure in order to improve the performances. Current applications of intelligent structures are mainly in the field of the active vibration control of aerospace structures, which often do not possess sufficient passive damping to reduce severe vibration often resulting from a minor disturbance force. In [SC93], [CS94] and [CSJ99] the optimum designs of intelligent structures for the active vibration control have been studied. These problems are mixed continuous-discrete optimization problems. There exist continuous and discrete design variables. The continuous design variables include dimensions and control gains of piezoelectric actuators. The location of piezoelectric actuators is the discrete design variable. Design criteria included the energy dissipated by the piezoelectric actuators, electric power requirements, vibration reduction and the fundamental frequency. Constraints were placed on total energy, input voltage, displacements and mass. The multiple design objectives and constraints were usually combined into a single unconstrained function which was then minimized. A simulated annealing approach was used for the discrete search. A deterministic gradient-based search was used for the continuous search. Gradients of the continuous design variables were computed by a finite-difference technique. In these works, however, the conflicts between objectives were not analyzed and Pareto-optimal solutions were not discussed. In [SWW93], [HL99] and [ZLG00] genetic algorithms have been used to find the optimal placement of piezoelectric actuators and sensors for active vibration control of a plate. The results showed that genetic algorithms are effective optimization tools. But multiobjective optimization was not mentioned in these studies. Besides the works described above, there are many publications about optimization of actuators and sensors for active control, see e.g. [HM03], [YV96] and [BMF00]. Active control using piezoelectric actuators has been the subject of attraction.

Topology optimization of piezoelectric actuators is another subject widely studied. The purpose of topology optimization is to find the optimal layout of a structure in a specified domain, i.e., the optimal distribution of the material and void phases in the design domain, in order to minimize (maximize) defined objective functions or achieve specified properties [BS03]. Topology optimization comprises several steps. First, the geometry of the design domain, boundary conditions and loading are prescribed. Second, the design domain is discretized by finite elements, and each element is assigned a design variable, which determines the absence or the presence of material at the particular location. Third, the finite-element analysis and sensitivity analysis are used to give the function value and the first-order sensitivity (gradient) of the objective and constraint. After that, the optimization algorithm is used to solve the optimization problem. Finally, the optimum topology is interpreted and refined. In the literature, there are two classes of methods to solve the topology optimization problem. One class is to solve the topology optimization problem directly as an integer 0-1 problem [Bec99] and [BS03]. The more effective method to solve this problem is to relax the design domain, i.e., to replace the integer variables with continuous variables. A material model that relates the material properties such as the elastic modulus in each point of the domain to some design variable must be defined, and this model must allow materials with intermediate properties and not only zero or full material [SNF98]. The relaxation can be realized by two approaches, namely the homogenization method and the SIMP method (Solid Isotropic Material with Penalization), see [BK88] and [BS03]. In the former the concept of perforated microstructure is introduced. The problem is posed as optimizing the material distribution in a perforated structure with infinite microscale voids. The size of each microvoid is the design variable. In the latter material properties are assumed constant within each element and the relative density of each element is the design variable. After relaxation the mathematical programming techniques with continuous design variables can be used to solve the optimization problem. The optimum result is a material distribution over mesh with some intermediate values of density ("gray scale") that represent the presence of intermediate materials (composite), which are difficult to fabricate in practice. They can be eliminated by using some form of penalty in the optimization procedure, see [BS03], or by applying the image-based technique (IBT), see [SNK00]. Topology optimization methods have been applied to design amplifying mechanisms (also termed mechanical amplifiers) of the displacement of piezoelectric actuators, see e.g. [LDG00], [DLL00], [SNK00], [CF00] and [BhF02]. Various formulations can be posed to obtain the optimum topology of the amplifying mechanisms. In [Sig97] an inverting displacement amplifier using the formulation of maximum mechanical advantage, namely the ratio of output force and input force, for static response was investigated. In [LDG00] and [DLL00] three formulations for the maximum output stroke, magnification factor and mechanical efficiency respectively were used for both static and dynamic operations. The design problem was solved as a 2D material distribution problem using Method of Moving Asymptotes (MMA). In [SNF98] and [SNK00] a flextensional actuator was designed for simultaneously maximizing mean transduction and mean stiffness. A multiobjective function was defined as the weighted sum of these two objectives. In [SK99] a topology optimization method was proposed for design piezoelectric transducers. The problem is posed as an eigenvalue optimization problem in structural optimization. Three multiobjective functions were defined. The first one consists of the maximization of the eletromechanical coupling factor for a specific mode or set of modes. The second one is related to the design of a transducer with specified resonance frequencies. The third one is related to the design of narrowband or broadband transducers. The sequential linear programming (SLP) was used to obtain the optimized solution. However, Pareto optima were not discussed. Topology optimization requires efficient and reliable large-scale nonlinear optimization algorithms, because a fine mesh is required and a large number of design variables are included in the problem. Usually, dual methods such as Method of Moving Asymptotes (MMA) are more efficient than primal methods such as sequential linear programming (SLP) and sequential quadratic programming (SQP) [DLL00]. Although the topology of the structure obtained by using topology optimization methods is generally difficult to manufacture, the topology optimization technique is one rational systematic design methodology for the structural design if the physical size and the shape and connectivity of the structure are unknown.

Some researchers have studied optimization problems concerning ultrasonic motors, transducers and piezoelectric transformers. In [PRF03] the optimization of the geometrical and material parameters defining the motor stator was studied, based on a parametric model of a traveling wave ultrasonic motor including stator, rotor and a simplified rotor-stator interface model. Three performance indicators, namely the piezoelectric coupling coefficient, the efficiency and the output power were used as objective functions. However, in this work the optimization process was based on single variable and no mathematical optimization algorithms were applied. In [Hem01] high efficiency, high shear force and velocity, small size and low cost were postulated as optimization goals for a novel piezoelectric linear motor. For each goal the corresponding design requirements for the oscillator, the contact, the rotor and the drive were introduced. No mathematical optimization methods were used in this work. In [JNL00] the optimization of the velocity of a piezoelectric ceramic actuator was performed, with driving voltage and system parameters being design variables. The Sequential Quadratic Programming (SQP) method was used. Each variable was explored individually. No optimization was performed for multivariable. The optimization of a piezoelectric transformer for maximum power transfer was studied in [HLH03], but no optimization algorithm was mentioned in this work. In [Lit03] the optimization of a power ultrasonic transducer based on an equivalent model was investigated. The optimization objectives, namely the vibration amplitude and efficiency were analyzed. However, no mathematical optimization methods were applied in this work.

Although a number of studies concerning optimization of piezoelectric actuators have been reported in the above reviewed literature, there is a necessity for further investigations, because an important class of optimization methods, namely multiobjective optimization methods (in particular MOEAs) have hardly been applied in the systematic design of piezoelectric actuators. Multiobjective optimization of piezoelectric actuators involving continuous and discrete design variables is scarcely reported. There is a need to present an integrated procedure for the piezoelectric transducer design via multiobjective optimization methods. This is concerned with the modeling, the problem formulation, the application of optimization algorithms and the selection of optimum results. In the next sections of this dissertation, the above mentioned several aspects will be discussed.

3 Multiobjective Optimization Methods

In Chapter 2 the modeling of the piezoelectric actuators has been introduced. The models of the actuators provide the base for formulating the multiobjective optimization problems (MOPs) for piezoelectric actuators. On the other hand, in order to solve MOPs, an appropriate optimization method is needed. Many multiobjective optimization methods have been developed over the past decades. A comprehensive summary of some of these methods can be found in [Mie99], [Deb02] etc. In this chapter, the multiobjective optimization methods which are most commonly used in engineering will be described. The study concentrates on those methods which will be used in the next chapter for solving the MOPs of piezoelectric actuators. The structure of this chapter is as follows: First, the basic concepts of multiobjective optimizations are described. Then basic multiobjective optimization methods are introduced. Finally, as the main part of this chapter, the most commonly used multiobjective evolution algorithms (MOEAs) will be studied.

3.1 Basic Concepts of Multiobjective Optimization

The MOP is an extension of the single-objective (scalar) optimization problem. In the MOP, a number of objective functions are to be optimized simultaneously. Losing no generality, a MOP can be stated as follows:

$$\min f_v(\mathbf{x}) \quad v=1,2,...,m \tag{3.1}$$

$$\begin{aligned} \text{subject to } \; & g_j(\mathbf{x})\geq 0, \quad j=1,2,...,J \\ & h_k(\mathbf{x})=0, \quad k=1,2,...,K \\ & x_i^l \leq x_i \leq x_i^u, \quad i=1,2,...,n \end{aligned}$$

where $\mathbf{x}\in R^n$ is a vector of n decision variables (design variables), which describe a solution. The side constraints $x_i^l \leq x_i \leq x_i^u$, the inequality constraints $g_j(\mathbf{x})\geq 0$ and the equality constraints $h_k(\mathbf{x})=0$ define a feasible region G in the decision variable space R^n. For each solution $\mathbf{x}$ in the feasible region G exists a point (objective vector) in the objective space R^m, denoted by $\mathbf{F}(\mathbf{x})\in R^m$, where $\mathbf{F}(\mathbf{x})=\mathbf{z}=(z_1,z_2,...,z_m)^T$, $z_v=f_v(\mathbf{x})$ for all $v=1,2,...,m$. The set of these objective vectors is called the feasible objective region Z. Fig. 3.1 represents the mapping from decision variable space into objective function space for a two-dimensional case. As a vector of objectives, instead of a single objective, is optimized, multiobjective optimization is also called vector optimization.

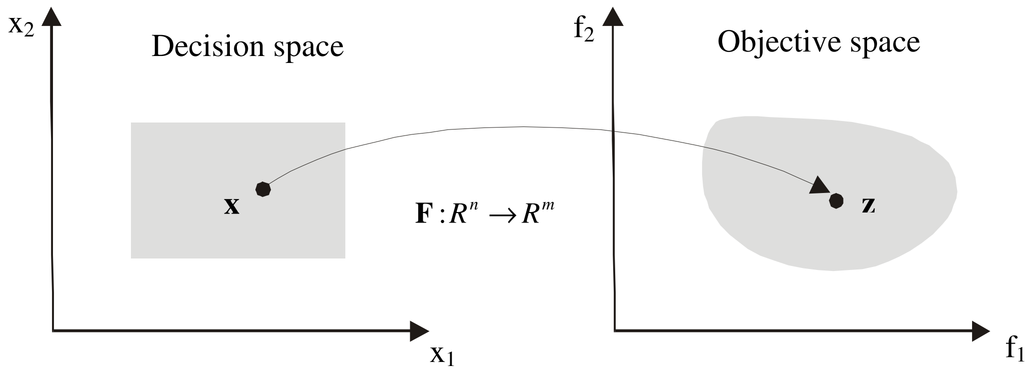

Fig. 3.1 Mapping from decision space into objective space

In the single-objective optimization, one can find a solution, which is absolutely best with respect to all other alternatives. In the MOP, because of incommensurability and conflict among objectives, it is not always possible to find a solution at which each objective function gets its optimal value simultaneously. The solutions of a MOP are therefore given in the non-dominance or Pareto optimality sense. For such solutions, no improvement in any objective function is possible without deterioration to at least one of the other objective functions. A more formal definition of non-dominance and Pareto optimality is as follows [Mie99] and [Deb02]:

Definition 3.1: A solution $\mathbf{x}^{(1)}$ is said to dominate the other solution $\mathbf{x}^{(2)}$ if $f_i(\mathbf{x}^{(1)}) \leq f_i(\mathbf{x}^{(2)})$ for all $i = 1,...,m$ and $f_j(\mathbf{x}^{(1)}) < f_j(\mathbf{x}^{(2)})$ for at least one index *j*.

If solution $\mathbf{x}^{(1)}$ dominates solution $\mathbf{x}^{(2)}$, the following terms are also commonly used:

- Solution $\mathbf{x}^{(1)}$ is non-dominated by solution $\mathbf{x}^{(2)}$
- Solution $\mathbf{x}^{(2)}$ is dominated by solution $\mathbf{x}^{(1)}$
- Solution $\mathbf{x}^{(1)}$ is non-inferior to solution $\mathbf{x}^{(2)}$

Definition 3.2: A decision vector $\hat{\mathbf{x}}$ is non-dominated with respect to a set *P* if it is not dominated by any other member of the set *P*. An objective vector $\hat{\mathbf{z}}$ is non-dominated if its image point in the set *P* is non-dominated.

The set of non-dominated solutions is called the non-dominated set and the set of non-dominated solutions in the objective space is called non-dominated front.

If the non-dominance concept is extended to the entire feasible space *G*, the Pareto-optimality can be defined as follows:

Definition 3.3: A decision vector $\hat{\mathbf{x}} \in G$ is Pareto-optimal if there does not exist another decision vector $\mathbf{x} \in G$ such that $f_i(\mathbf{x}) \leq f_i(\hat{\mathbf{x}})$ for all $i = 1,...,m$ and $f_j(\mathbf{x}) < f_j(\hat{\mathbf{x}})$ for at least one index *j*. An objective vector $\hat{\mathbf{z}} \in Z$ is Pareto-optimal if its image point in the set *G* is Pareto-optimal.

The set of Pareto-optimal solutions is called Pareto-optimal set and the set of Pareto-optimal solutions in the objective space is called Pareto-optimal front. Because of $G \supseteq P$, obviously a Pareto-optimal set is always a non-dominated set.

Fig. 3.2 shows the non-dominated and Pareto-optimal solutions in the objective space for a two-objective minimization problem. The fat line represents the Pareto front. Points A and B represent two Pareto-optimal points of the front. Although points C and D are non-dominated with respect to each other locally, they are not Pareto-optimal with respect to entire feasible region *Z*, because clearly point B dominates points C and D and point A dominates point C. Therefore, the non-dominated set is Pareto-optimal set if only if it is a non-dominated set with respect to the entire feasible space *Z*.

In many multi-objective optimization algorithms, Pareto-optimal solutions are usually found based on non-domination concept. Many approaches have been suggested for finding the non-dominated set of solutions from a given set of solutions. In [Deb02] three approaches (Naïve and Slow, Continuously Updated and Efficient Methods) have been described in detail.

3.2 Traditional Multiobjective Optimization Methods

Basically, there are three kinds of methods for handling MOPs: (1) generating approaches; (2) preference-based approaches (3) interactive methods [Coh85] and [Mie99]. In the generating methods, the entire set of Pareto optimal solutions is identified first, and then the best compromise solution is chosen from the obtained set by using higher-level information. No prior knowledge of preference structure over objectives is used. On the other hand, preference-based approaches require decision makers to give their preferences in a formal and structured way and then a composite single objective function is constructed. In interactive methods, the decision maker works with an interactive computer program and progressively provides preference information during the optimization process. The generating method is more practical and less subjective, while the preference-based method is more subjective and not straightforward. Interactive methods can be presumed to produce the most satisfactory results.

Most traditional methods convert the MOP into a single (scalar) or a family of single objective optimization problems by using some user-defined preference structures, and then solve the problem using the widely developed methods for single objective optimization. In the following, some most commonly used methods will be introduced. Details can be found in [Mie99], [GCh00] and [Deb02].

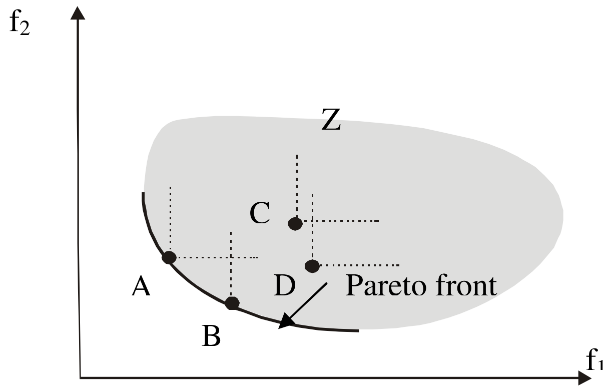

Fig. 3.2 Pareto-optimal solutions

3.2.1 Weighted Sum Method

The weighted sum method scalarizes a set of objectives into a single objective by assigning weights to each objective function. This method is the simplest and the most widely used method. It can be formulated as follows:

$$\min \quad F(\mathbf{x}) = \sum_{v=1}^{m} w_v f_v(\mathbf{x}) \tag{3.2}$$

$$\text{subject to} \quad g_j(\mathbf{x}) \geq 0, \qquad j = 1,2,\ldots,J$$
$$h_k(\mathbf{x}) = 0, \qquad k = 1,2,\ldots,K$$
$$x_i^l \leq x_i \leq x_i^u, \quad i = 1,2,\ldots,n$$

The weight w_v represents the relative importance of the objective and usually $\sum_{v=1}^{m} w_v = 1$. If all the weights are positive the optimal solution to the problem is Pareto optimal for the initial MOP. By choosing more than one set of positive weights other optimal solutions can be generated. If $F(\mathbf{x})$ is convex then all the optimal solutions of $F(\mathbf{x})$ are Pareto-optimal solutions. However, if $F(\mathbf{x})$ is non-convex certain Pareto-optimal solutions cannot be found. This can be illustrated geometrically. Consider the two-objective case in Fig. 3.3 (a). In the objective function space a straight line L1: $\sum_{v=1}^{2} w_v f_v(\mathbf{x}) = F_1$ is drawn. The minimization of equation (3.2) can be interpreted as finding the value of F_1 for which the line L1 is tangential to the boundary of objective space Z and lies in the bottom-left corner of the objective space Z. If different weight vector is selected, then the different slope of the straight line L1 is defined. This leads to the different optimal solution point where the line L1 is tangential to the boundary of objective space Z. However, when the lower boundary of the search space Z is non-convex, the Pareto-optimal solutions between A and B is not available, see Fig. 3.3 (b).

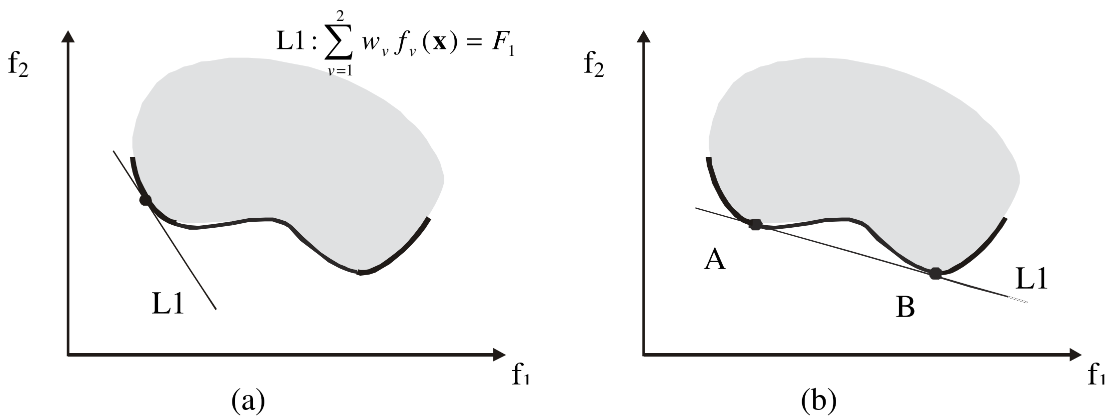

Fig. 3.3 The weighted sum method for (a) convex (b) non-convex part of objective functions

3.2.2 ε-Constraint Method

ε-Constraint method can overcome some of the convexity problems of the weighted sum method. In this method the MOP is reformulated by just keeping one of the objectives and transfer the others into constraints. This approach is able to identify a number of Pareto-optimal solutions on a non-convex boundary. It is formulated as

$$\min \; f_q(\mathbf{x}) \tag{3.3}$$

$$\begin{aligned} \text{subject to} \quad & f_v(\mathbf{x}) \le \varepsilon_v \qquad v = 1,2,\dots,m \quad m \ne q \\ & g_j(\mathbf{x}) \ge 0, \qquad j = 1,2,\dots,J \\ & h_k(\mathbf{x}) = 0, \qquad k = 1,2,\dots,K \\ & x_i^l \le x_i \le x_i^u, \quad i = 1,2,\dots,n \end{aligned}$$

3.2.3 Weighted metric methods

The weighted metric method (or compromise method) identifies solutions closest to the ideal point $\mathbf{z}^*$. The ideal point (objective vector) $\mathbf{z}^*$ is defined as $\mathbf{z}^* = \mathbf{F}^* = \left(f_1^*, f_2^*, \dots, f_m^*\right)^T$, where $f_v^*, v = 1,2,\dots,m$ is the minimum value for the *v*-th objective function individually. For the conflicting objectives the ideal point is not attainable because the conflicting objective functions are impossible to be minimized simultaneously. However, it is obvious the closer to the ideal point the solutions are, the better the solutions. Therefore the ideal point is usually used as a reference point. For a point $\mathbf{z} \in Z$ the distance from $\mathbf{z}$ to the $\mathbf{z}^*$ may be approximated by a L_p-norm as follows

$$L_p(\mathbf{z}) = \left\| \mathbf{z} - \mathbf{z}^* \right\|_p = \left[\sum_{v=1}^{m} \left| z_v - z_v^* \right|^p \right]^{1/p} \tag{3.4}$$

where $p \in [1,\infty]$. If different degrees of importance for objectives are considered, a weight vector $\mathbf{w} = (w_1, w_2, ..., w_m)$ is used. Therefore, for non-negative weights, the weighted L_p-norm is as follows

$$L_{p,w}(\mathbf{x}) = \left[\sum_{v=1}^{m} w_v \left| f_v(\mathbf{x}) - z_v^* \right|^p \right]^{1/p} \tag{3.5}$$

where $\mathbf{x} \in G$. The MOP is then transferred to a problem of minimizing the weighted L_p – norm. The parameter p will affect the optimal results. When p=1 the resulting method is equal to the weighted sum method. When $p = \infty$ the problem reduces to weighted Tchebycheff problem:

$$\min \quad L_{\infty,w}(\mathbf{x}) = \max \left\{ w_v \left| f_v(\mathbf{x}) - z_v^* \right|, \; v = 1,2,...,m \right\} \tag{3.6}$$

$$\begin{aligned} \text{subject to} \quad & g_j(\mathbf{x}) \geq 0, \quad j = 1,2,...,J \\ & h_k(\mathbf{x}) = 0, \quad k = 1,2,...,K \\ & x_i^l \leq x_i \leq x_i^u, \quad i = 1,2,...,n \end{aligned}$$

The parameter p will affect the optimal results. With $p = 1 \text{or} \, 2$, not all Pareto optimal solutions can be obtained. Although the weighted Tchebycheff method can find any Pareto-optimal solution, as p increases the problem becomes complex.

3.2.4 Value Function Method

In the value function (or utility function) method, a preference structure is mathematically represented using a value function $U : R^q \to R$, which maps solutions in the objective space into a real number so that the greater the number, the more preferred the solution in the objective space. The problem is then as follows:

$$\max U(\mathbf{F(x)}) \tag{3.7}$$

$$\begin{aligned} \text{subject to} \quad & g_j(\mathbf{x}) \geq 0, \quad j = 1,2,...,J \\ & h_k(\mathbf{x}) = 0, \quad k = 1,2,...,K \\ & x_i^l \leq x_i \leq x_i^u, \quad i = 1,2,...,n \end{aligned}$$

where $\mathbf{F(x)} = \left(f_1(\mathbf{x}), ..., f_q(\mathbf{x}) \right)^T$. The solution to the problem entirely depends on the chosen value function. Because of the difficulty in obtaining value function, this method is limited for solving MOPs.

In addition to the above described methods, there are many interactive methods and other conventional multi-objective optimization methods like e.g. NIMBUS (Nondifferentiable Interactive Multiobjective BUndle-based optimization System). A detailed discussion on these approaches can refer to [Mie 99].

3.3 Multiobjective Evolutionary Algorithms

In a MOP, different decision makers with different preferences may select different Pareto-optimal solutions. Therefore, it is important to find as many Pareto-optimal solutions as possible so that the decision maker can choose the best one according to his preference. Therefore, there are two goals in a multi-objective optimization [Deb 02]:

1. to find a set of solutions as close as possible to the true Pareto-optimal front
2. to find a set of solutions as diverse as possible

Conventional multi-objective optimization methods solve the MOP by scalarization. For these methods, there exist many difficulties in finding multiple Pareto optimal solutions. For example, they require some problem knowledge before optimization is performed. Some techniques such as weighted sum methods may be sensitive to the shape of the Pareto-optimal front. Moreover, they require several optimization runs to obtain an approximation of the Pareto-optimal set [Zit99]. Over the past decade, multi-objective evolutionary algorithms (MOEAs) have been developed. The basic feature of MOEAs is multiple directional and global search through maintaining a population of potential solutions from generation to generation [GCh00]. Due to their population-approach, MOEAs can find multiple Pareto-optimal solutions in one single simulation run. Moreover, by using a diversity-preserving mechanism, MOEAs also can find widely different Pareto-optimal solutions. In the next section, the basic principles of evolution algorithms are first described, and then the mostly used MOEAs are introduced.

3.3.1 Basic Principles of Evolutionary Algorithms

EAs imitate natural evolutionary principles to constitute search and optimization procedures. The best known EAs include genetic algorithms (GAs), evolution strategies and evolutionary programming. GAs are the mostly widely used EAs in the field of optimization.

The terminology used in GAs is borrowed from natural genetics. Individuals (solutions) in a population are called strings or chromosomes. Chromosomes are made of units called genes, each of which encodes a particular feature of the organism. The position of a gene in a chromosome also reflects a particular characteristic of organism. Each chromosome consists of several segments. Each segment refers to a particular value of a variable. In the simplest case a chromosome contains only a segment, which refers to a particular value of a variable and by a binary string, for example, 0110 in which each digit is treated as a gene. If 0110 is transformed into the decimal system as follows:

$$0 \cdot 2^3 + 1 \cdot 2^2 + 1 \cdot 2^1 + 0 \cdot 2^0 = 6$$

The value 6 may represent the value of a variable, which is used to calculate the value of an objective function in optimization. In order to use GA to find the optimal decision variables, various methods are used to encode them into a chromosome. Binary encoding and real-number encoding are two mostly used encoding methods [GCh00]. In the binary encoding, each decision variable is encoded as a bit using standard binary coding. For a problem having N variables, $\mathbf{x}=(x_1,\ldots,x_n)$, a chromosome contains n segments of a bit string as follows:

$$\underbrace{11...01}_{x_1}\underbrace{11...01}_{x_2}\cdots\underbrace{10...11}_{x_n}$$

Therefore, if each variable x_i is coded in m_i bits, the length of a complete chromosome is

$\sum_{i=1}^{n} m_i$. As the binary encoding of continuous variable usually results in many difficulties [Deb02], a real-number presentation is usually used in the problems having continuous variables. In the real-number encoding, each chromosome is represented as a vector of real numbers (decimal system). For example, for a problem with n variables, the real-number vector is

$$\mathrm{x}=\left(\underbrace{23}_{x_1},\underbrace{6}_{x_2},\cdots,\underbrace{168}_{x_n}\right)$$

Fig. 3.4 shows a standard GA flowchart.

Initialization An initial population of N individuals (solutions) is generated randomly. Each individual refers to a design, which contains n design variables. Each individual is represented by a chromosome (string), which contains n segments corresponding to n design variables

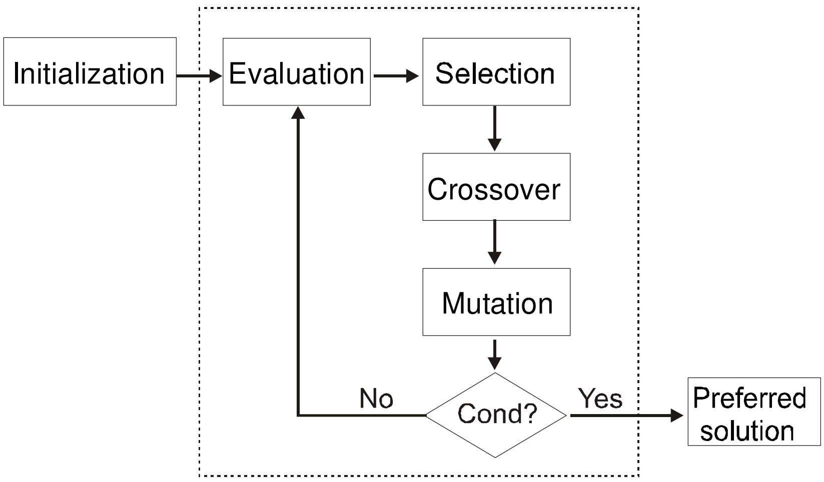

Fig. 3.4 The standard GA flowchart

Evaluation During evaluation, each individual is evaluated to give some measure of its fitness. In the unconstrained single-objective optimization problem, the fitness of a solution is assigned a value which is a function of the value of the corresponding objective function. In MOPs, special approaches are needed to determine the fitness value of a solution according to multiple objectives. These approaches will be introduced in the next sections.

Selection The primary task of the selection operator is to select and duplicate good solutions to create a new mating pool of *N* parent solutions. There exist a number of selection methods. Tournament selection, proportionate selection and ranking selection are some common types [Deb02].

In the tournament selection, tournaments are played between two randomly chosen chromosomes and the better chromosome is chosen and placed in the mating pool. The process is repeated *N* times until the mating pool is full.

In the proportionate selection, the selection probability or survival probability for each chromosome is determined in proportion to its fitness value. Then a roulette wheel can be constructed displaying these probabilities. Thereafter, the wheel is spun *N* (population size) times, each time selecting a chromosome. The wheel features the selection method as a random sampling procedure. Therefore, the chromosome that has higher fitness value will be copied into mating pool more often than the chromosome with lower fitness. The roulette-wheel concept can be simulated on a computer. A random and deterministic version of the above method is stochastic remainder roulette-wheel selection (SRWS) operator. In this operator, the selection probabilities are multiplied by the population size and the expected number of copies is calculated. Each chromosome is allocated copies according to the integer part of the expected number, and then the remaining slots in the mating pool is filled by using the RWS operator on the entire population with the fractional part of the expected number as fitness. In [Bak85] the stochastic universal sampling (SUS), another version of RWS is proposed. In this method, *N* (population size) numbers, which have equal space distances, are generated as follows:

$$\mathbf{LR} = \left\{ rn,\ rn + \frac{1}{N}, rn + \frac{2}{N}, \ldots, rn + \frac{N-1}{N} \right\} \bmod 1 \tag{3.8}$$

where *rn* is a random number between 0 and 1. Each element of LR represents a location of the roulette wheel, see Fig. 3.5. Therefore, only a random number is needed in order to select N solutions.

In ranking selection, the population is sorted from the best (rank *N*) to the worst (rank 1) according to their fitness, and then the selection probability of each chromosome is assigned according to the ranking but not its raw fitness. Thereafter a roulette wheel is applied with the selection probability and *N* chromosomes are chosen for the mating pool.

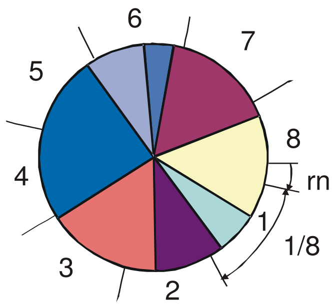

Fig. 3.5 Roulette wheel with a population of 8 solutions

Crossover The crossover operator provides the search mechanism of the GA. It creates new solutions (offspring) by exchanging features of two parent solutions picked from the mating pool at random. For a binary-coded chromosome, the single-point crossover operator and the two-point crossover operator are usually used. In a single-point crossover operator, the crossover operation is performed by choosing a crossing site along the string at random and exchanging all bits on the right side of the crossing site, as shown in the following example:

$$\begin{array}{c} \text{Parents} \\ \begin{array}{ccc:cccc} 0 & 1 & 0 & 1 & 0 & 0 & 1 \\ 1 & 0 & 1 & 0 & 0 & 1 & 0 \end{array} \end{array} \longrightarrow \begin{array}{c} \text{Offspring} \\ \begin{array}{ccc:cccc} 0 & 1 & 0 & 0 & 0 & 1 & 0 \\ 1 & 0 & 1 & 1 & 0 & 0 & 1 \end{array} \end{array}$$

In a two-point crossover operator, two different crossing sites are chosen randomly and the crossover operation is completed by exchanging middle substrings. Following this idea, n-point crossover can also be implemented. With the increase of crossover sites the extent of string preservation reduces. In order to preserve some good chromosomes, not all strings in the mating pool are used in a crossover. Usually, a crossover probability of p_c is used.

For a real-parameter GA, crossover operation is implemented by using a pair of real-parameter decision variable vectors to create a new pair of offspring vectors. Linear crossover, blend crossover (BLX-α), and boundary operator are some commonly used crossover.

In linear crossover operator, three solutions, $0.5x_i^{(1,t)} + 0.5x_i^{(2,t)}$, $1.5x_i^{(1,t)} - 0.5x_i^{(2,t)}$ and $-0.5x_i^{(1,t)} + 1.5x_i^{(2,t)}$ are generated from two parent solutions $x_i^{(1,t)}$ and $x_i^{(2,t)}$ at generation t. The best two solutions will be chosen as offspring [Deb02].

In BLX-α [ES93], parent solutions $x_i^{(1,t)}$ and $x_i^{(2,t)}$ give birth to offspring $x_i^{(1,t+1)}$ and $x_i^{(2,t+1)}$ according to

$$\begin{aligned} x_i^{(1,t+1)} &= \gamma_i x_i^{(1,t)} + (1-\gamma_i)x_i^{(2,t)} \\ x_i^{(2,t+1)} &= (1-\gamma_i)x_i^{(1,t)} + \gamma_i x_i^{(2,t)} \end{aligned} \tag{3.9}$$

where $\gamma_i = (1+2\alpha)u_i - \alpha$. u_i is a random number in [0,1] and α is user-specified parameter. It is reported that BLX-α with $\alpha = 0.5$ performs better than BLX operators with any other α value [Deb02].

Boundary operator was proposed in [SM97]. Considering that the global solution for many optimization problems usually lies on the boundary of the feasible region, for many constrained optimization problems, it may be beneficial to search just the boundary of the search space defined by the constraints. An example of such an approach is sphere crossover. Two parent solutions $x_i^{(1,t)}$ and $x_i^{(2,t)}$ create one offspring $x_i^{(1,t+1)}$ according to

$$x_i^{(1,t+1)} = \sqrt{\alpha x_i^{(1,t)} + (1-\alpha) x_i^{(2,t)}} \tag{3.10}$$

where i =1,…, n , α is a random number in [1, n].

There exist many other crossovers, such as simulated binary crossover (SBX), unimodal normally distributed crossover (UNDX), fuzzy connectives based crossover and direction-based crossover, etc. For details refer to [GCh00].

Mutation The mutation operator is used to perform a local search to find an improved solution. For the binary-coded chromosome, the bitwise mutation operator changes a 1 to 0 and vice versa with a mutation probability of p_m . For the real-parameter coded chromosome, random mutation, non-uniform mutation and Gaussian mutation are the most commonly used real-parameter mutation operators [Deb02].

The above three operators, namely selection, crossover and mutation operators constitute the main part of a GA. Through them a new population is created in every generation (iteration). Finally, termination conditions are checked. If the specified maximum number of generations is arrived, or another stopping criterion is satisfied, the iteration stops, otherwise the surviving population become the starting population for the next generation.

Preferred Solution Generally**,** a best solution needs to be selected for the implementation.

In addition to GAs, evolution strategies and evolutionary programming are also usually used. Good introduction material for the latter two methods can be found in [Bäc96].

3.3.2 Fitness Assignment and Fitness Sharing

As EAs can find multiple optimal solutions in a single run due to their population-to-population approach, it is natural to apply them in MOPs. According to two goals in a multi-objective optimization stated before, two aspects must be addressed in order to adapt EAs to MOPs. First, special approaches are needed for accomplishing fitness assignment and selection respect to multiple objectives, respectively, in order to guide the search towards the Pareto-optimal front. Second, appropriate techniques are needed for maintaining population diversity in order to achieve a well distributed and well spread non-dominated set.

During the past decade several fitness assignment methods have been developed. These methods can be classified as follows [GCh00]:

- Vector evaluation approach
- Weighted-sum method
- Goal programming approach
- Pareto-based approach

According to these different fitness assignment methods, various MOEAs have been proposed. These will be described in subsequent section.

In order to maintain population diversity, fitness sharing technique [GR87] is usually applied in MOEAs. The basic idea is to reduce the reproduction ability of a solution crowded by many solutions through degrading its fitness value f_i using the sharing function concept. Typically the following function is defined as the sharing function:

$$\mathrm{Sh}(d_{ij}) = \begin{cases} 1-\left(\dfrac{d_{ij}}{\sigma_{share}}\right)^{\alpha} & \text{if } d_{ij} < \sigma_{share} \\ 0 & \text{otherwise} \end{cases} \tag{3.11}$$

where α is a constant, σ_{share} is the niche radius, which represents the minimal distance between two solutions desired by the designer. The parameter d_{ij} is the metric of distance between any two solutions i and j. Therefore, if $d_{ij} = 0$, then $\mathrm{Sh}(d_{ij}) = 1$. This means a solution has full sharing on itself. If $d_{ij} \geq \sigma_{share}$, then $\mathrm{Sh}(d_{ij}) = 0$. This means two solutions which are at least a distance away from each other do not have any sharing effect on each other. For any other distance d two solutions have partial effect. A niche count nc_i, which gives an estimation of the extent of the crowding near the i-th solution, is then calculated as follows:

$$nc_i = \sum_{j=1}^{N} \mathrm{Sh}(d_{ij}) \tag{3.12}$$

The sum includes the ith solution itself. Thus, nc_i is always greater than or equal to one because at least $\mathrm{Sh}(d_{ii}) = 1$. Finally, the shared fitness value $f_i^{'}$ for the i-th solution is calculated as follows

$$f_i^{'} = \frac{f_i}{nc_i} \tag{3.13}$$

Thus, if the *i*th solution does not have any sharing effect on any other solution in the population, namely $nc_i = 1$, its fitness value will not be degraded. Otherwise, the sharing function will degrade fitness according to the crowding extent near the *i*-th solution.

3.3.3 General Procedures of Multi-objective Evolutionary Algorithms

As stated before, the dual goals in a multi-objective optimization are to find a set of solutions as close as possible to the Pareto-optimal front and simultaneously as diverse as possible. According to different ways to maintain the two goals, various MOEAs have been proposed. In [Deb02] and [GCh00] one can find the detailed descriptions for various MOEAs. Here only the Pareto-based MOEAs, which will be applied in the next chapter, are introduced.

Except the fitness assignment (evaluation) method for multiple objectives, the basic structure of a Pareto-based MOEA is similar to that of an GA described before. The general procedures are as follows:

Step1. *Initialization*: randomly create an initial population

Step2. *Evaluation*: identify non-dominated individuals from the population, assign the fitness of each individual using an appropriate fitness assignment method

Step3. *Selection*: select parents for genetic operations using an appropriate selection approach

Step4. *Generation*: generate offspring using genetic (crossover and mutation) operators,

Step5. *Elite Preservation*: ensure that the elite individuals enter the next generation using an elite-preserving strategy

Step6. *Termination*: if the prespecified maximal number of generations is reached, stop; otherwise return to step2

Step7. *Determination of the preferred solution*: a best solution is selected for implementation

It is noted that in most single-objective EA, the best α solutions (α=1 to 0.1N, N is the population size) are used as the elitist solutions [Deb 02]. In MOEA implementations, the best α non-dominated fronts (for example the fronts with rank 1 and rank 2) are used as the elitists. The proportion of the elitists from the population must be chosen carefully. If the proportion is too large, the population will lose its diversity, whereas the convergence performance can not be improved if the proportion is too small. In the following, some salient Pareto-based MOEAs including Pareto ranking or Pareto tournament are introduced.

In Pareto ranking methods, the fitness of individuals is assigned not according to the values of the objective functions, but in terms of the Pareto ranking of individuals. The basic procedure of the Pareto ranking (Goldberg's ranking) is as follows [Gol89]: first, non-dominated individuals with respect to the population are identified and assigned rank 1. Then these solutions are removed from the population. Next, the non-dominated solutions with respect to the remaining population are found and assigned rank 2. This procedure is continued until the entire population is ranked. Fig. 3.6 illustrates this approach for a two-objective minimisation problem. The multi-objective GA [FF93] and the non-dominated sorting GA [SD95] are two representative methods based on Pareto ranking.

3.3.4 Multiobjective Genetic Algorithm (MOGA)

In this method, the population is ranked according to the follow expression:

$$r_i = 1 + n_i \tag{3.14}$$

where r_i presents the rank of the i-th solution. n_i is the number of the solutions which dominate the solution i. Obviously, the minimum rank is 1 (for the non-dominated solutions with respect to population) and the maximum rank is no more than the size of the population. The smaller the rank r_i , the better the solution is. The population is sorted according to the ranks and a raw fitness is assigned to a solution by using a mapping function from the best solution to the worst solution. And then the raw fitnesses of the solutions within the same rank are averaged. In order to maintain diversity among non-dominated solutions, the shared fitness as described in the previous section is applied. Here a normalized distance of solution i from each solution j having the same rank is calculated in objective space as follows

$$d_{ij} = \sqrt{\sum_{n=1}^{q} \left(\frac{f_n^{(i)} - f_n^{(j)}}{f_n^{\max} - f_n^{\min}} \right)^2} \tag{3.15}$$

where $f_n^{\max}$ and $f_n^{\min}$ are maximum and minimum objective function values of the n-th objective. Except the fitness assignment method, the rest of this method is the same as that in a standard GA.

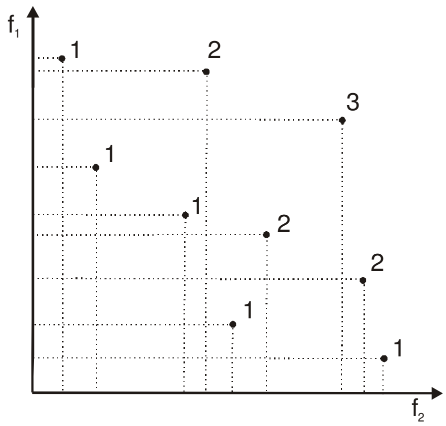

Fig. 3.6 Goldberg's ranking

3.3.5 Non-dominated Sorting Genetic Algorithm (NSGA)

In this method, the population is first ranked using the basic procedures of the Pareto ranking. A large fitness value is assigned to the individuals in the first non-dominated front, namely the set of the non-dominated individuals with rank 1. In order to maintain the goal of diversity, the sharing strategy is applied and the shared fitness of each individual in front 1 is obtained. Then a fitness value that is smaller than the minimum shared fitness value of the previous front is assigned to the individuals in the next front. The sharing strategy is used and the shared fitness of each individual in front 2 are obtained. This procedure is continued until the shared fitnesses of individuals in all fronts are obtained. A stochastic remainder roulette-wheel selection (SRWS) operator is used to generate new population. By means of this method, the non-dominated solutions in front 1 are emphasized and simultaneously the diversity is maintained.

In this method, the normalized Euclidean distance d_{ij} of the solution i from another solution j in the front 1 (Fr_1) is calculated in the parameter space as follows:

$$d_{ij} = \sqrt{\sum_{n=1}^{|Fr_1|}\left(\frac{x_n^{(i)} - x_n^{(j)}}{x_n^{\max} - x_n^{\min}}\right)^2} \tag{3.16}$$

Where $x_n^{\max}$ and $x_n^{\min}$ are the maximum and minimum objective decision variable values of the n-th decision variable, respectively. $|Fr_1|$ represents the number of non-dominated solutions in front 1. The sharing function value and niche count are then calculated using equations (3.11) and (3.12) respectively. Finally the shared fitness of the solution i is obtained by using equation (3.13). Once again, the sharing is performed in the solutions in front 2 (Fr_2) and the corresponding shared fitness value computed. This process continues until the shared fitnesses of all solutions are obtained.

In the above two methods, no mechanism is used to assure that the non-dominated solutions generated during evolutionary process enter the next generation, therefore, some non-dominated solutions obtained may get lost during evolution. In order to avoid this problem, in the following MOEAs an elite-preserving strategy is used.

3.3.6 Strength Pareto Evolutionary Algorithm (SPEA and SPEA2)

SPEA [ZT99] introduces the elite-preserving strategy by using an archive P' containing the non-dominated solutions found so far (the so-called external non-dominated set). At each generation, all non-dominated individuals in the current population P are copied to the archive P'. Then domination-check is performed among the members of the archive. Any dominated individuals are removed from P'. If the size of P' still exceeds a given limit, further non-dominated solutions stored in P' are deleted by means of clustering without destroying the characteristics of the non-dominated front. The fitness of each member in the current population *P* and archive P' is then assigned. For each individual in the archive P' a strength value $s_i \in [0,1)$ is computed, which represents the fitness value of the corresponding individual. The strength s_i is calculated as follows:

$$s_i = \frac{n_i}{N+1} \tag{3.17}$$

Where n_i is the number of current population members that are dominated by an archive member *i*. *N* is the size of the current population *P*. The fitness of an individual *j* in the current population *P* is calculated by summing the strengths of all archive members *i* that dominate *j*. It is given by

$$f_j = 1 + \sum_{i \in P' \wedge i \preceq j} s_i \tag{3.18}$$

This definition guarantees that members of P' have better fitness than members of *P*. Here a small fitness corresponds to a high reproduction probability. According to this definition, individuals near the Pareto-optimal front are preferred and simultaneously distributed along the Pareto-optimal front. This kind of fitness assignment provides a niching method based on Pareto domination.

After fitness values are assigned, individuals for the mating pool are selected from $P + P'$ by using a binary tournament selection operator. Finally the crossover and mutation operations as usual can be performed. In original study, a clustering approach, the average linkage method, has been used to reduce the size of the external non-dominated set.

In [ZLT02], an improved version of SPEA has been proposed. SPEA2 uses an improved fitness assignment scheme, a nearest neighbor density estimation technique and a new archive truncation method. In SPEA2, the size of archive P' (external non-dominated set) is fixed. All non-dominated individuals in $P + P'$ are copied to the archive. If the number of non-dominated individuals exceeds the archive size, the truncation operator is used. If the number of non-dominated individuals is less than the archive size, the archive is filled up by dominated individuals according to the fitness values. In order to fill the mating pool, the binary tournament selection is performed on the archive. Similarly, the crossover and mutation operators are applied to the mating pool to generate the offspring population. Unlike SPEA, in SPEA2 each individual *i* in the population *P* and archive P' is assigned a strength value s_i, which represents the number of individuals in $P + P'$ which are dominated by the individual *i*. The raw fitness f_i of an individual *i* is calculated by summing the strengths of all individuals that dominate *i*. A nearest neighbor density estimation technique is introduced to distinguish between individuals that have identical raw fitness values. The density d_i corresponding to *i*-th individual is calculated as follows

$$d_i = \frac{1}{\sigma_i^k + 2} \tag{3.19}$$

where σ_i^k represents the distance to the k-th nearest individual. Here h is equal to the square root of the size of $P + P'$. The final fitness of an individual i is defined by

$$F_i = f_i + d_i \tag{3.20}$$

In archive truncation, the non-dominated individual having the minimum distance is first removed from the archive. If there are several individuals having minimum distance the individual with the second smallest distances is deleted and so on.

3.3.7 Elitist Non-dominated Sorting Genetic Algorithm (NSGA-II)

In NSGA-II [Deb02], an offspring population Q_t is first generated from the parent population P_t . Then these two populations are combined to form a population R_t of size $2N$ and a non-dominated sorting is performed. Then the new population of size N is filled by the first non-dominated front, the second non-dominated front, and so on, until all slots in the new population P_{t+1} is filled up. The remaining fronts are deleted. When the solutions in the last front that is used to fill the new population are more than the remaining slots in the new population P_{t+1}, a niching strategy is used and the solutions that locate in the least crowded region are selected. This algorithm provides not only an elite-preservation but also maintains a better spread among the solutions. Fig. 3.7 illustrates the procedure of NSGA-II.

In this algorithm, a crowded tournament selection operator is used. In the tournament selection, two solutions i and j are compared. If they have different ranks, the solution that has a better rank wins. If they have same rank, the solution that has a better crowding distance wins. The crowding distance represents a measure of the density of solutions in the neighborhood. It estimates half of the perimeter of the cuboids formed by the nearest neighbors as the vertices.

The distance-based Pareto genetic algorithm is another commonly used elitist MOEA [OK 95] and [OK 96]. The basic idea is to assign fitness to each solution according to a distance measure with respect to the non-dominated solutions in the proceeding generation.

3.4 Constraint Handling in Multiobjective Evolutionary Algorithms

Most constraint handling methods in MOEAs can be classified into three categories: methods based on preserving feasibility of solutions, methods based on penalty functions and methods based on feasibility and domination of solutions.

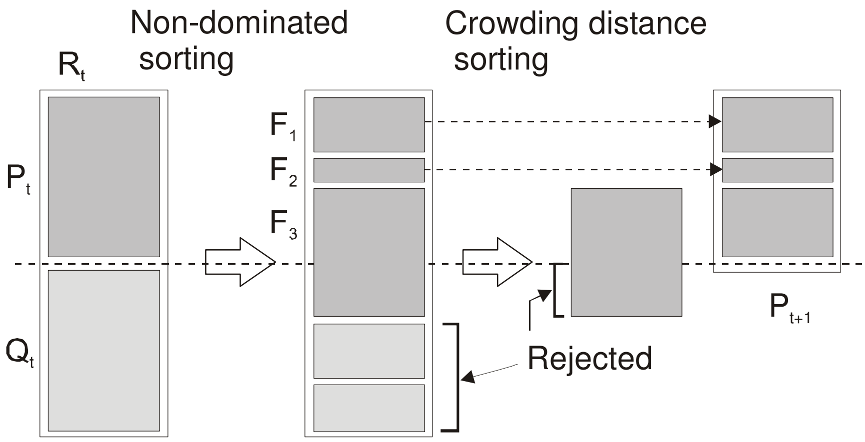

Fig.3.7 Schema of NSGA-II [Deb02]

3.4.1 Methods based on Preserving Feasibility of Solutions

In this method, solution that violates any of the constraints is discarded. An equality constraint can be handled using explicit or implicit method. In the explicit method, the explicit expression of a decision variable is derived from the equality constraint and then substituted into all objective functions and other constraint functions. In this way, the number of decision variables is reduced and this equality constraint is automatically satisfied in the optimization process. When a variable is difficult to be expressed explicitly, the implicit method can be used. For example, for each solution vector $\mathbf{x}=(x_1, x_2,\ldots,x_n)$, the value of a variable x_1 is determined by finding the root of an equality constraint $h(\mathbf{x})=0$ in terms of variable x_1. Therefore, the equality constraint is also automatically satisfied in the optimization process.

3.4.2 Methods based on Penalty Functions

The penalty technique is probably the most common technique to for constrained MOPs. In this method, a constrained MOP is transformed into an unconstrained MOP by penalizing infeasible solutions, where a penalty term is added to each objective function for any constraint violation. Based on the objective function $f_m(\mathrm{x})$ and the penalty term $p_m(\mathrm{x})$, the new objective function is given by

$$\tilde{f}_m(\mathrm{x}) = f_m(\mathrm{x}) + p_m(\mathrm{x}) \tag{3.21}$$

Once the new objective functions are formed, any unstrained multi-objective optimization methods described before can be used.

Generally, there are two classes of penalty function: static penalty and dynamic penalty. The static penalty function is usually given by

$$p_m(\mathrm{x}) = r_m \sum_{j=1}^{J} \tilde{g}_j(\mathrm{x}) \tag{3.22}$$

where r_m is a penalty parameter for the m-th objective function. $\tilde{g}_j(\mathrm{x})$ is constraint violation of the j-th constraint for the solution $\mathbf{x}$. For the minimization problem and the inequality constraints of the form "$\geq$", the constraint violation is calculated as follows:

$$\tilde{g}_j(\mathbf{x}) = \begin{cases} |\underline{g}_j(\mathbf{x})|, & \text{if } \underline{g}_j(\mathbf{x}) < 0 \\ 0, & \text{otherwise} \end{cases} \quad j = 1,2,...,J \tag{3.23}$$

where $\underline{g}_j(\mathbf{x})$ is the normalized constraint function of the constraint $g_j(\mathbf{x})$. That is, J constraint violations $|\underline{g}_j(\mathbf{x})|$ ($j = 1,2,...J$) have the same order of magnitude.

In the dynamic penalty function method, the penalty parameter is changed with the generation. There are many dynamic penalty methods. A commonly used method is as follows [JH94]:

$$p_m(\mathrm{x}) = (C_n \cdot t)^{\gamma} \sum_{j=1}^{J} \left[\tilde{g}_j(\mathrm{x})\right]^{\beta} \tag{3.24}$$

where t is generation counter. C_n , γ and β are user-defined constants. It is suggested that γ=1 and β=2.

3.4.3 Methods based on Feasibility and Domination of Solutions

The basic idea of these methods is to determine the winner of a tournament selection mainly according to three criteria: prefer the feasible solution to the infeasible solution, prefer the non-dominated solution to the dominated solution and prefer the solution residing in a less crowded region of the objective space or decision variable space to the solution residing in more crowded region.

In [JVG99] feasible and infeasible solutions are evaluated and a niche strategy is used to maintain the diversity of Pareto-optimal solutions. A binary tournament selection operator is used and a basic procedure is proposed: first, two solutions are picked up from the parent population. Then a tournament is played. If one solution is feasible and the other is infeasible, the former wins. If two solutions are feasible, a subpopulation of feasible solutions is selected from parent population and then a procedure similar to the niched Pareto GA described before is used. If two solutions are infeasible, a subpopulation of infeasible solutions is selected from parent population and a procedure similar to the niched Pareto GA is followed, where the constraint violation or nearness to a constraint boundary can be used as a criterion for comparison.

The constrained tournament method [Deb02] is another commonly used method. In this method, a constrain-domination concept is used to sort the population and then a binary tournament selection is performed. A solution $\mathbf{x}^{(i)}$ is said to constrain-dominate the other solution $\mathbf{x}^{(j)}$, if any of the following conditions is true:

1. solution $\mathbf{x}^{(i)}$ is feasible and solution $\mathbf{x}^{(j)}$ is infeasible
2. two solutions $\mathbf{x}^{(i)}$ and $\mathbf{x}^{(j)}$ are both infeasible, but solution $\mathbf{x}^{(i)}$ has a smaller constraint violation
3. both solution $\mathbf{x}^{(i)}$ and $\mathbf{x}^{(j)}$ are feasible and solution $\mathbf{x}^{(i)}$ dominates solution $\mathbf{x}^{(j)}$

Therefore, this allows a non-dominated sorting in the feasible region, and the solutions in the infeasible region are classified according to their constraint violation values. Similarly, the set of non-constraint dominated solutions can be defined as those that are not constrain-dominated by any member of the population. On the analogy of the procedure of the non-dominated sorting described in the previous section, the non-constrain-dominated sorting for the population is performed. A binary tournament selection operator is then used. First, two solutions are picked from the non-constrain-dominated population. If one solution belongs to a better non-constrain-dominated front, this solution wins. If two solutions belong to the same non-constrain-dominated front, the solution, which resides in a less crowded region based on a niched distance measure, will be chosen. A niched distance can be calculated using niche count metric based on sharing function, head count metric or crowding distance metric.

Instead of defining constraint-domination for infeasible solutions based on an overall constraint violation obtained by simply adding all constraint violations together, the non-domination check of constraint violations for infeasible solutions is suggested in [RTS01]. In this method, three different non-dominated sorting procedures, namely a non-dominated sorting only with respect to the objective functions, a non-dominated sorting only according to the constraint violation values and a non-dominated sorting with respect to a combined objective function and constraint violation values, are performed. And then solutions are chosen with these three different rankings and a new population is constructed.

3.5 Performance Metrics for Evaluating MOEAs

In the multi-objective optimization of piezoelectric transducers, it is expected that the obtained non-dominated solutions are not only closer to the true Pareto-optimal front but also convenient to be selected. These are also two general goals from the point of view of engineering.

As stated before, there are two goals in multi-objective optimization: 1. find solutions as close to the true Pareto-optimal front as possible. 2. find solutions as diverse as possible in the obtained non-dominated front. These are also two general goals from the point of view of engineering. The former emphasizes the precision of the optimized results. The latter emphasizes the convenience of the selection of the results. In order to evaluate an optimization method in terms of these two aspects, a number of performance metrics have been developed. These performance metrics can be classified into three groups [Deb02]: The first group is used to measure the extent of the solutions close to the Pareto-optimal solutions. The second group is used to measure the diversity of the obtained solutions. The third group is used to measure both aspects above using two metrics in an implicit manner. In this work, set coverage metric is used to evaluate the closeness to the Pareto-optimal front. The diversity among obtained non-dominated solutions is evaluated using two metrics that take into account the uniformity of distribution and the extent of spread of solutions, respectively.

If A and B represent two sets of no-dominated solutions obtained using two different optimization methods, the set coverage metric *C (A, B)* calculates the proportion of solutions in the set B, which are dominated by solutions in the set A as follows[Zit99]:

$$C(A,B) = \frac{\text{The number of solutions in } B\text{, which are dominated by solutions of } A}{\text{The number of solutions of } B} \tag{3.25}$$

Unlike those comparisons of different multi-objective optimization algorithms where one or several test problems are designed artificially and true Pareto-optimal front are known, the true Pareto-optimal fronts for the multi-objective optimization problems of discussed here are difficult to be known. Therefore, the set coverage metric *C (A, B)* can only be used to evaluate the relative convergence of the two sets of solutions with respect to the Pareto-optimal front of the optimization problem.

In order to evaluate the diversity of the non-dominated solutions obtained by using the three MOEAs, the following metric is used [Deb02]:

$$SP = \sqrt{\frac{1}{|Ns|}\sum_{i=1}^{|Ns|}(d_i - \bar{d})^2} \tag{3.26}$$

where $d_i = \min_{k \in Ns \wedge k \neq i} \sum_{v=1}^{m} \left| f_v^i - f_v^k \right|$ represents the minimum value of the sum of the distances in the objective space between the i-th solution and any other solution. $\bar{d} = \sum_{i=1}^{|Ns|} d_i / |Ns|$ represents the mean value of these distances. $|Ns|$ represents the number of the members in the non-dominated set Ns . m is the number of the objectives, here $m = 2$. The more uniformly the solutions are spaced, the smaller the metric *SP*.

In order to evaluate the extent of spread of the solutions the following metric is applied [Zit99]:

$$DI = \sqrt{\sum_{v=1}^{m}\left(\max_{i=1}^{|Ns|} f_v^i - \min_{i=1}^{|Ns|} f_v^i\right)^2} \tag{3.27}$$

For the two-objective problem, the metric DI measures the length of the hypotenuse of a triangle formed by the extreme solutions in the objective space. The larger the value of the metric DI is, the larger the extent of spread of the solutions.

In this chapter, the basic concepts of multi-objective optimization were introduced. The basic ideas behind various multi-objective optimization methods using scalarization technique and evolutionary algorithms were described. Some representative MOEAs have been introduced in detail. In the next chapter, multi-objective optimization of piezoelectric actuators using several MOEAs will be discussed.

4 Multiobjective Optimization of Piezoelectric Transducers

As the basis for multi-objective optimization of piezoelectric actuators two different kinds of techniques have been studied in chapter 2 and chapter 3. In this chapter, an integrated procedure for piezoelectric transducer design via multi-objective optimization is studied. The structure of this chapter is as follows: First, the Langevin transducer and its performance criteria are introduced. Then based on lumped parameter models the optimal prestress for transducers considering multiple objectives is studied. After analytical models based on the transfer matrix method are introduced, several multi-objective optimization problems of piezoelectric transducers are studied. In these problems two types of mechanical boundary conditions, the freely vibrating transducer and the transducer subjected to a mechanical load are considered.

4.1 Langevin Transducers

In ultrasonic machining and bonding as well as in many other applications, ultrasonic transducers are used to transfer high frequency electrical energy into high frequency mechanical vibration of a tool. The ultrasonic process is performed by the tool, which vibrates at a resonance frequency, generally between 20 kHz and 100 kHz. Piezoelectric transducers are the most commonly used type of ultrasonic transducers. Fig. 4.1 gives the principle description of an ultrasonic machining (or bonding) system. Fig. 4.2 shows two typical applications of piezoelectric transducers.

Most of the piezoelectric transducers have a setup, which can be in principle reduced to a sandwich construction, where piezoelectric material is sandwiched between metal end blocks (back section and front section or horn). They are known as so-called Langevin transducers or sandwiched transducers, see Fig. 4.3. Langevin transducers have the following advantages [Hul73], [Nep73] and [Rus95]:

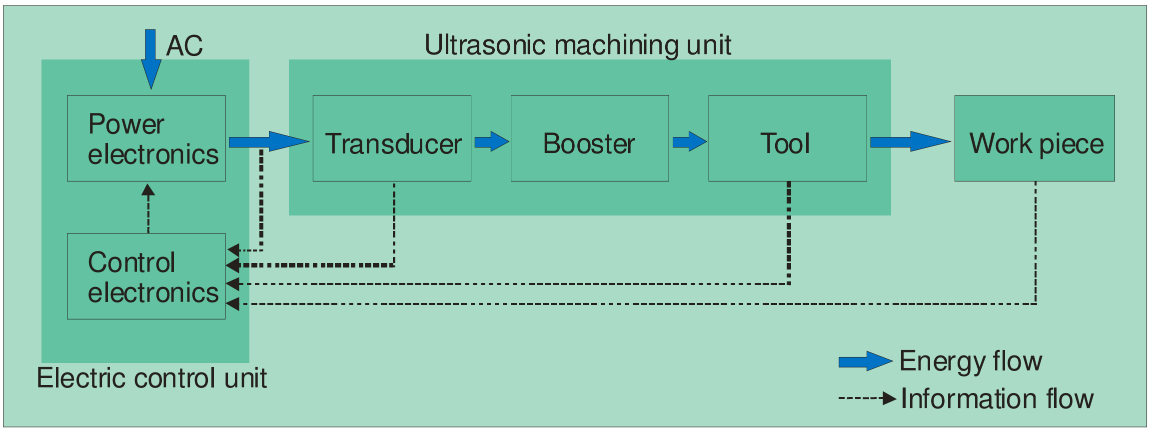

Fig. 4.1 Ultrasonic machining (bonding) system

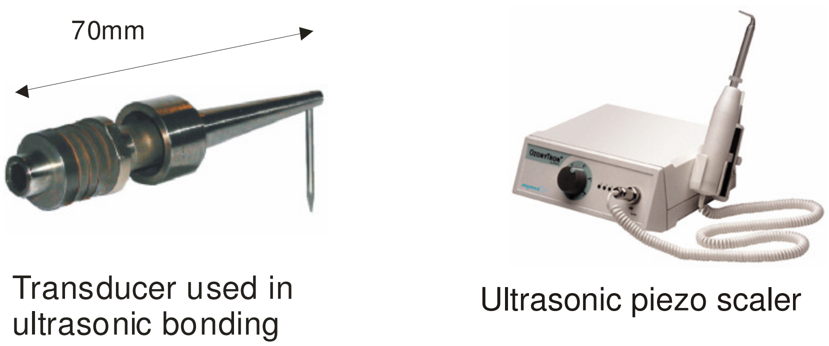

Fig.4.2 Typical piezoelectric transducers

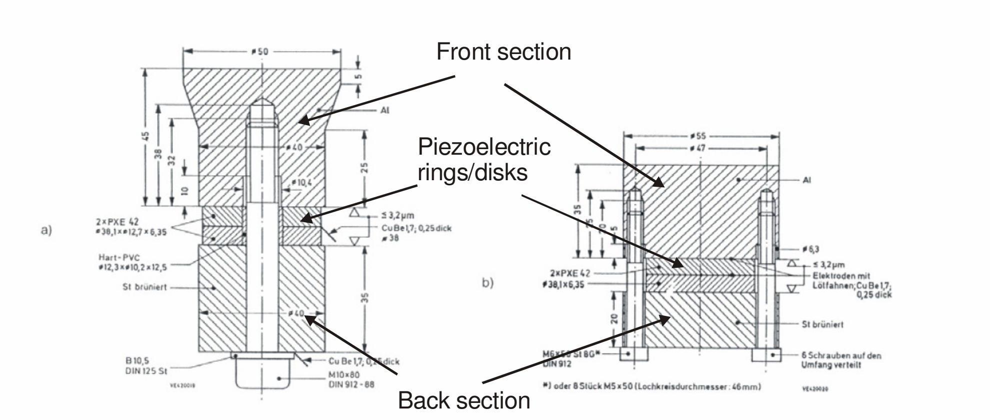

Fig. 4.3 Basic construction of Langevin-type transducers [Phi91]

1. A mechanical prestress may be imposed on the piezoelectric elements by means of a central bolt or peripheral sleeve. Thus, the admissible dynamic stress amplitude and hence the maximum power intensity are considerably increased. The mechanical contact between the parts is improved and hence the mechanical damping decreases.

2. The mechanical quality factor of metal is generally higher than that of piezoelectric material. The metal end sections are good heat-sinks, so that the transducer can be driven at higher vibration levels than other types of ultrasonic transducers.

3. As the manufacture of metal is much easier than that of piezoelectric materials, more variations of the shape and dimension of transducers are available.

4. As a part of piezoelectric material is replaced by metal, material costs decrease, also the influence of active material on characteristics of transducers.

As the displacement of the piezoelectric material is limited, a horn is used to amplify this limited displacement. There are four general designations of horns: constant, linear, exponential and stepped, which refer to the degree to which the area changes from the base to the tip. The thesis work concentrates on the design of constant-horn (also symmetrical) and stepped-horn transducers via multiobjective optimization methods. In the practical applications, piezoelectric transducers, like almost all mechanical systems, are always expected to be “optimal”. In order to achieve optimum performances, optimum pre-stress, geometrical and material parameters of the transducer must be determined.

4.2 Performance Criteria

There exist different performance criteria for piezoelectric transducers in the different applications. For the piezoelectric transducers used in ultrasonic machining and bonding devices, the most commonly applied performance criteria (some of which have been already described in chapter 2) are collected here.

Resonance frequency The resonance frequency of the transducer should be equal to the specified working frequency. Commonly, this resonance frequency is that of the first longitudinal vibration mode, which is often known as so-called λ/2 vibration mode. The cause of designing a transducer based on the λ/2 vibration mode is that the transducer can be combined with other λ/2 parts like booster and tool to form a whole ultrasonic machining device without obvious changes of the eigenform compared with that of each part before synthesis [Lit03]. The advantage of the λ/2-synthesis is that in the ideal case no forces act at the interfaces between individual parts. Therefore, the boundary conditions of each part in the whole synthesized system are the same of those of each part free at both sides. Under this condition, each part (transducer, booster or tool) can be first developed according to the specified resonance frequency and then they are synthesized into a whole device. Fig. 4.4 describes the λ/2-synthesis principle schematically.

Electrical input power The input power of the transducer is:

$$p_e(t) = U(t) \cdot I(t) \tag{4.1}$$

where *U(t)* and *I(t)* are the AC input voltage and current respectively. If the system is not driven exactly at resonance it will show a capacitive or inductive behavior. The mean power or effective power is then given by

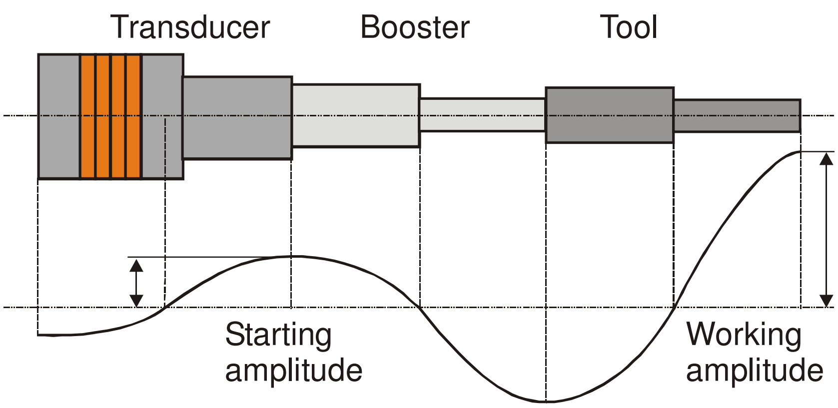

Fig. 4.4 The principle of the λ/2-synthesis

$$P_e = \frac{1}{T}\int_0^T U(t)I(t)dt \tag{4.2}$$

In the case of harmonic *U(t)* and *I(t)* the effective power results as

$$\hat{P}_e = \frac{1}{2}\hat{U}\,\hat{I}\cos\varphi_e = \hat{P}_a\cos\varphi_e \tag{4.3}$$

where $\hat{P}_a = \frac{1}{2}\hat{U}\,\hat{I}$ is the apparent power, φ_e is the phase difference between the *U(t)* and *I(t)*. $\cos\varphi_e$ is the power factor representing the proportion of the effective power which can be obtained from the apparent power. Obviously the power factor should approach 1 as closely as possible. The apparent power determines the size of the power electric device used to drive transducers. Therefore, in order to reduce the size of the power electric device, the apparent power should be minimized for a given output requirement such as a given amplitude or mechanical power.

Mechanical output power By analogy with the definition of the electrical power the moment mechanical output power of a transducer can be calculated as follows

$$p_m(t) = F(t)v(t) \tag{4.4}$$

In a work period *T*, the effective mechanical power of the transducer is then given by

$$P_m = \frac{1}{T}\int_0^T F(t)v(t)dt \tag{4.5}$$

For the harmonic vibration the effective power results as follows

$$\hat{P}_m = \frac{1}{2}\hat{F}\,\hat{v}\cos\varphi_m = \hat{P}_{ma}\cos\varphi_m \tag{4.6}$$

where $\hat{P}_{ma} = \frac{1}{2}\hat{F}\,\hat{v}$ is the apparent mechanical output power, φ_m is the phase difference between the *F(t)* and *v(t)*. $\cos\varphi_m$ is the power factor representing the proportion of the effective mechanical output power which can be obtained from the apparent mechanical output power. Similarly the power factor should approach 1 as closely as possible. For a given input power or input voltage, the effective mechanical output power should be maximized.

Coupling factor A coupling factor (also called the electromechanical coupling coefficient) *k* can be defined for each vibration mode in the piezoelectric transducer. Besides the definitions described given in chapter 2 there exist several definitions for the coupling factor depending on the manner in which the ratio of mechanical and electrical energy is computed [Ike96]. For optimization problems of piezoelectric transducers the definition of the coupling factor based on the equations of a four-pole network element may be preferred since they include the transducer dimensions. Generally, the fundamental relation for a piezoelectric transducer can be expressed in integral form as follows:

$$\begin{aligned} \underline{\hat{I}} &= \underline{y}_{11}\underline{\hat{U}} + \underline{y}_{12}\underline{\hat{F}} \\ \underline{\hat{v}} &= \underline{y}_{21}\underline{\hat{U}} + \underline{y}_{22}\underline{\hat{F}} \end{aligned} \tag{4.7}$$

Where $\underline{\hat{I}}$, $\underline{\hat{v}}$, $\underline{\hat{U}}$ and $\underline{\hat{F}}$ are the complex amplitudes of electric current, vibration velocity, voltage and force, respectively. Each admittance expression $\underline{y}_{ij}$ is a function of the driving frequency Ω. That is, the admittances depend on the excitation frequency Ω. From equation (4.7) the coupling factor can be derived as follows

$$k_{eff}{}^2 = \frac{\underline{y}_{12}{}^2}{\underline{y}_{11}\underline{y}_{22}} \tag{4.8}$$

For quasi-static operation, the coupling factor k_{eff} results as

$$k^{\,2} = \lim_{\Omega \to 0} k_{eff}{}^2 \tag{4.9}$$

The coupling factor is an overall measure for the excitation and energy conversion. It is noted that the coupling factor does not represent conversion efficiency.

Power efficiency The power efficiency λ_p can be defined as the ratio between the mechanical energy delivered and the electrical energy absorbed by the transducer, see [Cer00]. For the harmonic vibration of the transducer, this results in

$$\lambda_p = \frac{\hat{P}_m}{\hat{P}_a} = \frac{\hat{F}\hat{v}\cos\varphi_m}{\hat{U}\,\hat{I}} \tag{4.10}$$

i.e. the power efficiency is the quotient of the effective mechanical output power and apparent electrical input power of the transducer. Obviously, the power efficiency of the transducer should be maximized.

Efficiency The efficiency η is defined as a ratio of the output mechanical energy to the consumed electrical energy or the output electrical energy to the consumed mechanical energy. In a work cycle, the input electrical energy is transformed into mechanical energy partially and the remaining is stored as electrical energy in a transducer if there is no electrical loss. The stored energy can be returned to the source during discharge of the transducer. For the harmonic vibration of the transducer, the efficiency η can be calculated as follows

$$\eta = \frac{\hat{P}_m}{\hat{P}_e} = \frac{\hat{F}\hat{v}\cos\varphi_m}{\hat{U}\,\hat{I}\cos\varphi_e} \tag{4.11}$$

The efficiency η refers to the quotient of the effective mechanical output power and effective electrical input power of the transducer. It should be maximized.

The above performance criteria can also be explained according to the energy balance of the transducer as shown in Fig. 4.5. Respectively, they can be defined as follows

$$k^2 = \frac{W_{mA} + W_m}{W_a}, \quad \lambda_p = \frac{W_m}{W_a}, \quad \eta = \frac{W_m}{W_a - W_{eA}} \tag{4.12}$$

Mechanical quality factor As described in Chapter 2, the mechanical quality factor Q_m describes the resonance rise of the piezoelectric transducer. It is defined as an inverse of the loss factor $\tan\delta_m$. Obviously, a large mechanical quality factor Q_m corresponds to a large efficiency of the piezoelectric transducer and a large resonant amplitude. The material and structural damping of the piezoelectric transducer mainly determine the mechanical quality factor.

Piezoelectric quality number According to the description in chapter 2, the piezoelectric quality number M presents the phase rise or descend of the admittance functions of the piezoelectric transducer. When M<2, the resonance and anti-resonance frequencies do not exist any more, the transducer can not be driven with zero reactive power. More apparent power is needed resulting a large power electric device. Therefore, the piezoelectric quality number of the transducer used in ultrasonic bonding and machining should be larger than two. Furthermore, the larger the value of M is, the better the phase reserve of the transducer, compare Fig. 2.11 and Fig. 2.12 in chapter 2. M>2 assures that the resonance frequency exists and that the transducer can be driven with zero reactive power even though the load damping may be large.

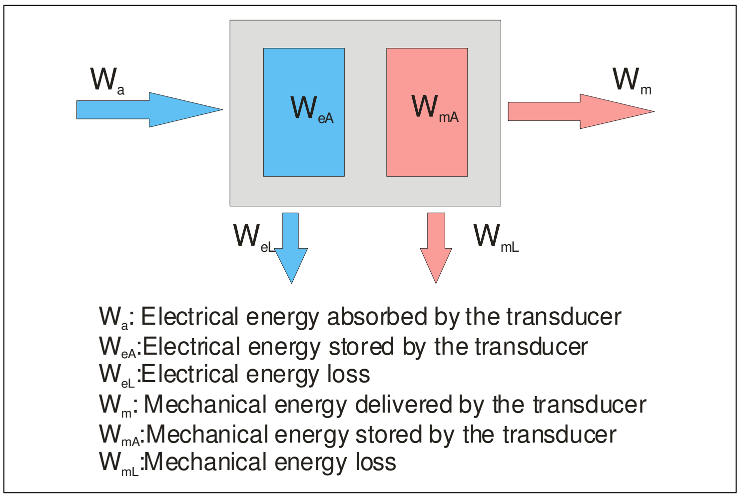

Fig. 4.5 The energy balance of the transducer

Volume of piezoelectric materials In general, piezoelectric materials are expensive. Therefore, the volume of piezoelectric materials should be minimized in order to reduce the cost of the whole transducer. However, the small volume will result in the increase of the strain in the piezoelectric material and further leads to the rise of the temperature of the piezoelectric material when the transducer is driven at resonance. This will increase the mechanical loss of the transducer. Therefore a trade-off for the volume of piezoelectric material should be considered.

Mass and size For the ultrasonic hand machining or drilling device the light and small piezoelectric transducer is expected. The material type of the metal end blocks mainly determines the mass and size of the piezoelectric transducer. For a given vibration mode and resonant frequency, different mass and size of the transducer will be obtained if different material types are used. Therefore the material types must be selected carefully in order to optimize the mass and size of the transducer.

There are two cases when the above performance criteria are used as objective functions in Multi-objective optimization problems. One case is that all performance criteria used as objective functions can be improved simultaneously in the optimization process. This means that the minimum solution corresponding to any objective function is the same. Therefore, one can find the optimum design variables for all considered performance criteria using only one criterion as the objective functions. The other case is that all performance criteria used as objective functions cannot be improved simultaneously in the optimization process. This means that the objectives are conflicting to each other. There exist multiple Pareto-optimal solutions. Indeed, the latter is more interesting and also the concentration of this thesis work. In [Sat03] the variations of the values of some performance criteria with respect to some geometrical and material parameters of a transducer have been studied qualitatively. This can be used as reference for determining objective functions in the following optimization problems.

In the following, the optimal prestress for the transducer is first determined. Then optimum geometrical and material parameters for each type of the transducer are discussed respectively.

4.3 Determination of Optimal Prestress

Prestress is a very sensitive parameter in the design of the Langevin transducer. As the influence of the prestress on the resonance performance of the transducer can not be modeled in theory, experimental study will be applied. The basic steps are: first, lumped parameter models are applied and optimization problems are described using model parameters. Then, model parameters are identified from experimental results according to different prestress. Finally, the optimum prestress for multiple objectives is determined. Because the model parameters are estimated from experiments, this approach can be applied for any transducer configuration. Losing no generality, a bolt-clamped Langevin-type piezoelectric transducer of length 70 mm has been constructed as shown in Fig. 4.6. A piezoelectric stack consisting of 4 piezoelectric rings, 4 copper electrodes and a force washer are clamped between two same steel rods by means of a bolt. The bolt is insulated from the center electrode using a thin PVC sleeve. The force washer based on strain gauge techniques was used to monitor pres-stress.

An experimental setup including an impedance analyzer (HP4192) and a laser vibrometer was used for measure of admittance frequency responses $\underline{\hat{I}}/\underline{\hat{U}}$ and $\underline{\hat{v}}/\underline{\hat{U}}$ with respect to various levels of the prestress between 20MPa and 100MPa. Fig.4.7 shows the measured admittance function $\underline{\hat{I}}/\underline{\hat{U}}$ and $\underline{\hat{v}}/\underline{\hat{U}}$ in the vicinity of the first longitudinal vibration mode according to different pre-stress. Obviously, the locations of resonance and anti-resonance frequencies as well as admittance maxima and minima vary when prestress varies.

When a piezoelectric transducer operates in the vicinity of a resonance frequency, an equivalent electrical or mechanical model shown in Fig. 2.8 in chapter 2 can describe its vibration behavior. Similarly, the electrical and mechanical admittance functions $\underline{\hat{I}}/\underline{\hat{U}}$ and $\underline{\hat{v}}/\underline{\hat{U}}$ can be approximated as follows:

$$\underline{\hat{Y}}_e = \frac{\underline{\hat{I}}}{\underline{\hat{U}}} = \frac{j\Omega}{jR\Omega + \dfrac{1}{C}} + \frac{j\Omega\alpha^2}{-m\Omega^2 + jd\Omega + c} \tag{4.13}$$

$$\underline{\hat{Y}}_m = \frac{\underline{\hat{v}}}{\underline{\hat{U}}} = \frac{j\Omega\alpha}{-m\Omega^2 + jd\Omega + c} \tag{4.14}$$

Model parameters can be calculated analytically from measured admittances [Kro99] and [Hem01]. In this work, the nonlinear least-square estimation technique was used for the parameter identification, based on the measurement of the electrical admittance frequency response $\underline{\hat{Y}}_e$ only.

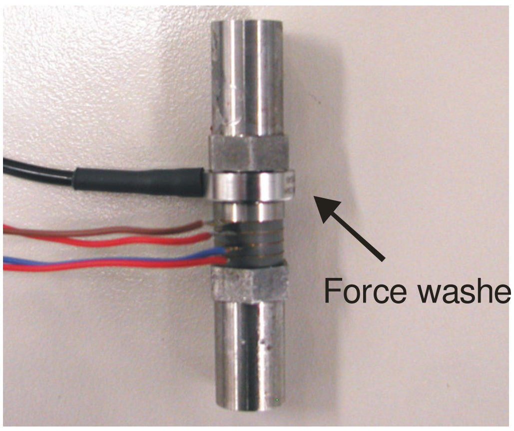

Fig. 4.6 Bolt-clamped Langevin transducer

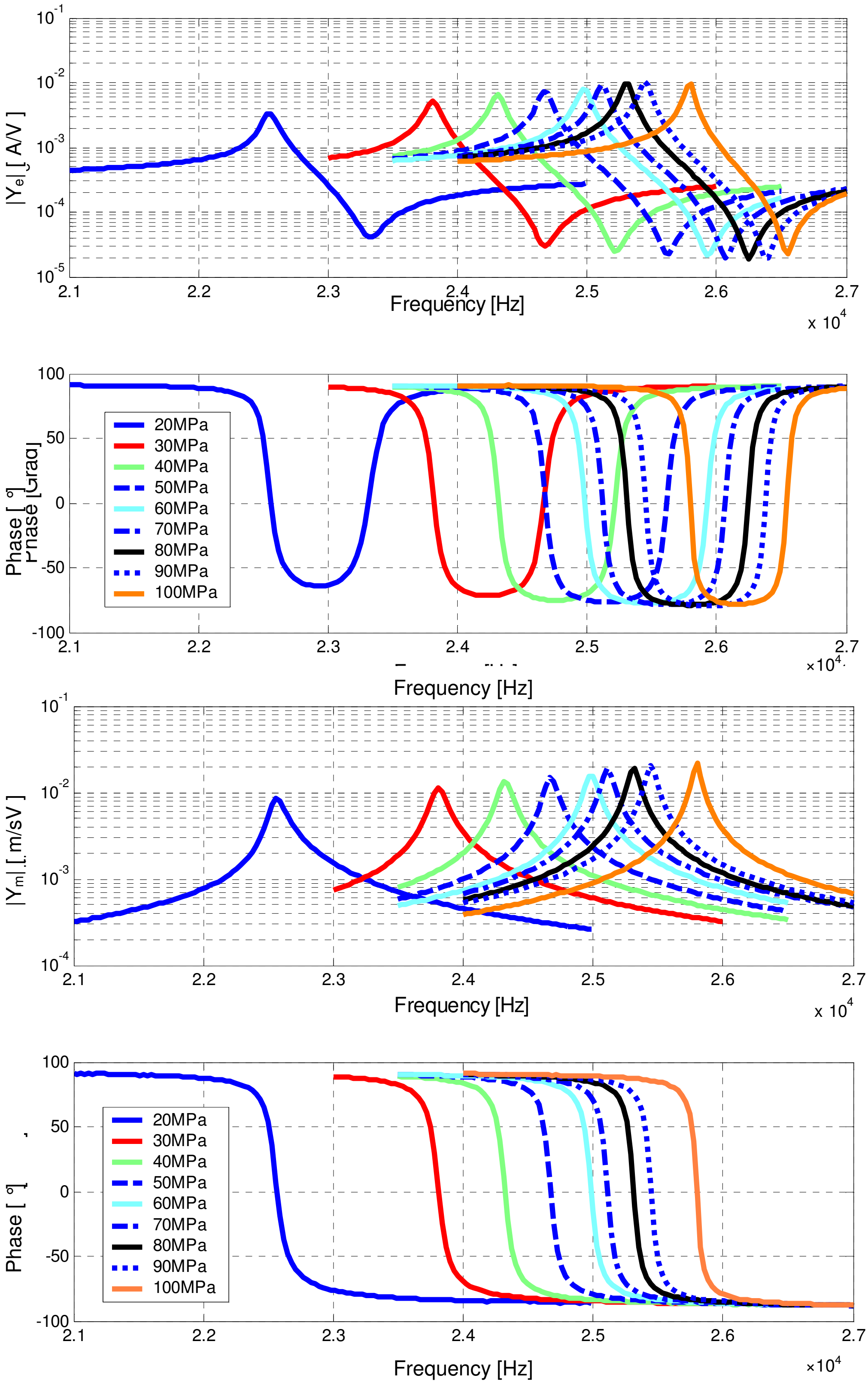

Fig. 4.7 Admittances as functions of prestress

The parameter identification problem can be formulated as a least-square optimization problem as follows

$$\min_{\boldsymbol{\varphi}\in R^6} f(\boldsymbol{\varphi}) = \frac{1}{2}\sum_{i=1}^{q}\left[\left(Y_i - \overline{Y}_i\right)^2 + \left(\angle Y_i - \angle\overline{Y}_i\right)^2\right] \tag{4.15}$$

where $\boldsymbol{\varphi} = [c\ m\ \alpha\ C\ d\ R]^T$ is estimated parameter vector. Y_i and $\overline{Y}_i$ are the measured and estimated magnitudes of admittance function $\hat{\underline{Y}}_e$ at the i-th sample point frequency (i=1, 2,…, q), respectively. $\angle Y_i$ and $\angle\overline{Y}_i$ are the measured and estimated phases of admittance function $\hat{\underline{Y}}_e$ at the i-th sample frequency point frequency (i=1,2,…, q). Here q=200 sample frequency points are used for parameter identification. Fig. 4.8 shows model parameters estimated with respect to varying prestress levels between 20MPa to 110MPa. The functional expressions of the model parameters with respect to the prestress Pr were then acquired by means of curve fitting with polynomials in the least-square sense. The resulting expressions are:

$$c = 1.28\times10^9\,\frac{\mathrm{N}}{\mathrm{m}}\left(-4\times10^{-5}\left(\frac{1}{\mathrm{MPa}}\right)^2 Pr^2 + 0.0081\frac{1}{\mathrm{MPa}}Pr + 0.5818\right) \tag{4.16}$$

$$m = 0.05\,\mathrm{kg}\left(0.0004\frac{1}{\mathrm{MPa}}Pr + 0.9133\right) \tag{4.17}$$

$$\alpha = 0.5013\frac{\mathrm{N}}{\mathrm{V}}\left(-8\times10^{-5}\left(\frac{1}{\mathrm{MPa}}\right)^2 Pr^2 + 0.012\frac{1}{\mathrm{MPa}}Pr + 0.5008\right) \tag{4.18}$$

$$C = 2.85\times10^{-9}\,\mathrm{F}\left(0.0024\frac{1}{\mathrm{MPa}}Pr + 0.7391\right) \tag{4.19}$$

$$d = 41.59\frac{\mathrm{Ns}}{\mathrm{m}}\left(7\times10^{-5}\left(\frac{1}{\mathrm{MPa}}\right)^2 Pr^2 - 0.0142\frac{1}{\mathrm{MPa}}Pr + 1.2539\right) \tag{4.20}$$

$$R = 60.58\,\mathrm{Ohm}\times$$
$$\left(-3\times10^{-6}\left(\frac{1}{\mathrm{MPa}}\right)^3 Pr^3 + 0.0008\left(\frac{1}{\mathrm{MPa}}\right)^2 Pr^2 - 0.0723\frac{1}{\mathrm{MPa}}Pr + 2.1752\right) \tag{4.21}$$

Applying the above expressions, the performance criteria can be expressed as functions of prestress Pr if the transducer is modeled as a lumped mass system. Next some optimization problems related to prestress are discussed.

When only one performance criterion is considered as the optimization objective in every optimization process, single-objective optimization is performed. However, in most practical applications multiple performance criteria with conflicting objectives are encountered and Pareto-optimal solutions need to be found.

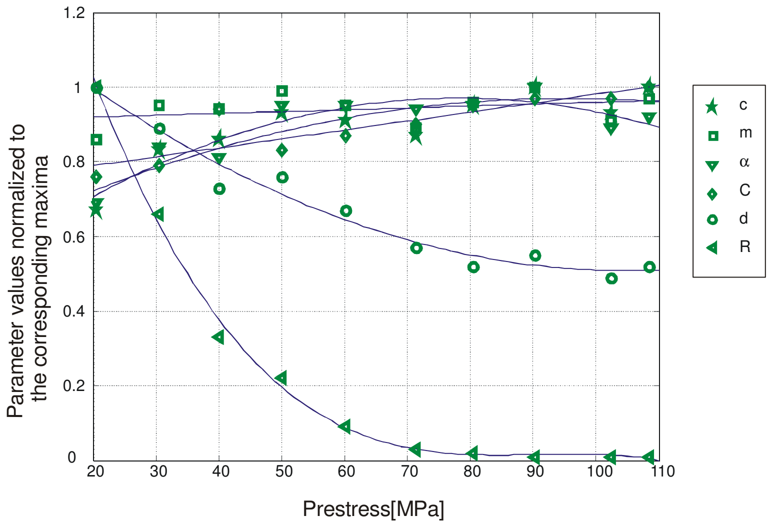

Fig. 4.8 Estimated model parameter values as functions of pre-stress. The values are normalized to the corresponding maxima.

4.3.1 Freely Vibrating Transducers

From the point of view of ultrasonic engineering the coupling factor k^2 and piezoelectric quality number M are two important performance criteria. Here they are considered as objective functions that need to be maximized simultaneously. The expressions of these two objectives can be obtained according to equations (2.12) and (2.60) in chapter 2, respectively. The optimization problem can then be formulated as follows:

$$\text{maximize } f_1(Pr) = k^2 = \frac{\omega_p{}^2 - \omega_s{}^2}{\omega_p{}^2} = \frac{\alpha^2}{cC + \alpha^2} \tag{4.22a}$$

$$\text{maximize } f_2(Pr) = M = \frac{\alpha^2}{\omega_s dC} \tag{4.22b}$$

$$\text{subject to } 20\text{MPa} \le Pr \le 110\text{MPa}$$

As there is only one design variable *Pr*, Pareto-optimal solutions can be readily found. Fig. 4.9(a) shows the two objectives k^2 and M as functions of pre-stress, respectively. The values of the objectives are normalized with respect to the corresponding maxima. The maximum of each objective function can be found using normal numerical optimization method. The prestress corresponding to the maximum effective coupling factor $k^2 = 0.068$ is Pr = 55.5MPa, to the maximum piezoelectric quality number M=22.3 is obtained for Pr = 80.7MPa. Obviously, the Pareto-optimal set is the interval [55.5MPa, 80.7MPa]. Fig. 4.9(b) presents values of objective functions in the objective space. Though this two-objective optimization problem appears to be trivial, it gives some interesting results:

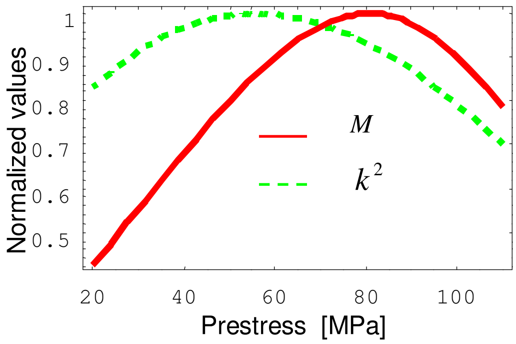

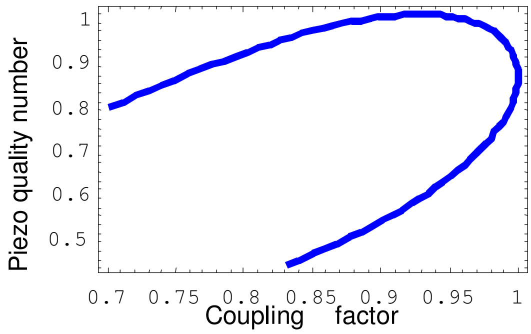

Fig. 4.9 (a) k^2 and M as functions of prestress (b) Pareo-optimal solutions in the objective space

1. Varying prestress will lead to the variation of the resonance frequencies of piezoelectric transducers. This will result in the change of resonance performances.

2. The performance criteria k^2 and M with respect to prestress can not arrive at optimum simultaneously. There exist Pareto-optimal solutions. For the transducer prototype here studied, the set of the Pareto optimal prestress is the interval [55.5 MPa, 80.7 MPa]. Correspondingly, the set of resonance frequencies is [25.09 kHz, 25.86 kHz].

Similarly, other two or multiple performance criteria can be considered as optimization objectives and the corresponding Pareto-optimal solutions with respect to prestress can be searched for.

4.3.2 Transducers with a Mechanical Load

In ultrasonic bonding and machining, piezoelectric transducers operate against loads (the bonded or machined work pieces). In general, for simplicity, the load can be modeled as a spring-damping load with a stiffness c_L and a damping d_L. Fig. 4.10 shows the equivalent mechanical model of the transducer with a mechanical load. Here, the effective coupling factor k^2 and the power efficiency λ_p are considered as objective functions.

According to the equivalent model shown in Fig. 4.10, the following equations are obtained:

$$m\ddot{u} + d\dot{u} + (c + c_L)u = -d_L\dot{u} + \alpha U \tag{4.23}$$

$$\frac{1}{C}(Q - \alpha u) + R(\dot{Q} - \alpha\dot{u}) = U \tag{4.24}$$

If the input voltage is $U(t) = \underline{\hat{U}} \cdot e^{j\Omega t}$, the following harmonic responses are obtained:

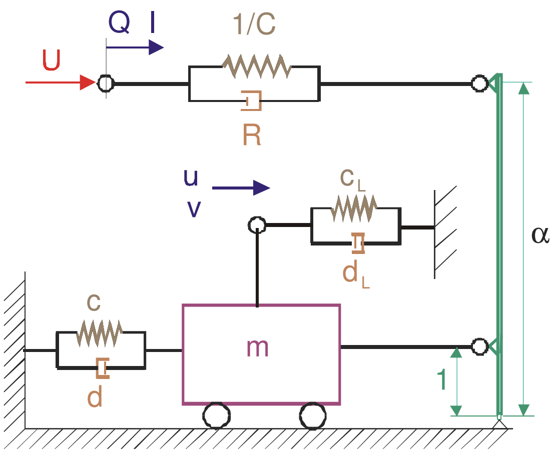

Fig. 4.10 Equivalent mechanical model of the transducer with a mechanical load

$$\hat{\underline{u}} = \frac{\alpha \hat{\underline{U}}}{c + c_L + j(d + d_L)\Omega - m\Omega^2} \tag{4.25}$$

$$\hat{\underline{v}} = j\Omega \cdot \hat{\underline{u}} = \frac{j\Omega \alpha \hat{\underline{U}}}{c + c_L + j(d + d_L)\Omega - m\Omega^2} \tag{4.26}$$

$$\hat{\underline{I}} = j\Omega \cdot \hat{\underline{Q}} = \frac{j\Omega \hat{\underline{U}}}{jR\Omega + \dfrac{1}{C}} + \frac{j\Omega \alpha^2 \hat{\underline{U}}}{c + c_L + j(d + d_L)\Omega - m\Omega^2} \tag{4.27}$$

By analogy with equations (2.53) and (2.54) in chapter 2, the series and parallel resonant frequencies in this case are calculated as follows:

$$\omega_s = \sqrt{\frac{c + c_L}{m}} \tag{4.28}$$

$$\omega_p = \sqrt{\frac{c + c_L + \dfrac{\alpha^2}{C}}{m}} \tag{4.29}$$

According to the definition of the coupling factor k^2, the first objective function is

$$f_1(Pr) = k^2 = \frac{\omega_p^2 - \omega_s^2}{\omega_p^2} = \frac{\alpha^2}{C(c + c_L) + \alpha^2} \tag{4.30}$$

When the transducer is driven at the resonant frequency, i.e. $\Omega = \omega_r \approx \omega_s$,

$$\hat{\underline{u}}_{res} = \frac{\alpha \hat{\underline{U}} \sqrt{m}}{j(d + d_L)\sqrt{c + c_L}} \tag{4.31}$$

$$\underline{\hat{v}}_{res} = \frac{\alpha \underline{\hat{U}}}{d + d_L} \tag{4.32}$$

$$\underline{\hat{I}}_{res} = \frac{j\sqrt{(c+c_L)/m}\,\underline{\hat{U}}}{jR\sqrt{(c+c_L)/m} + \frac{1}{C}} + \frac{\alpha^2 \underline{\hat{U}}}{d + d_L} \tag{4.33}$$

The output force of the transducer is given by

$$\underline{\hat{F}}_{res} = c_L \underline{\hat{u}}_{res} + d_L \underline{\hat{v}}_{res} = \frac{c_L \alpha \underline{\hat{U}} \sqrt{m}}{j(d + d_L)\sqrt{c + c_L}} + \frac{d_L \alpha \underline{\hat{U}}}{d + d_L} \tag{4.34}$$

Applying the equations (4.32) and (4.34), the effective mechanical power $\hat{P}_m$ delivered at resonance, with respect to Pr is given by

$$\hat{P}_m = \frac{1}{2} \hat{F}_{res} \hat{v}_{res} \cos \varphi_m \tag{4.35}$$

Where $\varphi_m = \angle \underline{\hat{v}}_{res} - \angle \underline{\hat{F}}_{res}$ is the phase difference between $\underline{\hat{v}}_{res}$ and $\underline{\hat{F}}_{res}$. The apparent electrical input power $\hat{P}_a$ at resonance can be calculated as follows:

$$\hat{P}_a = \frac{1}{2} \hat{I}_{res} \hat{U} \tag{4.36}$$

Applying equations (4.35) and (4.36), the second objective function, namely the power efficiency λ_p at resonance, with respect to Pr is given by

$$f_2(Pr) = \lambda_p = \frac{\hat{P}_m}{\hat{P}_a} \tag{4.37}$$

In the following the typical values $c_L = 1.27$ kN/μm and $d_L = 25.4/\omega_s$ Ns/m have been chosen. The optimization problem is then formulated as follows:

$$\begin{aligned} &\text{maximize}\, f_1(Pr) \\ &\text{maximize}\, f_2(Pr) \\ &\text{subject to } 20\text{MPa} \le Pr \le 110\text{MPa} \\ &\qquad\qquad\quad \hat{U} = 36\,\text{V} \end{aligned}$$

where model parameters α, d, c, m, C, and R in the expressions of the objective functions are determined by equations (4.16) to (4.21), respectively.

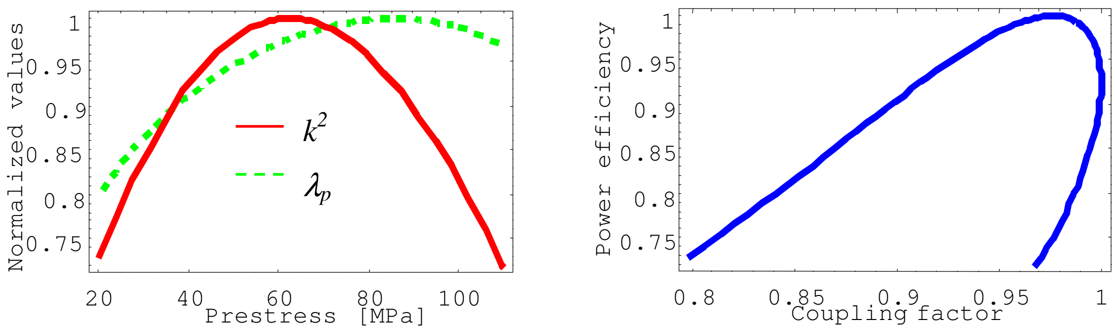

(a) (b)

Fig. 4.11 (a) k^2 and λ_p as functions of pre-stress (b) Pareto-optimal solutions in objective space

Similarly, as there is only one design variable, the Pareto-optimal solutions can be readily described by the plots as shown in Fig. 4.11. The values of the objectives are normalized with respect to the corresponding maxima. The maximum of each objective function (the inverse of the minimum of the objective function) can be found using normal numerical optimization method. The prestress corresponding to the maximum coupling factor k^2 =0.034 is Pr = 62.3 MPa, to the maximum power efficiency λp = 0.78 is Pr = 85.9 MPa. The Pareto-optimal set is the interval [62.3MPa, 85.9MPa].

In the above optimization problems, Pareto-optimal prestress has been studied individually based on experiments and lumped parameter models. Next, optimization of the piezoelectric transducer with respect to the design variables other than prestress will be discussed. First, modeling of the transducer using the transfer matrix method based on continuum models is introduced. This modeling method will be used in all optimization problems discussed later. Then, the optimization problems of the transducer with a constant horn (i.e. symmetrical transducers) and the transducer with a stepped horn will be discussed in turn.

4.4 Modeling of Langevin Transducers using Transfer Matrix Methods

The goal of modeling is to construct the mathematical expressions between the input quantities and output quantities of the transducer. As described in chapter 2, continuum models are directly related to dimensions, material parameters and boundary conditions and are suitable for the formulation of the optimization problem. However, they can generally only deal with simple and homogeneous elements. In order to apply continuum models in the design of Langevin transducers, here the transfer matrix method based on continuum models is introduced.

If the lateral dimensions of the whole transducer are smaller than one quarter of the wavelength in the frequency range of interest, the simple rod theory is well adequate for the approximation of their vibration behaviors. Therefore, the basic processes of the transfer matrix method are: First, the whole transducer is split into elementary mechanical and piezoelectric rod parts, which are homogeneous and geometrically simple and connected in series or in parallel. Second, for each rod part the transfer matrix relation is derived by means of the rod theory. Third, in terms of the deformation continuity and force equilibrium, all transfer matrix relations are concatenated to form a whole transfer matrix model for describing the electromechanical behavior of the whole transducer. In the following, the transfer matrix method is first introduced, and then the expressions of transfer matrixes are derived.

For each block the analytical model allows the computation of the vibration velocity and force at the right side of the block with respect to the vibration velocity and force at its left side. According to Fig. 4.12 a transfer matrix relation for each mechanical block can be written as follows

$$\begin{bmatrix} \underline{\hat{v}}_a \\ \underline{\hat{F}}_a \end{bmatrix} = \mathbf{A^m} \begin{bmatrix} \underline{\hat{v}}_e \\ \underline{\hat{F}}_e \end{bmatrix} \tag{4.38}$$

where $\mathbf{A^m}$ is the 2×2 transfer matrix , which is derived from analytical models. The expression can be reduced to the following form

$$\mathbf{X_a} = \mathbf{A^m X_e} \tag{4.39}$$

where

$$\mathbf{X_a} = \begin{bmatrix} \underline{\hat{v}}_a \\ \underline{\hat{F}}_a \end{bmatrix}, \quad \mathbf{X_e} = \begin{bmatrix} \underline{\hat{v}}_e \\ \underline{\hat{F}}_e \end{bmatrix} \tag{4.40}$$

In the case of a piezoelectric block (see Fig. 4.13), the transfer matrix relation can be written as

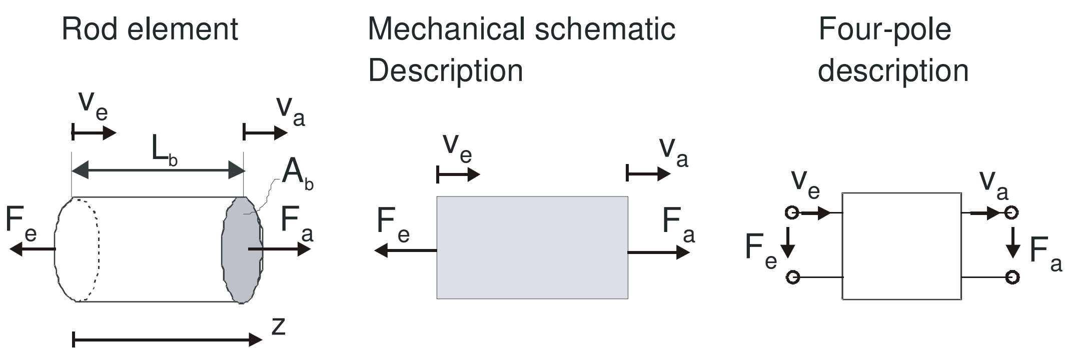

Fig. 4.12 Rod element, mechanical scheme and four-pole description

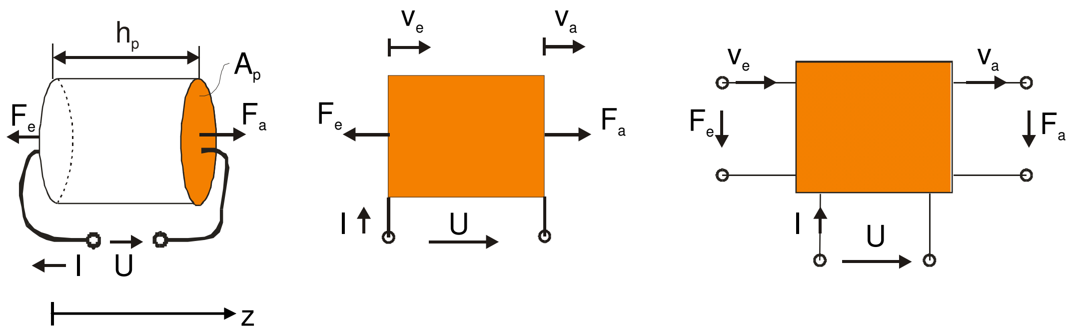

Fig. 4.13 Piezoelectric rod element, mechanical scheme and four-pole description

$$\begin{bmatrix} \underline{\hat{v}}_a \\ \underline{\hat{F}}_a \\ \underline{\hat{I}} \end{bmatrix} = \mathbf{A}^{\mathbf{P}} \begin{bmatrix} \underline{\hat{v}}_e \\ \underline{\hat{F}}_e \\ \underline{\hat{U}} \end{bmatrix} \tag{4.41}$$

where $\underline{\hat{I}}$ and $\underline{\hat{U}}$ are the electric current and voltage, respectively. $\mathbf{A}^{\mathbf{P}}$ is a 3×3 transfer matrix, which is derived from analytical models. Similarly, it can be rewritten as

$$\begin{bmatrix} \mathbf{X}_{\mathbf{a}} \\ \underline{\hat{I}} \end{bmatrix} = \begin{bmatrix} \mathbf{A}^{\mathbf{Pm}} & \mathbf{A}^{\mathbf{Pem}} \\ \mathbf{A}^{\mathbf{Pme}} & \mathbf{A}^{\mathbf{Pe}} \end{bmatrix} \begin{bmatrix} \mathbf{X}_{\mathbf{e}} \\ \underline{\hat{U}} \end{bmatrix} \tag{4.42}$$

where $\mathbf{A}^{\mathbf{Pm}}$, $\mathbf{A}^{\mathbf{Pem}}$ ($\mathbf{A}^{\mathbf{Pme}}$) and $\mathbf{A}^{\mathbf{Pe}}$ are 2×2, $2\times 1 (1\times 2)$ and 1×1 transfer matrices, respectively. They describe the mechanical field, electric field and electrometrical coupling effects of the piezoelectric block, respectively.

The whole transfer matrix relation of the transducer can be obtained by connecting transfer matrices of the elementary blocks in terms of interface conditions between two blocks. There are four fundamental connections shown in Table 4.1. Using these fundamental connections and the corresponding transfer matrices, the whole transfer matrices for various Langevin-type transducers can be assembled. The transfer matrices of these fundamental connections are derived as follows:

Connection 1: connection of two mechanical blocks in series

According to equations (4.38) and (4.39), the transfer matrix relations for block 1 and block 2 can be respectively written as follows

$$\mathbf{X}_{\mathbf{a1}} = \mathbf{A}_{\mathbf{1}}^{\mathbf{m}} \mathbf{X}_{\mathbf{e1}}, \mathbf{X}_{\mathbf{a2}} = \mathbf{A}_{\mathbf{2}}^{\mathbf{m}} \mathbf{X}_{\mathbf{e2}} \tag{4.43}$$

Assuming that the deformation is continuous at the interface of two block elements, there exist the following interface conditions

$$\underline{\hat{v}}_{a1} = \underline{\hat{v}}_{a2}, \ \underline{\hat{F}}_{a1} = \underline{\hat{F}}_{e2} \tag{4.44}$$

Table 4.1 Basic connections and their transfer matrices

	Mechanical schematic and four-pole description	Transfer matrix relations
1. Connection of two mechanical blocks	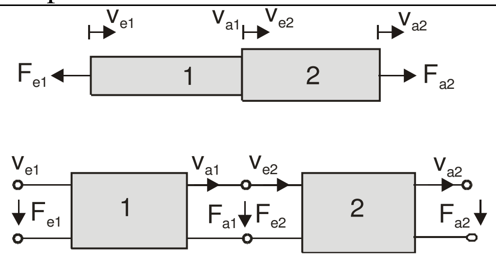	$\begin{bmatrix} v_{a2} \\ F_{a2} \end{bmatrix} = \mathbf{A}_2^{\mathbf{m}} \mathbf{A}_1^{\mathbf{m}} \begin{bmatrix} v_{e1} \\ F_{e1} \end{bmatrix}$ $\mathbf{X}_{\mathbf{a2}} = \mathbf{A}_2^{\mathbf{m}} \mathbf{A}_1^{\mathbf{m}} \mathbf{X}_{\mathbf{e1}}$
2. Connection of two piezoelectric blocks	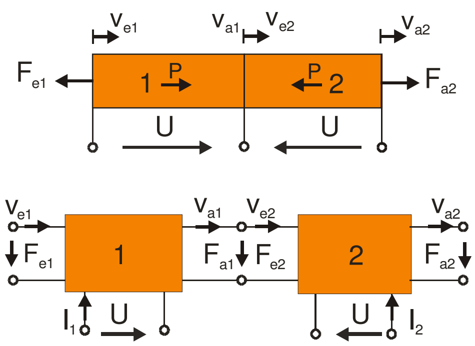	$\begin{bmatrix} \mathbf{X}_{\mathbf{a2}} \\ \underline{\hat{I}}_w \end{bmatrix} = \begin{bmatrix} \mathbf{A}_{\mathrm{w}}^{\mathbf{Pm}} & \mathbf{A}_{\mathrm{w}}^{\mathbf{Pem}} \\ \mathbf{A}_{\mathrm{w}}^{\mathbf{Pme}} & \mathbf{A}_{\mathrm{w}}^{\mathbf{Pe}} \end{bmatrix} \begin{bmatrix} \mathbf{X}_{\mathbf{e1}} \\ \underline{\hat{U}} \end{bmatrix}$ where $\mathbf{A}_{\mathrm{w}}^{\mathbf{Pm}} = \mathbf{A}_2^{\mathbf{Pm}} \mathbf{A}_1^{\mathbf{Pm}}$ $\mathbf{A}_{\mathrm{w}}^{\mathbf{Pem}} = \mathbf{A}_2^{\mathbf{Pm}} \mathbf{A}_1^{\mathbf{Pem}} + \mathbf{A}_2^{\mathbf{Pem}}$ $\mathbf{A}_{\mathrm{w}}^{\mathbf{Pme}} = \mathbf{A}_1^{\mathbf{Pme}} + \mathbf{A}_2^{\mathbf{Pme}} \mathbf{A}_1^{\mathbf{Pm}}$ $\mathbf{A}_{\mathrm{w}}^{\mathbf{Pe}} = \mathbf{A}_1^{\mathbf{Pe}} + \mathbf{A}_2^{\mathbf{Pe}} + \mathbf{A}_2^{\mathbf{Pme}} \mathbf{A}_1^{\mathbf{Pem}}$ $\underline{\hat{I}}_w = \underline{\hat{I}}_1 + \underline{\hat{I}}_2$
3. Connection of one mechanical block (left) and a piezo block (right)	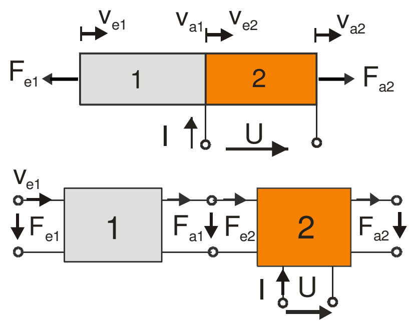	$\begin{bmatrix} \mathbf{X}_{\mathbf{a2}} \\ \underline{\hat{I}} \end{bmatrix} = \begin{bmatrix} \mathbf{A}_{\mathrm{w}}^{\mathbf{MPm}} & \mathbf{A}_{\mathrm{w}}^{\mathbf{MPem}} \\ \mathbf{A}_{\mathrm{w}}^{\mathbf{MPme}} & \mathbf{A}_{\mathrm{w}}^{\mathbf{MPe}} \end{bmatrix} \begin{bmatrix} \mathbf{X}_{\mathbf{e1}} \\ \underline{\hat{U}} \end{bmatrix}$ $\mathbf{A}_{\mathrm{w}}^{\mathbf{MPm}} = \mathbf{A}_2^{\mathbf{Pm}} \mathbf{A}_1^{\mathbf{m}}$ $\mathbf{A}_{\mathrm{w}}^{\mathbf{MPem}} = \mathbf{A}_2^{\mathbf{Pem}}$ $\mathbf{A}_{\mathrm{w}}^{\mathbf{MPme}} = \mathbf{A}_2^{\mathbf{Pme}} \mathbf{A}_1^{\mathbf{m}}$ $\mathbf{A}_{\mathrm{w}}^{\mathbf{MPe}} = \mathbf{A}_2^{\mathbf{Pe}}$
4. Connection of one piezo block (left) and a mechanical block (right)	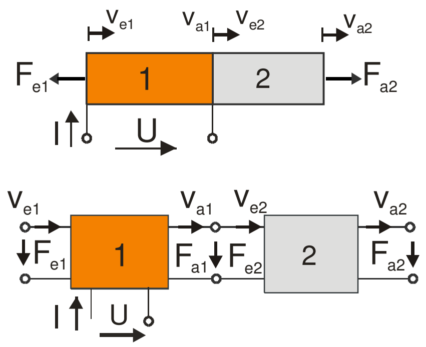	$\begin{bmatrix} \mathbf{X}_{\mathbf{a2}} \\ \underline{\hat{I}} \end{bmatrix} = \begin{bmatrix} \mathbf{A}_{\mathrm{w}}^{\mathbf{PMm}} & \mathbf{A}_{\mathrm{w}}^{\mathbf{PMem}} \\ \mathbf{A}_{\mathrm{w}}^{\mathbf{PMme}} & \mathbf{A}_{\mathrm{w}}^{\mathbf{PMe}} \end{bmatrix} \begin{bmatrix} \mathbf{X}_{\mathbf{e1}} \\ \underline{\hat{U}} \end{bmatrix}$ $\mathbf{A}_{\mathrm{w}}^{\mathbf{PMm}} = \mathbf{A}_2^{\mathbf{m}} \mathbf{A}_1^{\mathbf{Pm}}$ $\mathbf{A}_{\mathrm{w}}^{\mathbf{PMem}} = \mathbf{A}_2^{\mathbf{m}} \mathbf{A}_1^{\mathbf{Pem}}$ $\mathbf{A}_{\mathrm{w}}^{\mathbf{PMme}} = \mathbf{A}_1^{\mathbf{Pme}}$ $\mathbf{A}_{\mathrm{w}}^{\mathbf{PMe}} = \mathbf{A}_1^{\mathbf{Pe}}$

From equations (4.43) and (4.44), the whole transfer matrix relation is obtained as follows

$$\mathbf{X}_{\mathbf{a2}} = \mathbf{A}_{\mathbf{2}}^{\mathbf{m}} \mathbf{A}_{\mathbf{1}}^{\mathbf{m}} \mathbf{X}_{\mathbf{e1}} \tag{4.45}$$

Following this approach, the whole transfer matrix relation for *N* blocks in series can also be derived.

Connection 2: connection of two piezoelectric blocks mechanically in series and electrically in parallel

According to equation (4.42), the transfer matrix relations for piezoelectric block1 and block2 can be respectively written as follows

$$\begin{bmatrix} \mathbf{X}_{\mathrm{a1}} \\ \underline{\hat{I}}_1 \end{bmatrix} = \begin{bmatrix} \mathbf{A}_{\mathbf{1}}^{\mathbf{Pm}} & \mathbf{A}_{\mathbf{1}}^{\mathbf{Pem}} \\ \mathbf{A}_{\mathbf{1}}^{\mathbf{Pme}} & \mathbf{A}_{\mathbf{1}}^{\mathbf{Pe}} \end{bmatrix} \begin{bmatrix} \mathbf{X}_{\mathrm{e1}} \\ \underline{\hat{U}} \end{bmatrix}, \begin{bmatrix} \mathbf{X}_{\mathrm{a2}} \\ \underline{\hat{I}}_2 \end{bmatrix} = \begin{bmatrix} \mathbf{A}_{\mathbf{2}}^{\mathbf{Pm}} & \mathbf{A}_{\mathbf{2}}^{\mathbf{Pem}} \\ \mathbf{A}_{\mathbf{2}}^{\mathbf{Pme}} & \mathbf{A}_{\mathbf{2}}^{\mathbf{Pe}} \end{bmatrix} \begin{bmatrix} \mathbf{X}_{\mathrm{e2}} \\ \underline{\hat{U}} \end{bmatrix} \tag{4.46}$$

Similarly, using the interface conditions $\mathbf{X}_{\mathbf{a1}} = \mathbf{X}_{\mathrm{e2}}$, the whole transfer matrix relation can be obtained as follows

$$\begin{bmatrix} \mathbf{X}_{\mathbf{a2}} \\ \underline{\hat{I}} \end{bmatrix} = \begin{bmatrix} \mathbf{A}_{\mathbf{w}}^{\mathbf{Pm}} & \mathbf{A}_{\mathbf{w}}^{\mathbf{Pem}} \\ \mathbf{A}_{\mathbf{w}}^{\mathbf{Pme}} & \mathbf{A}_{\mathbf{w}}^{\mathbf{Pe}} \end{bmatrix} \begin{bmatrix} \mathbf{X}_{\mathbf{e1}} \\ \underline{\hat{U}} \end{bmatrix} \tag{4.47}$$

Where

$$\begin{aligned}
&\mathbf{A}_{\mathbf{w}}^{\mathbf{Pm}} = \mathbf{A}_{\mathbf{2}}^{\mathbf{Pm}} \mathbf{A}_{\mathbf{1}}^{\mathbf{Pm}} \\
&\mathbf{A}_{\mathbf{w}}^{\mathbf{Pem}} = \mathbf{A}_{\mathbf{2}}^{\mathbf{Pm}} \mathbf{A}_{\mathbf{1}}^{\mathbf{Pem}} + \mathbf{A}_{\mathbf{2}}^{\mathbf{Pem}} \\
&\mathbf{A}_{\mathbf{w}}^{\mathbf{Pme}} = \mathbf{A}_{\mathbf{1}}^{\mathbf{Pme}} + \mathbf{A}_{\mathbf{2}}^{\mathbf{Pme}} \mathbf{A}_{\mathbf{1}}^{\mathbf{Pm}} \\
&\mathbf{A}_{\mathbf{w}}^{\mathbf{Pe}} = \mathbf{A}_{\mathbf{1}}^{\mathbf{Pe}} + \mathbf{A}_{\mathbf{2}}^{\mathbf{Pe}} + \mathbf{A}_{\mathbf{2}}^{\mathbf{Pme}} \mathbf{A}_{\mathbf{1}}^{\mathbf{Pem}} \\
&I = I_1 + I_2
\end{aligned}$$

Following this approach, the whole transfer matrix relation for a piezoelectric stack consisting of *N* piezoelectric blocks is available.

Connection 3: a mechanical rod (left) + a piezoelectric element (right)

According to equations (4.39) and (4.42) the transfer matrix relations for the mechanical block 1 and the piezoelectric block 2 can be written as follows

$$\mathbf{X}_{\mathbf{a1}} = \mathbf{A}_{\mathbf{1}}^{\mathbf{m}} \mathbf{X}_{\mathbf{e1}} \tag{4.48}$$

$$\begin{bmatrix} \mathbf{X}_{\mathbf{a2}} \\ \underline{\hat{I}} \end{bmatrix} = \begin{bmatrix} \mathbf{A}_{\mathbf{2}}^{\mathbf{Pm}} & \mathbf{A}_{\mathbf{2}}^{\mathbf{Pem}} \\ \mathbf{A}_{\mathbf{2}}^{\mathbf{Pme}} & \mathbf{A}_{\mathbf{2}}^{\mathbf{Pe}} \end{bmatrix} \begin{bmatrix} \mathbf{X}_{\mathbf{e2}} \\ \underline{\hat{U}} \end{bmatrix} \tag{4.49}$$

Applying the interface conditions $\mathbf{X}_{\mathbf{a1}} = \mathbf{X}_{\mathbf{e2}}$ yields the whole transfer matrix relation as follows

$$\begin{bmatrix} \mathbf{X}_{a2} \\ \underline{\hat{I}} \end{bmatrix} = \begin{bmatrix} \mathbf{A}_{w}^{MPm} & \mathbf{A}_{w}^{MPem} \\ \mathbf{A}_{w}^{MPme} & \mathbf{A}_{w}^{MPe} \end{bmatrix} \begin{bmatrix} \mathbf{X}_{e1} \\ \underline{\hat{U}} \end{bmatrix} \tag{4.50}$$

where

$$\mathbf{A}_{w}^{MPm} = \mathbf{A}_{2}^{Pm}\mathbf{A}_{1}^{m}$$

$$\mathbf{A}_{w}^{MPem} = \mathbf{A}_{2}^{Pem}$$

$$\mathbf{A}_{w}^{MPme} = \mathbf{A}_{2}^{Pme}\mathbf{A}_{1}^{m}$$

$$\mathbf{A}_{w}^{MPe} = \mathbf{A}_{2}^{Pe}$$

Connection 4: a piezoelectric element (left) + a mechanical rod (right)

Applying a similar approach as in connection 3, the whole transfer matrix relation can be obtained as follows

$$\begin{bmatrix} \mathbf{X}_{a2} \\ \underline{\hat{I}} \end{bmatrix} = \begin{bmatrix} \mathbf{A}_{w}^{PMm} & \mathbf{A}_{w}^{PMem} \\ \mathbf{A}_{w}^{PMme} & \mathbf{A}_{w}^{PMe} \end{bmatrix} \begin{bmatrix} \mathbf{X}_{e1} \\ \underline{\hat{U}} \end{bmatrix} \tag{4.51}$$

where

$$\mathbf{A}_{w}^{PMm} = \mathbf{A}_{2}^{m}\mathbf{A}_{1}^{Pm}$$

$$\mathbf{A}_{w}^{PMem} = \mathbf{A}_{2}^{m}\mathbf{A}_{1}^{Pem}$$

$$\mathbf{A}_{w}^{PMme} = \mathbf{A}_{1}^{Pme}$$

$$\mathbf{A}_{w}^{PMe} = \mathbf{A}_{1}^{Pe}$$

The expressions of the transfer matrices of the fundamental block elements can be derived using the analytical models based on rod theory, respectively. A detailed derivation can be found in Appendix. In the next sections, the optimization problems of symmetric transducers and transducers with stepped horn will be discussed.

4.5 Optimization of Symmetrical Langevin-type Transducers

The symmetric Langevin-type transducer is the simplest Langevin-type transducer. Fig. 4.14 shows a typical design. A piezoelectric stack consisting of *N* (for example *N*=4) piezoelectric rings and copper electrodes is clamped between two same metal rods by means of a bolt. The piezoelectric rings and metal rods have the same outer diameter. Table 4.2 gives those parameters which affect the performances of the transducer.

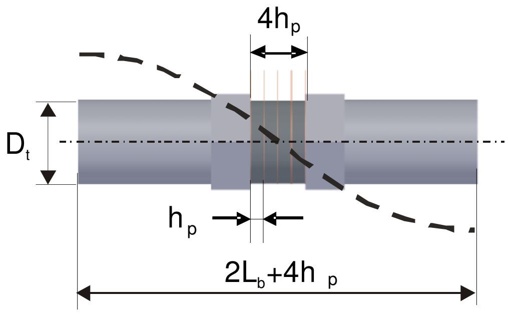

Fig. 4.14 A symmetrical Langevin transducer

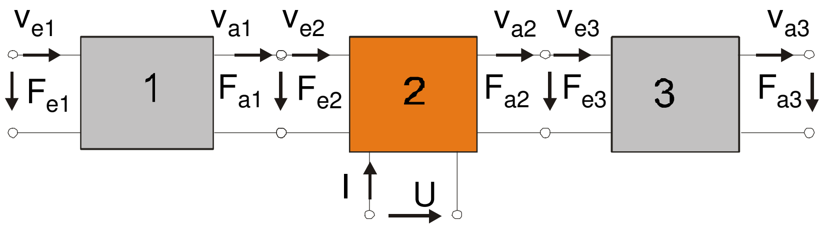

Fig. 4.15 Four-pole network element description of the symmetrical Langevin transducer

Table 4.2 Parameters that affect the performances of the transducer

$\underline{\hat{U}}$:	Input voltage
L_b:	Length of the metal parts
D_t:	Outer diameter of metal rods and piezo-disks/rings
D_i:	Inner diameter of piezo-rings and diameter of the bolt
L_{bt}:	Length of the bolt
h_p:	Thickness of piezoelectric rings
N:	Number of piezoelectric disks or rings
Typ_b:	Material parameters of metal end blocks
Typ_p:	Material parameters of piezo-rings

4.5.1 Derivation of the Whole Transfer Matrix

The whole transducer is considered as a combination of two mechanical rod elements and a piezoelectric stack in series. Then the whole transfer matrix relation of the transducer can be derived from the transfer matrices of the fundamental rod elements shown in Table 4.1. Fig. 4.15 gives the four-pole network element description. Considering the modeling in the earlier design stage, the bolt has not been modeled as a separate element. The actual piezoelectric rings are modeled as piezoelectric discs. The electrodes are not taken into account in the model. These simplifications will not cause obvious deterioration of the model.

Based on the transfer matrix relation of the fundamental connection 2 shown in Table 4.1, it is easy to obtain the transfer matrix relation for the piezoelectric stack consisting of N piezoelectric rings in series. It is noted that all piezoelectric rings here have the same thickness h_p. They are connected in parallel electrically and the whole current for the piezo-stack is

$$\underline{\hat{I}} = \left[\sum_{i=1}^{N} \mathbf{A}^{\mathbf{Pme}} \left(\mathbf{A}^{\mathbf{Pm}} \right)^{i-1} \right] \mathbf{X}_{\mathbf{e2}} + \left[\mathbf{A}^{\mathbf{Pe}} + \sum_{i=2}^{N} \left(\mathbf{A}^{\mathbf{Pe}} + \sum_{r=0}^{i-2} \mathbf{A}^{\mathbf{Pme}} \left(\mathbf{A}^{\mathbf{Pm}} \right)^{r} \mathbf{A}^{\mathbf{Pem}} \right) \right] \underline{\hat{U}} \tag{4.52}$$

The whole mechanical output (the vibration amplitude and force) on the right side of the piezoelectric stack is

$$\mathbf{X}_{\mathbf{a2}} = \left(\mathbf{A}^{\mathbf{Pm}} \right)^{N} \mathbf{X}_{\mathbf{e2}} + \left[\sum_{i=0}^{N-1} \left(\mathbf{A}^{\mathbf{Pm}} \right)^{i} \mathbf{A}^{\mathbf{Pem}} \right] \underline{\hat{U}} \tag{4.53}$$

According to equations (4.52) and (4.53), the whole transfer matrix relation for the piezoelectric stack can be written as follows

$$\begin{bmatrix} \mathbf{X}_{\mathbf{a2}} \\ \underline{\hat{I}} \end{bmatrix} = \begin{bmatrix} \mathbf{A}^{\mathbf{PSm}} & \mathbf{A}^{\mathbf{PSem}} \\ \mathbf{A}^{\mathbf{PSme}} & \mathbf{A}^{\mathbf{PSe}} \end{bmatrix} \begin{bmatrix} \mathbf{X}_{\mathbf{e2}} \\ \underline{\hat{U}} \end{bmatrix} \tag{4.54}$$

Where

$$\mathbf{X}_{\mathbf{a2}} = \begin{bmatrix} \underline{\hat{v}}_{a2} \\ \underline{\hat{F}}_{a2} \end{bmatrix}, \ \mathbf{X}_{\mathbf{e2}} = \begin{bmatrix} \underline{\hat{v}}_{e2} \\ \underline{\hat{F}}_{e2} \end{bmatrix}$$

$$\mathbf{A}^{\mathbf{PSm}} = \left(\mathbf{A}^{\mathbf{Pm}} \right)^{N}$$

$$\mathbf{A}^{\mathbf{PSem}} = \sum_{i=0}^{N-1} \left(\mathbf{A}^{\mathbf{Pm}} \right)^{i} \mathbf{A}^{\mathbf{Pem}}$$

$$\mathbf{A}^{\mathbf{PSme}} = \sum_{i=0}^{N-1} \mathbf{A}^{\mathbf{Pme}} \left(\mathbf{A}^{\mathbf{Pm}} \right)^{i}$$

$$\mathbf{A}^{\mathbf{PSe}} = \mathbf{A}^{\mathbf{Pe}} + \sum_{i=2}^{N} \left(\mathbf{A}^{\mathbf{Pe}} + \sum_{r=0}^{i-2} \mathbf{A}^{\mathbf{Pme}} \left(\mathbf{A}^{\mathbf{Pm}} \right)^{r} \mathbf{A}^{\mathbf{Pem}} \right)$$

Applying the above equation (4.54) and the transfer matrix relations of the fundamental connections 3 and 4 shown in Table 4.1 yields the whole transfer matrix relation for the symmetrical Langevin-type transducer as follows:

$$\begin{bmatrix} \mathbf{X}_{a3} \\ \underline{\hat{I}} \end{bmatrix} = \begin{bmatrix} \mathbf{A}^{\mathbf{PTm}} & \mathbf{A}^{\mathbf{PTem}} \\ \mathbf{A}^{\mathbf{PTme}} & \mathbf{A}^{\mathbf{PTe}} \end{bmatrix} \begin{bmatrix} \mathbf{X}_{e1} \\ \underline{\hat{U}} \end{bmatrix} \tag{4.55}$$

Where

$$\mathbf{X}_{e1} = \begin{bmatrix} \underline{\hat{v}}_{e1} \\ \underline{\hat{F}}_{e1} \end{bmatrix}, \quad \mathbf{X}_{a3} = \begin{bmatrix} \underline{\hat{v}}_{a3} \\ \underline{\hat{F}}_{a3} \end{bmatrix}$$

$$\mathbf{A}^{\mathbf{PTm}} = \mathbf{A}^{\mathbf{m}}\mathbf{A}^{\mathbf{PSm}}\mathbf{A}^{\mathbf{m}} = \begin{bmatrix} a_{11}^{PT} & a_{12}^{PT} \\ a_{21}^{PT} & a_{22}^{PT} \end{bmatrix}$$

$$\mathbf{A}^{\mathbf{PTem}} = \mathbf{A}^{\mathbf{m}}\mathbf{A}^{\mathbf{PSem}} = \begin{bmatrix} a_{13}^{PT} \\ a_{23}^{PT} \end{bmatrix}$$

$$\mathbf{A}^{\mathbf{PTme}} = \mathbf{A}^{\mathbf{PSme}}\mathbf{A}^{\mathbf{m}} = \begin{bmatrix} a_{31}^{PT} & a_{32}^{PT} \end{bmatrix}$$

$$\mathbf{A}^{\mathbf{PTe}} = \mathbf{A}^{\mathbf{PSe}} = a_{33}^{PT}$$

It should be pointed out that the matrix elements $a_{ij}^{PT}\ (i, j = 1,2,3)$ are functions of the material parameters, dimensional parameters and the vibration frequency of the transducer. Their explicit mathematical expressions are not given here because the expressions are very complex. They are derived automatically in the programs.

4.5.2 Problem Formulation of the Symmetrical Transducer without Loads

Optimization objectives For the resonant driven piezoelectric transducer, the free vibration amplitude and input power at the resonance operation are two important performance criteria. Here they are considered as objective functions. For a given exciting voltage, the vibration amplitude should be maximized. In the meantime, the input power of the transducer should be minimized. In the following, the mathematical descriptions of these two objectives will be derived from the above model. In order to predict vibration amplitude and current at resonance frequency, losses due to material properties are included in the model using complex moduli instead of real moduli.

For the transducer free at both sides, there exist the following boundary conditions

$$\underline{\hat{F}}_{e1}=0,\ \ \underline{\hat{F}}_{a3}=0 \tag{4.56}$$

Introducing (4.56) into (4.55) yield the following expressions

$$\underline{\hat{v}}_{e1} = -\frac{a_{23}^{PT}}{a_{21}^{PT}}\underline{\hat{U}} \tag{4.57}$$

$$\underline{\hat{v}}_{a3} = a_{11}^{PT}\,\underline{\hat{v}}_{e1} + a_{13}^{PT}\,\underline{\hat{U}} \tag{4.58}$$

$$\underline{\hat{I}} = a_{31}^{PT}\,\underline{\hat{v}}_{e1} + a_{33}^{PT}\,\underline{\hat{U}} \tag{4.59}$$

After inserting equation (4.57) into equation (4.58), the solution of $\underline{\hat{v}}_{a3}$ is obtained as follows:

$$\underline{\hat{v}}_{a3} = \left(a_{13}^{PT} - \frac{a_{11}^{PT} a_{23}^{PT}}{a_{21}^{PT}} \right) \underline{\hat{U}} \tag{4.60}$$

where

$$\mathrm{Im}\left[a_{13}^{PT} - \frac{a_{11}^{PT} a_{23}^{PT}}{a_{21}^{PT}} \right] = 0 \tag{4.61}$$

is the so-called characteristic equation representing the resonance of the transducer free at both sides.

When the transducer is driven by the voltage $\underline{\hat{U}} e^{j\Omega t}$, the vibration velocity $\underline{\hat{v}}_{a3}$ at resonance can be calculated from equation (4.60). Therefore, the vibration amplitude at the right side of the transducer can be obtained from

$$\underline{\hat{u}}_{a3} = \frac{1}{j\Omega} \left(a_{13}^{PT} - \frac{a_{11}^{PT} a_{23}^{PT}}{a_{21}^{PT}} \right) \underline{\hat{U}} \tag{4.62}$$

Equation (4.62) gives the expression of the first objective function, which should be maximized. As optimization methods applied in this work only handle minimization problems, the inverse of the above expression will be used as the objective function in the optimization problem. It is given by

$$f_1 = \left| \frac{a_{21}^{PT}}{a_{13}^{PT} a_{21}^{PT} - a_{11}^{PT} a_{23}^{PT}} \right| \frac{\Omega}{\hat{U}} \tag{4.63}$$

Introducing equation (4.57) into equation (4.59) yields the input current

$$\underline{\hat{I}} = \left(a_{33}^{PT} - \frac{a_{31}^{PT} a_{23}^{PT}}{a_{21}^{PT}} \right) \underline{\hat{U}} \tag{4.64}$$

Therefore the input electrical power (apparent power) for the harmonic vibration is

$$\hat{P}_a = \frac{1}{2} \hat{I} \hat{U} = \frac{\hat{U}^2}{2} \left| a_{33}^{PT} - \frac{a_{31}^{PT} a_{23}^{PT}}{a_{21}^{PT}} \right| \tag{4.65}$$

Equation (4.65) gives the expression of the second objective function. It is given by

$$f_2 = \hat{P}_a \tag{4.66}$$

Design variables The parameters that affect the performances of the transducer with specified resonance frequency and vibration mode have been shown in Table 4.2. There are two types of the parameters. The input voltage *U* and the dimensions of the transducer are of continuous type. The number of the piezoelectric rings and material of the backing rod, front rod and piezoelectric rings are of discrete type. In this work, the number of the piezoelectric rings *N* is assumed as one of the elements of the set {2, 4, 6}. The metal rods take one of 4 pre-specified material types (represented by corresponding density ρ, elastic modulus E and loss factor $tan\delta$). Not all parameters need to be determined by the optimization process. Some parameters can be given before optimization. Here the following parameters are considered as given quantities: the number of the piezoelectric rings $N \in \{2,4,6\}$, the input exciting voltage $\underline{\hat{U}}$ and the material type of the piezo-rings. As stated before**,** the inner diameter of the piezo-rings and the dimensions of the bolt will not be considered as design variables individually. The remaining design variables, which will be determined by the optimization process, are shown in Table 4.3. Table 4.4 gives material data.

Constraints The transducer should operate at the specified resonance frequency ω_r. Equation (4.61) gives the resonance condition of the transducer free at both sides. Under the condition that the values of the above given parameter are known, equation (4.61) describes an equality constraint g_1 with respect to the design variables L_b, h_p and the material type of the metal end rods. It is noted that there exist multi-mode solutions to equation (4.61) according to L_b and h_p for a given material type of the end rods. This can be illustrated with Fig. 4.16, which shows the locus of roots of equation (4.61) in the ranges $0.2\,\text{mm} \le h_p \le 5\,\text{mm}$ and $5\,\text{mm} \le L_b \le 200\,\text{mm}$ for the following given parameter values:

- the number of the piezoelectric rings N=2
- the material type of the backing and front rods: steel
- the piezoelectric material: PIC181
- the input voltage $\underline{\hat{U}} = 100V$
- the resonance frequency $f_r = 20kHz$

Table 4.3 Design variables for the symmetrical transducer

L_b:	Length of the metal parts
D_t:	Outer diameter of metal rods and piezo-rings
h_p:	Thickness of piezoelectric rings
Typ_b:	Material of metal end blocks (represented by corresponding density ρ, elastic modulus E and loss factor $tan\delta$)

Table 4.4 Material types and corresponding parameters

Material characteristics	Steel	Titanium	Aluminum bronze	Brass	PIC 181 (PI Ceramic Gmbh)
Density (ρ) $\left[\mathrm{kgm}^{-3}\right]$	7900	4430	8500	8400	7850
Elastic modulus (E) $\left[\times 10^{11}\,\mathrm{Nm}^{-2}\right]$	2.1	1.15	1.4	0.9	0.7
Loss factor($\tan\delta$) $\left[\times 10^{-4}\right]$	4.3	11.4	4.3	3.3	29
Charge constant (d_{33}) $\left[\times 10^{-12}\,\mathrm{mV}^{-1}\right]$	--	--	--	--	265
Voltage constant (g_{33}) $\left[\times 10^{-3}\,\mathrm{VmN}^{-1}\right]$	--	--	--	--	25.2
Relative permittivity $\left(\varepsilon_{33}^{T}/\varepsilon_0\right)$	--	--	--	--	1200
Binary String	00	01	10	11	
No.	1	2	3	4	

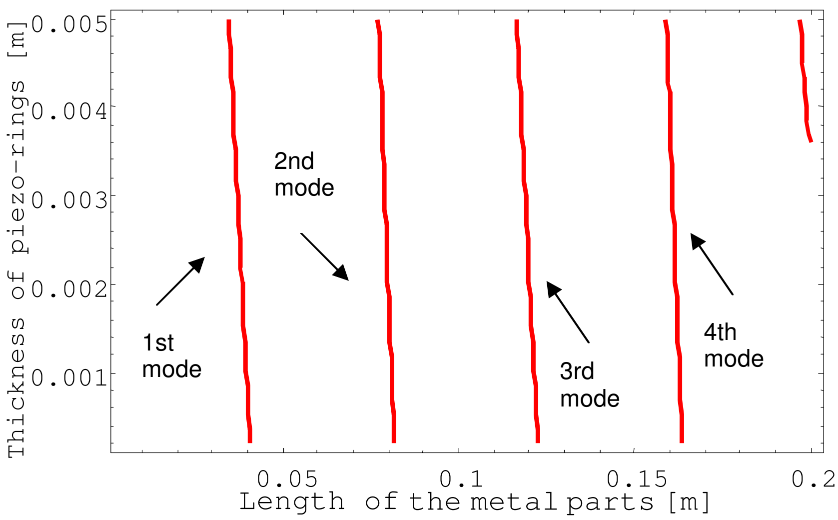

Fig. 4.16 Locus of roots of equation (4.61)

The locus of roots shown in Fig. 4.16 contains the first four vibration modes of the transducer. In order to obtain the solutions for a specified vibration mode (here the first vibration mode, also λ/2-mode) and to avoid the "switching" of the vibration modes during search, the search ranges of the variables h_p and L_b must be defined accordingly. The corresponding bounds of h_p and L are determined as follows: The lower bounds of h_p and L_b are specified by the designer. The upper bound of h_p is either set by the designer or obtained by searching the root of equation (4.61) corresponding to the lower bound of L_b. Similarly, the upper bound of L_b is determined by searching the root of equation (4.61) corresponding to the lower bound of h_p. As the derivative of the constraint function g_1 can not be found in a closed form analytical solution, the secant method is used to numerically search solutions of equation (4.61). The starting values must be picked carefully and tried sufficiently so that the secant method can find the solutions only for the λ/2 mode. The plot of solutions to equation (4.61) can be used for specifying the starting values for searching the upper bounds of L_b. For example, according to Fig. 4.16, the two starting values for searching the upper bound of L_b can be selected as 5 mm and 50 mm. Similarly, for the transducer with other material of metal end blocks and number of the piezo-rings, the corresponding locus of roots of equation (4.61) can be obtained and be used for specifying the starting values.

Considering design requirements for the electric driving device of the transducer, the maximum apparent input power $\hat{P}_{\max}$ and current $\hat{I}_{\max}$ need to be limited. The constraints can be concluded as follows:

$$g_1:\ \mathrm{Im}\left[a_{13}^{PT} - \frac{a_{11}^{PT} a_{23}^{PT}}{a_{21}^{PT}} \right] = 0, \text{ where } \Omega = \omega_r = 2\pi f_r$$

$$g_2:\ 10^{-6}\,\mathrm{VA} \le \hat{P}_a \le \hat{P}_{\max}$$

$$g_3:\ 10^{-6}\,\mathrm{A} \le \hat{I} \le \hat{I}_{\max}$$

$$g_4:\ Lb_D \le D_t \le Ub_D$$

$$g_5:\ Lb_h \le h_p \le Ub_h$$

$$g_6:\ Lb_L \le L_b \le Ub_L$$

The first constraint assures that the transducer operates at the specified resonance frequency f_r. The second and third constraints limit the input power and input current. $\hat{I}$ and $\hat{P}_a$ are given by the equations (4.64) and (4.65) respectively. Obviously, they must be positive quantities. Bounds of 10^{-6} VA and 10^{-6} A are imposed on $\hat{P}_a$ and $\hat{I}$ to avoid division by zero. The last three constraints give the region of search for the optimum. The values of Lb_D, Ub_D, $L\,b_h$, $U\,b_h$ and Lb_L are determined according to manufactory specifications and the requirements for the piezoelectric transducer. The value of the upper bound Ub_L is dynamic upper bound. It varies according to the selected material type of the end blocks. It is determined using the search method described before.

Denoting the variable vector $\mathbf{x} = (x_1, x_2, x_3, x_4) = (D_t, h_p, L_b, Typ_b)$, the objective vector $F(\mathbf{x}) = [f_1(\mathbf{x}), f_2(\mathbf{x})]$ and the constraint vector $G = [g_i, i = 1,...,6]$, the two-objective optimization problem is formulated as follows:

$$\begin{aligned} &Minimize \;\; F(\mathbf{x}) \\ &Subject\, to\; G \end{aligned} \tag{4.67}$$

4.5.3 Implementation of the Optimization Process

The optimization process can be divided into two levels. In the first level, optimization is performed individually for each given number *N* of piezoelectric rings. The respective non-dominated solutions are searched for. In the second level optimization, non-dominated solutions are searched again in the non-dominated solutions obtained in the first level optimization. Here only the first level optimization is performed. The second level optimization will be performed in chapter 5. For the optimization problem, the following parameter values are assumed:

- $f_r = 20$ kHz, λ/2 vibration mode
- $\hat{U} = 100$ V, $\hat{I}_{\max} = 4$ A
- $Lb_D = 8$ mm , $Ub_D = 50$ mm
- $Lb_h = 0.2$ mm, $Ub_h = 5$ mm
- $Lb_L = 5$ mm

For the given $\hat{U}$ and $\hat{I}_{\max}$, the maximum electrical input power $\hat{P}_{\max}$ is determined correspondingly. Therefore the constraint g_2 can be deleted. In the following, four MOEAs, namely MOGA, NSGA, SPEA and NSGA-II are first used to solve the constrained MOP of the transducer with 2 piezo-rings respectively. Then the most appropriate MOEA is selected from the four MOEAs according to their optimized results and is applied in optimization of the transducers with 4 and 6 piezo-rings.

Two strategies have been used to handle constraints. In MOGA, NSGA and SPEA, the constrained MOP is transferred into a non-constrained MOP by using the penalty function approach, whereas the constrain-domination concept is applied in NSGA-II.

In the penalty function approach, the constraints g_3 is normalized (converted into the "≥ „ form) as follows:

$$\begin{aligned} \underline{g}_{3u}(\mathbf{x}) &= \hat{I}_{\max}/\hat{I} - 1 \geq 0 \\ \underline{g}_{3l}(\mathbf{x}) &= \hat{I}/10^{-6}\,\mathrm{A} - 1 \geq 0 \end{aligned} \tag{4.68}$$

For each solution, the constraint violation for each constraint is calculated as follows:

$$\tilde{g}_i(\mathbf{x}) = \begin{cases} |\,\underline{g}_i(\mathbf{x})\,|, & if\ \underline{g}_i(\mathbf{x}) < 0 \\ 0, & if\ \underline{g}_i(\mathbf{x}) \geq 0 \end{cases} \qquad i = 3u, 3l \tag{4.69}$$

Then the new objective functions (penalized functions) are defined as follows:

$$\begin{aligned} \tilde{f}_1(\mathbf{x}) &= f_1(\mathbf{x}) + p_1[\tilde{g}_{3u}(\mathbf{x}) + \tilde{g}_{3l}(\mathbf{x})] \\ \tilde{f}_2(\mathbf{x}) &= f_2(\mathbf{x}) + p_2[\tilde{g}_{3u}(\mathbf{x}) + \tilde{g}_{3l}(\mathbf{x})] \end{aligned} \tag{4.70}$$

The penalty parameter p_1 and p_2 should be chosen so that both of $f_i(\mathbf{x})$ and $p_i[\tilde{g}_{3u}(\mathbf{x}) + \tilde{g}_{3l}(\mathbf{x})]$ have the same order of magnitude, where $i = 1, 2$. Many static and dynamic strategies can be used to choose penalty parameters. Here static values of penalty parameters are used. In order to determine penalty parameters, the optimization was first performed for a small number of generations. The values of penalty parameters were then determined according to the obtained values of the original objective functions and constraint violations. Here $p_1 = 2\times10^2$ and $p_2 = 4\times10^4$ are chosen.

The values of two penalty parameters must be chosen properly so that the algorithms work well. If the penalty parameter is not chosen adequately, Pareto-optimal solutions may not be found or a poor distribution of solutions may be occur. In order to avoid choosing any explicit penalty parameter, the constrain-domination concept instead of penalty function approach is used in NSGA-II.

Four MOEAs here used differ in the way each solution is evaluated and selected to fill the mating pool for offspring production. The rest of the algorithms (crossover and mutation operations) are the same. After the mating pool is filled up, a crossover operator and a mutation operator are applied to the strings of the mating pool to create new solutions.

In each MOEA, a mixed coding scheme with a mixed crossover and a mixed mutation operator is used. A mixed coding (chromosome) for a typical design (individual or solution) of the symmetric transducer with 4 design variables is as follow:

$$\underbrace{2.0}_{D_t}\quad \underbrace{01}_{Typ_b}\quad \underbrace{15.8}_{h_p}\quad \underbrace{37.6}_{L_b}$$

The first variable D_t is a continuous variable, which takes a real value in the range of $8\text{mm} \leq D_t \leq 50\text{mm}$. The second variable Typ_b is a discrete variable, which take a two-bit binary string representing a set values of ρ, E and $\tan\delta$ of a specified material type. The strings and corresponding material types are shown in Table 4.4. The third variable h_p is a continuous variable, which takes a value in the range of $0.2\text{mm} \le h_p \le 5\text{mm}$. The last variable L_b is continuous type, which takes a value in the range of $5\text{mm} \le L_b \le Ub_L$. The Ub_L is dynamic upper bound for the variable L_b. It varies from one generation to another and its value is determined by solving the equality constraint g_1 using the secant method.

In each generation, two chromosomes are selected from the mating pool randomly. A blended crossover (BLX-α) operation is performed on the continuous parts D_t and h_p. For the discrete part Typ_b a single-crossover is used. A bit-wise mutation is only performed on the discrete part. The value of the design variable L_b is determined by solving the equality constraint g_1 using the secant method. Hereto, one offspring solution consisting of 4 variable values has been obtained. Similarly, the other offspring solution can also be obtained.

Table 4.5 Parameters and techniques that are used in the four MOEAs.

Parameters and techniques	*MOEAs*			
	MOGA	NSGA	SPEA	NSGA-II
Constraint handling strategy	Penalty function	Penalty function	Penalty function	Constrain - domination
Approach to find non-dominated set	Continuous updated method	Continuous updated method	Continuous updated method	Continuous updated method
Fitness assignment	Pareto ranking (the rank of a certain individual corresponds to the number of individuals in the current population by which it is dominated) and the shared fitness	Pareto ranking (Goldberg's ranking) and the shared fitness	Pareto-based method (the fitness is assigned according to the strength of the individual)	Pareto ranking (Goldberg's ranking) and the shared fitness
Niching technique	Fitness sharing in objective space	Fitness sharing in parameter space	Pareto-based method in objective space	Fitness sharing in parameter space
Elite – preserving	No	No	Yes	Yes
Selection operation	SRWS	SRWS	Binary tournament selection	SRWS and the crowded tournament selection
Crossover probability	0.9	0.9	0.9	0.9
Mutation probability	0.5	0.5	0.5	0.5
δ_{share}	0.5	0.184	--	0.184
Population size	50	50	50	50

Table 4.5 gives some important parameters and techniques that are used in the four MOEAs. It is pointed out that in NSGA-II the crowded tournament selection operator here is only used in the process of creating the new population P_{t+1} of size N from the combined population R_t of size $2N$ consisting of the parent population P_t and the offspring population Q_t. The SRWS operator is still used to select the solutions in P_{t+1} into the mating pool.

Optimization is performed first for the transducer with 2 piezo-rings using the above four MOEAs, respectively. Figs. 4.17 to 4.20 show the respective non-dominated solutions in objective spaces after 300 generations. Tables 4.6 to 4.9 give the corresponding values of design variables and objective functions for the non-dominated solutions.

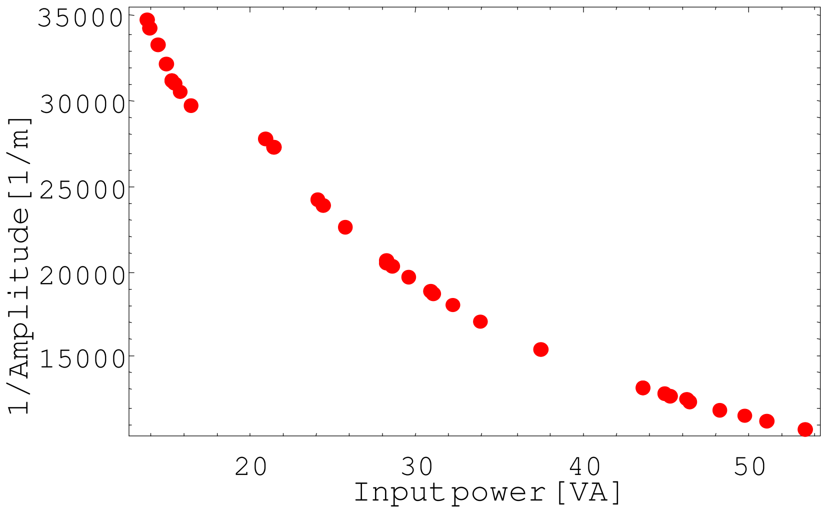

Fig. 4.17 Non-dominated solutions obtained by using MOGA for the symmetrical transducer with 2 piezo-rings

Table 4.6 Values of design variables and objective functions for non-dominated solutions obtained by using MOGA for the symmetrical transducer with 2 piezo-rings

Design	D_t [mm]	Typ_b	h_p [mm]	L_b [mm]	$\hat{u}_{a3}$ [µm]	$\hat{P}_a$ [VA]
1	8.	2	0.2	63.4	33.44	16.23
2	8.	4	0.2	40.7	92.19	53.43
3	8.	4	0.3	40.5	88.09	51.01
4	8.	4	0.4	40.5	85.94	49.77
5	8.	2	0.4	63.	32.64	15.59
6	8.	4	0.4	40.4	83.22	48.2
7	8.	4	0.5	40.2	80.15	46.42
8	8.	4	0.5	40.2	79.82	46.24
9	8.	4	0.6	40.1	78.12	45.26
10	8.	4	0.6	40.1	77.57	44.95
11	8.	2	0.6	62.7	32.14	15.33
12	8.	4	0.7	40.	75.29	43.63

Table 4.6 continued

Design	D_t [mm]	Typ_b	h_p [mm]	L_b [mm]	$\hat{u}_{a3}$ [µm]	$\hat{P}_a$ [VA]
13	8.	4	0.7	40.	75.14	43.55
14	8.	2	0.7	62.6	31.91	15.22
15	8.	2	0.7	62.5	31.85	15.19
16	8.	2	1.	62.	30.94	14.76
17	8.	4	1.5	39.	58.06	33.68
18	8.	2	1.4	61.4	29.91	14.27
19	8.	4	1.2	39.4	64.41	37.42
20	8.	2	1.9	60.6	28.61	13.66
21	8.	2	1.7	60.9	29.	13.85
22	8.	4	1.7	38.8	55.3	32.14
23	8.	4	1.9	38.5	52.84	30.71
24	8.	4	2.2	38.1	49.09	28.51
25	8.	4	1.8	38.6	53.15	30.9
26	8.	4	2.2	38.1	48.48	28.17
27	8.	4	2.	38.3	50.68	29.49
28	8.	4	2.2	38.1	48.38	28.14
29	8.	4	2.6	37.5	44.1	25.65
30	8.	4	3.	37.1	41.18	23.96
31	8.	4	2.9	37.2	41.77	24.31
32	8.1	4	3.6	36.3	36.54	21.25
33	8.1	4	3.7	36.1	35.83	20.84
34	8.1	4	3.6	36.3	36.5	21.24

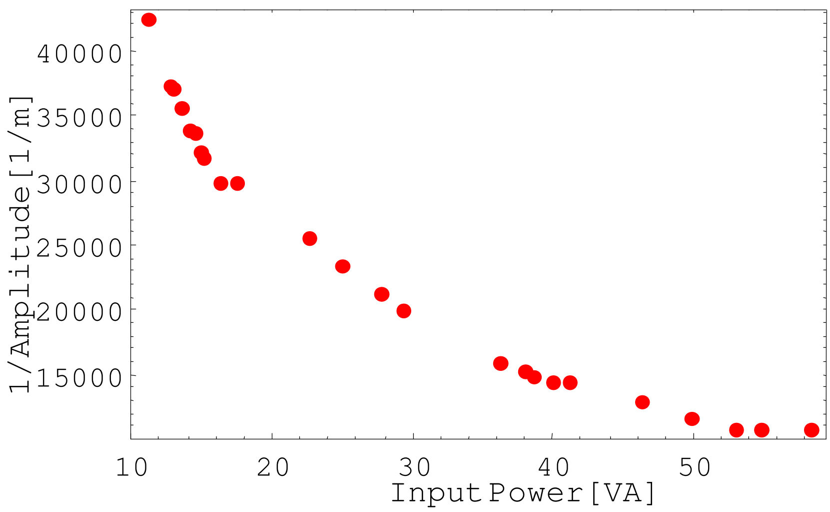

Fig. 4.18 Non-dominated solutions obtained by using NSGA for the symmetrical transducer with 2 piezo-rings

Table 4.7 Values of design variables and objective functions for non-dominated solutions obtained by using NSGA for the symmetrical transducer with 2 piezo-rings

Design	D_t [mm]	Typ_b	h_p [mm]	L_b [mm]	$\hat{u}_{a3}$ [µm]	$\hat{P}_a$ [VA]
1	8.	2	0.2	63.4	33.44	16.23
2	8.	2	4.4	56.5	23.54	11.13
3	8.	4	0.2	40.6	91.49	53.01
4	8.	4	1.	39.7	69.06	39.93
5	8.	4	1.1	39.6	66.6	38.49
6	8.	4	1.3	39.3	62.65	36.2
7	8.	4	3.2	36.8	39.13	22.48
8	8.	2	1.6	61.1	29.44	13.98
9	8.	2	2.7	59.3	26.73	12.68
10	8.	4	0.4	40.4	85.52	49.81
11	8.	2	2.1	60.3	28.09	13.42
12	8.	2	2.7	59.4	26.84	12.84
13	8.1	2	0.9	62.3	31.35	15.1
14	8.1	4	1.1	39.4	64.75	37.99
15	8.1	2	1.	62.	30.92	14.93
16	8.1	4	2.8	37.3	42.4	24.89
17	8.1	4	2.1	38.2	49.63	29.27
18	8.1	4	0.2	40.7	92.19	54.76
19	8.1	4	0.9	39.7	69.27	41.07
20	8.1	4	2.4	37.9	46.75	27.76
21	8.1	2	1.5	61.2	29.58	14.55
22	8.2	4	0.7	40.1	76.67	46.32
23	8.3	2	0.2	63.4	33.44	17.53
24	8.4	4	0.2	40.7	92.19	58.38

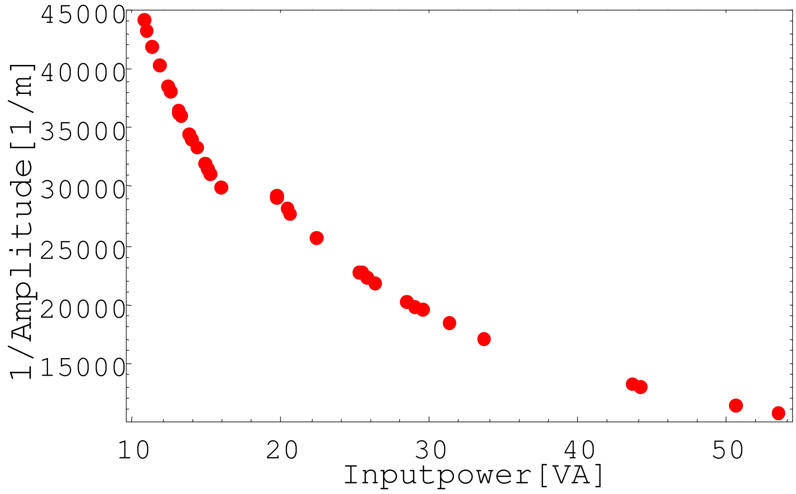

Fig. 4.19 Non-dominated solutions obtained by using SPEA for the symmetrical transducer with 2 piezo-rings

Table 4.8 Values of design variables and objective functions for non-dominated solutions obtained by using SPEA for the symmetrical transducer with 2 piezo-rings

Design	D_t [mm]	Typ_b	h_p [mm]	L_b [mm]	$\hat{u}_{a3}$ [μm]	$\hat{P}_a$ [VA]
1	8.	2	0.3	63.2	33.12	15.89
2	8.	2	0.7	62.6	31.92	15.19
3	8.	2	1.4	61.5	29.94	14.22
4	8.	2	1.6	61.	29.26	13.89
5	8.	2	5.	55.5	22.58	10.66
6	8.	4	0.2	40.7	92.19	53.43
7	8.	4	1.5	39.	58.08	33.55
8	8.	2	0.8	62.4	31.55	15.
9	8.	4	3.8	36.1	35.39	20.28
10	8.	4	0.3	40.5	87.19	50.47
11	8.	4	4.	35.8	34.09	19.52
12	8.	4	0.7	40.1	76.27	44.11
13	8.	4	4.	35.8	34.21	19.59
14	8.	2	4.7	56.	23.05	10.89
15	8.	2	1.	62.1	31.03	14.75
16	8.	2	1.8	60.8	28.9	13.72
17	8.	2	3.7	57.6	24.68	11.68
18	8.	4	3.7	36.1	35.81	20.53
19	8.	2	4.2	56.8	23.8	11.26
20	8.	4	2.5	37.7	45.56	26.25
21	8.	4	2.1	38.3	50.11	28.9
22	8.	2	3.1	58.6	25.92	12.28
23	8.	4	1.8	38.6	53.98	31.16
24	8.	4	2.7	37.5	43.76	25.2
25	8.	4	2.2	38.1	49.01	28.26
26	8.	2	0.9	62.2	31.13	14.8
27	8.	4	0.7	40.	75.12	43.45
28	8.	4	2.6	37.6	44.7	25.75
29	8.	4	2.7	37.5	43.84	25.25
30	8.	4	2.	38.3	50.9	29.37
31	8.	2	2.4	59.8	27.5	13.04
32	8.	2	2.4	59.7	27.31	12.95
33	8.	4	3.3	36.7	38.89	22.35
34	8.	2	3.	58.8	26.17	12.4
35	8.	2	2.3	59.9	27.59	13.09

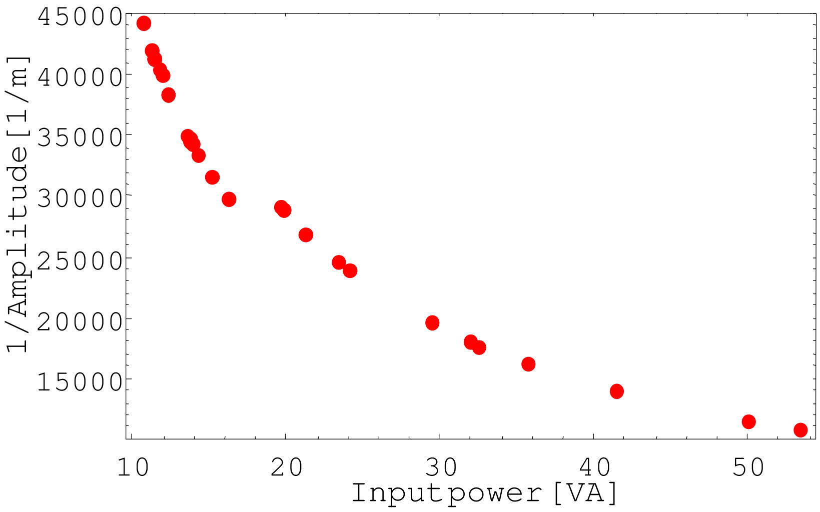

Fig. 4.20 Non-dominated solutions obtained by using NSGA-II for symmetrical transducer with 2 piezo-rings

Table 4.9 Values of design variables and objective functions for non-dominated solutions obtained by using NSGA-II for the symmetrical transducer with 2 piezo-rings

Design	D_t [mm]	Typ_b	h_p [mm]	L_b [mm]	$\hat{u}_{a3}$ [µm]	$\hat{P}_a$ [VA]
1	8.	2	0.2	63.4	33.44	16.23
2	8.	2	1.4	61.4	29.82	14.16
3	8.	2	3.	58.7	26.05	12.34
4	8.	4	0.3	40.5	86.43	50.02
5	8.	4	3.6	36.4	37.04	21.26
6	8.	2	0.8	62.4	31.61	15.03
7	8.	2	1.8	60.8	28.84	13.69
8	8.	2	1.9	60.7	28.69	13.62
9	8.	2	2.	60.5	28.43	13.49
10	8.	2	3.6	57.9	25.01	11.84
11	8.	2	4.	57.1	24.2	11.45
12	8.	4	0.2	40.7	92.19	53.43
13	8.	4	0.8	39.8	71.56	41.37
14	8.	4	1.3	39.3	61.75	35.68
15	8.	4	1.6	38.8	56.32	32.52
16	8.	4	1.7	38.7	55.15	31.84
17	8.	4	2.	38.3	50.89	29.36
18	8.	4	2.9	37.2	41.77	24.03
19	8.	4	3.1	37.	40.54	23.31
20	8.	4	4.	35.8	34.43	19.72
21	8.	4	4.	35.8	34.17	19.57
22	8.	2	1.7	60.9	29.07	13.8
23	8.	2	1.7	60.8	28.97	13.75
24	8.	2	3.	58.7	26.02	12.33
25	8.	2	3.1	58.7	26.01	12.33

Table 4.9 continued

Design	D_t [mm]	Typ_b	h_p [mm]	L_b [mm]	$\hat{u}_{a3}$ [μm]	$\hat{P}_a$ [VA]
26	8.	2	4.1	57.1	24.12	11.41
27	8.	2	4.1	57.	24.1	11.4
28	8.	2	4.2	56.8	23.83	11.27
29	8.	2	5.	55.5	22.58	10.66
30	8.	4	4.	35.8	34.26	19.62
31	8.	2	3.7	57.6	24.7	11.69

In the following, the above four MOEAs will be evaluated in terms of the relative convergence of the non-dominated solutions, the diversity of the non-dominated solutions, the computing cost and the ability of finding non-dominated solutions. Then the most appropriate MOEA will be selected and used to solve the optimization problems of the transducer with 4 and 6 piezo-rings.

In order to compare the optimized results visually, the non-dominated solutions obtained above are plotted again according to the same axes (see Fig. 4.21). Based on Fig. 4.21, however, it is difficult to identify which algorithm is better in terms of the convergence of non-dominated solutions. Therefore, the set coverage metric C (A, B) has been applied, see the definition of C (A, B) in chapter 3. Table 4.10 gives the calculated values of the set coverage metric C (A, B), where A represents a non-dominated set obtained by using a MOEA in the column and B represents a non-dominated set obtained by using a MOEA in the row correspondingly.

Since no member of the non-dominated set NSGA-II is dominated by the members of the others, the set NSGA-II has a better convergence to the Pareto-optimal front than the rest relatively. Compared with SPEA, however, NSGA-II has not an obvious advantage in terms of the convergence because the metric C(NSGA-II, SPEA) is very small.

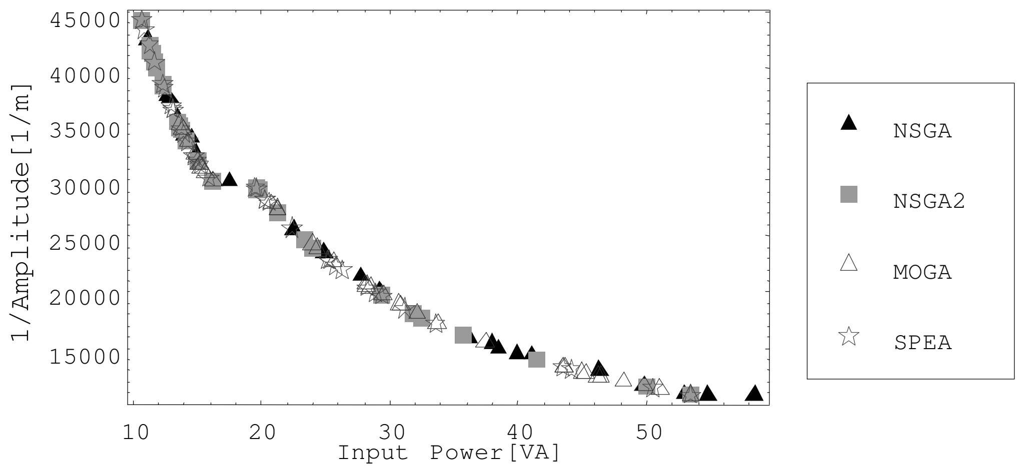

Fig. 4.21 Non-dominated solutions in objective space obtained by using four MOEAs after 300 generations for the symmetrical transducer with 2 piezo-rings

Table 4.10 The values of metrics C(A,B) for non-dominated solutions obtained by four MOEAs after 300 generations for the symmetrical transducer with 2 piezo-rings

A \ B	NSGA	NSGA-II	MOGA	SPEA
NSGA	**-**	**0**	**0**	0
NSGA-II	**4/24**	**-**	**4/34**	1/35
MOGA	**6/24**	**0**	**-**	0
SPEA	4/24	0	5/34	-

Table 4.11 Values of metrics SP and DI and the computation cost for non-dominated solutions obtained by four MOEAs after 300 generations for the symmetrical transducer with 2 piezo-rings

Metric	NSGA	NSGA-II	MOGA	SPEA
SP	1095	683	398	479
DI	31637	33434	24106	33434
Computation time [s]	1714	14656	5797	5146
Number of the non-dominated solutions	24	31	34	35

In order to compare the generated solutions in terms of the diversity, the metric SP and DI, which evaluate the uniformity of distribution of solutions and the extent of spread of solutions respectively, are applied. Table 4.11 gives the calculated values of the metrics. According to the definitions of SP and DI, the more uniformly the solutions are distributed, the smaller the metric SP; the larger the value of the metric DI is, the larger the extent of spread of the solutions. It is obvious that the algorithms MOGA and SPEA perform better than the algorithms NAGA and NSGA-II in terms of the uniformity of distribution of solutions in objective space, whereas the non-dominated set obtained by NSGA and SPEA has the largest extent of spread relatively.

The reason that the algorithms MOGA and SPEA perform better than the algorithms NAGA and NSGA-II in terms of the uniformity of distribution of solutions in objective space is that the former performs the niching strategy in the objective variable space, whereas the latter performs the niching strategy in the design variable (parameter) space. The better diversity of the solutions in objective space is expected if the niching strategy is performed in objective space. In general, a good diversity of the solutions in objective space may not result in a good diversity of the solutions in design variable space, and vice versa. The choice between decision-space niching or objective-space niching depends on what is desired in the obtained non-dominated set. If diversity in decision variable values is emphasized, decision-space niching should be performed. On the other hand, if diversity in objective function values is emphasized, objective-space niching should be performed.

Table 4.11 also shows the computation time and the number of the non-dominated solutions after 300 generations using the four MOEAs. Obviously, the computation cost of the NSGA is the lowest and the computation cost of NSGA-II is the largest. Although the short computation time is always expected, the closeness to the Pareto-optimal front and the diversity of non-dominated solutions are more important in the optimal design of transducers. In terms of finding non-dominated solutions, SPEA shows a better performance.

According to above results of the comparison, it is concluded that SPEA show the best overall performance for the two-objective optimization problem of the symmetrical transducer. Therefore, it has been applied for optimization of the symmetrical transducer with 4 and 6 piezoelectric rings, respectively. Figs. 4.22 and 4.23 show the respective non-dominated solutions after 300 generations for the transducer with 2 and 4 piezo-rings. Tables 4.12 and 4.13 give the values of the design variables and objective functions for the non-dominated solutions.

After all non-dominated solutions for the transducer with 2, 4 and 6 piezo-rings are obtained, the second-level optimization can be performed. This will be described in chapter 5.

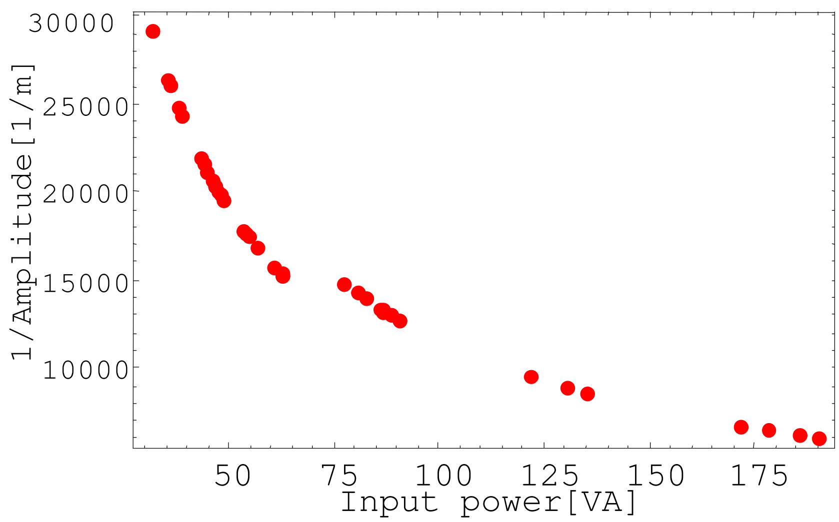

Fig. 4.22 Non-dominated solutions obtained by using SPEA for the symmetrical transducer with 4 piezo-rings

Table 4.12 Values of design variables and objective functions for the non-dominated solutions obtained by using SPEA for the symmetrical transducer with 4 piezo-rings

Design	D_t [mm]	Typ_b	h_p [mm]	L_b [mm]	$\hat{u}_{a3}$ [µm]	$\hat{P}_a$ [VA]
1	8.	2	5.	47.3	33.81	31.37
2	8.	2	3.9	50.8	37.88	35.49
3	8.	2	3.8	51.2	38.4	36.02
4	8.	2	3.4	52.5	40.22	37.84
5	8.	2	3.2	53.1	41.12	38.74
6	8.	2	2.3	56.1	46.22	43.75
7	8.	4	1.9	36.2	71.75	82.45
8	8.	2	1.9	57.5	49.14	46.61
9	8.	2	2.4	55.7	45.5	43.07
10	8.	4	2.1	35.7	67.2	77.11
11	8.	4	1.7	36.6	76.63	88.26
12	8.	2	2.2	56.6	47.21	44.75
13	8.	2	1.9	57.4	48.92	46.42
14	8.	4	1.9	36.	70.16	80.63
15	8.	2	1.9	57.5	49.14	46.64
16	8.	2	1.7	58.	50.28	47.75
17	8.	2	2.	57.1	48.27	45.8
18	8.	4	1.6	36.8	78.64	90.66
19	8.	4	0.8	39.	116.51	135.01
20	8.	4	1.7	36.5	75.22	86.64
21	8.	4	0.3	40.1	153.58	178.24
22	8.	4	0.4	40.	147.79	171.49
23	8.	2	1.1	60.2	56.17	53.48
24	8.	2	1.	60.5	56.83	54.11
25	8.	2	0.9	60.6	57.22	54.5
26	8.	4	0.9	38.5	105.04	121.66
27	8.	2	0.2	63.	65.57	62.85
28	8.	2	0.2	63.	65.41	62.67
29	8.	4	0.3	40.2	159.7	185.41
30	8.	4	0.8	38.8	112.31	130.16
31	8.	2	0.2	62.9	65.07	62.27
32	8.	4	0.2	40.3	163.97	190.41
33	8.	2	1.8	57.8	49.83	47.35
34	8.	2	0.7	61.2	59.22	56.44
35	8.	4	1.8	36.4	74.59	85.95
36	8.	4	1.7	36.5	74.81	86.21
37	8.	2	1.6	58.4	51.25	48.75
38	8.	2	0.4	62.4	63.22	60.37

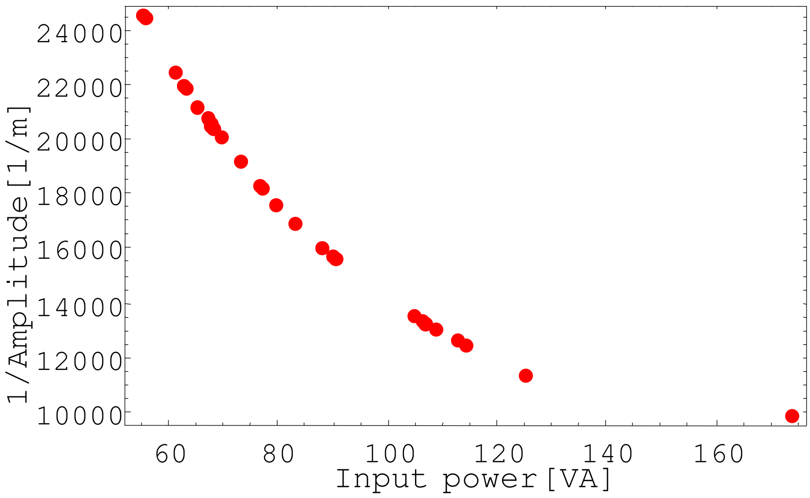

Fig. 4.23 Non-dominated solutions obtained by using SPEA for the symmetrical transducer with 6 piezo-rings

Table 4.13 Values of design variables and objective functions for the non-dominated solutions obtained by using SPEA for the symmetrical transducer with 6 piezo-rings

Design	D_t [mm]	Typ_b	h_p [mm]	L_b [mm]	$\hat{u}_{a3}$ [µm]	$\hat{P}_a$ [VA]
1	8.	2	5.	39.	40.75	55.03
2	8.	2	5.	39.1	40.91	55.28
3	8.	2	4.1	43.4	45.44	62.48
4	8.	2	3.9	44.7	47.09	65.04
5	8.	2	4.3	42.6	44.5	61.02
6	8.	2	4.1	43.4	45.5	62.58
7	8.	2	4.1	43.6	45.73	62.94
8	8.	2	3.7	45.5	48.17	66.72
9	8.	2	3.6	45.9	48.71	67.56
10	8.	2	3.6	46.2	49.09	68.15
11	8.	2	3.5	46.7	49.84	69.29
12	8.	2	3.6	45.7	48.45	67.16
13	8.	2	3.6	45.8	48.6	67.39
14	8.	2	3.1	48.2	52.15	72.83
15	8.	2	2.6	50.7	56.58	79.5
16	8.	2	2.9	49.6	54.54	76.45
17	8.	2	2.8	49.7	54.74	76.74
18	8.	2	1.	59.	79.09	112.57
19	8.	2	2.4	51.9	58.92	83.02
20	8.	2	2.1	53.3	62.19	87.89
21	8.	2	1.2	57.7	74.58	106.06
22	8.	4	1.4	35.7	101.1	173.83
23	8.	2	1.2	57.9	75.1	106.85
24	8.	2	2.	53.9	63.43	89.76
25	8.	2	0.9	59.2	80.14	114.16
26	8.	2	2.	54.	63.78	90.28
27	8.	2	1.3	57.5	73.72	104.85
28	8.	2	1.1	58.2	76.32	108.64
29	8.	2	0.6	61.	87.47	124.82

4.6 Optimization of Langevin-type Transducers with a Stepped Horn

In ultrasonic machining and bonding, it is generally required that piezoelectric transducers have a working frequency between 10 kHz and 100 kHz and in the meantime have a large vibration amplitude (10 to 50 micros at 20 kHz). It is difficult to achieve such large vibration amplitude using the transducer configurations described in sections 4.5. In order to magnify the vibration amplitude, the front block is usually designed as a linear (cone), exponential or stepped acoustic horn (sonotrode). Fig. 4.24 shows the three mostly used forms of horns. Here, a stepped-horn transducer is studied.

Fig. 4.25(a) shows a typical configuration of a Langevin-type transducer with a stepped horn. It has been shown that the impedance transformation ration in the case of both L_{f1} and L_{f2} being λ/4 long is given by $\left(A_{f1}/A_{f2}\right)^2$, and the amplitude transformation ratio is given by $\left(A_{f1}/A_{f2}\right)$. A_{f1} and A_{f2} are the profile areas of the input side and output side of the horn. The larger the ratio is, the larger is the vibration amplitude at the end of the horn [BPF91]. As seen before, in addition to the vibration amplitude there exist other important performance criteria. Therefore, multiple design goals should be considered.

4.6.1 Derivation of the Whole Transfer Matrix

The whole transducer is considered as a connection of a piezoelectric stack element and three mechanical elements in series, where the stepped horn consists of two mechanical elements. Fig. 4.25(b) gives four-pole network element description. Similarly, applying equation (4.94) and the transfer matrix relations of the fundamental connection 1, 3 and 4 shown in Table 4.1, the whole transfer matrix relation for this transducer can be written as follows:

$$\begin{bmatrix} \mathbf{X_{a4}} \\ \underline{\hat{I}} \end{bmatrix} = \begin{bmatrix} \mathbf{A_w^{Hm}} & \mathbf{A_w^{Hem}} \\ \mathbf{A_w^{Hme}} & \mathbf{A_w^{He}} \end{bmatrix} \begin{bmatrix} \mathbf{X_{e1}} \\ \underline{\hat{U}} \end{bmatrix} \tag{4.71}$$

where

$$\mathbf{X}_{e1} = \begin{bmatrix} \underline{\hat{v}}_{e1} \\ \underline{\hat{F}}_{e1} \end{bmatrix}, \quad \mathbf{X}_{a4} = \begin{bmatrix} \underline{\hat{v}}_{a4} \\ \underline{\hat{F}}_{a4} \end{bmatrix}$$

$$\mathbf{A}_w^{Hm} = \mathbf{A}_4^m \mathbf{A}_3^m \mathbf{A}_2^{PSm} \mathbf{A}_1^m = \begin{bmatrix} a_{11}^H & a_{12}^H \\ a_{21}^H & a_{22}^H \end{bmatrix}$$

$$\mathbf{A}_w^{Hem} = \mathbf{A}_4^m \mathbf{A}_3^m \mathbf{A}_2^{PSem} = \begin{bmatrix} a_{13}^H \\ a_{23}^H \end{bmatrix}$$

$$\mathbf{A}_w^{Hme} = \mathbf{A}_2^{PSme} \mathbf{A}_1^m = \begin{bmatrix} a_{31}^H & a_{32}^H \end{bmatrix}$$

$$\mathbf{A}_w^{He} = \mathbf{A}^{PSe} = a_{33}^H$$

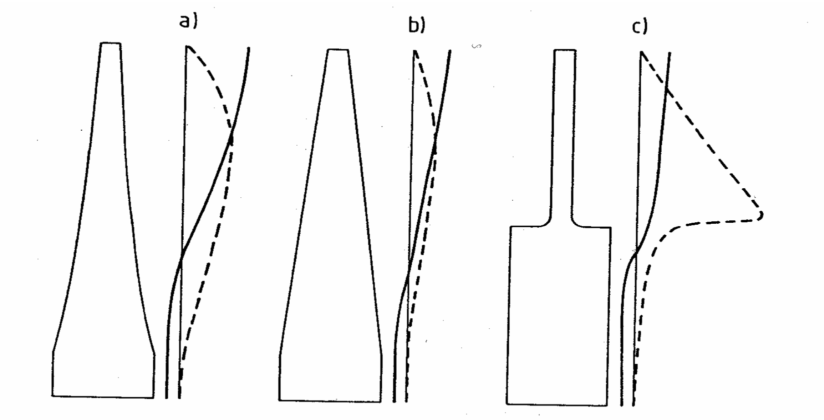

Fig. 4.24 Shape (-), vibration amplitude (-) and strain (--) on three horns: a) exponential horn, b) cone horn, c) stepped horn

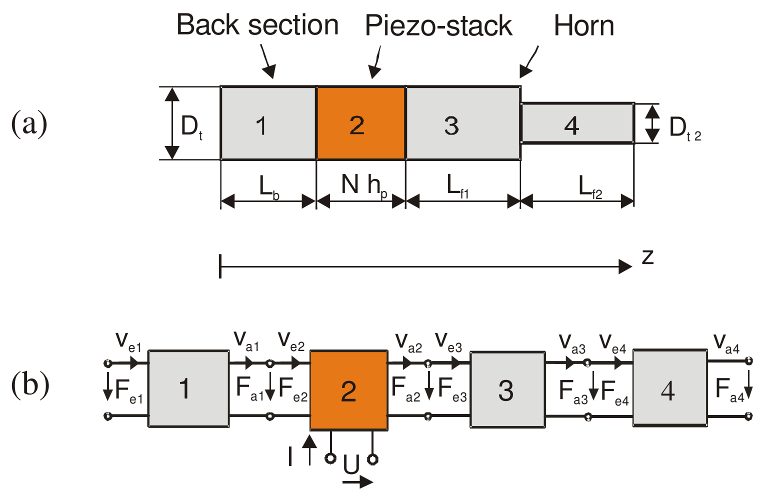

Fig. 4.25 Langevin transducer with a stepped horn (a) typical configuration (b) four-pole element descriptions

Similarly, the detailed expressions of the matrix elements a_{ij}^{H} $(i, j = 1, 2, 3)$ are not given here because the expressions are very complex. They are derived automatically in the programs.

4.6.2 Problem Formulation of Transducers without Loads

In this section, the objective functions, design variables and constraints are defined. The multi-objective optimization for the transducer at free vibration is discussed.

Optimization objectives Similarly, the free vibration amplitude and input electrical power at the resonance operation are considered as objective functions. For a given exciting voltage, the former should be maximized and the latter should be minimized. By analogy with equation (4.63), the first optimization objective, which represents the inverse of the vibration amplitude at resonance, is formulated as follows

$$f_1 = \left| \frac{a_{21}^H}{a_{13}^H a_{21}^H - a_{11}^H a_{23}^H} \right| \frac{\Omega}{\hat{U}} \tag{4.72}$$

According to equations (4.64) and (4.65) the expressions of the input current $\hat{I}$ and apparent power $\hat{P}_a$ for this problem are given by

$$\hat{I} = \left| a_{33}^H - \frac{a_{31}^H a_{23}^H}{a_{21}^H} \right| \hat{U} \tag{4.73}$$

$$\hat{P}_a = \frac{1}{2} \hat{I}\hat{U} = \frac{\hat{U}^2}{2} \left| a_{33}^H - \frac{a_{31}^H a_{23}^H}{a_{21}^{PT}} \right| \tag{4.74}$$

Equation (4.74) gives the expression of the second objective function. It is given by

$$f_2 = \hat{P}_a \tag{4.75}$$

Design variables The parameters which affect the performances of the transducer with a stepped horn are shown in Table 4.14. Similarly, there are two types of parameters. *N* and material are the discrete type. The others are continuous type. The inner diameter of piezo-rings and the dimensions of the bolt will not be considered as design variables individually. It is also assumed that the piezoelectric transducer has been pre-stressed optimally. In this problem, the following parameters are then considered as design variables:

The dimensional parameters: D_t, D_{t2} ($\zeta = D_{t2} / D_t$), L_b, h_p, L_{f1}, L_{f2}

The material type: Typ_b (ρ_b, E_b , $tg\delta_b$) and Typ_f (ρ_f, E_f , $tg\delta_f$)

The rest is considered as given quantities. *N* can take one of the elements of the set {2, 4, 6}.

Constraints On the analogy of equation (4.61), the resonance condition for the transducer with a stepped horn free at both sides is given by

$$\mathrm{Im}\left[a_{13}^H - \frac{a_{11}^H a_{23}^H}{a_{21}^H} \right] = 0 \tag{4.76}$$

The equation (4.76) describes an equality constraint for the design variables. Similarly, the secant method will be used in searching the solutions to equation (4.76). As there are multi-mode solutions to equation (4.76) in the specified variable ranges, the bounds of the variables and two starting points must be picked carefully using similar method described before so that only the solutions for the λ/2 mode are found.

Table 4.14 Parameters that affect the performances of the transducer

$\underline{\hat{U}}$: Input voltage
L_b: Length of back blocks
L_{f1}: Length of the first part of horns
L_{f2}: Length of the second part of horns
D_t: Outer diameter of back blocks, input end of horns and piezo-rings
D_{t2}: Outer diameter of the output end of horns
h_p: Thickness of piezoelectric rings
D_i: Inner diameter of piezo-rings and outer diameter of bolts
L_{bt}: Length of bolts

N: Number of piezoelectric disks or rings
Typ_b: Material of back blocks
Typ_f: Material of horns
Typ_p: Material of piezo-rings

In addition to equality constraint, there exist design requirements for electrical quantities and dimensional quantities. All constraints for this optimization problem can be concluded as follows:

g1: $\mathrm{Im}\left[a_{13}^H - \frac{a_{11}^H a_{23}^H}{a_{21}^H}\right] = 0$, where $\Omega = \omega_r = 2\pi f_r$

g2: $10^{-6}\,\mathrm{VA} \le \hat{P}_a \le \hat{P}_{\max}$

g3: $10^{-6}\,\mathrm{A} \le \hat{I} \le \hat{I}_{\max}$

g4: $D_{tl} \le D_t \le D_{tu}$

g5: $\zeta_l \le \zeta \le \zeta_u$

g6: $L_{bl} \le L_b \le L_{bu}$

g7: $h_{pl} \le h_p \le h_{ph}$

g8: $L_{f1l} \le L_{f1} \le L_{f1h}$

g9: $L_{f2l} \le L_{f2} \le L_{f2h}$

Similarly, the first constraint assures that the transducer operates at the specified resonance frequency f_r. The second and third constraints limit the input power and input current. Obviously, they must be positive quantities. Bounds of 10^{-6} VA and 10^{-6} A are imposed on $\hat{P}_a$ and $\hat{I}$ to avoid division by zero. The last six constraints give the region of search for the optimum. The values of the lower bounds and upper bounds of D_t, ζ, L_b and h_p as well as the values of lower bounds of L_{f1} and L_{f2} are determined according to manufactory specifications and the requirements for the piezoelectric transducer. The upper bounds L_{f1h} and L_{f2h} are dynamic upper bounds. They vary according to the selected material type of the end blocks and the values of other continuous design variables. They are searched using the secant method in the process of optimization.

Denoting the variable vector $\mathbf{x} = (x_1, x_2, x_3, x_4, x_5, x_6, x_7, x_8) = (D_t, \zeta, L_b, Typ_b, Typ_f, h_p, L_{f1}, L_{f2})$, the objective vector $F(\mathbf{x}) = [f_1(\mathbf{x}), f_2(\mathbf{x})]$ as well as the constraint vector $G = [g_i, i = 1,...,9]$, the two-objective optimization problem can be written as follows:

$$\begin{aligned} &Minimize\ \ F(\mathbf{x}) \\ &Subject\,to\ G \end{aligned} \tag{4.77}$$

4.6.3 Implementation of Optimization

Similarly, two-level optimization is performed. In the first level, the optimized solutions for each given number N of piezoelectric rings are searched. In the second level optimization, Pareto-optimal solutions are searched again in all optimized solutions which obtained from the first level optimization. For all optimization problems in the first level, the following parameter values are assumed:

- $f_r = 20kHz$, λ/2 vibration mode
- $\hat{U} = 100V$, $\hat{I}_{\max} = 4A$
- $D_{tl} = 8$ mm, $D_{tu} = 50$ mm, $\zeta_l = 0.2$, $\zeta_u = 1$
- $L_{bl} = 5$ mm, $L_{bu} = 58.5$ mm, $h_{pl} = 0.2$mm, $h_{pu} = 5$mm
- $L_{f1l} = 5$ mm, $L_{f2l} = 2$ mm

The optimization problem for 2 piezo-rings is first solved using MOGA, NSGA, NSGA-II and SPEA2. Then the most appropriate MOEA is selected and applied in optimization of the transducers with 4 and 6 piezo-rings. MOGA, NSGA and NSGA-II are the same methods as are used for symmetrical transducers before. SPEA2 is an improved version of SPEA. Unlike SPEA, SPEA2 uses an improved fitness assignment scheme, a nearest neighbor density estimation technique and an enhanced archive truncation method. Similarly, the parameters and techniques shown in Table 4.5 are also used in these methods.

The constraints are handled using the following methods. For the given $\hat{U}$ and $\hat{I}_{\max}$, the upper bound $\hat{P}_{\max}$ of the electrical input power is determined correspondingly. Therefore the constraint g_2 can be deleted. The g_3 is dealt with using the penalty function approach similar to that in section 4.5.3. The side constraints g_4 to g_9 are handled by directly limiting the values of the design variables in the regions given by the respective side constraints. When any value of the design variables goes outside the bounds, this value is replaced by the corresponding bound. The equality constraint will be dealt with in each generation using the following method: First, determine the upper bound L_{f1u} of the variable L_{f1} for the $\lambda/2$ mode using the secant method according to the obtained values of the variables ζ, L_b, Typ_b, Typ_f, h_p and the lower bound L_{f2l}. Replace the value of L_{f1} with the corresponding bound if the value of L_{f1} goes outside the range $L_{f1l} \le L_{f1} \le L_{f1u}$. Second, determine the value of the variable L_{f2} using the secant method.

As the design variables include continuous and discrete types, a mixed coding scheme with a mixed crossover and a mixed mutation operator are used in each MOEA. The chromosome for a typical design is as follows:

$$\underbrace{10.3}_{D_t}\quad \underbrace{0.27}_{\zeta}\quad \underbrace{22.6}_{L_b}\quad \underbrace{11}_{Typ_b}\quad \underbrace{01}_{Typ_f}\quad \underbrace{2.9}_{h_p}\quad \underbrace{19.6}_{L_{f1}}\quad \underbrace{63.3}_{L_{f2}}$$

The first variable D_t is continuous variable, which takes a real value in the range of $8\,\text{mm} \le D_t \le 50\,\text{mm}$. The second variable ζ takes a real value in the range of $0.2 \le \zeta \le 1$. The third variable L_b takes a real value in the range of $5\text{mm} \le L_b \le 58.5\,\text{mm}$. The fourth and fifth variables Typ_b and Typ_f are discrete variables, which take a two-bit binary string and represent a set values of ρ ,E and tgδ of a specified material type, respectively. The strings and corresponding material types are shown in Table 4.4. The sixth variable h_p is a continuous variable, which takes a value in the range of $0.2\,\text{mm} \le h_p \le 5\,\text{mm}$. The last two variables L_{f1} and L_{f2} are continuous type, which take a value in the rang of $5\,\text{mm} \le L_{f1} \le L_{f1u}$ and $2\,\text{mm} \le L_{f2} \le L_{f2u}$, respectively. L_{f1u} and L_{f2u} are dynamic upper bounds. They vary from one generation to another and their values are determined using the secant method.

In order to create offspring of the discrete parts Typ_b and Typ_f , two two-bit strings are connected into a four-bit string and the single-crossover operator is used. For the continuous variables the blended crossover (BLX-α) is applied. It is noted that the crossover and mutation operations will not be applied to the continuous variables L_{f2}, whose value is determined by solving the equality constraint according to other values of the variables.

The two-objective optimization problem of the stepped-horn transducer with two piezo-rings was solved by the four MOEAs, respectively. Figs. 4.26 to 4.29 show the respective optimization results in the objective function space after 300 generation. Tables 4.15 to 4.18 give the corresponding variable values and objective function values.

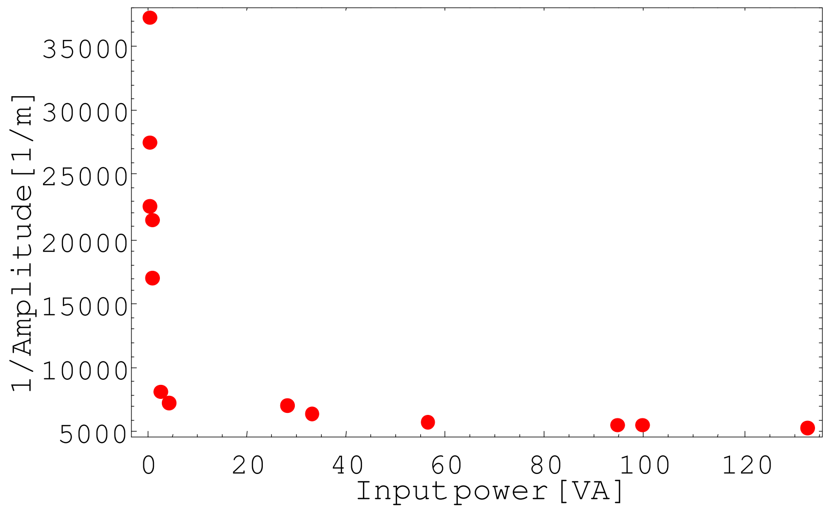

Fig. 4.26 Non-dominated solutions obtained by using MOGA for the freely vibrating stepped-horn transducer with 2 piezo-rings

Table 4.15 Values of design variables and objective functions for non-dominated solutions obtained by MOGA for the freely vibrating stepped-horn transducer with 2 piezo-rings

Design	D_t [mm]	ζ	L_b [mm]	Typ_b	Typ_f	h_p [mm]	L_{f1} [mm]	L_{f2} [mm]	$\hat{u}_{a4}$ [µm]	$\hat{P}_a$ [VA]
1	8.	0.2	5.	1	1	5.	68.2	63.6	44.12	0.48
2	8.	0.2	5.	1	2	5.	69.4	62.1	36.09	0.43
3	8.	0.2	5.	3	4	5.	55.5	38.7	119.46	2.43
4	8.3	0.2	6.2	1	1	4.9	60.	63.9	46.21	0.58
5	8.3	0.2	6.2	2	2	4.9	64.	62.6	26.81	0.29
6	8.4	0.21	6.6	2	3	4.9	68.2	48.8	58.02	0.89
7	8.6	0.21	7.5	1	4	4.8	54.6	38.3	133.61	4.25
8	12.7	0.26	22.1	1	4	3.5	45.7	36.2	149.76	32.63
9	15.2	0.3	31.	2	4	2.7	40.7	38.1	137.21	28.08
10	15.6	0.3	32.6	1	4	2.5	35.7	37.1	166.81	56.37
11	17.9	0.33	40.7	1	4	1.8	32.	36.6	173.56	94.16
12	19.9	0.36	48.	1	4	1.1	21.4	38.4	176.31	99.14
13	21.5	0.38	52.8	1	4	0.7	19.4	38.2	181.57	132.65

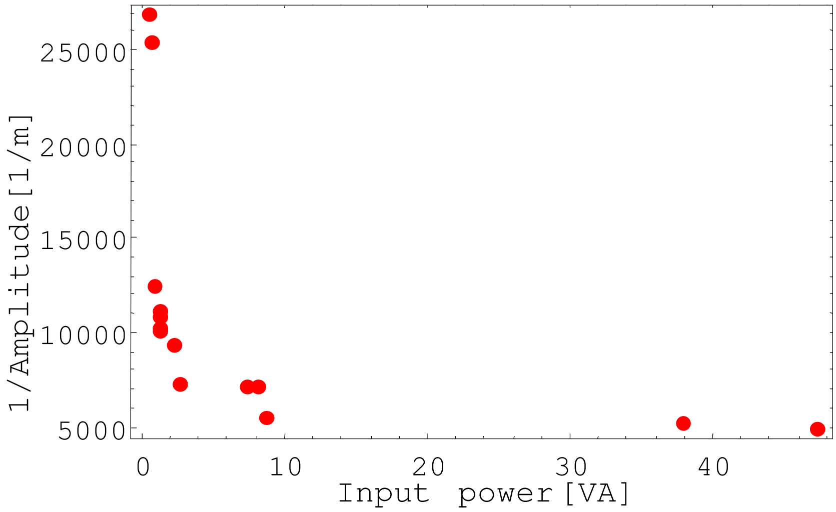

Fig. 4.27 Non-dominated solutions obtained by using NSGA for the freely vibrating stepped-horn transducer with 2 piezo-rings

Table 4.16 Values of design variables and objective functions for non-dominated solutions obtained by NSGA for the freely vibrating stepped-horn transducer with 2 piezo-rings

Design	D_t [mm]	ζ	L_b [mm]	Typ_b	Typ_f	h_p [mm]	L_{f1} [mm]	L_{f2} [mm]	$\hat{u}_{a4}$ [µm]	$\hat{P}_a$ [VA]
1	8.	0.2	5.	3	4	5.	5.	42.	97.32	1.23
2	8.	0.2	5.4	3	4	4.7	5.	42.	99.28	1.28
3	8.	0.2	5.	1	2	5.	5.3	65.4	37.18	0.44
4	8.	0.2	5.	2	4	5.	5.8	42.2	79.73	0.86
5	8.	0.21	5.	4	4	5.	6.4	42.	92.32	1.19
6	8.	0.21	14.7	4	4	2.3	5.9	41.7	135.65	2.54
7	8.	0.21	5.	4	4	5.	7.4	41.9	89.19	1.14
8	8.	0.27	5.	2	3	5.	19.3	52.3	39.34	0.62
9	9.2	0.22	9.2	4	4	4.7	8.5	41.6	106.27	2.28
10	10.	0.2	35.1	3	3	0.2	5.	51.1	140.94	8.04
11	10.3	0.2	34.7	3	4	0.2	5.5	41.1	181.13	8.62
12	12.3	0.22	21.7	1	4	3.6	8.7	41.2	139.06	7.19
13	15.8	0.26	35.1	4	4	1.9	18.4	39.5	192.13	37.77
14	17.9	0.25	38.6	4	4	1.5	15.9	39.6	203.49	47.31

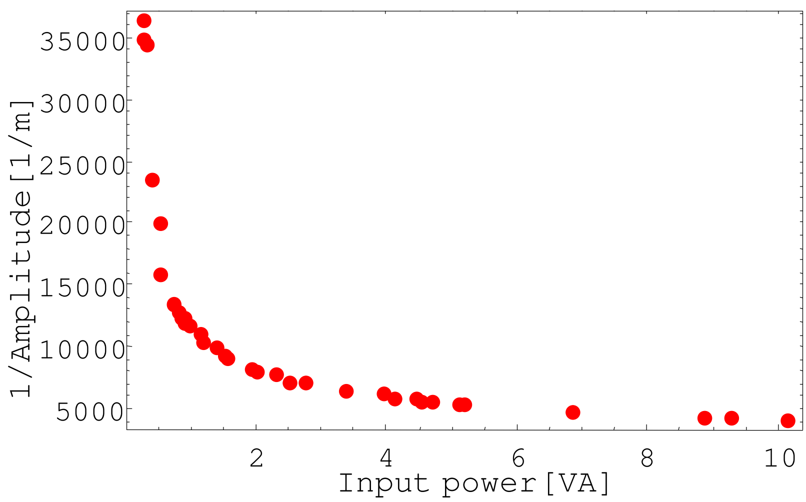

Fig. 4.28 Non-dominated solutions obtained by using NSGA-II for the freely vibrating stepped-horn transducer with 2 piezo-rings

Table 4.17 Values of design variables and objective functions for non-dominated solutions by using NSGA-II for the freely vibrating stepped-horn transducer with 2 piezo-rings

Design	D_t [mm]	ζ	L_b [mm]	Typ_b	Typ_f	h_p [mm]	L_{f1} [mm]	L_{f2} [mm]	$\hat{u}_{a4}$ [µm]	$\hat{P}_a$ [VA]
1	8.	0.2	5.	2	4	5.	8.1	42.	73.74	0.7
2	8.	0.2	5.	3	3	5.	46.5	50.3	49.71	0.51
3	8.	0.2	5.	3	2	5.	28.2	64.	28.51	0.28
4	8.	0.2	5.	1	4	5.	9.7	41.7	83.12	0.89
5	8.	0.2	5.	1	2	5.	21.5	64.4	28.98	0.29
6	8.	0.2	7.1	3	4	3.5	5.	42.1	107.97	1.51
7	8.	0.2	5.6	2	4	4.9	41.9	40.3	62.98	0.51
8	8.	0.2	5.7	2	2	4.9	14.6	64.9	27.43	0.26
9	8.	0.2	10.2	3	4	3.5	9.	41.6	110.07	1.55
10	8.	0.2	6.2	3	4	4.9	25.	40.9	78.11	0.79
11	8.	0.21	17.7	4	4	3.7	23.	40.6	139.87	2.73
12	8.	0.2	8.4	2	3	4.6	37.2	50.7	42.33	0.39
13	8.	0.21	27.5	4	4	2.7	21.4	40.2	184.81	5.11
14	8.	0.21	7.4	3	4	5.	14.5	41.3	90.83	1.12
15	8.	0.2	15.7	2	4	3.9	13.	41.4	94.67	1.19
16	8.	0.2	10.8	2	4	4.4	13.2	41.5	81.04	0.88
17	8.	0.2	11.8	2	4	4.1	15.4	41.4	80.1	0.84
18	8.	0.2	13.6	3	4	3.5	10.7	41.3	120.76	1.91
19	8.	0.2	14.6	1	4	3.2	8.2	41.5	124.03	2.01
20	8.	0.2	16.3	1	4	2.4	5.	41.7	138.67	2.48
21	8.	0.21	14.5	2	4	4.	18.7	41.2	85.14	0.97

Table 4.17 continued

Design	D_t [mm]	ζ	L_b [mm]	Typ_b	Typ_f	h_p [mm]	L_{f1} [mm]	L_{f2} [mm]	$\hat{u}_{a4}$ [µm]	$\hat{P}_a$ [VA]
22	8.1	0.21	20.7	2	4	3.3	19.7	41.1	100.77	1.38
23	8.1	0.21	17.8	1	4	3.7	12.	41.1	128.38	2.27
24	8.1	0.21	36.7	1	4	1.6	12.4	40.8	170.71	4.12
25	8.1	0.21	30.4	3	4	2.6	16.	40.5	171.48	4.42
26	8.1	0.21	37.9	4	4	1.6	15.	40.1	210.13	6.83
27	8.1	0.21	37.	2	4	1.5	5.8	41.4	151.31	3.35
28	8.1	0.22	55.9	3	4	0.4	16.3	39.6	245.08	10.15
29	8.1	0.21	45.3	2	4	1.	13.1	40.8	158.23	3.93
30	8.2	0.21	43.3	1	4	0.8	5.	41.	180.33	4.67
31	8.2	0.21	41.8	1	4	1.	6.5	41.	177.65	4.52
32	8.2	0.22	53.2	4	4	0.2	8.8	39.6	232.59	9.26
33	8.2	0.22	53.2	4	4	0.2	7.8	39.7	225.94	8.87
34	8.2	0.21	44.3	3	4	0.7	5.	40.8	188.06	5.18

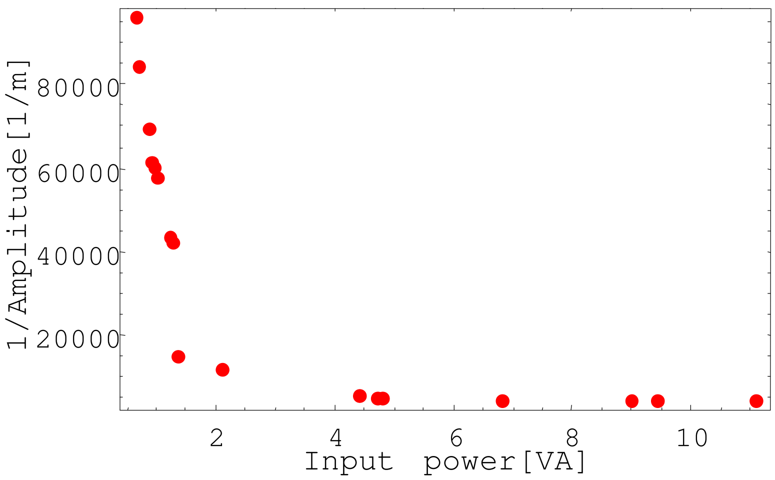

Fig. 4.29 Non-dominated solutions obtained by using SPEA2 for the freely vibrating stepped-horn transducer with 2 piezo-rings

Table 4.18 Values of design variables and objective functions for non-dominated solutions obtained by SPEA2 for the freely vibrating stepped-horn transducer with 2 piezo-rings

Design	D_t [mm]	ζ	L_b [mm]	Typ_b	Typ_f	h_p [mm]	L_{f1} [mm]	L_{f2} [mm]	$\hat{u}_{a4}$ [µm]	$\hat{P}_a$ [VA]
1	8.	0.2	58.1	1	4	0.6	5.3	40.7	192.92	4.8
2	8.	0.25	52.9	4	4	0.2	9.1	39.2	224.91	11.1
3	8.	0.7	5.	2	1	2.7	47.3	68.8	14.32	0.88
4	8.	0.72	5.	2	2	2.6	48.9	64.	10.4	0.65
5	8.	0.64	5.3	2	1	3.2	42.3	69.7	17.35	1.02
6	8.	0.67	5.	2	2	3.1	44.6	65.1	11.84	0.68

Table 4.18 continued

Design	D_t [mm]	ζ	L_b [mm]	Typ_b	Typ_f	h_p [mm]	L_{f1} [mm]	L_{f2} [mm]	$\hat{u}_{a4}$ [μm]	$\hat{P}_a$ [VA]
7	8.	0.65	5.1	2	1	3.1	42.7	69.8	16.56	0.95
8	8.	0.65	5.	2	1	3.1	42.9	69.8	16.27	0.93
9	8.	0.59	6.2	2	3	3.4	38.	51.7	23.02	1.21
10	8.	0.58	6.4	2	3	3.5	37.5	51.8	23.78	1.26
11	8.	0.22	55.7	4	4	0.2	7.1	39.4	222.9	8.98
12	8.	0.23	55.	4	4	0.2	7.6	39.3	223.51	9.4
13	8.	0.2	58.5	2	4	0.4	5.	40.8	175.81	4.39
14	8.	0.2	58.2	1	4	1.2	5.2	40.7	190.54	4.7
15	8.1	0.2	58.2	4	4	1.2	5.2	39.4	213.8	6.8
16	8.1	0.2	58.5	2	2	2.7	5.	63.3	65.41	1.34
17	8.1	0.2	58.5	4	2	2.7	5.	61.5	82.98	2.11

Similarly, the four MOEAs are evaluated in order to select the most appropriate MOEA, which will be used to solve the optimization problems of the transducer with 4 and 6 piezo-rings. Fig. 4.30 shows non-dominated solutions in objective space obtained above. In order to evaluate their convergence and diversity, the performance metric C(A, B), SP and DI have been calculated. The corresponding results are shown in Table 4.19 and Table 4.20.

According to Table 4.19, it is obvious that the set NSGA-II has the best convergence to the Pareto-optimal front than the rest relatively. According to the values of SP and DI shown in Table 4.20, NSGA and NSGA-II distribute do better than the others in terms of the uniformity of distribution of solutions, whereas the set of solutions obtained by SPEA2 has the largest spread.

Table 4.20 also shows the computation time and the number of the non-dominated solutions after 300 generations using the four MOEAs. Obviously, the computation cost of the NSGA is the lowest and the computation cost of SPEA2 is the largest. In terms of finding non-dominated solutions, NSGA-II shows the best performance.

Considering that NSGA-II shows the obvious advantage in terms of the convergence of solutions and the ability of finding non-dominated solutions in this optimization problem, it has been applied for optimization of the stepped horn transducer with 4 and 6 piezoelectric rings, respectively. Figs. 4.31 and 4.32 show the respective non-dominated solutions after 300 generations for 4 and 6 piezo-rings. Table 4.21 and Table 4.22 give the values of the design variables and objective functions for the non-dominated solutions.

After all non-dominated solutions for the transducer with 2, 4 and 6 piezo-rings are obtained, the second-level optimization can be performed. The results will be described in chapter 5.

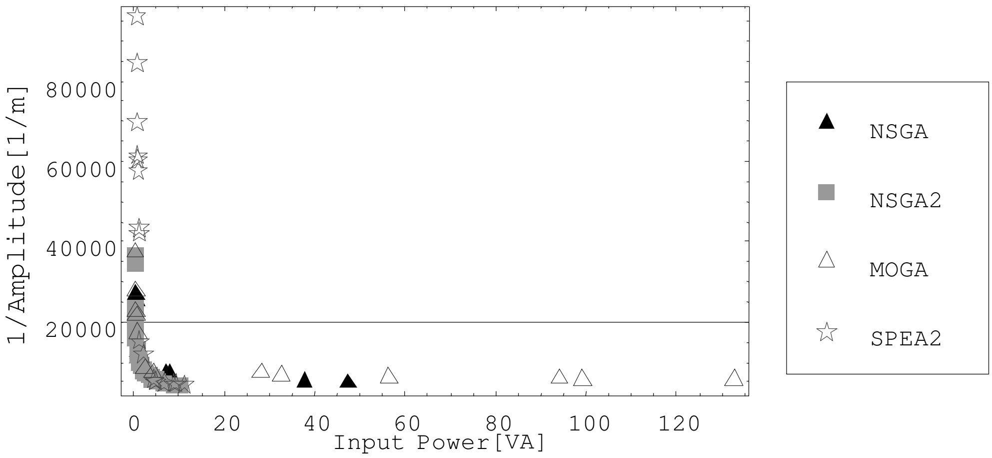

Fig.4.30 Non-dominated solutions in objective space obtained by using four MOEAs for the freely vibrating stepped-horn transducer with 2 piezo-rings

Table 4.19 Values of metrics C (A, B) for the freely vibrating stepped-horn transducer without 2 piezo-rings

A \ B	NSGA	NSGA-II	MOGA	SPEA2
NSGA	**-**	**0**	**8/13**	10/17
NSGA-II	**11/14**	**-**	**12/13**	13/17
MOGA	**1/14**	**0**	**-**	8/17
SPEA2	5/14	4/34	6/13	-

Table 4.20 Values of metrics SP and DI and the computation cost for the freely vibrating stepped-horn transducer with 2 piezo-rings

Metric	NSGA	NSGA-II	MOGA	SPEA2
SP	487	857	2734	3849
DI	21982	32372	31793	91739
Computation time [s]	4290	23373	17393	52200
Number of the non-dominated solutions	14	34	13	17

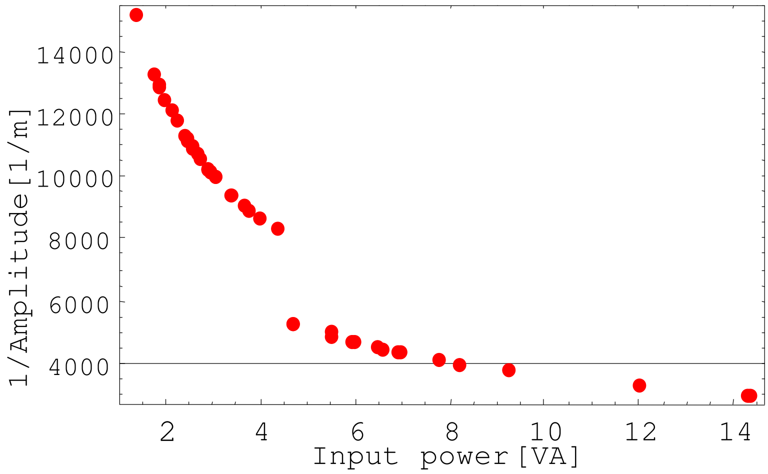

Fig. 4.31 Non-dominated solutions obtained by using NSGA-II for the freely vibrating stepped-horn transducer with 4 piezo-rings

Table 4.21 Values of design variables and objective functions for the non-dominated solutions obtained by NSGA-II for the freely vibrating stepped-horn transducer with 4 piezo-rings

Design	D_t [mm]	ζ	L_b [mm]	Typ_b	Typ_f	h_p [mm]	L_{f1} [mm]	L_{f2} [mm]	$\hat{u}_{a4}$ [μm]	$\hat{P}_a$ [VA]
1	8.	0.2	12.4	1	4	2.5	6.	41.5	242.77	7.77
2	8.	0.2	10.2	4	2	3.2	5.9	64.4	91.74	2.57
3	8.	0.2	5.	4	2	4.1	5.9	64.6	77.01	1.82
4	8.	0.2	8.5	2	2	3.8	5.6	64.8	75.07	1.75
5	8.	0.2	21.5	2	4	1.	5.8	41.9	251.75	8.18
6	8.	0.2	5.	2	2	3.2	6.2	65.2	65.81	1.37
7	8.	0.2	5.	1	4	3.3	6.1	41.7	188.67	4.65
8	8.	0.2	9.4	3	2	4.3	5.3	64.2	90.93	2.53
9	8.	0.2	11.5	2	4	3.2	5.7	41.7	203.43	5.48
10	8.	0.2	13.1	3	2	3.	5.6	64.3	98.5	2.95
11	8.	0.2	14.1	2	2	3.	5.4	64.8	84.6	2.21
12	8.	0.2	15.	2	4	2.8	5.4	41.7	220.03	6.44
13	8.	0.2	8.8	3	2	4.1	5.4	64.3	89.05	2.43
14	8.	0.2	11.3	1	2	3.8	5.3	64.3	92.88	2.64
15	8.	0.2	17.1	2	4	2.7	5.5	41.6	228.54	6.95
16	8.	0.2	18.7	3	2	1.9	5.5	64.3	109.33	3.62
17	8.	0.2	13.1	2	2	2.6	5.7	65.	82.4	2.11
18	8.	0.2	14.3	3	4	3.	5.4	41.3	259.74	9.22
19	8.	0.2	16.8	2	4	3.	5.6	41.5	226.91	6.9
20	8.	0.2	17.	2	2	2.8	5.3	64.7	89.27	2.45
21	8.	0.2	8.6	3	4	3.1	6.1	41.5	222.46	6.55
22	8.	0.2	24.8	4	2	1.6	5.2	63.9	120.12	4.35
23	8.	0.2	11.	4	2	3.8	5.2	64.2	94.65	2.74
24	8.	0.2	9.9	1	2	3.	6.	64.6	88.45	2.38
25	8.	0.2	8.9	2	4	3.	5.8	41.8	188.88	4.66

Table 4.21 continued

Design	D_t [mm]	ζ	L_b [mm]	Typ_b	Typ_f	h_p [mm]	L_{f1} [mm]	L_{f2} [mm]	$\hat{u}_{a4}$ [μm]	$\hat{P}_a$ [VA]
26	8.	0.2	18.5	1	2	2.7	5.4	64.1	105.75	3.38
27	8.	0.2	26.6	4	4	1.	5.2	41.1	334.68	14.33
28	8.	0.2	26.5	4	4	1.1	5.2	41.1	332.49	14.26
29	8.	0.2	13.8	1	2	3.1	5.4	64.3	97.66	2.89
30	8.	0.2	15.2	1	2	2.6	5.8	64.3	100.06	3.03
31	8.	0.2	5.3	3	2	3.5	5.8	64.7	77.53	1.84
32	8.	0.2	12.4	2	4	3.4	5.2	41.6	210.05	5.89
33	8.	0.2	21.9	1	2	1.6	5.3	64.3	111.42	3.76
34	8.	0.2	13.6	1	2	3.3	5.4	64.2	97.27	2.87
35	8.	0.2	22.2	3	2	1.6	5.3	64.2	114.75	3.97
36	8.	0.2	12.7	2	4	3.6	5.4	41.5	211.34	5.99
37	8.	0.2	20.6	4	4	1.8	5.2	41.2	301.42	11.96
38	8.	0.2	13.6	3	2	3.2	5.2	64.2	99.86	3.02
39	8.	0.2	5.8	1	2	4.7	5.1	64.4	80.15	1.96
40	8.	0.2	5.	1	4	5.	5.2	41.4	199.08	5.47

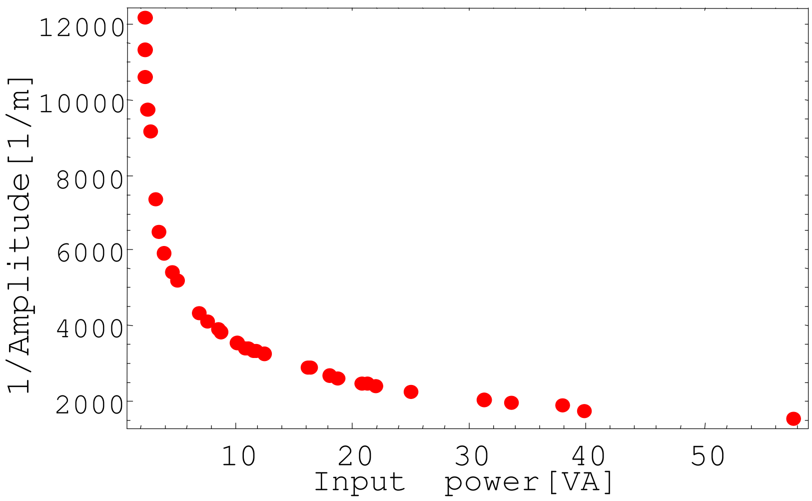

Fig.4.32 Non-dominated solutions obtained by using NSGA-II for the freely vibrating stepped-horn transducer with 6 piezo-rings

Table 4.22 Values of design variables and objective functions for the non-dominated solutions obtained by using NSGA-II for the freely vibrating stepped-horn transducer with 6 piezo-rings

Design	D_t [mm]	ζ	L_b [mm]	Typ_b	Typ_f	h_p [mm]	L_{f1} [mm]	L_{f2} [mm]	$\hat{u}_{e4}$ [μm]	$\hat{P}_a$ [VA]
1	8.	0.2	7.9	4	4	1.2	48.8	39.6	340.97	16.15
2	8.	0.2	50.	1	4	0.2	5.6	40.9	561.83	39.66
3	8.	0.2	20.4	4	4	0.7	21.8	40.7	441.49	24.83
4	8.	0.2	25.	1	4	0.2	5.	41.5	487.2	31.15
5	8.	0.2	18.6	3	4	0.8	24.7	40.6	412.6	21.82
6	8.	0.2	58.5	4	4	0.2	5.	39.6	648.77	57.59
7	8.	0.2	5.	2	4	1.3	42.4	40.4	153.78	3.36
8	8.	0.2	18.6	3	4	0.8	23.9	40.7	406.38	21.17
9	8.	0.2	5.	2	3	1.5	49.7	50.3	102.15	2.52
10	8.	0.2	5.	2	3	1.4	43.7	50.6	93.85	2.32
11	8.	0.2	17.	1	4	1.	27.8	40.6	380.69	18.72
12	8.	0.2	15.8	1	4	1.1	29.8	40.5	372.16	17.95
13	8.	0.2	16.8	2	4	1.	29.4	40.8	260.58	8.71
14	8.	0.2	5.	2	1	1.3	40.3	65.	81.81	2.23
15	8.	0.2	18.8	2	4	0.7	16.8	41.3	277.37	10.15
16	8.	0.2	5.	2	3	1.2	35.3	51.	87.8	2.3
17	8.	0.2	11.7	1	4	1.	27.9	40.8	289.66	10.78
18	8.	0.2	15.6	2	4	0.9	24.1	41.	239.88	7.52
19	8.	0.2	5.6	2	3	1.5	47.3	50.4	108.23	2.72
20	8.1	0.2	6.6	2	4	1.3	39.4	40.5	168.02	3.9
21	8.1	0.2	29.2	1	4	1.	20.6	40.5	499.12	33.44
22	8.1	0.2	26.2	3	4	1.	22.8	40.3	521.78	37.77
23	8.1	0.2	5.	4	4	1.3	31.3	40.8	191.9	4.9
24	8.1	0.2	5.2	2	4	1.	21.5	41.4	134.86	3.09
25	8.1	0.2	19.4	1	4	1.	23.1	40.7	398.55	20.83
26	8.1	0.2	8.9	3	4	1.4	34.9	40.4	296.52	11.53
27	8.1	0.2	8.4	3	4	1.6	36.	40.3	306.24	12.42
28	8.1	0.2	9.6	1	4	1.4	35.2	40.4	297.58	11.63
29	8.1	0.2	8.4	4	4	1.6	41.6	40.	343.39	16.34
30	8.1	0.2	5.7	1	4	1.4	39.2	40.4	227.89	6.86
31	8.1	0.2	6.3	4	4	1.5	37.5	40.4	253.2	8.43
32	8.1	0.2	9.2	1	4	1.6	30.5	40.6	290.1	11.02
33	8.1	0.2	5.5	2	4	1.8	35.8	40.6	183.69	4.43

4.6.4 Problem Formulation of Transducers with a Mechanical Load

Optimization objectives In ultrasonic machining and bonding, piezoelectric transducers operate against loads. The load has much influence on the behavior and vibration form of the transducer. In order to study the effect of loads on the resonance performances, a simple spring-damping load model is studied here. In the case of loading, the mechanical output power and electrical input power are two important performance criteria. Here they are considered as optimization objectives. For a given exciting voltage, the former should be maximized, and in the meantime the latter should be minimized

For the transducer with a spring-damping load on one end (see Fig. 4.33), there exist the following boundary conditions

$$\underline{\hat{F}}_{e1} = 0 \tag{4.78}$$

$$\underline{\hat{F}}_{a4} = \left(\frac{c_L}{j\Omega} + d_L\right)\underline{\hat{v}}_{a4} \tag{4.79}$$

Substituting the boundary conditions (4.78) and (4.79) into (4.71), with simple computations the following equations can be obtained

$$\underline{\hat{v}}_{e1} = \left(\frac{j\Omega a_{23}^{H} - j\Omega d_L a_{13}^{H} - c_L a_{13}^{H}}{j\Omega d_L a_{11}^{H} - j\Omega a_{21}^{H} + c_L a_{11}^{HT}}\right)\underline{\hat{U}} \tag{4.80}$$

$$\underline{\hat{v}}_{a4} = a_{11}^{H}\,\underline{\hat{v}}_{e1} + a_{13}^{H}\,\underline{\hat{U}} \tag{4.81}$$

$$\underline{\hat{I}} = a_{31}^{H}\,\underline{\hat{v}}_{e1} + a_{33}^{H}\,\underline{\hat{U}} \tag{4.82}$$

Applying equation (4.80) into equation (4.81), the solution of $\underline{\hat{v}}_{a4}$ is obtained as follows:

$$\underline{\hat{v}}_{a4} = \left(\frac{j\Omega a_{23}^{H} a_{11}^{H} - j\Omega a_{21}^{H} a_{13}^{H}}{j\Omega d_L a_{11}^{H} - j\Omega a_{21}^{H} + c_L a_{11}^{HT}}\right)\underline{\hat{U}} \tag{4.83}$$

where

$$\mathrm{Im}\left[\frac{j\Omega a_{23}^{H} a_{11}^{H} - j\Omega a_{21}^{H} a_{13}^{H}}{j\Omega d_L a_{11}^{H} - j\Omega a_{21}^{H} + c_L a_{11}^{HT}}\right] = 0 \tag{4.84}$$

is the characteristic equation representing the resonance of the transducer free at one end and with a load on the other end.

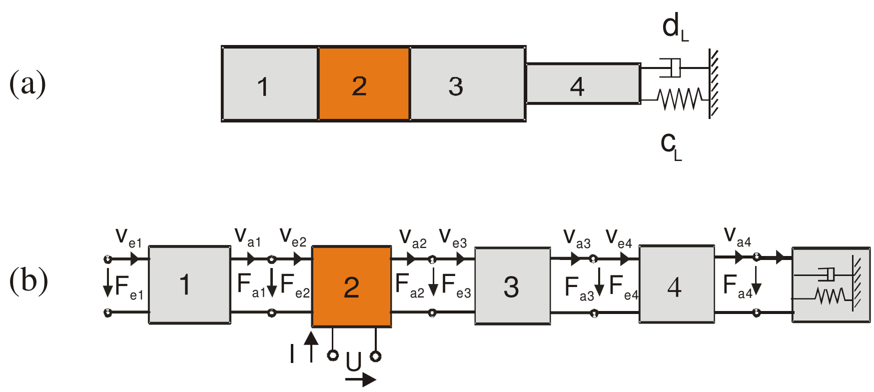

Fig.4.33 Scheme of a stepped-horn transducer with a mechanical load

The effective mechanical output power is

$$\hat{P}_m = \frac{1}{2}\hat{F}_{a4}\hat{v}_{a4}\cos\varphi_m \tag{4.85}$$

where φ_m is the phase difference between $\underline{\hat{F}}_{a4}$ and $\underline{\hat{v}}_{a4}$. Applying equations (4.79) and equations (4.83) yields

$$\hat{P}_m = \frac{1}{2}\left|\frac{c_L}{j\Omega}+d_L\right|\left|\frac{j\Omega a_{23}^H a_{11}^H - j\Omega a_{21}^H a_{13}^H}{j\Omega d_L a_{11}^H - j\Omega a_{21}^H + c_L a_{11}^{HT}}\right|\hat{U}^2\cos\varphi_m \tag{4.86}$$

Equation (4.86) gives the expression of the first optimization objective, which should be maximized. Because only minimization problems will be handled in all algorithms here applied, the above objective for maximization is transformed into an objective for minimization by using the inverse of the original objective. Therefore, the first objective function is defined as

$$f_1 = \frac{1}{\hat{P}_m} \tag{4.87}$$

Introducing equation (4.80) into equation (4.82) yields the input current

$$\underline{\hat{I}} = \left(\frac{j\Omega a_{23}^H a_{31}^H - j\Omega d_L a_{31}^{PT} a_{13}^{PT} - c_L a_{31}^{PT} a_{13}^{PT}}{j\Omega d_L a_{11}^H - j\Omega a_{21}^H + c_L a_{11}^{HT}} + a_{33}^{PT}\right)\underline{\hat{U}} \tag{4.88}$$

Therefore the input apparent power can be expressed as

$$\hat{P}_a = \frac{1}{2}\hat{I}\hat{U} = \frac{1}{2}\left|\frac{j\Omega a_{23}^H a_{31}^H - j\Omega d_L a_{31}^{PT} a_{13}^{PT} - c_L a_{31}^{PT} a_{13}^{PT}}{j\Omega d_L a_{11}^H - j\Omega a_{21}^H + c_L a_{11}^{HT}} + a_{33}^{PT}\right|\hat{U}^2 \tag{4.89}$$

Equation (4.89) gives the expression of the second objective function, which should be minimized. It can be written as

$$f_2 = \hat{P}_a \tag{4.90}$$

Design variables The given quantities and design variables are the same as those of the stepped-horn transducer without load described before. It is assumed that the load is a typical spring-damping load for ultrasonic bonding [Brö02], which has the following parameter values:

$$c_L\text{=1.27 kN/µm,} \tag{4.91}$$

$$d_L\text{=25.4/}\Omega\text{ Ns/µm} \tag{4.92}$$

where Ω is the vibration frequency of the transducer.

Constraints Equation (4.84) gives the resonance condition of the transducer with a load at the given resonance frequency f_r. It describes an equality constraint for the design variable. The constraints g_2 to g_9 in section 4.6.2 are also here used.

The two-objective optimization problem for the stepped-horn transducer with a mechanical load can be written as follows:

$$\begin{aligned} &Minimize \;\; F(\mathbf{x}) \\ &Subject\,to \;\; G(\mathbf{x}) \end{aligned} \tag{4.93}$$

Where $F(\mathbf{x}) = [f_1(\mathbf{x}), f_2(\mathbf{x})]$,

$$G(\mathbf{x}) = [g_i(\mathbf{x}), i = 1,...,9],$$

$$\mathbf{x} = (x_1, x_2, x_3, x_4, x_5, x_6, x_7, x_8) = (D_t, \zeta, L_b, Typ_b, Typ_f, h_p, L_{f1}, L_{f2})$$

4.6.5 Implementation of Optimization

Considering that NSGA-II shows a better overall performance in the optimization of the freely vibrating transducer with a stepped horn, NSGA-II is here applied for the all optimization problems of the transducer with 2, 4 and 6 piezo-rings. The optimization procedures similar to those in section 4.6.3 are used.

Figs. 4.34 to 4.36 show the obtained optimized solutions in the objective space after 300 generations for the number of the piezo-rings N =2, 4 and 6 respectively. Tables 4.23 to 4.25 give the corresponding design variable values and objective functions values. Similarly, the second level optimization can be performed in the obtained all non-dominated solutions for the transducer with 2 , 4 and 6 piezo-rings. This will be described in chapter 5.

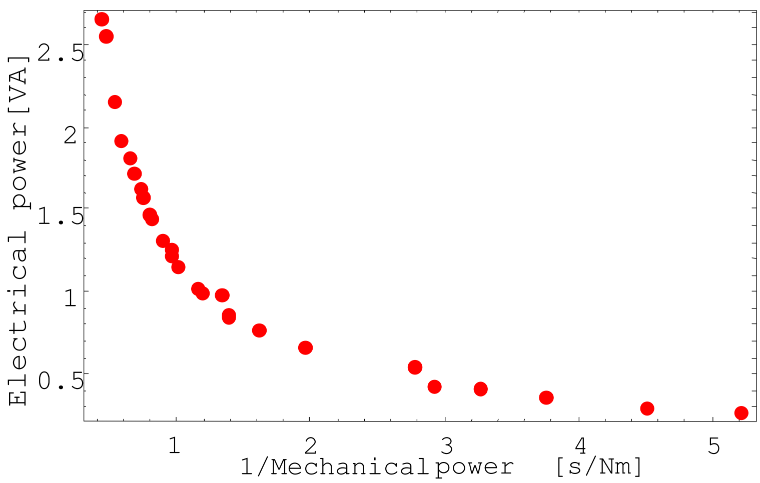

Fig. 4.34 Non-dominated solutions for the stepped horn transducer with a mechanical load and 2 piezo-rings

Table 4.23 Values of design variables and objective functions corresponding to non-dominated solutions for the stepped horn transducer with a mechanical load and 2 piezo-rings

Design	D_t [mm]	ζ	L_b [mm]	Typ_b	Typ_f	h_p [mm]	L_{f1} [mm]	L_{f2} [mm]	$\hat{P}_m$ [Nm/s]	$\hat{P}_a$ [VA]
1	8.	0.86	34.3	3	3	4.6	29.9	24.3	0.22	0.3
2	8.	0.96	18.3	4	1	5.	15.3	72.9	0.19	0.27
3	8.5	0.88	34.8	4	3	4.5	32.6	12.8	0.34	0.43
4	8.8	0.86	35.7	4	4	4.2	33.9	2.	0.27	0.36
5	9.2	0.85	28.	3	3	4.7	32.7	29.6	0.31	0.41
6	9.4	0.86	41.5	3	1	4.	42.4	16.7	0.72	0.85
7	9.7	1.	44.3	1	3	3.3	31.8	20.	0.62	0.77
8	10.2	0.98	51.3	2	3	4.	8.7	41.7	0.73	0.87
9	10.3	0.79	42.9	3	1	4.1	43.1	14.4	1.	1.16
10	10.4	0.8	45.	2	1	4.	32.6	48.9	0.51	0.67
11	10.4	0.91	34.8	4	3	3.8	41.8	4.	0.84	1.
12	10.5	0.9	34.6	4	1	3.8	42.	17.7	1.14	1.31
13	10.5	0.89	34.8	4	3	3.9	41.7	3.9	0.87	1.02
14	10.5	0.9	46.	3	1	3.5	31.4	23.4	1.04	1.22
15	10.7	0.97	43.7	1	2	3.5	30.	35.4	0.36	0.54
16	11.	0.89	44.3	3	1	3.5	31.9	26.1	1.25	1.45
17	11.3	0.93	40.8	1	3	3.4	39.3	16.9	1.05	1.26
18	11.4	0.99	53.1	2	1	3.9	6.9	53.5	1.73	1.93
19	11.7	0.8	40.7	3	1	3.7	39.2	26.6	1.49	1.72
20	11.8	0.92	36.7	4	1	3.4	49.2	5.9	1.91	2.17
21	11.8	0.81	46.1	3	1	3.5	28.3	30.6	1.35	1.58
22	11.9	0.86	41.4	1	1	3.5	37.9	36.7	1.39	1.63
23	11.9	0.86	40.2	2	3	3.5	39.3	30.2	0.76	0.98
24	11.9	0.78	41.7	4	3	3.7	34.2	2.	1.26	1.47
25	12.	0.78	42.	3	1	3.7	38.1	26.4	1.57	1.82
26	12.8	0.66	47.8	3	1	3.9	42.3	9.1	2.37	2.66
27	13.2	1.	40.9	3	3	2.6	36.2	14.2	2.2	2.56

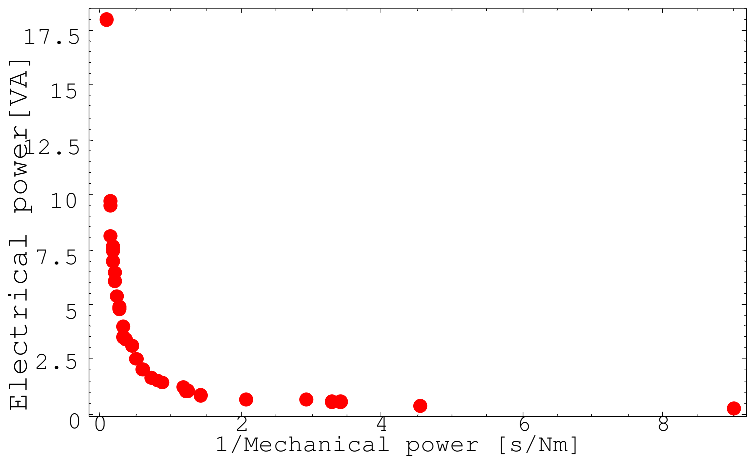

Fig. 4.35 Non-dominated solutions for the stepped horn transducer with a mechanical load and 4 piezo-rings

Table 4.24 Values of design variables and objective functions corresponding to non-dominated solutions for the stepped horn transducer with a mechanical load and 4 piezo-rings

Design	D_t [mm]	ζ	L_b [mm]	Typ_b	Typ_f	h_p [mm]	L_{f1} [mm]	L_{f2} [mm]	$\hat{P}_m$ [Nm/s]	$\hat{P}_a$ [VA]
1	8.	0.56	20.3	3	1	3.9	48.2	45.9	0.34	0.68
2	8.	0.64	24.9	2	4	3.7	44.3	16.	0.3	0.59
3	8.	0.76	31.6	4	4	3.1	33.3	2.	0.71	0.92
4	8.	0.8	24.2	4	1	2.7	69.2	5.7	1.39	1.68
5	8.	0.81	16.2	3	4	3.7	47.7	2.	0.49	0.69
6	8.	0.89	5.	3	2	5.	32.2	53.8	0.11	0.33
7	8.1	0.61	27.4	1	3	3.5	45.5	17.5	0.83	1.1
8	8.2	0.66	22.6	1	3	4.	27.5	38.9	0.29	0.58
9	8.5	0.71	10.2	4	3	5.	28.4	42.6	0.22	0.46
10	8.7	0.62	27.3	4	1	4.	28.2	40.7	0.82	1.09
11	9.2	0.89	53.3	2	4	2.1	9.7	30.7	0.86	1.3
12	10.5	0.66	22.2	3	3	4.2	31.1	32.5	1.26	1.64
13	11.6	0.9	18.	2	1	4.2	32.9	60.4	1.72	2.11
14	11.6	0.51	44.7	1	4	3.8	29.8	2.	3.12	3.59
15	11.6	0.35	33.	4	3	3.6	33.9	9.7	4.27	4.94
16	11.8	0.54	50.1	3	4	3.	20.6	17.	2.01	2.6
17	12.1	0.6	32.9	3	1	3.5	36.1	34.4	4.16	4.82
18	12.4	0.32	57.7	4	4	4.1	6.8	2.	1.15	1.48
19	12.8	0.69	24.8	3	3	3.	53.5	5.3	6.89	7.72
20	12.9	0.79	32.	4	4	4.1	27.8	2.	4.84	5.44
21	13.	0.32	39.2	4	3	3.4	28.3	2.	6.23	6.97
22	13.2	0.82	29.8	2	4	4.4	28.2	21.8	2.89	3.42
23	13.4	0.65	28.4	3	4	3.2	39.3	2.	5.69	6.48
24	13.6	0.44	27.8	2	4	4.1	42.8	19.7	2.36	3.15
25	13.7	0.2	44.9	3	3	3.1	32.9	2.	8.79	9.8
26	14.	0.24	51.1	2	4	4.5	27.8	2.	6.8	7.51
27	14.1	0.73	35.5	3	4	3.	34.7	2.	7.29	8.23
28	14.1	0.49	34.4	4	3	3.8	28.8	12.5	8.66	9.6
29	15.	0.73	31.1	2	4	4.2	26.3	26.5	3.38	4.08
30	15.	0.8	33.8	4	2	3.9	33.	21.2	5.4	6.17
31	16.3	0.76	37.1	4	3	3.8	27.1	2.	16.89	18.06

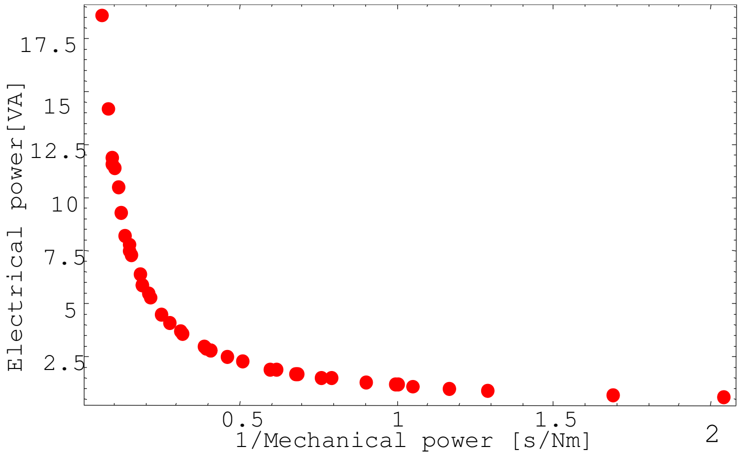

Fig.4.36 Non-dominated solutions for the stepped horn transducer with a mechanical load and 6 piezo-rings

Table 4.25 Values of design variables and objective functions corresponding to non-dominated solutions for the stepped horn transducer with a mechanical load and 6 piezo-rings

Design	D_t [mm]	ζ	L_b [mm]	Typ_b	Typ_f	h_p [mm]	L_{f1} [mm]	L_{f2} [mm]	$\hat{P}_m$ [Nm/s]	$\hat{P}_a$ [VA]
1	8.	1.	58.5	2	1	5.	6.6	4.4	0.96	1.11
2	8.	1.	46.6	2	2	4.9	12.8	19.4	1.01	1.2
3	8.	1.	46.8	4	2	5.	3.1	2.	0.49	0.62
4	8.	1.	52.1	2	1	4.8	13.	3.9	1.32	1.51
5	8.	1.	53.7	2	3	5.	5.	8.2	1.12	1.29
6	8.	1.	58.5	3	1	4.7	3.4	2.	0.59	0.73
7	8.1	1.	40.6	3	4	5.	10.1	2.	1.	1.17
8	8.1	0.94	40.1	1	1	5.	5.8	13.6	1.46	1.67
9	8.3	0.99	39.9	1	3	5.	5.	11.6	1.49	1.7
10	8.3	0.68	40.6	4	3	5.	5.	5.1	0.86	1.02
11	8.5	0.92	54.9	3	2	5.	5.	5.3	0.78	0.94
12	8.7	0.95	48.3	2	4	4.9	10.6	7.4	1.62	1.87
13	8.7	0.95	48.1	1	2	4.9	10.4	15.6	1.26	1.49
14	9.2	0.91	45.7	3	1	4.9	8.1	3.7	1.68	1.93
15	9.2	0.91	45.7	2	3	4.9	8.	14.1	2.57	2.9
16	9.3	0.91	41.5	1	1	4.9	7.8	11.8	2.48	2.81
17	9.4	0.92	47.7	1	4	4.8	8.9	6.	1.98	2.28
18	10.	0.89	48.6	3	1	4.7	8.9	2.	2.18	2.5
19	10.	0.85	45.4	2	4	4.9	6.4	16.3	2.59	2.98
20	10.5	0.82	45.2	3	4	4.9	5.	7.9	2.5	2.87
21	10.5	0.94	27.	3	4	4.7	7.2	16.7	3.68	4.17
22	10.6	0.85	43.6	3	1	4.8	5.8	10.2	3.26	3.69
23	10.7	0.77	51.9	1	3	4.3	12.3	6.3	3.99	4.51
24	10.8	0.97	33.3	3	2	5.	5.	25.4	3.17	3.62
25	11.2	0.92	49.6	1	3	4.	7.3	13.3	5.28	5.93

Table 4.25 continued

Design	D_t [mm]	ζ	L_b [mm]	Typ_b	Typ_f	h_p [mm]	L_{f1} [mm]	L_{f2} [mm]	$\hat{P}_m$ [Nm/s]	$\hat{P}_a$ [VA]
26	11.2	0.78	36.5	2	3	4.3	11.1	29.9	4.85	5.5
27	11.3	0.91	40.6	3	1	4.8	6.7	9.7	4.75	5.31
28	11.3	0.92	28.4	1	1	4.6	8.6	25.8	8.58	9.35
29	11.5	0.9	41.9	1	1	4.4	18.5	4.9	7.44	8.2
30	11.5	0.92	37.7	3	3	4.8	6.3	10.3	5.27	5.88
31	11.8	0.66	45.7	2	3	3.8	15.4	25.6	5.64	6.45
32	12.	0.77	34.	2	1	4.1	25.3	31.	11.02	11.99
33	12.	0.94	32.4	1	1	4.6	13.1	16.2	10.74	11.62
34	12.	0.93	32.8	1	4	4.6	13.3	10.3	7.02	7.8
35	12.2	0.96	27.4	3	4	5.	5.	16.2	6.84	7.59
36	12.5	0.9	47.3	2	3	3.6	7.6	24.8	10.42	11.44
37	12.7	0.92	23.7	2	4	4.9	5.2	30.4	6.52	7.31
38	13.2	0.79	49.8	1	1	3.6	8.3	26.1	8.84	10.52
39	13.3	0.48	58.1	2	1	3.2	21.5	17.3	13.03	14.3
40	13.4	0.93	46.8	2	1	4.1	10.5	21.2	17.69	18.73

In this chapter, several two-objective optimization problems for Langevin-type transducers have been studied. Based on experiments, applying lumped parameter models and parameter identification the optimal pre-stress for multiple objectives have been found. Using transfer matrix methods, the optimization problems for the symmetrical transducer and the transducer with a stepped horn were formulated. Optimizations were performed using MOGA, NSGA, NSGA-II, SPEA and SPEA2 and the results have been obtained. In next chapter, the results obtained will be analyzed and discussed.

5 Results and Discussions

In chapter 4, non-dominated solutions for transducers with 2, 4 and 6 piezoelectric rings have been obtained. In order to identify the final Pareto-optimal solutions of each optimization problem, the non-domination check (the second level optimization) needs to be performed in these solutions. After the second level optimization is finished, an important problem is how to determine the preferred solution for the implementation of the optimal design. In this chapter, first, the results of the second level optimization are presented and analyzed. Then the preferred solution is selected by means of different selection methods. Finally, the load characteristics of the Pareto-optimal stepped-horn transducer are studied.

5.1 Discussion of the Results for the Symmetrical Transducer

The non-dominated solutions for the symmetrical Langevin transducer with 2, 4 and 6 piezo-rings under the condition of no load have been given in chapter 4 (refer to Figs. 4.19, 4.22 and 4.23 as well as Tables 4.8, 4.12 and 4.13). Here they are plotted in Fig. 5.1. The Pareto-optimal solutions were searched again in these non-dominated solutions. Fig 5.2 shows the non-dominated solutions in objective space after the search is finished.

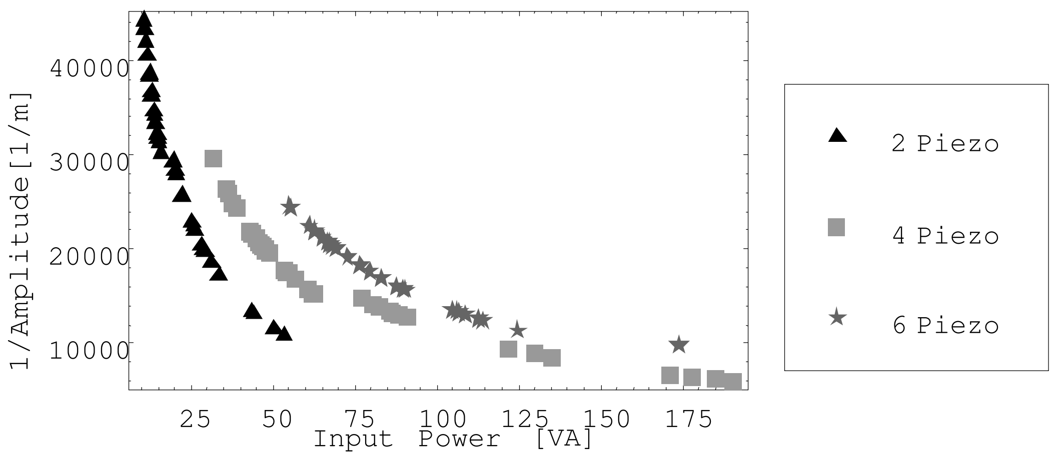

Fig. 5.1 Non-dominated solutions in objective space for the symmetrical transducers with 2, 4 and 6 piezo-rings

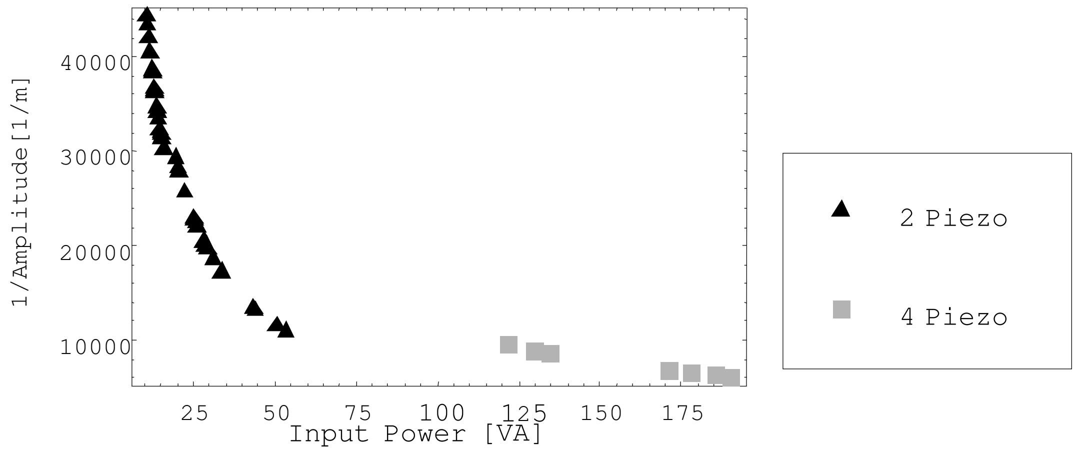

Fig. 5.2 Non-dominated solutions in objective space for the symmetrical transducer obtained after the second level optimization

5.1.1 Analysis of the Results of the Optimization

It is obvious that the set of non-dominated solutions for the transducer with 6 piezo-rings are dominated by members of the non-dominated sets of the transducers with 2 and 4 piezo-rings. Therefore, they do not appear in the final results. The final set of Pareto-optimal solutions consists of all 35 members of the non-dominated set for 2 piezo-rings and 7 members for 4 piezo-rings. Table 5.1 gives the values of the design variables and objective functions for these Pareto-optimal solutions. It is noted that the value of the diameter of the transducer for all solutions is equal to the lower bound of this design variable. This situation can be explained from the point of view of engineering. The smaller the diameter of the transducer is, the smaller the capacitance of the piezo-rings and the loss of the material. This will result in the decrease of the input power and the increase of the vibration amplitude. Table 5.1 also shows that the front and back metal sections of the symmetrical transducer should be made of titanium or brass when the electrical input power and the vibration amplitude at the resonance are considered as objective functions. In addition, compared with the transducers with 2 piezo-rings, the transducers with 4 piezo-rings have the larger electrical input power and vibration amplitude. It is also noticed that the total length of the transducers with two end blocks made of brass is shorter than that of the transducers with two end blocks made of titanium. The end blocks of the all transducers with 4 piezo-rings are made from brass.

Table 5.1 Values of design variables and objective functions as well as the corresponding pseudo weights after the second level optimization for the symmetrical transducer

Design	D_t [mm]	Typ_b	h_p [mm]	L [mm]	N	$\hat{u}_{a3}$ [µm] (Obj1)	$\hat{P}_a$ [VA] (Obj2)	w_1	w_2
1	8.	2	0.3	63.2	2	33.12	15.89	0.28	0.72
2	8.	2	0.7	62.6	2	31.92	15.19	0.26	0.74
3	8.	2	1.4	61.5	2	29.94	14.22	0.23	0.77
4	8.	2	1.6	61.	2	29.26	13.89	0.21	0.79
5	8.	2	5.	55.5	2	22.58	10.66	0.	1.
6	8.	4	0.2	40.7	2	92.19	53.43	0.53	0.47
7	8.	4	1.5	39.	2	58.08	33.55	0.45	0.55
8	8.	2	0.8	62.4	2	31.55	15.	0.25	0.75
9	8.	4	3.8	36.1	2	35.39	20.28	0.31	0.69
10	8.	4	0.3	40.5	2	87.19	50.47	0.52	0.48
11	8.	4	4.	35.8	2	34.09	19.52	0.29	0.71
12	8.	4	0.7	40.1	2	76.27	44.11	0.5	0.5
13	8.	4	4.	35.8	2	34.21	19.59	0.29	0.71
14	8.	2	4.7	56.	2	23.05	10.89	0.02	0.98
15	8.	2	1.	62.1	2	31.03	14.75	0.24	0.76
16	8.	2	1.8	60.8	2	28.9	13.72	0.21	0.79
17	8.	2	3.7	57.6	2	24.68	11.68	0.09	0.91
18	8.	4	3.7	36.1	2	35.81	20.53	0.31	0.69
19	8.	2	4.2	56.8	2	23.8	11.26	0.06	0.94
20	8.	4	2.5	37.7	2	45.56	26.25	0.39	0.61
21	8.	4	2.1	38.3	2	50.11	28.9	0.41	0.59
22	8.	2	3.1	58.6	2	25.92	12.28	0.13	0.87
23	8.	4	1.8	38.6	2	53.98	31.16	0.43	0.57
24	8.	4	2.7	37.5	2	43.76	25.2	0.38	0.62
25	8.	4	2.2	38.1	2	49.01	28.26	0.41	0.59
26	8.	2	0.9	62.2	2	31.13	14.8	0.25	0.75
27	8.	4	0.7	40.	2	75.12	43.45	0.5	0.5
28	8.	4	2.6	37.6	2	44.7	25.75	0.39	0.61
29	8.	4	2.7	37.5	2	43.84	25.25	0.38	0.62
30	8.	4	2.	38.3	2	50.9	29.37	0.42	0.58
31	8.	2	2.4	59.8	2	27.5	13.04	0.17	0.83
32	8.	2	2.4	59.7	2	27.31	12.95	0.17	0.83
33	8.	4	3.3	36.7	2	38.89	22.35	0.34	0.66
34	8.	2	3.	58.8	2	26.17	12.4	0.14	0.86
35	8.	2	2.3	59.9	2	27.59	13.09	0.18	0.82
36	8.	4	0.8	39.	4	116.51	135.01	0.75	0.25
37	8.	4	0.3	40.1	4	153.58	178.24	0.94	0.06
38	8.	4	0.4	40.	4	147.79	171.49	0.9	0.1
39	8.	4	0.9	38.5	4	105.04	121.66	0.7	0.3
40	8.	4	0.3	40.2	4	159.7	185.41	0.97	0.03
41	8.	4	0.8	38.8	4	112.31	130.16	0.73	0.27
42	8.	4	0.2	40.3	4	163.97	190.41	1.	0.

5.1.2 Determination of the Preferred Solution

In the practical design of piezoelectric actuators, generally, only one solution needs to be implemented. Therefore, how to select a particular solution from the set of non-dominated solutions obtained is an important task from point of view of engineering**.**

The methods to determine the preferred solution from the obtained non-dominated solutions can be divided into two classes. One class is to choose the preferred solution from the whole set of non-dominated solutions according to high-level information. Since every solution is considered in these methods, the best solution according to the high-level selection information will not be lost. However, the cost to evaluate solutions in these methods is high because in general the size of the non-dominated set is large. The other class is first to reduce the size of the set of non-dominated solutions and then to determine the preferred solution from the remaining solutions according to high-level information. The advantages of this class of methods are the low cost to evaluate solutions and the convenience to determine the preferred solution. However, the best solution may be lost in the process of reducing the size of the non-dominated set.

If certain high level information is known, the preferred solution can be chosen according to this high level information. As far as optimization problems of piezoelectric actuators are concerned, any performance except those performance criteria used as optimization objectives in the optimization problem can be considered as the high level information. From the point of view of the ultrasonic technique, the piezoelectric quality number, the power efficiency and the effective coupling factor are some important performance criteria. In addition to using performance criteria of piezoelectric actuators, many techniques for multiple criteria decision-making can also be adopted to select the preferred solution [Mie98]. One of the techniques is using pseudo-weight vectors

After the non-dominated solutions were obtained, a pseudo-weight vector can be calculated for each solution according to the following equation:

$$w_i = \frac{\left(f_i^{\max} - f_i\right) / \left(f_i^{\max} - f_i^{\min}\right)}{\sum_{j=1}^{m} \left(f_j^{\max} - f_j\right) / \left(f_j^{\max} - f_j^{\min}\right)} \tag{5.1}$$

where $f_i^{\max}$ and $f_i^{\min}$ represent the maximum (worst) and minimum (best) values of the i-th objective function in the obtained non-dominated solutions. m is the number of the optimization objectives. The weight vector w_i gives a relative important factor for the i-the objective corresponding to the solution. Obviously, the weight w_i is maximum for the best solution for the i-th objective function.

The clustering technique is a technique usually used to reduce the size of the set of non-dominated solutions. Here, for the two-objective optimization problem the following procedures of the clustering are used [Zit99]: first, sort the obtained non-dominated solutions in ascending order of the value of objective function 1. Second, consider each of the solutions as a separate cluster and find the centroid of each cluster, then calculate the Euclidean distance between all pairs of the clusters in order. Third, combine the two clusters which have a minimum distance. Next, find the centroid of each cluster, calculate the Euclidean distance between all pairs of the clusters, and combine the two clustering having a minimum distance into a cluster. Continue these steps until the required number of the clusters is achieved. Finally, in each cluster the solution closest to the centroid is kept and the rest is abandoned. In the whole process of clustering the two extreme solutions are always taken into account as separate clusters.

In the following, the preferred design for implementation will be determined using the methods described above.

Selection according to weight vectors The preferred solution can be determined according to pseudo-weight vectors. Table 5.1 gives the calculated weights w_1 and w_2, where w_1 is for the vibration amplitude and w_2 for the electrical input power. A solution can be selected according to a designer-preferred weight vector. For example, if a weight value of 70% is assigned to the objective 1 (the vibration amplitude) and a weight value of 30% to the objective 2 (the input power), solution (design) 39, which has a similar weight vector, can be chosen. Design 5 and Design 42 are two extreme solutions among the obtained non-dominated solutions. The former represents the Pareto-optimal design of a symmetrical transducer which has the smallest electrical input power. The latter represents the Pareto-optimal design of a symmetrical transducer which has the largest vibration amplitude. It is noted that the larger the pseudo-weight of the objective function 1 (namely the larger the vibration amplitude) is, the smaller the thickness of the piezo-stacks. On the other hand, the larger the pseudo-weight of the objective function 2 (namely the smaller the input electrical power) is, the larger the thickness of the piezo-stacks.

Table 5.2 Four designs used for explaining how to determine the preferred solution for the symmetrical transducer

Design	D_t [mm]	Typ_b	h_p [mm]	L_b [mm]	N	$\hat{u}_{a3}$ [µm] (Obj1)	$\hat{P}_a$ [VA] (Obj2)	w_1	w_2
3	8	2	1.4	61.5	2	29.94	14.22	0.23	0.77
5	8	2	5	55.5	2	22.58	10.66	0	1
23	8	4	1.8	38.6	2	53.98	31.16	0.43	0.57
42	8	4	0.2	40.3	4	163.97	190.41	1	0

Selection according to performance criteria In the optimization problem of the symmetrical transducer, the input electrical power and the vibration amplitude at resonance have been considered as optimization objectives. The rest of performance criteria can be used as high-level information for the selection of optimized results. As stated before, the piezoelectric quality number, the power efficiency, the effective coupling factor are important performance criteria. Here the effective coupling factor *k* is first considered.

As described in chapter 2 and chapter 4, the effective coupling factor *k* describes the effective energy conversion in piezoelectric transducers. The larger the value of *k*, the more electrical energy is transferred into mechanical energy. The effective coupling factor *k* corresponds to the distance between resonance frequency and anti-resonance frequency for a vibration mode. Therefore, the design corresponding to the largest distance between resonant and anti-resonant frequencies should be chosen. The resonance and anti-resonance frequencies can be readily obtained if the frequency response of the admittance function $\underline{\hat{I}}/\underline{\hat{U}}$ is plotted. The frequency response of the admittance function $\underline{\hat{I}}/\underline{\hat{U}}$ for the symmetrical transducer can be calculated from equation (4.64). Therefore, the frequency responses of the admittance functions $\underline{\hat{I}}/\underline{\hat{U}}$ for every members of the set of the final Pareto-optimal solutions shown in Table 5.1 can be plotted and the preferred design having the best coupling factor *k* can be determined. Here, as an example to explain how to determine the preferred selection according to the high level information *k*, 4 designs in Table 5.1 have been studied. These designs are shown in Table 5.2. Fig. 5.3 shows the frequency responses of the admittance functions $\underline{\hat{I}}/\underline{\hat{U}}$ for the 4 designs. It is shown in Fig. 5.3 that the distance between the resonance and anti-resonance frequencies increases with the increase of the thickness $N \cdot h_p$ of the piezoelectric stack. Design 5, which has the largest thickness of the piezo-stack ($N \cdot h_p = 2 \times 5 = 10\text{mm}$), has the largest distance between resonance and anti-resonance frequencies. Therefore, according to the coupling factor *k* Design 5 is the preferred design among these 4 Pareto-optimal designs.

Selection by means of clustering technique In order to perform the required selection more easily, the size of Pareto-optimal solutions can be reduced by means of the above described clustering technique before the selection is performed. Fig. 5.4 shows the results after clustering operation with a choice of 6 final solutions in the objective space. Table 5.3 gives the values of the design variables and objective functions for the 6 final solutions. The configurations of the transducers for the 6 final solutions are shown in Fig. 5.5.

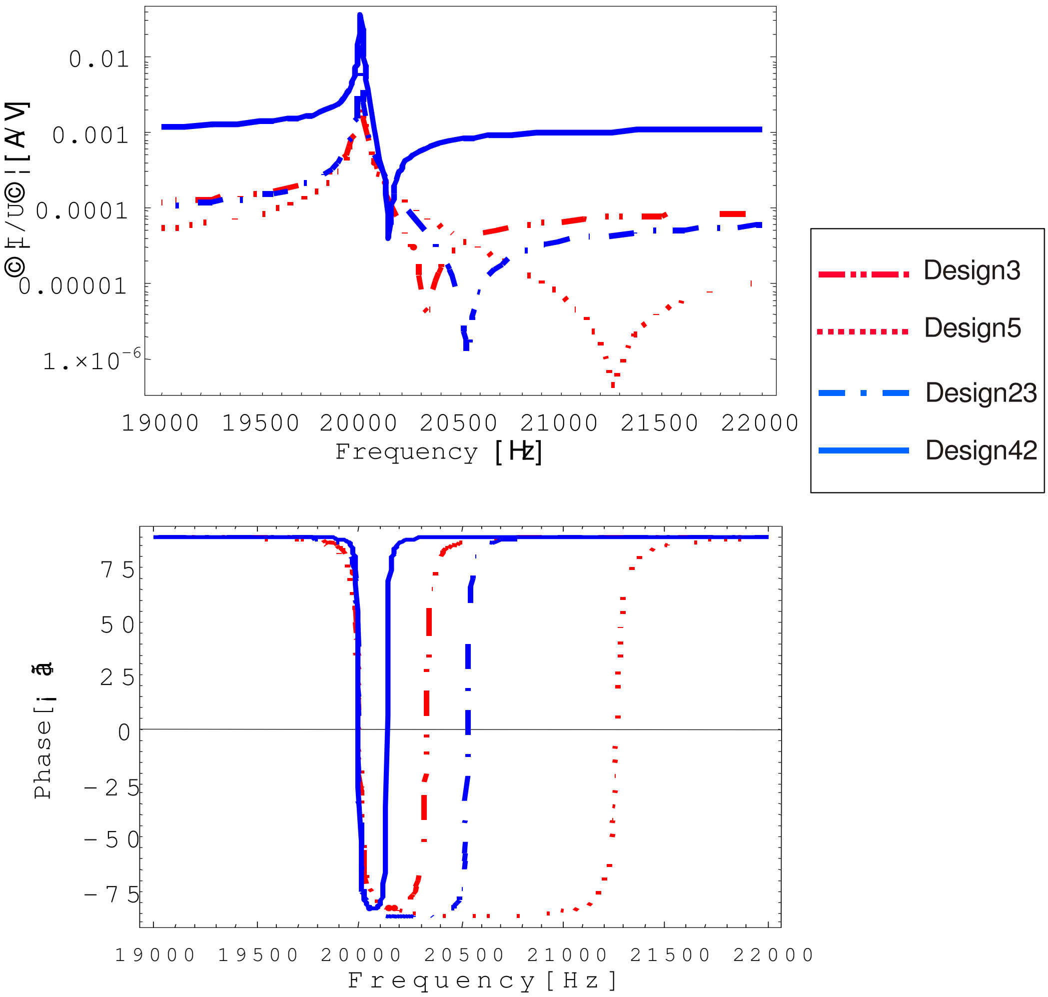

Fig.5.3 Admittance frequency responses for the 4 designs given by Table 5.2

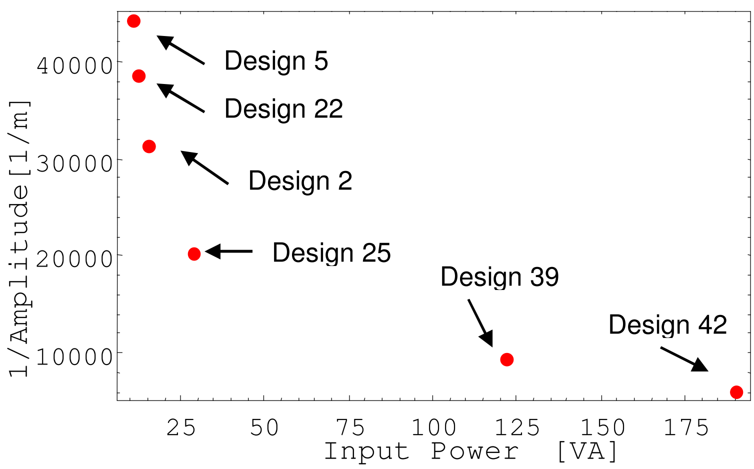

Fig. 5.4 Six final Pareto-optimal solutions after clustering for the symmetrical transducer

Table 5.3 Values of design variables and objective functions as well as weights for 6 Pareto-optimal solutions after clustering for the symmetrical transducer

Design	D_t [mm]	Typ_b	h_p [mm]	L_b [mm]	N	$\hat{u}_{a3}$ [µm] (Obj1)	$\hat{P}_a$ [VA] (Obj2)	w_1	w_2
2	8	2	0.7	62.6	2	31.39	15.19	0.26	0.74
5	8	2	5	55.5	2	22.58	10.66	0	1
22	8	2	3.1	58.6	2	25.92	12.28	0.13	0.87
25	8	4	2.2	38.1	2	49.01	28.26	0.41	0.59
39	8	4	0.9	38.5	4	105.04	121.66	0.7	0.3
42	8	4	0.2	40.3	4	163.97	190.41	1	0

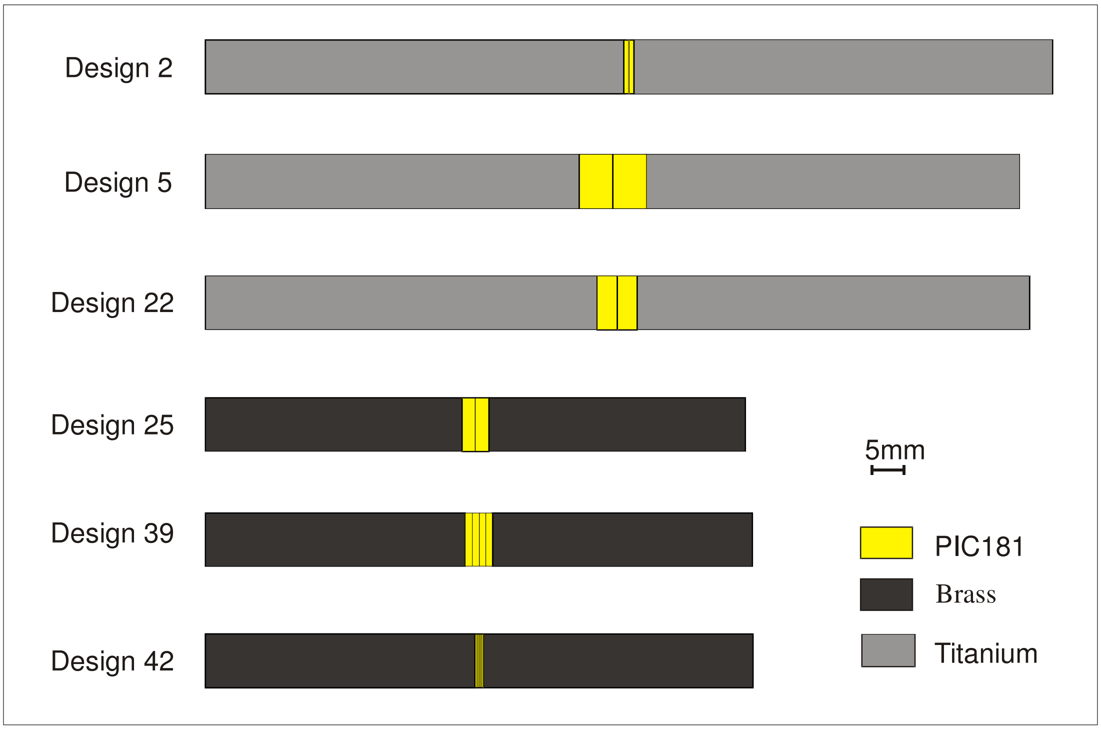

Fig. 5.5 Configurations of the symmetrical transducers for 6 Pareto-optimal solutions after clustering

After clustering is finished, similarly, the high level information described before can then be applied to determine a preferred design from the results of clustering for implementation. It is pointed out that in the optimization problems in chapter 4 the set of Pareto-optimal solutions is searched under the condition of a given voltage $\hat{U} = 100V$. If the range of the working voltage is given, the ranges of the objective function values are also determined. This information is available for determining the preferred solution. The variations of two objective function values with respect to different values of the input voltage between 10V to 300V for six Pareto-optimal designs obtained after clustering (see Table 5.3) have been calculated. Fig. 5.6 shows the results for the input power at resonance smaller than 100 VA and the vibration amplitude at resonance larger than 10µm. The number of the piezo-rings will affect the range of the input power and the vibration amplitude of the transducer for the given range of voltage. For example, the vibration amplitude of Design 42 with 4 piezo-rings is not smaller than about 16 µm (refer to point A). The vibration amplitude of Design 5 with 2 piezo-rings will not be larger than about 57 µm (refer to point B). Its input power will not be more than about 67 VA. Obviously, Design 42 is the best design because the others do not dominate the set of its Pareto-optimal solutions with respect to the input voltage. That is, in order to arrive at a given vibration amplitude (here not smaller than about 16 µm), the transducer corresponding to Design 42 needs the minimum input power among the 6 Pareto-optimal designs. Therefore Design 42 is the preferred design for implementation. It is noticed that the material of the end blocks and the total thickness of the piezo-stack affects the performances of transducers for a given range of the input voltage. However, the performances are first determined by material and then by the thickness. The transducers with the end blocks made of brass have better performance than those with the end blocks of titanium. Under the condition of the same material, the transducers with a thin piezo-stack have better performances than the others.

In the above sections, the Pareto-optimal solutions for the symmetrical freely vibrating transducer have been analyzed. The methods to determine the preferred design have been discussed. Some important rules for designing the symmetrical Langevin-type transducers via multiobjective optimization are concluded as follows:

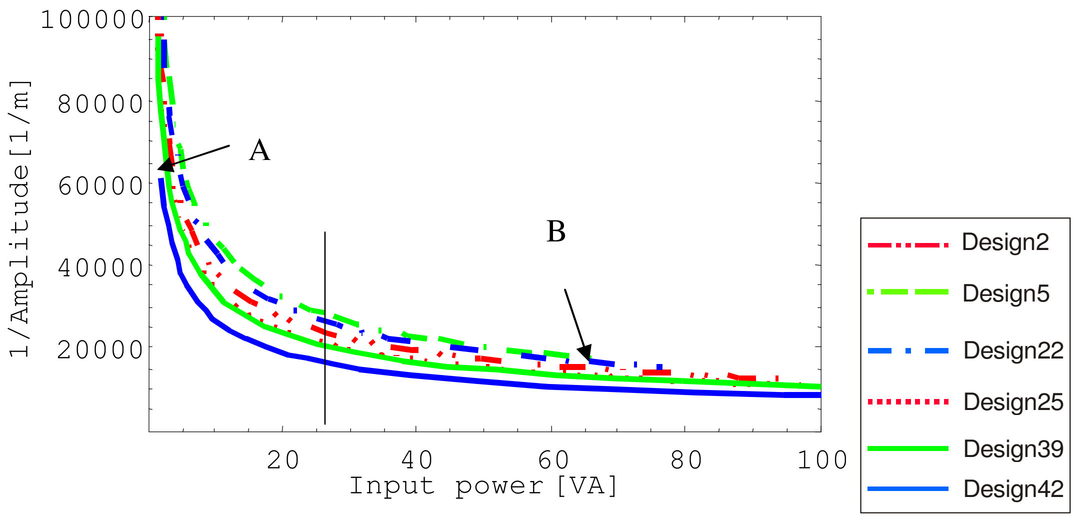

Fig. 5.6 Values of the input power and the vibration amplitude of the symmetrical transducers for 6 Pareto-optimal designs obtained after clustering for a given range of the input voltage from 10V to 300V

1. Brass and titanium are two kinds of preferred material of the end blocks for Pareto-optimal designs. If a Pareto-optimal transducer is expected to have good performance (lower electric input power and higher vibration amplitude) in a given range of the voltage, brass is the preferred material for the end blocks. Furthermore, the total thickness of the piezo-stack should be as small as possible. However, if a larger effective coupling factor is expected, a thicker piezo-stack needs to be used.

2. The number of the piezoelectric rings will affect the ranges of the values of objective functions. For a given voltage range, the maximum input power of the transducer with 2 piezo-rings is smaller than that of the transducer with 4 piezo-rings. On the other hand, the minimum vibration amplitude of the transducer with 2 piezo-rings is lower than that of the transducer with 4 piezo-rings.

It should be pointed out the implemented Pareto-optimal solution here is selected from many known candidates which are obtained using MOEAs. This is different from the process of obtaining a Pareto-optimal solution by using a traditional scalarization method, where a preference structure over objectives is given in advance and then an implemented Pareto-optimal solution is found. Obviously, the approach in which the entire set of Pareto-optimal solutions is first identified and the preferred solution is then chosen is more practical and less subjective.

5.2 Discussion of the Results for Stepped-horn Transducers without Load

Fig. 5.7 shows three sets of non-dominated solutions for the stepped-horn transducers with 2, 4 and 6 piezo-rings obtained in the first level optimization (refer to Figs. 4.28, 4.31 and 4.32 as well as Tables 4.17, 4.21 and 4.22). Similarly, the Pareto-optimal solutions were searched again in these non-dominated solutions. Fig 5.8 shows the results after non-domination check. Table 5.4 gives the values of the design variables and objective functions for these Pareto-optimal solutions after the second level optimization.

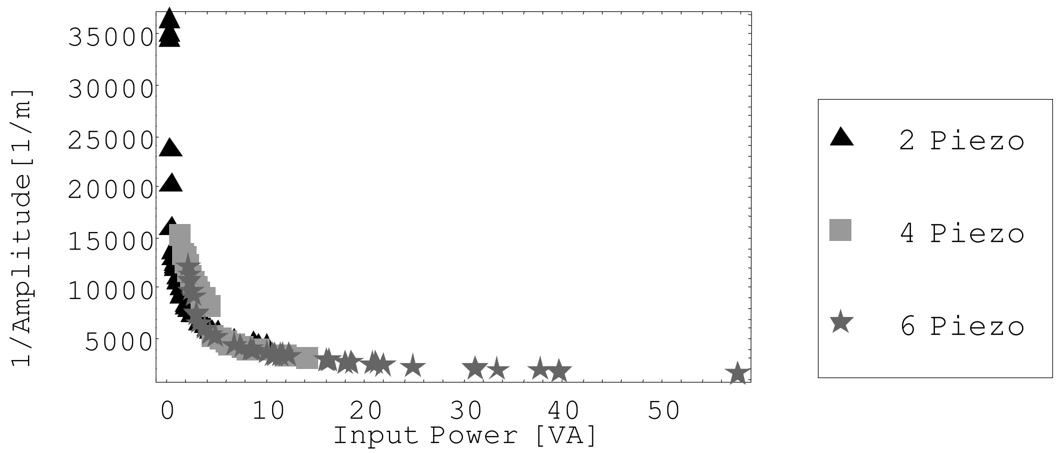

Fig. 5.7 Non-dominated solutions in objective space for the freely vibrating stepped-horn transducer with 2 , 4 and 6 piezo-rings

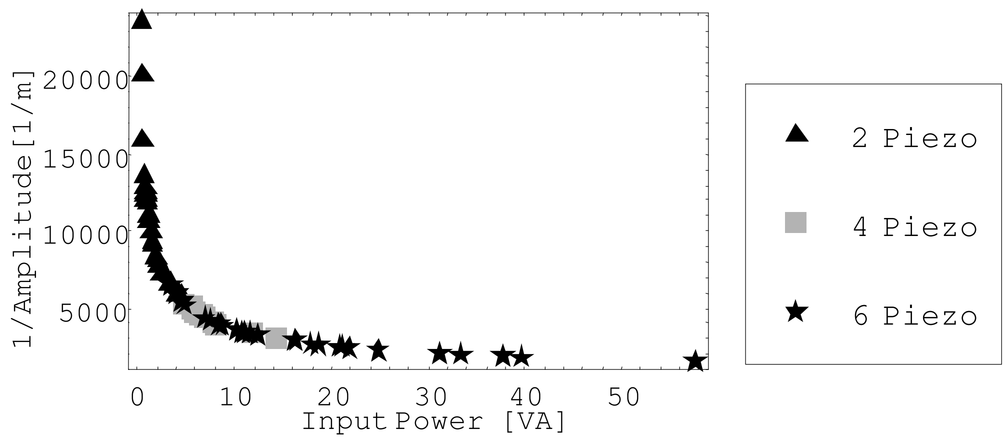

Fig. 5.8 Non-dominated solutions in objective space for the freely vibrating stepped-horn transducer obtained after the second level optimization

Table 5.4 Values of design variables and objective functions for the non-dominated solutions obtained after the second-level optimization for the freely vibrating stepped-horn transducer

Design	D_t [mm]	ζ	L_b [mm]	Typ_b	Typ_f	h_p [mm]	L_{f1} [mm]	L_{f2} [mm]	N	$\hat{u}_{a4}$ [μm]	$\hat{P}_a$ [VA]
1	8.	0.2	5.	2	4	5.	8.1	42.	2	73.74	0.7
2	8.	0.2	5.	3	3	5.	46.5	50.3	2	49.71	0.51
3	8.	0.2	5.	1	4	5.	9.7	41.7	2	83.12	0.89
4	8.	0.2	7.1	3	4	3.5	5.	42.1	2	107.97	1.51
5	8.	0.2	5.6	2	4	4.9	41.9	40.3	2	62.98	0.51
6	8.	0.2	10.2	3	4	3.5	9.	41.6	2	110.07	1.55
7	8.	0.2	6.2	3	4	4.9	25.	40.9	2	78.11	0.79
8	8.	0.21	17.7	4	4	3.7	23.	40.6	2	139.87	2.73
9	8.	0.2	8.4	2	3	4.6	37.2	50.7	2	42.33	0.39
10	8.	0.21	7.4	3	4	5.	14.5	41.3	2	90.83	1.12
11	8.	0.2	15.7	2	4	3.9	13.	41.4	2	94.67	1.19
12	8.	0.2	10.8	2	4	4.4	13.2	41.5	2	81.04	0.88
13	8.	0.2	11.8	2	4	4.1	15.4	41.4	2	80.1	0.84
14	8.	0.2	13.6	3	4	3.5	10.7	41.3	2	120.76	1.91
15	8.	0.2	14.6	1	4	3.2	8.2	41.5	2	124.03	2.01
16	8.	0.2	16.3	1	4	2.4	5.	41.7	2	138.67	2.48
17	8.	0.21	14.5	2	4	4.	18.7	41.2	2	85.14	0.97
18	8.1	0.21	20.7	2	4	3.3	19.7	41.1	2	100.77	1.38
19	8.1	0.21	17.8	1	4	3.7	12.	41.1	2	128.38	2.27
20	8.1	0.21	36.7	1	4	1.6	12.4	40.8	2	170.71	4.12
21	8.1	0.21	30.4	3	4	2.6	16.	40.5	2	171.48	4.42
22	8.1	0.21	37.	2	4	1.5	5.8	41.4	2	151.31	3.35
23	8.	0.2	12.4	1	4	2.5	6.	41.5	4	242.77	7.77
24	8.	0.2	21.5	2	4	1.	5.8	41.9	4	251.75	8.18
25	8.	0.2	5.	1	4	3.3	6.1	41.7	4	188.67	4.65
26	8.	0.2	11.5	2	4	3.2	5.7	41.7	4	203.43	5.48

Table 5.4 continued

Design	D_t [mm]	ζ	L_b [mm]	Typ_b	Typ_f	h_p [mm]	L_{f1} [mm]	L_{f2} [mm]	N	$\hat{u}_{a4}$ [µm]	$\hat{P}_a$ [VA]
27	8.	0.2	15.	2	4	2.8	5.4	41.7	4	220.03	6.44
28	8.	0.2	17.1	2	4	2.7	5.5	41.6	4	228.54	6.95
29	8.	0.2	8.6	3	4	3.1	6.1	41.5	4	222.46	6.55
30	8.	0.2	8.9	2	4	3.	5.8	41.8	4	188.88	4.66
31	8.	0.2	26.6	4	4	1.	5.2	41.1	4	334.68	14.33
32	8.	0.2	26.5	4	4	1.1	5.2	41.1	4	332.49	14.26
33	8.	0.2	12.4	2	4	3.4	5.2	41.6	4	210.05	5.89
34	8.	0.2	12.7	2	4	3.6	5.4	41.5	4	211.34	5.99
35	8.	0.2	20.6	4	4	1.8	5.2	41.2	4	301.42	11.96
36	8.	0.2	5.	1	4	5.	5.2	41.4	4	199.08	5.47
37	8.	0.2	7.9	4	4	1.2	48.8	39.6	6	340.97	16.15
38	8.	0.2	50.	1	4	0.2	5.6	40.9	6	561.83	39.66
39	8.	0.2	20.4	4	4	0.7	21.8	40.7	6	441.49	24.83
40	8.	0.2	25.	1	4	0.2	5.	41.5	6	487.2	31.15
41	8.	0.2	18.6	3	4	0.8	24.7	40.6	6	412.6	21.82
42	8.	0.2	58.5	4	4	0.2	5.	39.6	6	648.77	57.59
43	8.	0.2	5.	2	4	1.3	42.4	40.4	6	153.78	3.36
44	8.	0.2	18.6	3	4	0.8	23.9	40.7	6	406.38	21.17
45	8.	0.2	17.	1	4	1.	27.8	40.6	6	380.69	18.72
46	8.	0.2	15.8	1	4	1.1	29.8	40.5	6	372.16	17.95
47	8.	0.2	16.8	2	4	1.	29.4	40.8	6	260.58	8.71
48	8.	0.2	18.8	2	4	0.7	16.8	41.3	6	277.37	10.15
49	8.	0.2	11.7	1	4	1.	27.9	40.8	6	289.66	10.78
50	8.	0.2	15.6	2	4	0.9	24.1	41.	6	239.88	7.52
51	8.1	0.2	6.6	2	4	1.3	39.4	40.5	6	168.02	3.9
52	8.1	0.2	29.2	1	4	1.	20.6	40.5	6	499.12	33.44
53	8.1	0.2	26.2	3	4	1.	22.8	40.3	6	521.78	37.77
54	8.1	0.2	5.	4	4	1.3	31.3	40.8	6	191.9	4.9
55	8.1	0.2	19.4	1	4	1.	23.1	40.7	6	398.55	20.83
56	8.1	0.2	8.9	3	4	1.4	34.9	40.4	6	296.52	11.53
57	8.1	0.2	8.4	3	4	1.6	36.	40.3	6	306.24	12.42
58	8.1	0.2	9.6	1	4	1.4	35.2	40.4	6	297.58	11.63
59	8.1	0.2	8.4	4	4	1.6	41.6	40.	6	343.39	16.34
60	8.1	0.2	5.7	1	4	1.4	39.2	40.4	6	227.89	6.86
61	8.1	0.2	6.3	4	4	1.5	37.5	40.4	6	253.2	8.43
62	8.1	0.2	9.2	1	4	1.6	30.5	40.6	6	290.1	11.02
63	8.1	0.2	5.5	2	4	1.8	35.8	40.6	6	183.69	4.43

5.2.1 Analysis of the Results of the Optimization

The final set of Pareto-optimal solutions for the stepped-horn transducer consists of 22 members from the set of the non-dominated solutions for 2 piezo-rings, 14 members from the set for 4 piezo-rings and 27 members from the set for 6 piezo-rings. Unlike the final results after the second level optimization for the symmetrical transducer, the final results for the stepped-horn transducer include some members of the set of non-dominated solutions for 6 piezo-rings. This is because not all members of the set of non-dominated solutions of the stepped-horn transducer with 6 piezo-rings are dominated by the members of the set of non-dominated solutions of the transducer with 2 and 4 piezo-rings. It is noted that the diameter of the transducers for all solutions is equal or nearly equal to the lower bound of this design variable. The reason for this phenomenon has been given in section 5.1.1. Furthermore, all amplitude transformation ratios ζ, namely the ratio of the diameter between the output side and input side of the horn, are equal or nearly equal to the lower bound of this design variable. This is because a horn with the ratio $\zeta < 1$ is a mechanical amplifier. For a given vibration amplitude at the input side of the horn, the smaller the ratio ζ is, the larger the vibration amplitude at the output side. Therefore, in order to obtain the maximum vibration amplitude at the output side of the horn, ζ needs to be as small as possible. It should be noted that a large transformation will result in a “sensitive” transducer, i.e. a transducer where the output load has a large influence on the system’s behavior. In the present optimization problem, however, this effect has not been taken into account in the formulation of the objective functions. In all Pareto-optimal designs, there are four types of material (steel, titanium, aluminum bronze and brass) for the back section but only two types (aluminum bronze and brass) for the horn. Most horns are made of brass. Since a horn is used as mechanical amplifier, the stepped-horn transducer can produce the larger vibration amplitude for a given input power compared with the symmetrical transducer.

5.2.2 Determination of the Preferred Solution

Similarly, there are two classes of methods to determine the preferred design for implementation from the results of the second level optimization. One class is to determine the preferred solution directly from the whole set. The other is to determine the preferred solution from the reduced set of Pareto-optimal solutions. In the following, several methods are discussed respectively.

Selection according to weight vectors The pseudo-weight vectors of two design objectives for all Pareto-optimal solutions shown in Table 5.4 have been calculated using equation (5.1). They are shown in Table 5.5. Then the preferred solution can be selected according to a designer-preferred weight vector. For example, if a weight value of 40% is prepared for objective 1 (the vibration amplitude) and a weight value of 60% for the objective 2 (the input power), Design 4 can be chosen. Design 9 and Design 42 are two extreme solutions among the obtained non-dominated solutions. The former represents the Pareto-optimal design of a stepped-horn transducer that consumes the smallest electrical input power among all designs. The latter represents the Pareto-optimal design of a stepped-horn transducer that has the largest vibration amplitude.

Table 5.5 Values of the pseudo-weight vectors of the objective function for the non-dominated solutions obtained after the second level optimization for the freely vibrating stepped-horn transducer

Design	w_1	w_2	Design	w_1	w_2	Design	w_1	w_2
1	0.314	0.686	22	0.448	0.552	43	0.45	0.55
2	0.137	0.863	23	0.504	0.496	44	0.601	0.399
3	0.346	0.654	24	0.507	0.493	45	0.583	0.417
4	0.399	0.601	25	0.473	0.527	46	0.578	0.422
5	0.26	0.74	26	0.482	0.518	47	0.512	0.488
6	0.402	0.598	27	0.491	0.509	48	0.522	0.478
7	0.33	0.67	28	0.496	0.504	49	0.528	0.472
8	0.438	0.562	29	0.493	0.507	50	0.502	0.498
9	0.	1.	30	0.473	0.527	51	0.46	0.54
10	0.367	0.633	31	0.553	0.447	52	0.699	0.301
11	0.375	0.625	32	0.552	0.448	53	0.739	0.261
12	0.34	0.66	33	0.486	0.514	54	0.475	0.525
13	0.337	0.663	34	0.487	0.513	55	0.598	0.402
14	0.417	0.583	35	0.536	0.464	56	0.532	0.468
15	0.42	0.58	36	0.48	0.52	57	0.539	0.461
16	0.435	0.565	37	0.564	0.436	58	0.533	0.467
17	0.352	0.648	38	0.759	0.241	59	0.565	0.435
18	0.387	0.613	39	0.628	0.372	60	0.496	0.504
19	0.426	0.574	40	0.679	0.321	61	0.509	0.491
20	0.463	0.537	41	0.606	0.394	62	0.529	0.471
21	0.464	0.536	42	1.	0.	63	0.47	0.53

It is noticed that the weight vectors are not uniformly distributed, because the final Pareto-optimal solutions are not distributed evenly in the objective space. Therefore, not all designer-preferred weight vectors can find corresponding designs in the set of the Pareto-optimal solutions. In this case, other high level information is needed. It needs to be pointed out that the pseudo weight of the electrical input power doesn't increase with the increase of the thickness of the piezo-stack any more. For example, the total thickness of the piezo-stack for Design 36 is larger than the total thickness for Design 5 and the weight of the input power for the former is smaller than that for the latter. This is different from the situation for the symmetrical transducer. Moreover, in most cases, the larger the number of the piezo-rings is, the larger the input power.

Selection according to performance criteria Any performance criterion which is not used as the objective function can be considered as high level information to determine the preferred design. For the symmetrical transducer, the effective coupling factor k has been considered. Here, however, another important performance parameter of transducers, namely the piezoelectric quality number M is considered as high-level information.

As described in chapter 2 and 4, the piezoelectric quality number M presents the phase descend of the admittance function of the transducer. The larger the value of M is, the higher the extent of the phase reserve. A large phase reserve ensures that a resonance frequency exists in the true sense of the meaning, and the transducer can be driven with zero reactive power even though the damping of the load may be large. The frequency response of the admittance function $\underline{\hat{I}}/\underline{\hat{U}}$ for the stepped horn can be calculated according to equation (4.73). Figs. 5.9 and 5.10 show the Bode plot and the Nyquist plot of the admittance function $\underline{\hat{I}}/\underline{\hat{U}}$ for 6 Pareto-optimal designs (Design 8 to Design 13). According to Fig. 5.9, it can be obtained that Design 8 has a largest phase descend. That is, it has the largest piezoelectric quality number *M*. This can be explained more clearly by Fig. 5.10. As stated in section 2.3.1, the piezoelectric quality number is geometrically defined as the ratio between the diameter Y_r of the locus of $\underline{\hat{I}}/\underline{\hat{U}}$ and the offset Y_c of its center from the real axis, namely $M = Y_r/Y_c$ (see Fig. 5.9). Obviously, Design 8 has the largest *M* and should be preferred for implementation.

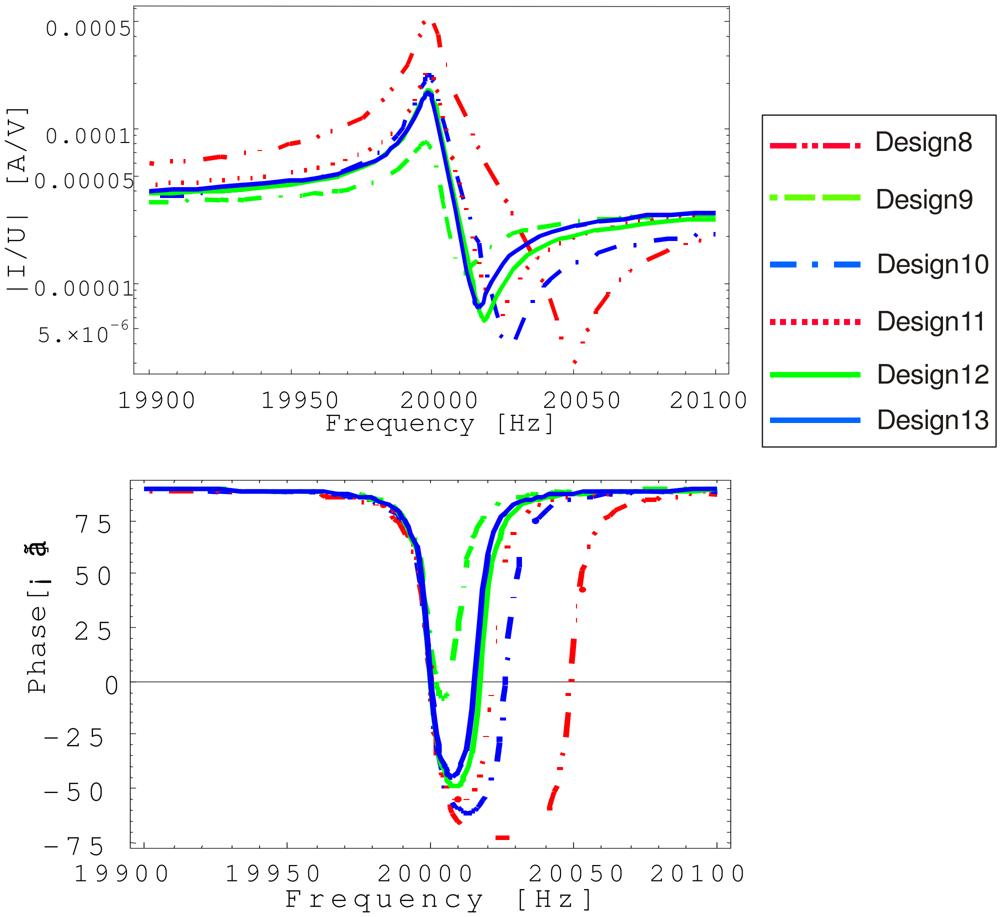

Fig. 5.9 Admittances $\underline{\hat{I}}/\underline{\hat{U}}$ of 6 designs from Table 5.4 as functions of frequencies (the Bode plot)

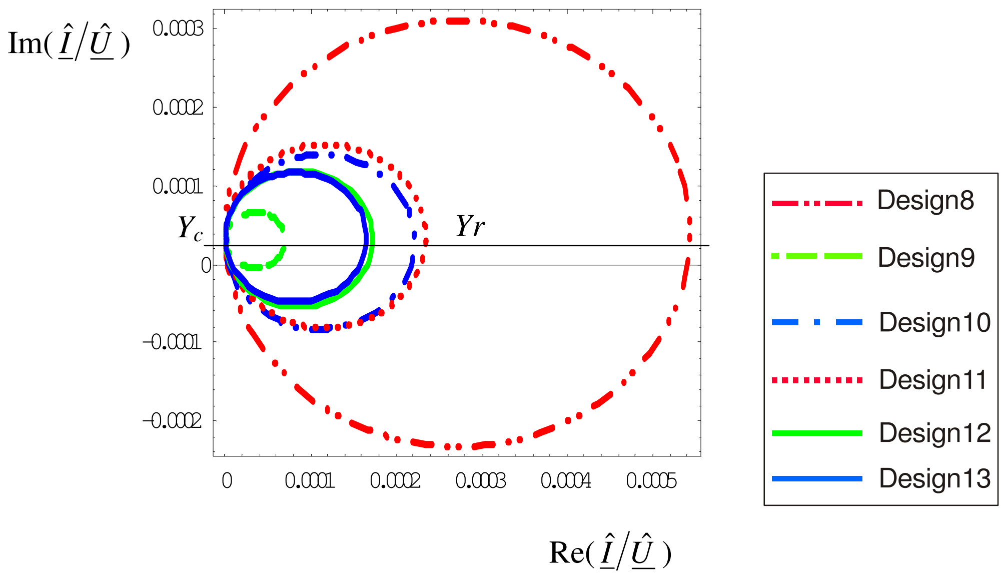

Fig. 5.10 Admittances $\hat{\underline{I}}/\hat{\underline{U}}$ of 6 designs from Table 5.4 as functions of frequencies in the complex plane (the Nyquist plot)

It is noticed that the 0°-line in Fig. 5.9 is almost tangential to the phase-frequency plots of Design 9. Correspondingly the real axis in Fig. 5.10 is nearly tangential to the Nyquist plot of Design 9. That is, the piezoelectric quality number of Design 9 is nearly equal to 2. If the load damping is large, it is possible that the intersections do not exist any more. The transducer can not be driven with zero reactive power. Therefore, it is avoided to select Design 9 as the optimal design of the transducer for ultrasonic bonding and machining.

It can be seen that Design 8 also has the largest distance between resonance and anti-resonance frequencies. That is, Design 8 has the largest coupling factor. It should be pointed out that for the Pareto-optimal stepped-horn, increasing the thickness of the piezo-stack doesn't mean the coupling factor will increase. Here, the material of the end blocks will affect the coupling factor. For these 6 Pareto-optimal designs, the designs whose end blocks are made of brass have better coupling factor than the others.

Similarly, these selection methods can be applied in other Pareto-optimal designs shown in Table 5.4. Therefore, all solutions can be compared according to high level information and the preferred design can be determined.

Selection by means of clustering technique There are 63 members in the set of Pareto-optimal solutions obtained after the second level optimization. If all Pareto-optimal solutions are evaluated according to high level information, the computation cost is large. In order to reduce the size of the set of Pareto-optimal solutions, the clustering technique is used here. Fig. 5.11 shows the results after performing the clustering operation similar to that used for the symmetrical transducer with a choice of 5 final solutions in the objective space. Tables 5.6 and 5.7 give their corresponding values of the design variables, objective functions and weights.

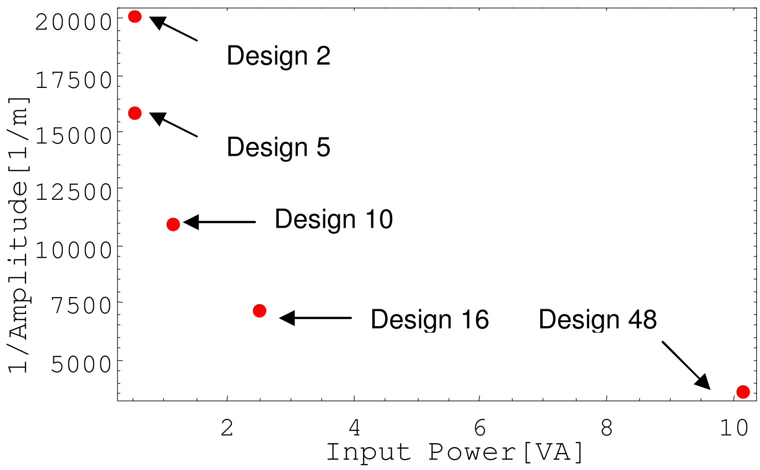

Fig. 5.11 Five final Pareto-optimal solutions after clustering for the stepped-horn transducer

Table 5.6 Values of 5 Pareto-optimal solutions in design variable spaces after clustering for the stepped-horn transducer

Design	D_t [mm]	ζ	L_b [mm]	Typ_b	Typ_f	h_p [mm]	L_{f1} [mm]	L_{f2} [mm]	N
2	8	0.2	5.	3	3	5	46.5	50.3	2
5	8	0.2	5.6	2	4	4.9	41.9	40.3	2
10	8	0.21	7.4	3	4	5	14.5	41.3	2
16	8	0.2	16.3	1	4	2.4	5.	41.7	2
48	8	0.2	18.8	2	4	0.7	16.8	41.3	6

Table 5.7 Values of objective functions for 5 Pareto-optimal solutions and corresponding weights for the stepped-horn transducer

Design	Amplitude [µm] (Obj1)	Input Power [VA] (Obj2)	w_1	w_2
2	49.71	0.51	0.14	0.86
5	62.98	0.51	0.26	0.74
10	90.83	1.12	0.37	0.63
16	138.67	2.48	0.43	0.57
48	277.37	10.15	0.52	0.48

The configurations of the stepped-horn transducers for the above 5 Pareto-optimal solutions are shown in Fig. 5.12. It is noticed that the diameter and amplitude transformation factor ς of the transducers for all 6 designs are equal to the lower bounds of the design variables D_t and ς, respectively. That is, for this two optimization objectives (maximizing the vibration amplitude and minimizing the input power of the transducer) the lower bounds of design variables D_t and ς will affect the optimized results. They should be defined according to practical design requirements. Design 2 is the minimum input power design, but the vibration amplitude is the smallest. Design 48 is the maximum vibration amplitude design. However its input electrical power is the largest. The material types of the back section and horn affect the length of the whole transducer. Among the 5 designs, the transducer with the back section of steel and the horn of brass has small length. If a short transducer is expected, the transducer corresponding to Design 16 is preferred. A finally implemented design can also be selected from these 5 designs according to a designer-preferred weight vector or other high level information such as piezoelectric quality number M, coupling factor k or the like. In the following, the coupling factor k is considered.

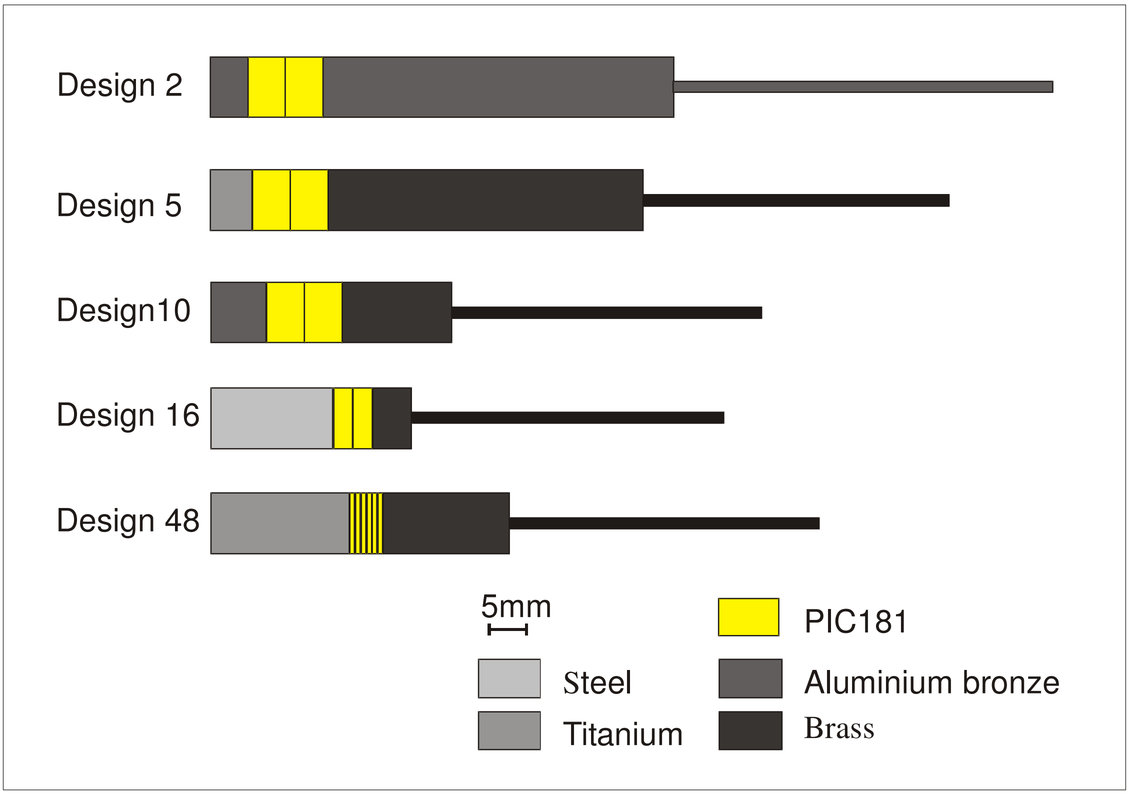

Fig. 5.12 Configurations of the stepped horn transducers without load for 5 Pareto-optimal solutions after clustering

As stated before, the effective coupling factor k can be represented by the distance between the resonance and anti-resonance frequencies for a vibration mode of the transducer. The resonance and anti-resonance frequencies can be determined by the frequency response of the admittance function $\underline{\hat{I}}/\underline{\hat{U}}$. Fig. 5.13 gives the frequency responses of the admittance function $\underline{\hat{I}}/\underline{\hat{U}}$ for the 5 designs, where the frequency at which the admittance is maximum corresponds to the resonance frequency. The frequency at which the admittance is minimum corresponds to the anti-resonance frequency. Obviously, Design 10 and 16 have larger distances between the resonance and anti-resonance frequencies. Considering that the length of the transducer with Design 16 is shorter than that of the transducer with Design 10, therefore, Design 16 is preferred.

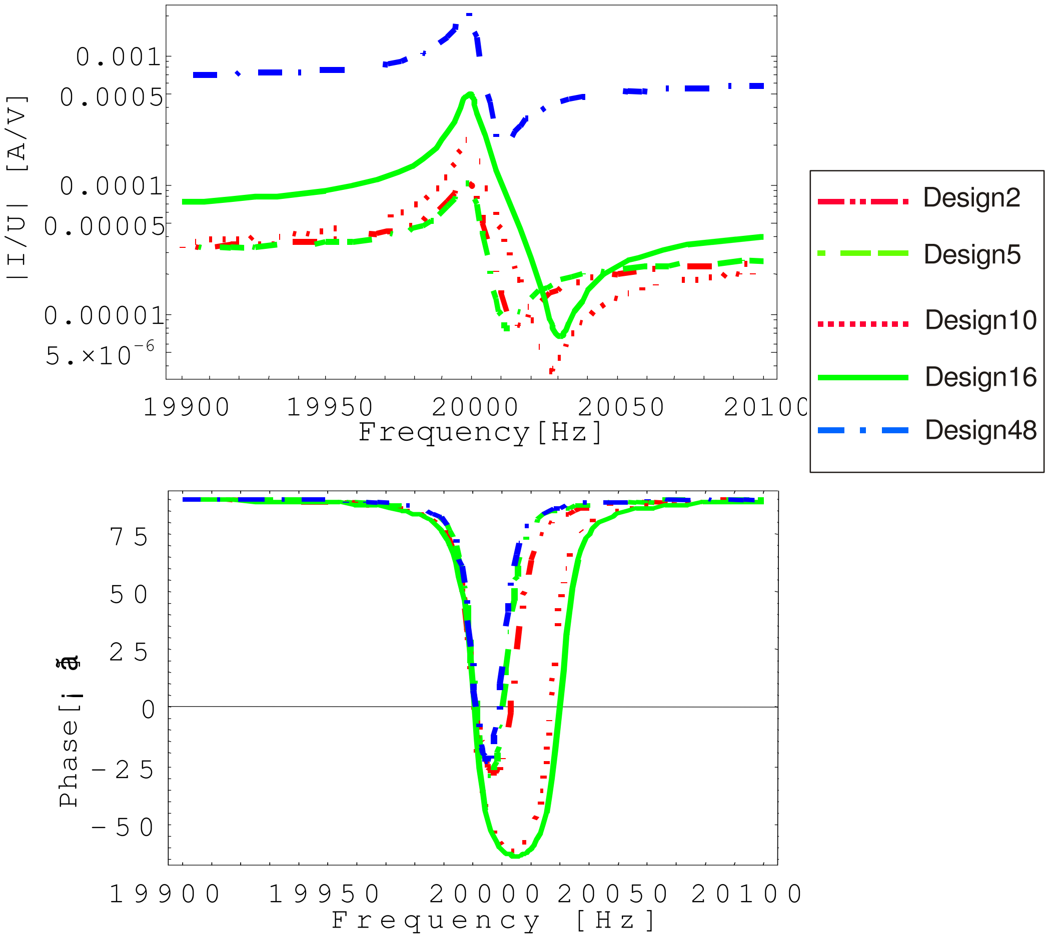

Fig. 5.13 Admittance $\underline{\hat{I}}/\underline{\hat{U}}$ as functions of frequencies for 5 Pareto-optimal designs of stepped-horn transducers without load obtained after clustering.

5.3 Discussion of the Results for Stepped-horn Transducers with Load

The non-dominated solutions of the transducers with 2, 4 and 6 piezo-rings under a mechanical load have been obtained in chapter 4 (refer to Figs. 4.34, 4.35 and 4.36 as well as Tables 4.23, 4.24 and 4.25). Here they are plotted in Fig.5.14. The non-dominated solutions were searched for again in these solutions and the results are shown in Fig.5.15 and Table 5.8

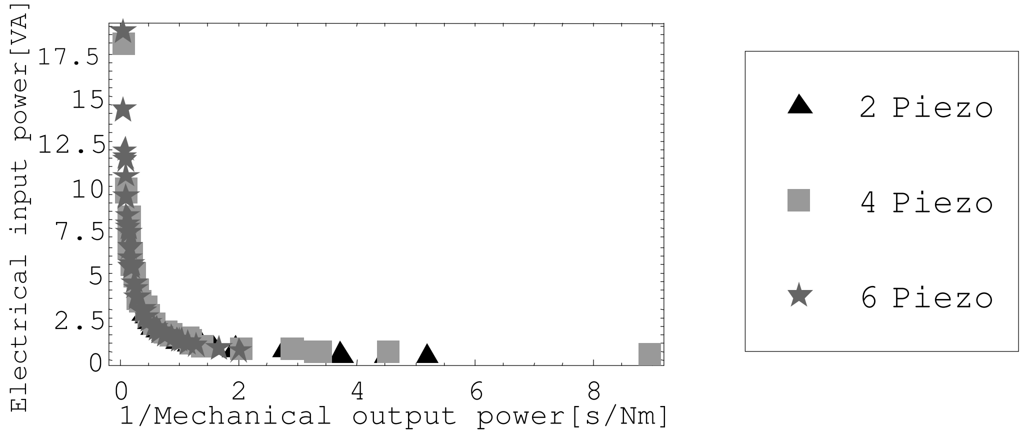

Fig. 5.14 Three sets of non-dominated solutions of the stepped-horn transducer with load for 2, 4 and 6 piezo-rings

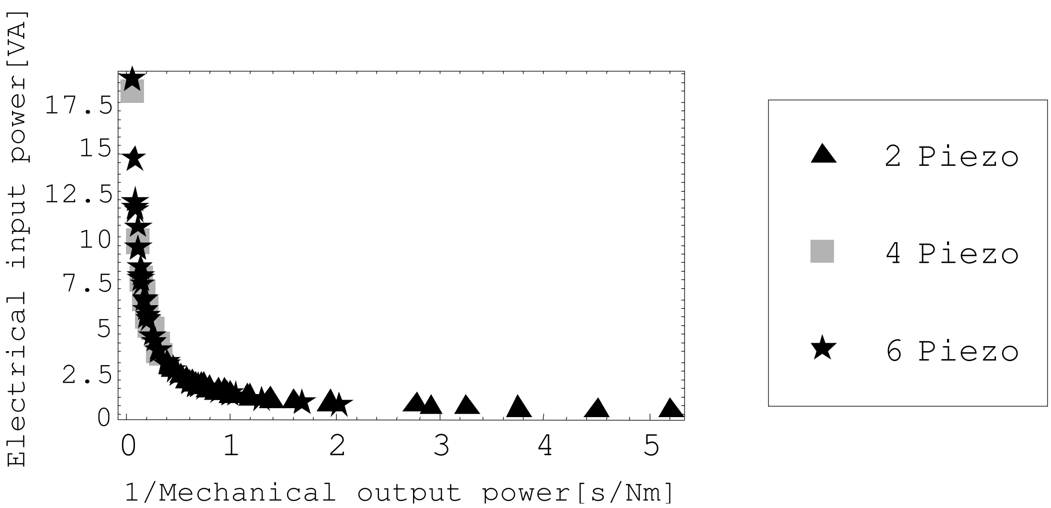

Fig. 5.15 Non-dominated solutions of the stepped-horn transducer with load for 2, 4 and 6 piezo-rings after the second level optimization

Table 5.8 Values of design variables and objective functions for the non-dominated solutions obtained after the second level optimization for the stepped-horn transducer with load

Design	D_t [mm]	ζ	L_b [mm]	Typ_b	Typ_f	h_p [mm]	L_{f1} [mm]	L_{f2} [mm]	N	$\hat{P}_m$ [Nm/s]	$\hat{P}_a$ [VA]
1	8.	0.86	34.3	3	3	4.6	29.9	24.3	2	0.22	0.3
2	8.	0.96	18.3	4	1	5.	15.3	72.9	2	0.19	0.27
3	8.5	0.88	34.8	4	3	4.5	32.6	12.8	2	0.34	0.43
4	8.8	0.86	35.7	4	4	4.2	33.9	2.	2	0.27	0.36
5	9.2	0.85	28.	3	3	4.7	32.7	29.6	2	0.31	0.41
6	9.4	0.86	41.5	3	1	4.	42.4	16.7	2	0.72	0.85
7	9.7	1.	44.3	1	3	3.3	31.8	20.	2	0.62	0.77
8	10.2	0.98	51.3	2	3	4.	8.7	41.7	2	0.73	0.87
9	10.3	0.79	42.9	3	1	4.1	43.1	14.4	2	1.	1.16
10	10.4	0.8	45.	2	1	4.	32.6	48.9	2	0.51	0.67
11	10.4	0.91	34.8	4	3	3.8	41.8	4.	2	0.84	1.
12	10.5	0.9	34.6	4	1	3.8	42.	17.7	2	1.14	1.31
13	10.5	0.89	34.8	4	3	3.9	41.7	3.9	2	0.87	1.02
14	10.5	0.9	46.	3	1	3.5	31.4	23.4	2	1.04	1.22
15	10.7	0.97	43.7	1	2	3.5	30.	35.4	2	0.36	0.54
16	11.	0.89	44.3	3	1	3.5	31.9	26.1	2	1.25	1.45
17	11.3	0.93	40.8	1	3	3.4	39.3	16.9	2	1.05	1.26
18	11.4	0.99	53.1	2	1	3.9	6.9	53.5	2	1.73	1.93
19	11.7	0.8	40.7	3	1	3.7	39.2	26.6	2	1.49	1.72
20	11.8	0.92	36.7	4	1	3.4	49.2	5.9	2	1.91	2.17
21	11.8	0.81	46.1	3	1	3.5	28.3	30.6	2	1.35	1.58
22	11.9	0.86	41.4	1	1	3.5	37.9	36.7	2	1.39	1.63
23	11.9	0.78	41.7	4	3	3.7	34.2	2.	2	1.26	1.47
24	12.	0.78	42.	3	1	3.7	38.1	26.4	2	1.57	1.82
25	12.8	0.66	47.8	3	1	3.9	42.3	9.1	2	2.37	2.66
26	13.2	1.	40.9	3	3	2.6	36.2	14.2	2	2.2	2.56
27	11.6	0.51	44.7	1	4	3.8	29.8	2.	4	3.12	3.59
28	11.6	0.35	33.	4	3	3.6	33.9	9.7	4	4.27	4.94
29	12.1	0.6	32.9	3	1	3.5	36.1	34.4	4	4.16	4.82
30	12.8	0.69	24.8	3	3	3.	53.5	5.3	4	6.89	7.72
31	12.9	0.79	32.	4	4	4.1	27.8	2.	4	4.84	5.44
32	13.	0.32	39.2	4	3	3.4	28.3	2.	4	6.23	6.97
33	13.2	0.82	29.8	2	4	4.4	28.2	21.8	4	2.89	3.42
34	13.4	0.65	28.4	3	4	3.2	39.3	2.	4	5.69	6.48
35	13.7	0.2	44.9	3	3	3.1	32.9	2.	4	8.79	9.8
36	14.	0.24	51.1	2	4	4.5	27.8	2.	4	6.8	7.51
37	14.1	0.49	34.4	4	3	3.8	28.8	12.5	4	8.66	9.6
38	15.	0.73	31.1	2	4	4.2	26.3	26.5	4	3.38	4.08
39	15.	0.8	33.8	4	2	3.9	33.	21.2	4	5.4	6.17
40	16.3	0.76	37.1	4	3	3.8	27.1	2.	4	16.89	18.06

Table 5.8 continued

Design	D_t [mm]	ζ	L_b [mm]	Typ_b	Typ_f	h_p [mm]	L_{f1} [mm]	L_{f2} [mm]	N	$\hat{P}_m$ [Nm/s]	$\hat{P}_a$ [VA]
41	8.	1.	58.5	2	1	5.	6.6	4.4	6	0.96	1.11
42	8.	1.	46.6	2	2	4.9	12.8	19.4	6	1.01	1.2
43	8.	1.	46.8	4	2	5.	3.1	2.	6	0.49	0.62
44	8.	1.	52.1	2	1	4.8	13.	3.9	6	1.32	1.51
45	8.	1.	53.7	2	3	5.	5.	8.2	6	1.12	1.29
46	8.	1.	58.5	3	1	4.7	3.4	2.	6	0.59	0.73
47	8.1	0.94	40.1	1	1	5.	5.8	13.6	6	1.46	1.67
48	8.3	0.99	39.9	1	3	5.	5.	11.6	6	1.49	1.7
49	8.5	0.92	54.9	3	2	5.	5.	5.3	6	0.78	0.94
50	8.7	0.95	48.3	2	4	4.9	10.6	7.4	6	1.62	1.87
51	9.2	0.91	45.7	2	3	4.9	8.	14.1	6	2.57	2.9
52	9.3	0.91	41.5	1	1	4.9	7.8	11.8	6	2.48	2.81
53	9.4	0.92	47.7	1	4	4.8	8.9	6.	6	1.98	2.28
54	10.	0.89	48.6	3	1	4.7	8.9	2.	6	2.18	2.5
55	10.	0.85	45.4	2	4	4.9	6.4	16.3	6	2.59	2.98
56	10.5	0.82	45.2	3	4	4.9	5.	7.9	6	2.5	2.87
57	10.5	0.94	27.	3	4	4.7	7.2	16.7	6	3.68	4.17
58	10.6	0.85	43.6	3	1	4.8	5.8	10.2	6	3.26	3.69
59	10.7	0.77	51.9	1	3	4.3	12.3	6.3	6	3.99	4.51
60	10.8	0.97	33.3	3	2	5.	5.	25.4	6	3.17	3.62
61	11.2	0.92	49.6	1	3	4.	7.3	13.3	6	5.28	5.93
62	11.2	0.78	36.5	2	3	4.3	11.1	29.9	6	4.85	5.5
63	11.3	0.91	40.6	3	1	4.8	6.7	9.7	6	4.75	5.31
64	11.3	0.92	28.4	1	1	4.6	8.6	25.8	6	8.58	9.35
65	11.5	0.9	41.9	1	1	4.4	18.5	4.9	6	7.44	8.2
66	11.5	0.92	37.7	3	3	4.8	6.3	10.3	6	5.27	5.88
67	11.8	0.66	45.7	2	3	3.8	15.4	25.6	6	5.64	6.45
68	12.	0.77	34.	2	1	4.1	25.3	31.	6	11.02	11.99
69	12.	0.94	32.4	1	1	4.6	13.1	16.2	6	10.74	11.62
70	12.	0.93	32.8	1	4	4.6	13.3	10.3	6	7.02	7.8
71	12.2	0.96	27.4	3	4	5.	5.	16.2	6	6.84	7.59
72	12.5	0.9	47.3	2	3	3.6	7.6	24.8	6	10.42	11.44
73	12.7	0.92	23.7	2	4	4.9	5.2	30.4	6	6.52	7.31
74	13.2	0.79	49.8	1	1	3.6	8.3	26.1	6	8.84	10.52
75	13.3	0.48	58.1	2	1	3.2	21.5	17.3	6	13.03	14.3
76	13.4	0.93	46.8	2	1	4.1	10.5	21.2	6	17.69	18.73

5.3.1 Analysis of the Results of the Optimization

There are 76 individuals in the final set of Pareto-optimal solutions for the stepped-horn transducer with load, where 26 individuals come from the set of the non-dominated solutions for 2 piezo-rings, 14 individuals from the set for 4 piezo-rings and 36 individuals from the set for 6 piezo-rings. It is noticed that not all diameters of the transducers are equal or nearly equal to the lower bound of this design variable. Unlike the amplitude transformation ratio ζ under the condition of no load, here the ζ of most transducers are near to the lower bound of this design variable, but rather have values around $\zeta = 0.8$. Some of them are near to 1, which refers to a constant horn, a special type of the stepped horn. Furthermore, four material types have been applied for both the back section and horn. The thickness of all piezo-rings is more than 3mm.

5.3.2 Determination of the Preferred Solution

In the front sections, two classes of methods and some high-level information have been used to determine the preferred design for implementation. Here the similar methods and high level information can be adopted. In the following, first, the size of the set of solutions is reduced by clustering operation. Then, the coupling factor, the piezoelectric quality number and the power efficiency as high-level information are applied in determining a preferred design.

Reduction of size of the set of non-dominated solutions There are 76 solutions in the set of Pareto-optimal solutions obtained after the second level optimization. In order to reduce the size of the set of Pareto-optimal solutions, a clustering technique similar to that used before is applied here. Fig. 5.16 shows the results with a choice of 5 final solutions in the objective space after clustering. Tables 5.9 and 5.10 give their corresponding values of the design variables, objective functions and pseudo weights. Fig. 5.17 shows their respective configurations.

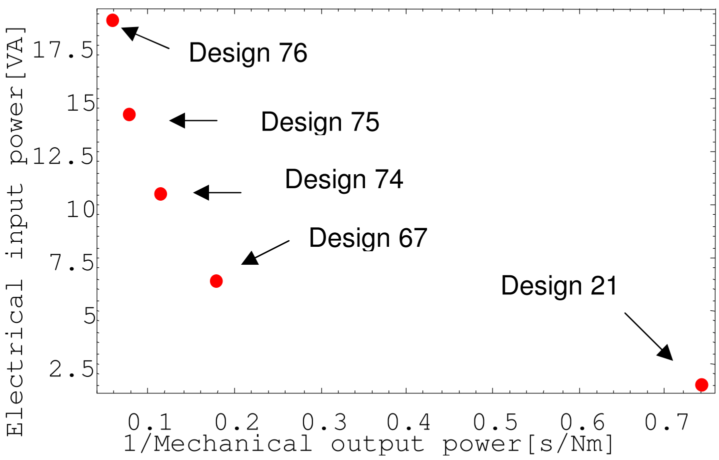

Fig. 5.16 Five Pareto-optimal designs obtained after clustering operation for the stepped-horn transducer with load

Table 5.9 Values of 5 Pareto-optimal designs in design variable spaces after clustering for the stepped-horn transducer with load

Design	D_t [mm]	ζ	L_b [mm]	Typ_b	Typ_f	h_p [mm]	L_{f1} [mm]	L_{f2} [mm]	N
76	13.4	0.93	46.8	2	1	4.1	10.5	21.2	6
75	13.3	0.48	58.1	2	1	3.2	21.5	17.3	6
74	13.2	0.79	49.8	1	1	3.6	8.3	26.1	6
67	11.8	0.66	45.7	2	3	3.8	15.4	25.6	6
21	11.8	0.81	46.1	3	1	3.5	28.3	30.6	2

Table 5.10 Values of objective functions for 5 Pareto-optimal designs after clustering and corresponding weights for the stepped-horn transducer with load

Design	Mechanical output power [Ns/m] (Obj1)	Electrical Input power [VA] (Obj2)	w_1	w_2	Efficiency
76	17.69	18.73	1	0	0.94
75	13.03	14.3	0.81	0.19	0.91
74	8.84	10.52	0.69	0.31	0.84
67	5.64	6.45	0.59	0.41	0.87
21	1.35	1.58	0.48	0.52	0.85

Selection according to performance criteria For the stepped-horn transducer under the condition of load, the effective coupling factor k, and piezoelectric quality number M as well as the power efficiency are important characteristics. They can be considered as high level information to determine the preferred design from the 5 solutions obtained after clustering.

In order to compare the coupling factors and piezoelectric quality numbers of these 5 designs, the frequency responses of the admittance functions $\underline{\hat{I}}/\underline{\hat{U}}$ for the 5 solutions were calculated according to equation (4.88). The respective Bode plots and the Nyquist plots are shown in Figs. 5.18 and 5.19.

Obviously, Design 76 has the largest distance between the resonance and anti-resonance frequencies among those of the five designs. This is means the coupling factor k of Design 76 is the best. Furthermore, Design 76 has also the largest phase descend (the largest offset of the center of the Nyquist plot from the real axis). Therefore the piezoelectric quality number M of Design 76 is the largest among those of these designs. For the transducer operating against load, the power efficiency is one of the most important characteristics as well. It can be used as high-level information for determining a preferred solution. The power efficiency of the stepped-horn transducer under the condition of load can be readily derived from equations (4.86) and (4.89). It is given by

$$\lambda_p = \frac{\hat{P}_m}{\hat{P}_a} \tag{5.2}$$

The power efficiencies of the above 5 Pareto-optimal transducers have been calculated and the results are shown in Table 5.10. It is obvious that Design 76 has the highest power efficiency.

Compared with the other designs, Design 76 has the advantages in terms of the coupling factor, the piezoelectric quality number and the power efficiency. Therefore, it is the preferred design for implementation.

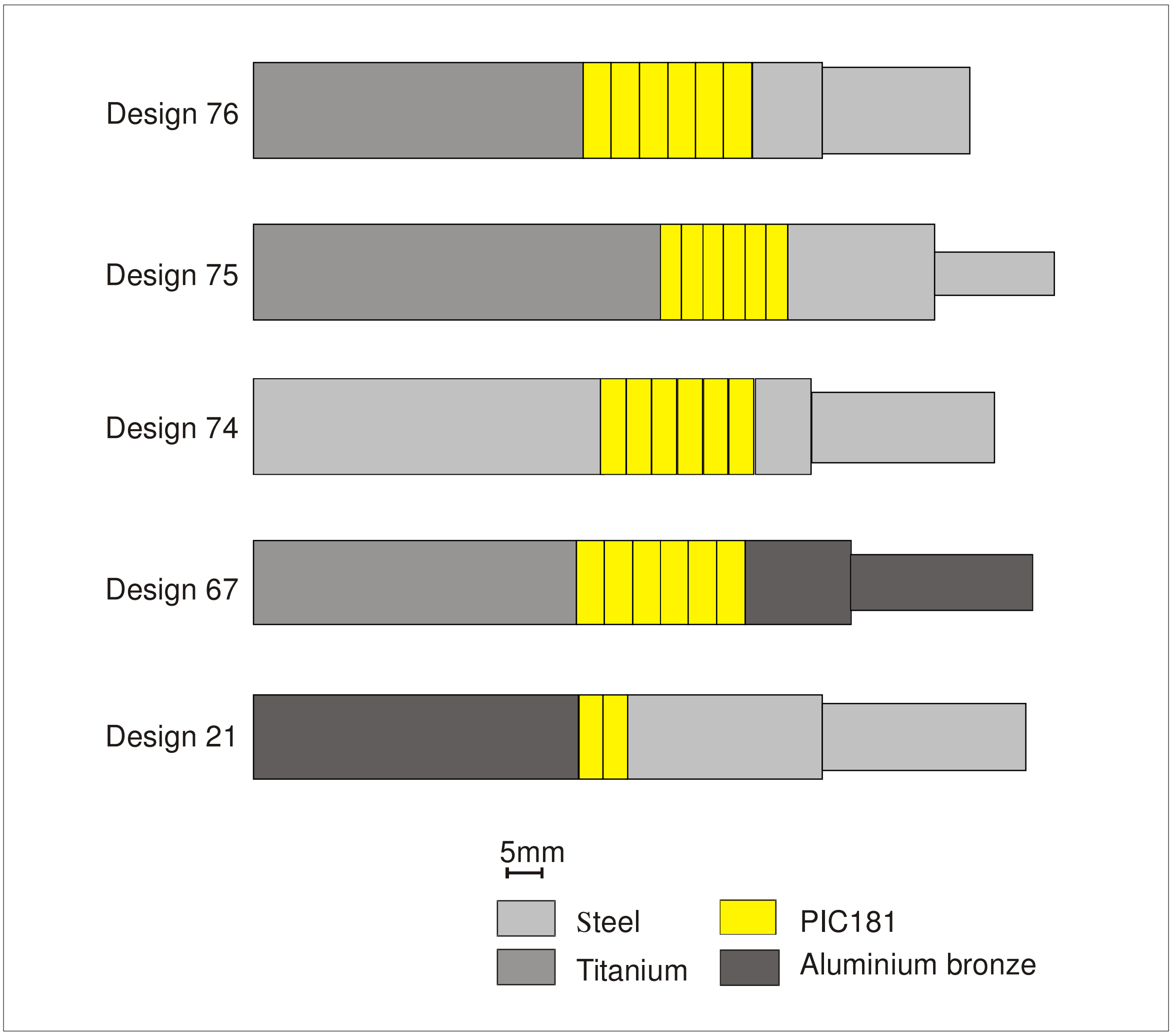

Fig. 5.17 Configurations of the stepped horn transducers with load for 5 Pareto-optimal solutions after clustering

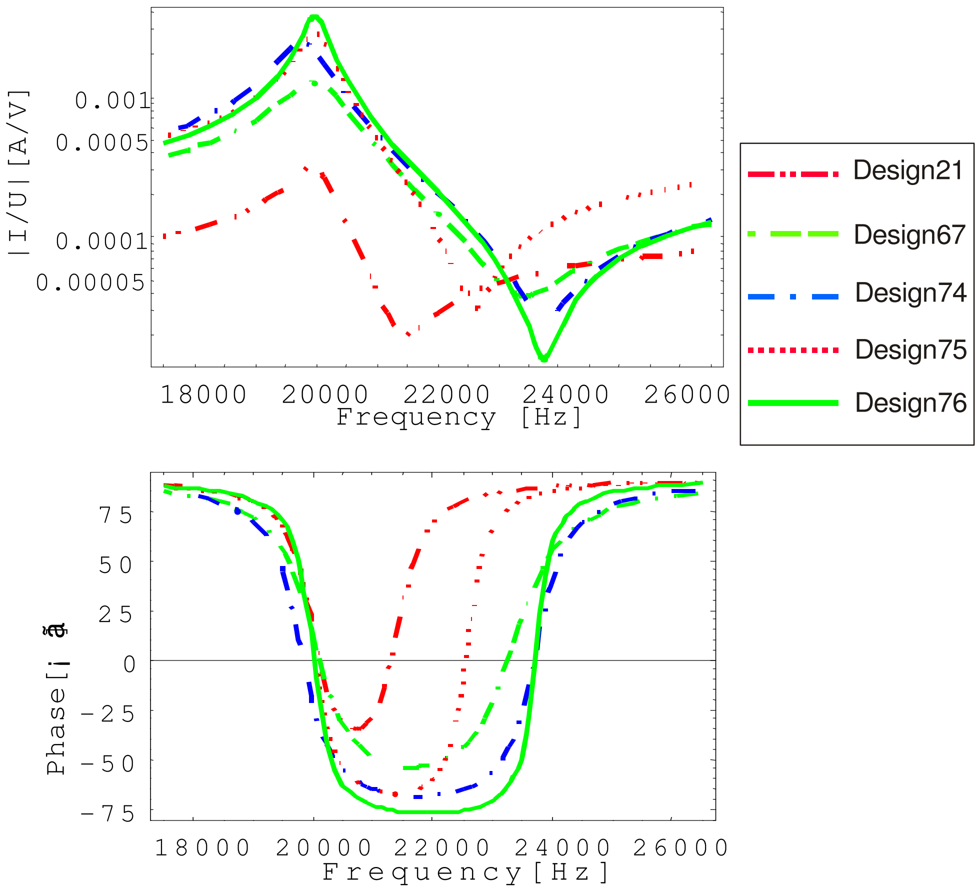

Fig. 5.18 Admittances $\underline{\hat{I}}/\underline{\hat{U}}$ *of 5 designs in Table 5.9 for the stepped-horn transducers with load as functions of frequencies (the Bode plot)*

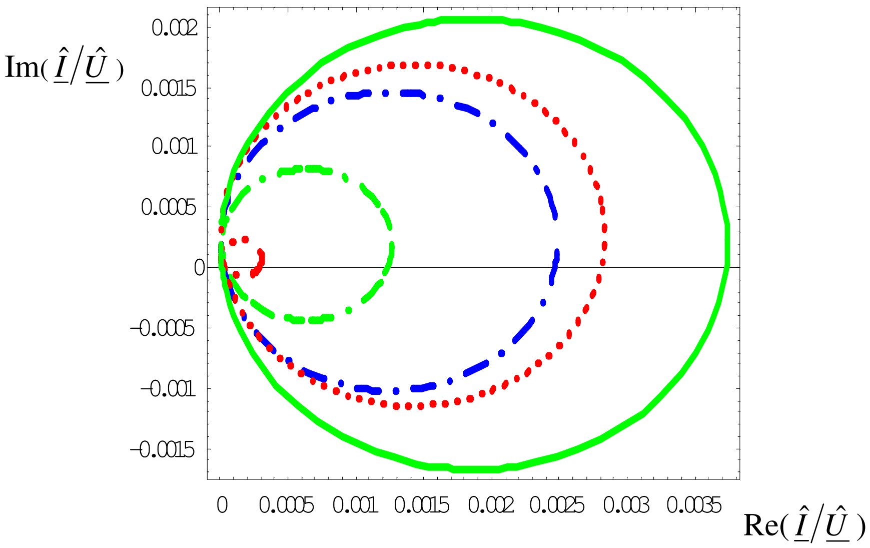

Fig. 5.19 Admittances $\underline{\hat{I}}/\underline{\hat{U}}$ *of the 5 designs in Table 5.9 for the stepped-horn transducers with load as functions of frequencies in the complex plane (the Nyquist plot)*

5.3.3 Load Characteristics of Stepped-horn Transducers

In the above multiobjective optimization problem of the stepped-horn transducer with load, a spring-damping load has been assumed. For the given load, the set of Pareto-optimal designs of the transducer has been obtained by means of MOEAs. In ultrasonic machining and bonding, piezoelectric transducers operate against loads. It is then a natural question how the load affects the behavior. In order to study the effect of loads on the resonance performances, in the following, the damping is not a fixed value, whereas the other parameters are not changed.

The power efficiency and mechanical output power of the 5 Pareto-optimal transducers as functions of the damping were calculated according to equations (5.2) and (4.86) and plotted in Figs. 5.20 and 5.21, respectively. The efficiencies of the 5 solutions increase rapidly in the range of less than about d_L=80Ns/m (for Design 21, Design 67, Design75 and Design 76) as well as d_L=500Ns/m (for Design 74) and decrease with increasing the load damping gradually. It is noted that the efficiencies have maxima at the region of about 25-80 Ns/m for Design 21, Design 67, Design75 and Design 76. For Design 74 the range is around 400-500 Ns/m. The mechanical output powers of Designs 67, 75 and 76 increase rapidly in the range of about less than 40Ns/m and rapidly decrease with the increase of the load damping, whereas for Designs 21 and 74 the variation of mechanical power is not obvious. It is noticed that Design 76 has larger power efficiency and mechanical power than the others in a wide range of the damping load.

If the damping of the transducer matches the load damping, the maximum power efficiency and mechanical power can be obtained. Generally, for a given load damping, the match of damping can be achieved by changing the structure of the transducer. It should be pointed out that the power efficiencies and mechanical powers of 5 Pareto-Optimal designs for the stepped-horn transducer didn't arrive at their respective maximum values in the multiobjective optimization problem before, where the load damping d_L is equal to about 202 Ns/m (see section 4.6.4). Since two trade-off objectives must be considered simultaneously, it is not possible to achieve a match of the transducer to the load damping by changing the structure of the transducer. However, the electrical input power and mechanical output power of the 5 designs are Pareto-optimal, respectively.

The load characteristics of other Pareto-optimal transducer designs can be analyzed similarly. Obviously, load characteristics can be used a high level information to determine the preferred transducer for implementation.

In this chapter, the optimized results of the optimization problems for Langevin-type transducers have been evaluated and discussed. In order to search for the preferred solutions various selection methods and high level information can be applied. The optimized results show that the performances of the Pareto-optimal transducer are obviously affected by the material of the end blocks. Titanium and brass are preferred materials. The load has much influence on the behavior and vibration form of the Pareto-optimal transducer obtained under the condition of no load. In all multiobjective optimization problems discussed here, only two-objective optimization problem considering the vibration amplitude and electrical input power at a given resonance frequency as design objectives have been studied. For other optimal design objectives, similar methods can be used. The methods and procedures for designing piezoelectric transducers via multiobjective optimization can be applied in other MOPs.

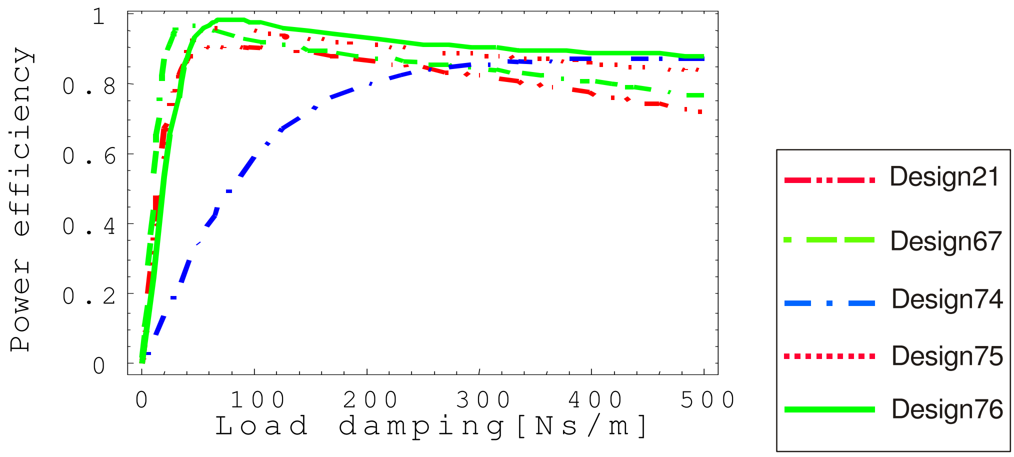

Fig. 5.20 Power efficiencies of 5 designs shown in Table 5.9 as functions of the load damping for the stepped-horn transducer

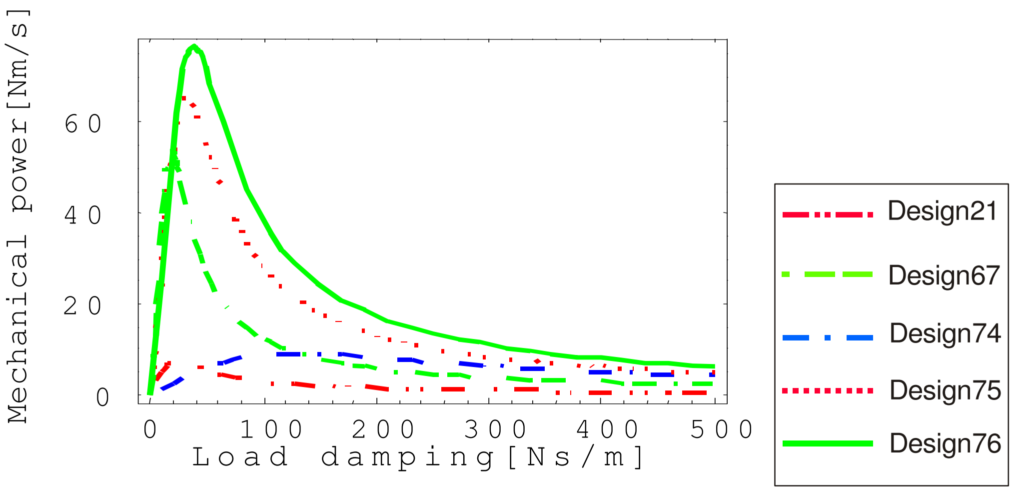

Fig. 5.21 Mechanical output powers of 5 designs shown in Table 5.9 as functions of the load damping for the stepped-horn transducer

6 Summary and Outlook

The design of piezoelectric actuators is usually based on single-objective optimization only. In most practical applications of piezoelectric actuators, however, there exist multiple design objectives which often are contradictory to each other by their very nature. This dissertation has studied various multiobjective optimization methods and applied them in the design of piezoelectric transducers. The main contribution has been to formulate the design of a piezoelectric transducer as a constrained multiobjective optimization problem involving continuous and discrete design variables and to find Pareto-optimal solutions using multiobjective evolutionary algorithms. The determination of the preferred designs using high level information was also addressed.

As the basis for the optimization of piezoelectric actuators the most important fundamentals concerning piezoelectric actuators were first described. In order to formulate optimization problems, the behaviors of piezoelectric actuators were modeled. The fundamental equations for describing electromechanical behaviors of piezoelectric actuators are piezoelectric constitutive equations. Four models that can be applied to describe the vibration behavior of the piezoelectric actuator were described by using the modeling of a longitudinal piezoelectric actuator as an example. These models are nonparameter models, continuum models, finite element models and lumped parameter models. Nonparameter models are predominantly applied in the experimental characterization of dynamic behaviors of piezoelectric actuators. As no parameters are used in the models, they are not suitable to the optimization problem. Continuum models can well describe the vibration behavior of piezoelectric actuators with simple geometry. As material data and geometrical parameters are taken into account in models, continuum models can be used in the design process for the formulation of optimization problems. Finite element models can describe the vibration behavior of piezoelectric actuators with complex geometry and boundary conditions. However, the cost of numerical computation in the finite element models is notably higher than the cost in continuum models. They are not well suited for optimization problems occurring in the early design stages. Lumped parameter models can well describe the vibration behavior of the piezoelectric actuator operating in the vicinity of one of its resonant frequencies. Their advantage is that the vibration behavior of the actuator can be described by simple algebraic equations and it is convenient to formulate the performance criteria for actuators using these models. Piezoelectric actuators have been widely used in different fields. For different applications, there exist different design goals. The typical design goals of piezoelectric actuators for one stroke driving and resonant driving were introduced. The state of the art of optimization of piezoelectric actuators was reviewed. Although various optimization problems have been studied in literature, piezoelectric actuator design via multiobjective optimization was scarcely reported. A latent need for studying the integrated optimal design procedure of piezoelectric actuators including modeling, mathematical formulation, optimization algorithms and implementation was identified.

The models of the piezoelectric actuators provide the base for formulating MOPs. In combination with an appropriate optimization method the underlying MOP can be solved. In a MOP, because of conflict among objectives, it is not always possible find a solution for which each objective arrives at its optimal value simultaneously. Therefore, the concepts of non-domination and Pareto-optimality were introduced. The solutions of a MOP were given in the non-domination or Pareto-optimality sense. To find solutions belonging to a better non-dominated front and simultaneously to maintain diversity in the non-dominated solutions are two important goals in a multiobjective optimization.

Most traditional multiobjective optimization methods convert the MOP into a single objective problem and then solve the problem using widely developed methods for single objective optimization. Some commonly used traditional multiobjective optimization methods including weighted sum methods, ε-constraint methods, weighted metric methods and value function methods were described in brief. These methods require some problem knowledge before optimization is performed. Some techniques may be sensitive to the shape of the Pareto-optimal front. Moreover, they require several optimization runs to obtain an approximation of the Pareto-optimal set. Evolutionary algorithms (EAs), on the other hand, are able to find multiple Pareto-optimal solutions in a single simulation run due to their population-approach. They are well suited for multiobjective optimization and the problems with discrete variables. By using a diversity-preserving mechanism, moreover, MOEAs can also find widely different Pareto-optimal solutions. The basic structure of a MOEA is similar to a single-objective GA. Since a scalar fitness is needed for reproduction in an EA, the essence of a MOEA is how to assign a scalar fitness to each individual from multiple objective functions. According to different fitness assignment methods, various MOEAs have been developed over the past decades. In this dissertation, the multi-objective GA (MOGA), the non-dominated sorting GA (NSGA), the elitist NSGA (NSGA-II), the strength Pareto EA (SPEA) and the improved SPEA (SPEA2) were studied. In MOGA and NSGA, the fitness of each individual is first assigned according to their respective Pareto-ranking methods. Then the shared fitness is calculated in order to maintain diversity among non-dominated solutions. Proportionate selection operators are used in the two GAs. In the two GAs mentioned above, no elite-preservation is performed. NSGA-II, SPEA and SPEA2 are three MOEAs with elite-preservation. In NSGA-II, non-dominated sorting is first performed among a population of size 2N consisting of offspring and parent populations. A new population of size N is then filled by individuals first according to their ranks and then according to the crowding distances. This provides an elite-preservation. The crowded tournament selection operator is used for obtaining the mating pool. In SPEA, the elites are preserved by using an external population. The fitness (strength) of each elite individual and the fitness of each individual in the current population are assigned according to respective expressions related to the number of dominated solutions. A clustering technique is used to reduce the size of external population when its size is larger than the specified size. A binary tournament selection operation is performed in this MOEA. SPEA2 is an improved version of SPEA. An improved fitness assignment scheme, a nearest neighbor density estimation technique and a new archive truncation method are used in this MOEA. The methods for handling constraints in MOPs were studied. The penalty function approach and the constrained tournament method are two commonly used methods.

Based on modeling and multiobjective optimization techniques, multiobjective optimal design problems of Langevin-typed piezoelectric transducers were studied. For the transducers used in ultrasonic bonding and machining, the most important design criteria are the resonance frequency, electrical input power, mechanical output power, coupling factor, power efficiency, efficiency, mechanical quality factor, piezoelectric quality number, volume of piezoelectric materials and mass and size of the transducer. These performance criteria can be considered as objective functions in MOPs of transducers. In this dissertation, two-objective optimization problems were studied. As the influence of prestress on the resonance performance of the transducer can not be modeled in theory, experimental study was applied in determining optimal prestress. The coupling factor and piezoelectric quality number were considered as design objectives. Lumped parameter models and parameter identification were used in the formulation of optimization problems. The Pareto-optimal pre-stresses for the freely vibrating transducer and the transducer with a mechanical load were found respectively. Two kinds of Langevin-typed transducers (the symmetrical transducer as well as the transducer with a stepped horn) were designed via multiobjective optimization. The transfer matrix method based on continuum models was applied in formulations of MOPs. For the MOPs of freely vibrating transducers, the minimum electrical input power and the maximum resonant amplitude were considered as two design objectives. For the MOPs of transducers with a mechanical load, the maximum mechanical output power and the minimum electrical input power were considered as design objectives. In all problems, an equality constraint is used to assure that the transducer operates at the specified resonance frequency and several inequality constraints are used to specify the ranges of the input power, input current and dimensions of the transducer respectively. Each MOP of the freely vibrating transducer with 2 piezoelectric rings was solved by using MOGA, NSGA, NSGA-II and SPEA (SPEA2), where penalty functions were used to transfer constrained MOPs into non-constrained MOPs. Each MOP of the freely vibrating transducer with 2 piezoelectric rings was also solved by using NSGA-II where constrained tournament method instead of the penalty function approach was used. Unlike the common NSGA-II, the crowded tournament selection operation was performed only for creation of the new population. In MOGA and SPEA (SPEA2), the niching strategy was performed in the objective space. The other MOEAs used parameter-space niching. As the design variables include continuous and discrete types, a mixed coding scheme was used in each MOEA. The blended crossover (BLX-α) was applied to the continuous variables. For the discrete variables a single-crossover was used. The mutation operation was only applied to discrete variables.

Optimization results were evaluated in terms of the extent of the obtained non-dominated solutions close to the true Pareto-optimal front and the diversity in the obtained non-dominated solutions. For MOPs of symmetrical transducers, the SPEA did better than the others relatively. It was then applied in the MOPs of symmetrical transducers with 4 and 6 piezoelectric rings, respectively. For MOPs of the transducer with a stepped horn, NSGA2 using the penalty function method did better than the others. It was then used to solve the MOPs of the transducer with a stepped horn. In each MOP, after all non-dominated solutions for transducers with 2, 4 and 6 piezoelectric rings were obtained, the second level optimization was performed and Pareto-optimal solutions were searched among all obtained non-dominated solutions. In the practical design of piezoelectric transducers, generally, only one solution is needed to be implemented finally. Methods for determining preferred solutions from obtained Pareto-optimal solutions were studied. The preferred solution was chosen according to the specified weight vector and the performance criteria which were not used as design objectives, respectively. The coupling factor, the piezoelectric quality number and power efficiency as high-level information have been applied in determining the preferred designs. In order to reduce the size of obtained Pareto-optimal solutions, a clustering technique was applied. The NSGA2 using the penalty function method was also applied in the MOP of the stepped-horn transducers with a mechanical load. The second level optimizations and clustering were performed .The preferred solutions were determined using similar methods. The load characteristics were discussed.

This dissertation has presented an integrated procedure for piezoelectric transducer design via multiobjective optimization methods. The integrated procedure can be applied in other two-objective or Mutiobjective optimization problems of piezoelectric actuators. In order to obtain better optimized results, further investigations can be performed in two aspects. First, the quality of models of piezoelectric actuators can be improved if fewer simplifications are used. In this dissertation, some simplifications have been introduced into the modeling. For example, the bolt was not modeled as a separate element, but the characteristics of the bolt were incorporated in the backing and front rods. The actual piezoelectric rings were modeled as piezoelectric discs. The electrodes were not taken into account in the model. The nonlinear characteristic of piezoelectric material under high electrical field strength was not considered. Second, in addition to MOEAs used here there exist other MOEAs and other multiobjective optimization methods such as set oriented subdivision algorithms (see [DSH04] and [SMD03]) and multi-objective particle swarm optimization (MOPSO) methods [MT03]. They can also be applied to MOPs of piezoelectric actuators.

Appendix A

Derivation of Individual Transfer Matrix

In this section, the expressions of the transfer matrices of the fundamental block elements are derived using the analytical models based on rod theory, respectively. In the following expressions, all material moduli are considered as real values. If material loss is taken into account, complex moduli can be applied instead of real moduli.

Mechanical Rod Elements The vibration behavior of a mechanical rod element (see Fig. 4.12) can be described by the one-dimensional wave equation

$$\ddot{u}(z,t) = c_m^{\ 2} u''(z,t) \tag{A.1}$$

with motion and force boundary conditions. Where c_m is the wave propagation speed

$$c_m = \sqrt{\frac{E}{\rho}} \tag{A.2}$$

The axial force and vibration velocity in the rod element are

$$F(z,t) = A_b \cdot T(z,t) = A_b \cdot Eu'(z,t) \tag{A.3}$$

$$v(z,t) = \dot{u}(z,t) \tag{A.4}$$

There are the following motion and force boundary conditions

$$\dot{u}(0,t) = v_e(t), \quad \dot{u}(L_b,t) = v_a(t) \tag{A.5}$$

$$A_b Eu'(0,t) = F_e(t), \quad A_b Eu'(L_b,t) = F_a(t) \tag{A.6}$$

As the complex expressions will be used in the computation, the velocity and force quantities at both sides of the rod element for harmonic vibrations are written as

$$\underline{v}_e(t) = \underline{\hat{v}}_e\, e^{j\Omega t}, \quad \underline{v}_a(t) = \underline{\hat{v}}_a\, e^{j\Omega t}, \tag{A.7}$$

$$\underline{F}_e(t) = \underline{\hat{F}}_e\, e^{j\Omega t}, \quad \underline{F}_a(t) = \underline{\hat{F}}_a\, e^{j\Omega t}, \tag{A.8}$$

The above boundary value problem can be solved by means of the separation-of-variables method described in chapter 2 for the case of harmonic vibrations. That is

$$\underline{u}(z,t) = \left(C_1 e^{jk_m z} + C_2 e^{-jk_m z}\right) e^{j\Omega t} \tag{A.9}$$

where $k_m = \Omega / c_m$ is the wave number.

Substituting the equation (A.9) into the equations (A.5) and (A.6) and considering the equations (A.7) and (A.8) yield the following transfer matrix relation

$$\begin{bmatrix} \underline{\hat{v}}_a \\ \underline{\hat{F}}_a \end{bmatrix} = \frac{1}{2} \begin{bmatrix} \left(e^{-jk_mL_b} + e^{jk_mL_b}\right) & \frac{\Omega}{A_bEk_m}\left(e^{jk_mL_b} - e^{-jk_mL_b}\right) \\ \frac{A_bEk_m}{\Omega}\left(e^{jk_mL_b} - e^{-jk_mL_b}\right) & \left(e^{-jk_mL_b} + e^{jk_mL_b}\right) \end{bmatrix} \cdot \begin{bmatrix} \underline{\hat{v}}_e \\ \underline{\hat{F}}_e \end{bmatrix} \tag{A.10}$$

Using Euler's equation this may be written as

$$\begin{bmatrix} \underline{\hat{v}}_a \\ \underline{\hat{F}}_a \end{bmatrix} = \begin{bmatrix} \cos(k_mL_b) & \frac{j\Omega}{A_bEk_m}\sin(k_mL_b) \\ \frac{jA_bEk_m}{\Omega}\sin(k_mL_b) & \cos(k_mL_b) \end{bmatrix} \cdot \begin{bmatrix} \underline{\hat{v}}_e \\ \underline{\hat{F}}_e \end{bmatrix} \tag{A.11}$$

Therefore, the transfer matrix of the mechanical rod element is obtained as follows

$$\mathbf{A^m} = \frac{1}{2} \begin{bmatrix} \cos(k_mL_b) & \frac{j\Omega}{A_bEk_m}\sin(k_mL_b) \\ \frac{jA_bEk_m}{\Omega}\sin(k_mL_b) & \cos(k_mL_b) \end{bmatrix} \tag{A.12}$$

Piezoelectric Elements The transfer model matrix for a piezoceramic element can be derived by means of the method described in chapter 2. Here the brief derivation is given.

According to equations (2.17) and (2.18) in chapter 2 the axial force and the current applied in the piezoceramic element (see Fig. 4.13) can be described as follows

$$F(z,t) = A_p \cdot T(z,t) = A_p c_{33}^E u'(z,t) + A_p e_{33} \phi'(z,t) \tag{A.13}$$

$$I(z,t) = A_p \cdot \dot{D}(z,t) = e_{33}\dot{u}'(z,t) - \varepsilon_{33}^S \dot{\phi}'(z,t) \tag{A.14}$$

Besides mechanical boundary quantities shown in equations (A.7) and (A.8), for the piezoceramic element there exist electrical boundary quantities

$$\underline{U}(t) = \underline{\hat{U}} e^{j\Omega t}, \quad \underline{I}(t) = \underline{\hat{I}} e^{j\Omega t} \tag{A.15}$$

According to equations (2.27) and (2.28) the governing equations for describing the vibration behaviors of the piezoceramic element are

$$\ddot{u}(z,t) = c_p^{\,2} u''(z,t) \tag{A.16}$$

$$\varphi''(z,t) = \frac{e_{33}}{\varepsilon_{33}^S} u''(z,t) \tag{A.17}$$

According to equations (2.33) and (2.34), solutions of the above governing equations can be written as

$$\underline{u}(z,t) = (C_1 e^{jk_p z} + C_2 e^{-jk_p z}) e^{j\Omega t} \tag{A.18}$$

$$\underline{\varphi}(z,t) = \left[\frac{e_{33}}{\varepsilon_{33}^S}(C_1 e^{jk_p z} + C_2 e^{-jk_p z}) + C_3 z + C_4 \right] e^{j\Omega t} \tag{A.19}$$

There are the following mechanical and electric boundary conditions (see Fig. 4.13)

$$\dot{u}(0,t) = v_e(t), \quad \dot{u}(h_p,t) = v_a(t) \tag{A.20}$$

$$A_p c_{33}^E u'(0,t) + A_p e_{33} \varphi'(0,t) = F_e(t), \quad A_p c_{33}^E u'(h_p,t) + A_p e_{33} \varphi'(h_p,t) = F_a(t) \tag{A.21}$$

$$A_p e_{33} \dot{u}'(0,t) - A_p \varepsilon_{33}^S \dot{\varphi}'(0,t) = I(t), \quad \varphi(0,t) - \varphi(h_p,t) = U(t) \tag{A.22}$$

Substituting the equations (A.18) and (A.19) into (A.20), (A.21) and (A.22) it follows

$$j\Omega(C_1 + C_2) = \underline{\hat{v}}_e \tag{A.23}$$

$$j\Omega(C_1 e^{jk_p h_p} + C_2 e^{-jk_p h_p}) = \underline{\hat{v}}_a \tag{A.24}$$

$$jk_p A_p c_{33}^E (C_1 - C_2) + jk_p A_p \frac{e_{33}^2}{\varepsilon_{33}^S}(C_1 - C_2) + A_p e_{33} C_3 = \underline{\hat{F}}_e \tag{A.25}$$

$$jk_p A_p c_{33}^E (C_1 e^{jk_p h_p} - C_2 e^{-jk_p h_p}) + jk_p A_p \frac{e_{33}^2}{\varepsilon_{33}^S}(C_1 e^{jk_p h_p} - C_2 e^{-jk_p h_p}) + A_p e_{33} C_3 = \underline{\hat{F}}_a \tag{A.26}$$

$$-jA_p \varepsilon_{33}^S \Omega C_3 = \underline{\hat{I}} \tag{A.27}$$

$$\frac{e_{33}}{\varepsilon_{33}^S}(C_1 + C_2) - \frac{e_{33}}{\varepsilon_{33}^S}(C_1 e^{jk_p h_p} + C_2 e^{-jk_p h_p}) - C_3 h_p = \underline{\hat{U}} \tag{A.28}$$

Eliminating C_1, C_2, and C_3 and getting $\underline{\hat{v}}_a$, $\underline{\hat{F}}_a$ and $\underline{\hat{I}}$ in terms of $\underline{\hat{v}}_e$, $\underline{\hat{F}}_e$ and $\underline{\hat{U}}$ from the above equations, the transfer matrix relation can be obtained as follows

$$\begin{bmatrix} \underline{\hat{v}}_a \\ \underline{\hat{F}}_a \\ \underline{\hat{I}} \end{bmatrix} = \begin{bmatrix} A_{11}^p & A_{12}^p & A_{13}^p \\ A_{21}^p & A_{22}^p & A_{23}^p \\ A_{31}^p & A_{32}^p & A_{33}^p \end{bmatrix} \begin{bmatrix} \underline{\hat{v}}_e \\ \underline{\hat{F}}_e \\ \underline{\hat{U}} \end{bmatrix} \tag{A.29}$$

where

$$A_{11}^p = \frac{h_p k_p (e_{33}^2 + c_{33}^E \varepsilon_{33}^S)\cos(h_p k_p) - e_{33}^2 \sin(h_p k_p)}{h_p k_p (e_{33}^2 + c_{33}^E \varepsilon_{33}^S) - e_{33}^2 \sin(h_p k_p)} \tag{A.30}$$

$$A_{12}^{p} = \frac{j\Omega h_p \varepsilon_{33}^{S} \sin(h_p k_p)}{A_p h_p k_p (e_{33}^2 + c_{33}^{E}\varepsilon_{33}^{S}) - Ae_{33}^2 \sin(h_p k_p)} \tag{A.31}$$

$$A_{13}^{p} = \frac{j\Omega e_{33} \varepsilon_{33}^{S} \sin(h_p k_p)}{h_p k_p (e_{33}^2 + c_{33}^{E}\varepsilon_{33}^{S}) - e_{33}^2 \sin(h_p k_p)} \tag{A.32}$$

$$A_{21}^{p} = \frac{A_p k_p (e_{33}^2 + c_{33}^{E}\varepsilon_{33}^{S})(-2e_{33}^2 + 2e_{33}^2 \cos(h_p k_p) + h_p k_p (e_{33}^2 + c_{33}^{E}\varepsilon_{33}^{S}) \sin(h_p k_p))}{j\Omega \varepsilon_{33}^{S} (h_p k_p (e_{33}^2 + c_{33}^{E}\varepsilon_{33}^{S}) - e_{33}^2 \sin(h_p k_p))} \tag{A.33}$$

$$A_{22}^{p} = \frac{h_p k_p (e_{33}^2 + c_{33}^{E}\varepsilon_{33}^{S}) \cos(h_p k_p) - e_{33}^2 \sin(h_p k_p)}{h_p k_p (e_{33}^2 + c_{33}^{E}\varepsilon_{33}^{S}) - e_{33}^2 \sin(h_p k_p)} \tag{A.34}$$

$$A_{23}^{p} = \frac{A_p e_{33} k_p (e_{33}^2 + c_{33}^{E}\varepsilon_{33}^{S})(-1 + \cos(h_p k_p))}{h_p k_p (e_{33}^2 + c_{33}^{E}\varepsilon_{33}^{S}) - e_{33}^2 \sin(h_p k_p)} \tag{A.35}$$

$$A_{31}^{p} = \frac{A_p e_{33} k_p (e_{33}^2 + c_{33}^{E}\varepsilon_{33}^{S})(-1 + \cos(h_p k_p))}{h_p k_p (e_{33}^2 + c_{33}^{E}\varepsilon_{33}^{S}) - e_{33}^2 \sin(h_p k_p)} \tag{A.36}$$

$$A_{32}^{p} = \frac{j\Omega e_{33} \varepsilon_{33}^{S} \sin(h_p k_p)}{h_p k_p (e_{33}^2 + c_{33}^{E}\varepsilon_{33}^{S}) - e_{33}^2 \sin(h_p k_p)} \tag{A.37}$$

$$A_{33}^{p} = \frac{j\Omega A_p k_p \varepsilon_{33}^{S} (e_{33}^2 + c_{33}^{E}\varepsilon_{33}^{S})}{h_p k_p (e_{33}^2 + c_{33}^{E}\varepsilon_{33}^{S}) - e_{33}^2 \sin(h_p k_p)} \tag{A.38}$$

Similarly, (A.29) may be written as

$$\begin{bmatrix} \mathbf{X_a} \\ \underline{\hat{I}} \end{bmatrix} = \begin{bmatrix} \mathbf{A^{Pm}} & \mathbf{A^{Pem}} \\ \mathbf{A^{Pme}} & \mathbf{A^{Pe}} \end{bmatrix} \begin{bmatrix} \mathbf{X_e} \\ \underline{\hat{U}} \end{bmatrix} \tag{A.39}$$

Appendix B

Developed Programs

B.1 Multiobjective Optimization of Symmetrical Langevin Transducers

1. Optimal design of symmetrical Langevin transducers using MOGA
2. Optimal design of symmetrical Langevin transducers using NSGA
3. Optimal design of symmetrical Langevin transducers using SPEA
4. Optimal design of symmetrical Langevin transducers using NSGA-II

B.2 Multiobjective Optimization of Stepped-horn Transducers

1. Optimal design of stepped-horn transducers without load using MOGA
2. Optimal design of stepped-horn transducers without load using NSGA
3. Optimal design of stepped-horn transducers without load using SPEA2
4. Optimal design of stepped-horn transducers without load using NSGA-II
5. Optimal design of stepped-horn transducers with load using NSGA-II

Bibliography

[Abb98] Abboud, N. N.; Wojcik, G. L.; Vaughan, D. K.; Mould, J.; Powell, D. J. and Nikodym, L.: Finite element modelling for ultrasonic transducers. Proceedings of the International Symposium on Medical Imaging, SPIE, 1998

[Ans01] ANSYS 6.0 User Manual, 2001

[Bak85] Baker, J. E.: Adaptive selection methods for genetic algorithms. In Proceedings of an International Conference on Genetic Algorithms and Their Application, pp.101-111, 1985

[Bäc96] Bäck, T.: Evolutionary Algorithms in Theory and Practice. Oxford University Press, 1996, ISBN 0-19-509971-0

[BCJ64] Berlincourt, D. A.; Curran, D. R. and Jaffe, H.: Piezoelectric and piezomagnetic materials and their function in transducers. Chapter 3 in Mason, W.P.: Physical Acoustics. Vol. 1A, 1964

[Bec99] Beckers, M.: topology optimization using a dual method with discrete variables. Structural and Multidisciplinary Optimization, Vol.17, No.1, pp.14-24, 1999

[BhF02] Bharti, S. and Frecker, M.I.: Topology optimization and detailed finite element modeling of piezoelectric actuators: effect of external loads and detail geometers on actuator output. Proceedings of SPIE, Vol.4693, pp.124-135, 2002

[BK88] Bendsøe, M. P. and Kikuchi, N.: Generating optimal topologies in optimal design using a homogenization method. Computer Methods in Applied Mechanics and Engineering, Vol.71, pp.197-224, 1988

[BMF00] Barboni, R.; Mannini, A.; Fantini, E. and Gaudenzi, P.: Optimal plancement of PZT actuators for the control of beam dynamics. Smart Materials and Structures, Vol.9, pp.110-120, 2000

[BPF91] Bangviwat, A.; Ponnekanti, H. and Finch, R.D.: Optimizing the performanece of piezoelectric drivers that use stepped horns. Journal of the Acoustic Society of America, Vol.90, pp.1223-1229, 1991

[Brö02] Brökelmann, M. : Modellierung und Simulation piezoelektrischer Aktoren zum resonanten Betrieb bei nichtlinearen mechanischer Randbedingungen. Diplomarbeit, Heinz Nixdorf Institut, Universität Paderborn, Mechatronik und Dynamik, 2002

[BS03] Bendsøe, M. P. and Sigmund, O. : Topology Optimization – Theory, Methods and Applications. Springer-Verlag Berlin Heidelberg, 2003, ISBN 3-540-42992-1

[Cer00] Monolithic Multilayer Actuators Operation and Applications. CeramTec AG, Lauf, Germany, 2000. http://www.ceramtec.de

[CF00] Canfield, S. and Frecker, M.: Topology optimization of compliant mechanical amplifiers for piezoelectric actuators. Struktural and Multidisciplinary Optimization, Vol.20, pp.269-279, 2000

[CL87] Crawley, E. F. and Luis, J.: Use of piezoelectric actuators as elements of intelligent structures. AIAA Journal, Vol.25, pp.1373-1385, 1987

[Coh85] Cohon, J. L.: Multicriteria programming: Brief review and application. Design Optimization, pp.163-191. Academic Press, New York, 1985

[Cra94] Crawley, E. F.: Intelligent structures for aerospace: a technology overview and assessment. AIAA Journal, Vol.32, No.8, pp.1689-99, 1994

[CSe94] Chattopadhyay, A. and Seeley, C.E.: A multiobjective optimization for the design of rotating composites box beams with discrete piezoelectric actuators. Proceedings-SPIE the International Society for Optical Engineering, Vol.2190, pp.38-51, 1994

[CS94] Chattopadhyay, A. and Seeley, C.E.: A simulated annealing technique for multiobjective optimization of intelligent structures. Smart Materials and Structures, Vol.3, pp.98-106, 1994

[CSJ99] Chattopadhyay, A.; Seeley, C. E. and Jha, R.: Aeroelastic tailoring using piezoelectric actuation and hybrid optimization. Smart Materials and Structures, Vol.8, pp.83-91, 1999

[CTS02] Chee, C.; Tong, L. and Steven, G. P.: Piezoelectric actuator orientation optimization for static shape control of composite plates. Composite structures, Vol.55, pp.169-184, Elsevier, 2002

[Cul96] Culshaw, B.: Smart structures and materials. Artech House, INC., 1996, ISBN 0-89006-681-7

[Deb02] Deb, Kalyanmoy: Multi-Objective Optimization using Evolutionary Algorithms. John Wiley & Sons, Ltd, 2002, ISBN 0-471-87339-X

[DI483] Leitfaden zur Bestimmung de dynamischen Eigenschaften von piezoelektrischer Keramik mit hohem elecktromechanischen Koppelfaktor. DIE IEC 483, Beuth Verlag GmbH, Berlin, 1988

[DI324] Piezoelektrische Eigenschaften von keramischen Werkstoffen und Komponenten. DIN EN 50324, VDE VERLAG GMBH, 2002

[DLL00] Du, H.; Lau, G. K.; Lim, M. K. and Qui, J.: Topological optimization of mechanical amplified for piezoelectric actuators under dynamic motion. . Smart Materials and Structures, Vol.9, pp.788-800, 2000

[DSH04] Dellnitz, M.; Schütze, O. and Hestermeyer, T.: Covering Pareto Sets by Multilevel Subdivision Techniques. Journal of Optimization, Theory and Applications, 2004

[ES93] Eschelman, L. J. and Schaffer, J. D.: Real-coded genetic algorithms and interval schemata. In Foundations of Genetic Algorithms 2, pp.187-202, 1993

[FF93] Fonseca, C. M. and Fleming, P. J.: Genetic algorithm for multiobjective optimization: Formulation, discussion, and generalization. In Proceedings of Fifth International Conference on Genetic Algorithms, pp.416-423, 1993

[Fu04] Fu, B.; Hemsel, T. and Wallaschek, J.: Model-based Diagnosis for Sandwiched Ultrasonic Transducers. In: Proceedings of the 18th International Congress on Acoustics, ICA 2004, 4-9 April 2004, Kyoto, Japan Bd. 3, 2004, pp. 2243-2246

[GCh00] Gen, M. and Cheng, R.: Genetic algorithms and engineering optimizaiton. Wiley-Interscience Publication, USA, 2000, ISBN 0-471-31531-1

[Gen95] Genta, G.: Vibration of structures and machines: practical aspects. Springer-Verlag, New York, 1995, ISBN 0-387-94403-6

[Gol89] Goldberg, D.: Genetic Algorithms in Search, Optimization and Machine Learning, Addison-Wesley, Reading, MA, 1989

[GR87] Goldberg, D. and Richardson, J.: Genetic algorithm with sharing for multi-modal function optimization, in Proceedings of the 2nd International Conference on Genetic Algorithms, Lawrence Erlbaum Associates, Hillsdale,N.J.,pp41-49,1987

[Hem01] Hemsel, T. : Untersuchung und Weiterentwicklung linearer piezoelecktrischer Schwingungsantriebe. Dissertation, Heinz Nixdorf Institut, Universität Paderborn, 2001, ISBN 3-935433-10-7

[Hen01] Henke, A.: Modellbildung, Simulation und Optimierung piezoelektrischer Stellsysteme. Dissertation, Heinz Nixdorf Institut, Universität Paderborn, 2001

[HKL98] Hemsel, T.; Krome, J. W.; Littmann, W. and Wallaschek, J.: Modellierung piezoelektrischer Stapel- und Vielschichtaktoren für dynamischen Betrieb. 2. Polnisch-deutscher Workshop: Werkzeuge der Mechatronik, Ilmenau, 1998, ISBN 3-00-002556-1, pp.224-233

[HL99] Han, J. H. and Lee, I.: Optimal placement of piezoelectric sensors and actuators for vibration control of a composite plate using genetic algorithms. Smart Materials and Structures, Vol.8, pp.257-267, 1999

[HLH03] Hsu, Y.; Lee, C. and Hsiao, W.: Optimizing piezoelectric transformer for maximum power transfer. Smart Materials and Structures, Vol.12, pp.373-383, 2003

[HM03] Halim, D. and Moheimani, S.O.: An optimization approach to optimal placement of collocated piezoelectric actuators and sensors on a thin plate. Mechatronics, vol.13, pp.27-47, 2003

[Hul73] Hulst, A. P.: On a family of high-power transducers. In Proceeding of Ultrasonic International Conference, pp.285-294, 1973

[IE87] IEEE Standard on Piezoelectricity. American Standards National Institut, New York, 1987

[Ike96] Ikeda, T.: Fundamentals of Piezoelectricity. Oxford University Press, 1996, ISBN 0-19-856339-6

[JC71] Jaffe, B. and Cook, W. R.: Piezoelectric Ceramics. Academic Press, 1971, ISBN 0-12-379550-8

[JH94] Joines, J.A. and Houck, C. R.: On the use of nonstationary penalty functions to solve nonlinear constrained optimization problems with GAs. In Proceedings of the International Conference on Evolutionary Computation, pp.579-584

[JNL00] Jiang, T. Y.; Ng, T. Y. and Lam, K. Y.: Optimization of a piezoelectric ceramic actuators. Sensors and Actuators, Vol.84, pp.81-94, 2000

[JVG99] Jiménez, F.,Verdegay, J. L. and Goméz-Skarmeta, A. F.: Evolutionary techniques for constrained multiobjective optimization problems. In proceedings of the workshop on Multi-Criterion Optimization Using Evolutionary Methods held at Genetic and Evolutionary Computation Conference (GECCO-1999), pp. 115-116

[Kro99] Krome, J. W.: Modelle zur Untersuchung des Schwingungsverhaltens von Statoren für piezoelektrische Ultraschallwanderwellenmotoren. Dissertation, Heinz Nixdorf Institut, Universität Paderborn, HNI-Verlagsschriftenreihe, Bd.59, 1999, ISBN 3-931466-58-2

[LDG00] Lau, G. K.; Du, H.; Guo, N. and Lim, M. K. : Systematic design of displacement-amplifying mechanisms for piezoelectric stacked actuators using topology optimization. Journal of Intelligent Material Systems and Structures, Vol.11, pp.685-695, 2000

[LeI75] Lenk, A. and Irrgang, B.: Elektromechanische Systeme. Band 2:Systeme mit verteilten Parametern. VEB Verlag Technik, Berlin, 1975

[Len75] Lenk, A.: Elektromechanische Systeme. Band 1: Systeme mit Konzentrierten Parametern. VEB Verlag Technik, Berlin, 1975

[Ler90] Lerch, R.: Simulation of piezoelectric devices by two- and three-dimensional finite elements. IEEE Transactions on Ultrasonics, Ferroelectrics and Frequency Control, Vol.37, pp.233-247, 1990

[Lit03] Littmann, W.: Piezoelektrische, resonant betriebene Ultraschall-Leistungswandler mit nichtlinearen mechanischen Randbedingungen. Dissertation, Heinz Nixdorf Institut, Universität Paderborn, 2003, ISBN

[LOM00] Li, Y.; Onoda, J. and Minesugi, K.: Simultaneous optimization of piezoelectric actuator placement and feedback for vibration suppression. Acta Astronautica, Vol.50, No.6, pp.335-341, Elsevier, 2002

[Mie99] Miettinen, K.: Nonlinear multiobjective optimization. Kluwer Academic Publishers, 1999, ISBN 0-7923-8278-1

[MT03] Mostaghim, S. and Teich, J: Strategies for finding good local guides in Multi-objective Particle Swarm Optimization (MOPSO). Proceedings of IEEE Swarm Intelligence Symposium, April 24-26, 2003, Indianapolis, Indiana, USA

[Nep73] Neppiras, E. A.: the pre-stressed piezoelectric sandwich transducer. In Proceeding of Ultrasonic International Conference, pp.295-302, 1973

[OK95] Osyczka, A. and Kundu, S.: A new method to solve generalized multicriterion optimization problems using genetic algorithm, Structual Optimization, Vol.10, No.2, pp.94-99,1995

[OK96] Osyczka, A. and Kundu, S.: A modified distance method for multicriterion optimization problems using genetic algorithm, Computers and Industrial Engineering, Vol.30, No.4, pp.871-882,1996.

[Phi88] Valvo Unternehmenbereich Bauelemente der Philips GmbH: PIEZOXIDE (PXE) Eigenschaften und Anwendungen. Dr.Alfred Hüthig Verlag Gmbh, Heidelberg, 1988, ISBN 3-7785-1755-4

[Phi91] Waanders, J. W.: Piezoelectric Ceramics-Properties and Applications. Philips Components, Eindhoven, 1991

[Pre02] Preumont, A.: Responsive Systems for Active Vibration Control. Kluwer Academic Publishers, Dordrecht, 2002, ISBN 1-4020-0898-8

[PRF03] Pons, J. L.; Rodriguez, H.; Fernández, J. F.; Villegas, M. and Seco, F. : Parameter optimization of ultrasonic motors. Sensors and actuators, Vol.107, pp.169-182, Elsevier, 2003

[RTS01] Ray, T.; Tai, K. and Seow, K. C.: An evolutionary algorithm for multiobjective optimization. Engineering Optimization, Vol.33, 399-424, 2001

[Rus95] Ruschmeyer, K.: Piezokeramik- Grundlagen, Werkstoffe, Applikationen. Renningen-Malmsheim, Expert Verlag, 1995, ISBN 3-8169-1152-8

[Sat03] Sattel, T.: Mechatronisches System zur schwingungsüberlagerten Bearbeitung von Baustoffen. III . Quartalsbericht 2003

[SC93] Seeley, C.E. and Chattopadhyay, A.: The development of an optimization procedure for the design of intelligent structures. Smart Materials and Structures, Vol.2, No.2, pp.135-146, 1993

[Sch96] Schäufele, A.: Ferroelastische Eigenschaften von Blei-Zirkoat-Titanat-Keramiken. Dissertation, VDI Verlag Gmbh, Düsseldorf, 1996, ISBN 3-18-344505

[SD95] Srinivas, N. and Deb, K.: Multi-Objective function optimization using non-dominated sorting genetic algorithms. Evolutionary Computation, Vol. 2, pp. 221-248, 1995

[Set02] Setter, N.: Piezoelectric materials in devices: extended reviews on current and emerging piezoelectric materials, technology, and applications. EPFL, Swiss Federal Inst. of Technology, 2002, ISBN 2-9700346-0-3

[Sig97] Sigmund, O.: On the design of compliant mechanisms using topology optimization. Mechanics of Structures and Machines, Vol. 25, pp.493-524, 1997

[SK99] Silva, E. C. N. and Kikuchi, N.: Design of piezoelectric transducers using topology optimization. Smart Materials and Structures, Vol.8, pp.350-364, 1999

[SM95] Statnikov, R. B. and Matusov, J.: Multicriteria Optimization and Engineering. Chapman & Hall, 1995, ISBN 0-412-99231-0

[SMD03] Schütze, O.; Mostaghim, S.; Dellnitz, M. and Teich, J.: Covering Pareto Sets by Multilevel Evolutionary Subdivision Techniques. In Proceeding of Evolutionary Multi-Criterion Optimization: Second International Conference, EMO 2003, Faro, Portugal, April 8-11, pp. 118-132, 2003

[SNF98] Silva, E.; Nishiwaki, S.; Fonseca, J.; Crumm, A; Brady, G.; de Espinosa, F.; Halloran, J. and Kikuchi, N.: Topology optimization applied to the design of piezocomposite materials and piezoelectric actuators. Proceedings of SPIE, Vol.3323, pp.216-227, 1998

[SNK00] Silva, E.; Nishiwaki, S. and Kikuchi, N.: Topology optimization design of flextensional actuator. IEEE Transaction on Ultrasonics, Ferroelectrics, and Frequency Control. Vol.47, No.3, pp.657-671, 2000

[SWW93] Sadri, A.M.; Wright, J.R. and Wynne, R.J.: Modelling and optimal placement of piezoelectric actuators in isotropic plates using genetic algorithms. Smart Materials and Structures, Vol.8, pp.490-498, 1993

[Uch97] Uchino, K.: Piezoelectric Actuators and Ultrasonic Motors. Kluwer Academic Publishers, USA, 1997, ISBN 0-7923-9811-4

[Uch04] Uchino, K.: Materials, design, drive/control, modelling and application. In Proceeding of Actuator 2004, 9th International Conference on New Actuators, 14-16 June 2004, Bremen, Germany, pp.38-47

[Wal00] Wallaschek, J.: Systementwurf piezoelektrischer Aktoren. VDI Bildungswerk, Mechatronik Workshop, Düsseldorf , 2000

[WH00] Wallaschek, J. and Hemsel, T.: Piezoelektrische Werkstoffe und ihre technische Anwendung. Heinz Nixdorf Institut, Universität Paderborn, Mechtronik und Dynamik, 2000

[YV96] Yousefi-Koma, A. and Vukovich, G.: Shape and location optimization of piezoelectric actuators in active control systems. Proceedings of the ASME Aerospace Division, AD-vol.52, pp.559-566, 1996

[Zit99] Zitzler, E.: Evolutionary algorithms for multiobjective optimization: methods and applications. Dissertation, Technische Wissenschaften ETH Zürich, Nr. 13398, Shaker Verlag, 1999, ISBN 3-8265-6831-1

[ZLG00] Zhang, H.W.; Lennox, B.; Goulding, P.R. and Leung, A.Y.T.: A float-encoded genetic algorithm technique for integrated optimization of piezoelectric actuator and sensor placement and feedback gains. Smart Materials and Structures, Vol.9, pp.552-557, 2000

[ZLT02] Zitzler, E.; Laumanns, M. and Thiele, L.: SPEA2: Improving the strength Pareto evolutionary algorithm. Evolutionary Methods for Design, Optimization and Control with Applications to Industrial Problems, 2002

[ZT99] Zitzler,E. and Thiele,L.: Multiobjective Evolutionary Algorithms: A Comparative Case Study and the Strength Pareto Approach. IEEE Transactions on Evolutionary Computation, Vol.3, No.4, pp.257-271, 1999